SEMI-SYNTHESIS OF AROMATIC DIACIDS AND BIOSYNTHESIS OF KANOSAMINE IN *ESCHERICHIA COLI*

By

Kelly Miller

A DISSERTATION

Submitted to
Michigan State University
in partial fulfillment of the requirements
for the degree of

Chemistry—Doctor of Philosophy

2018

ABSTRACT

SEMI-SYNTHESIS OF AROMATIC DIACIDS AND BIOSYNTHESIS OF KANOSAMINE IN *ESCHERICHIA COLI*

By

Kelly Miller

Microbial synthesis of chemicals from biobased feedstocks is an alternative to manufacture of materials derived from petroleum or unconventional gases, such as shale gas and coalbed methane. Aromatic diacids, terephthalic acid, isophthalic acid , and phthalic acid, are valuable compounds for the polymers and plasticizers industry. These diacids are currently manufactured via Amoco Mid-Century oxidation of petroleum-derived *para*-, *meta*- and *ortho*-xylenes, respectively; a process not without environmental and economic challenges.

In this work, a semi-synthesis of terephthalic, isophthalic, and phthalic acids is outlined using 2-hydroxymuconic acid as a common synthetic precursor. Recombinant *Escherichia coli* was utilized combining protocatechuic acid anabolic and catabolic pathways to achieve 1.2 g/L 2-hydroxymuconic acid from D-glucose in fed-batch fermentation. Lewis-acid catalysis was explored in a cycloaddition of 2-hydroxymuconic acid with ethylene to produce terephthalic acid. Cyclization of 2-hydroxymuconic acid afforded 6-carboxy-2-pyrone which was reacted with propiolic acid to afford mixtures of isophthalic and phthalic acids. Propiolic acid from biogas methane and ethylene from bioethanol could maximize the amount of renewable carbon in this semi-synthetic strategy, producing all three petroleum-derived aromatic diacids without the need for Amoco Mid-Century oxidation process.

In an additional research trajectory, the production of kanosamine (3-amino-3-deoxy-D-glucose) is evaluated in fed-batch fermentation of recombinant *E. coli*. Two biosynthesis pathways are reported in the literature: one native to *Bacillus subtilis* and the other reported in *Amycolatopsis mediterranei* and *Bacillus pumilus*. Genes encoding kanosamine biosynthetic enzymes from *B. subtilis*, *A. mediterranei*, and *B. pumilus* are expressed in *Escherichia coli* to determine whether heterologous expression results in kanosamine accumulation and if the system can be manipulated to maximize kanosamine production. Recombinant *E. coli* expressing genes from *B. subtilis* 168 produces 12.7 ± 0.6 g/L kanosamine in a 6% mol/mol yield from D-glucose. Kanosamine yields were increased to 18 ± 1% mol/mol by blocking the Embden-Meyerhoff-Parnas pathway through a mutation in *pgi*-encoded phosphoglucose isomerase. Enzymes native to *A. mediterranei* proved to be challenging to efficiently express in *E. coli*, prompting examination of *B. pumilus* kanosamine biosynthesis. Expression of *B. pumilus* SH-B11 genes in *E. coli* results in 6.3 g/L kanosamine titers in 4.4% mol/mol yield from D-glucose in fed-batch fermentation. *In vitro* feeding experiments suggest a departure from what is in the literature regarding kanosamine production in *Bacillus pumilus*.

TABLE OF CONTENTS

LIST OF TABLES

LIST OF FIGURES

KEY TO ABBREVIATIONS

AHBA	3-amino-5-hydroxybenzoic acid
aminoDAHP	4-amino-3,4-dideoxy-D-*arabino*-heptulosonate-7-phosphate
aminoDHQ	5-amino-5-deoxy-3-dehydroquinate
aminoDHS	5-amino-5-deoxy-3-dehydroshikimate
aminoF6P	3-amino-3-deoxy-D-fructose-6-phosphate
AMP	2-amino-2-methyl-1-propanol
ATP	adenosine triphosphate
BTX	benzene, toluene, xylenes
cAMP	cyclic adenosine monophosphate
4-CBA	4-carboxybenzaldehyde
CHMS	5-carboxy-2-hydroxymuconic semialdehyde
CoA	coenzyme A
DAHP	3-deoxy-D-*arabino*-heptulosonate 7-phosphate
DEHP	di-(2-ethylhexyl) phthalate
DEPT	distortionless enhancement by polarization transfer
DINCH	diisononyl cyclohexane-1,2-dicarboxylate
DHQ	3-dehydroquinate
DHS	3-dehydroshikimate
DMF	dimethylfuran
DMT	dimethylterephthalate

DNA	deoxyribonucleic acid
D.O.	dissolved oxygen
E4P	D-erythrose-4-phosphate
F6P	D-fructose-6-phosphate
FDCA	2,5-furandicarboxylic acid
GA	gallic acid
G6P	D-glucose-6-phosphate
GC	gas chromatography
Glu	L-glutamate
Gln	L-glutamine
GlcN	glucosamine (2-amino-2-deoxy-D-glucose)
h	hour
2-HMA	2-hydroxymuconic acid
HMF	hydroxymethylfurfural
HMS	2-hydroxymuconic semialdehyde
HOMO	highest occupied molecular orbital
HPLC	high performance liquid chromatography
IED DA	inverse electron demand Diels-Alder
iminoE4P	1-imino-1-deoxy-D-erythrose-4-phosphate
IPA	isophthalic acid
IPTG	β-D-isopropylthiogalactopyranoside
k	rate constant

kb	kilobase
kD	kilodalton
αKG	α-ketoglutarate
K6P	kanosamine-6-phosphate
LUMO	lowest occupied molecular orbital
M	molar
mC7N	six-membered carbocycle with *meta*-substituted carbon and nitrogen groups
mg	milligram
mL	milliliter
mM	millimolar
min	minute
NAD^+	nicotinamide adenine dinucleotide, oxidized form
NADH	nicotinamide adenine dinucleotide, reduced form
NMR	nuclear magnetic resonance
NOE	nuclear Overhauser effect
NTA	nitrilotriacetic acid
OD	optical density
PA	phthalic acid
PCA	protocatechuic acid
PCR	polymerase chain reaction
PEP	phosphoenolpyruvate

PET	poly(ethylene terephthalate)
PLP	pyridoxal phosphate
PMP	pyridoxamine phosphate
psi	pounds per square inch
PTA	terephthalic acid
RNA	ribonucleic acid
R5P	ribose-5-phosphate
SDS-PAGE	sodium dodecylsulfate polyacrylamide gel electrophoresis
TCA	citric acid
U	unit; μmol/min
UDP	uridine diphosphate
UDPGlc	UDP-3-keto-D-glucose
UTP	uridine triphosphate

CHAPTER ONE: SYNTHESIS OF RENEWABLE TEREPHTHALIC ACID, ISOPHTHALIC ACID, AND PHTHALIC ACID FROM MICROBE-SYNTHESIZED 2-HYDROXYMUCONIC ACID

INTRODUCTION

1. Chemicals manufacture from natural hydrocarbon sources: shale gas and petroleum

Commercial manufacture of fuels and chemicals relies heavily on non-renewable natural resources such as natural gas and petroleum. Reserves of these fossil fuels are widespread and the composition of each varies from one location to another.[1] In North America, natural gas trapped in pores of underground shale rock beds is an abundant source of hydrocarbons. A map of the shale gas reserves in the contiguous United States presented by the United States Energy Information Administration is shown in Figure 1.[2]

Though the precise composition of shale gas differs from one wellhead to another, the primary component is always methane.[3] Ethane, propane, and higher hydrocarbons may be present as well as compounds such as carbon dioxide, nitrogen, and hydrogen sulfide. The Marcellus shale gas play is the largest in the U.S. and one of the most productive in the world.[4] The composition of the Marcellus shale gas play is described in Table 1.[1] Because shale gas is trapped much deeper than conventional natural gas, new technologies were required to access it. Horizontal drilling and hydraulic fracturing, or fracking, were developed explicitly for this purpose.[5]

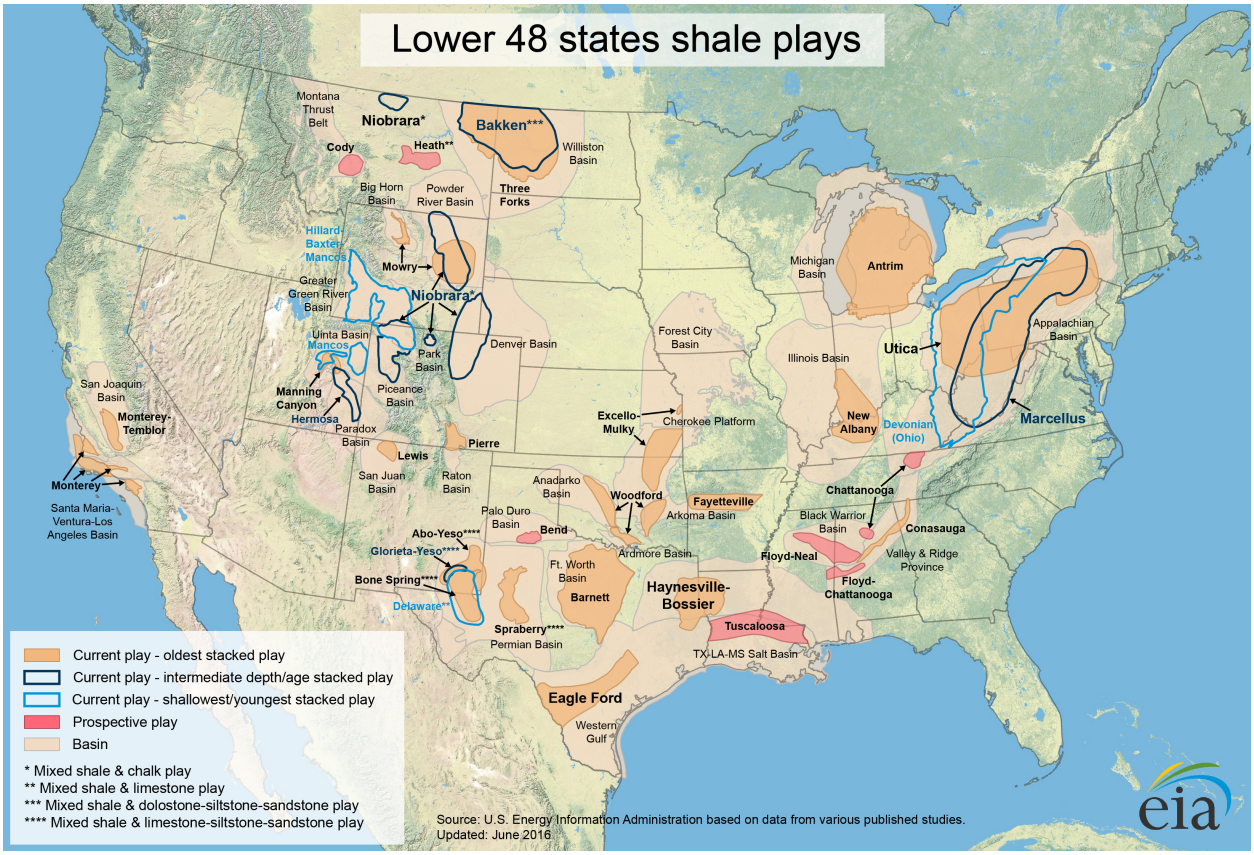

Figure 1. Map of shale gas reserves in the contiguous United States.

Table 1. Composition of Marcellus shale gas play in Appalachia.

Component	Mol percentage
Methane	76.9
Ethane	13.4
Propane	4.5
Butanes	1.6
Pentanes	1.3
CO_2	1.0
N_2	1.0

Briefly, a well bore drills vertically downward until it reaches a layer of shale rock. The bore is then turned horizontally and drilling continues through the rock, providing much greater

recovery of gas trapped in rock pores than vertical drilling. A steel casing equipped with explosive charges surrounds the horizontal portion of the well. Detonation of the charges creates large fractures in the shale rock which are kept open by highly pressurized water. The water contains fine-grained silica (SiO_2) and other chemicals that prevent the fractures collapsing once the water pump is shut off. Reducing the water pressure allows the shale gas to flow through the open fractures and into the well.[5]

Petroleum contains a wider distribution of hydrocarbons than natural or shale gas. When organic compounds such as fatty acids and steroids are pressurized for millions of years within the earth, a crude oil forms in which molecules containing forty or more carbon atoms may be present.[6,7] In order for crude oil to serve as a useful source of hydrocarbons for chemicals manufacture, it must be separated into useful fractions. Table 2 describes some characteristic properties of petroleum fractions from a Middle-Eastern crude oil.[8] Each fraction contains a different distribution of paraffins, aromatics, and cycloaliphatics (naphthenes).

Table 2. Characteristic data of a Middle-Eastern petroleum reserve.

Fraction	Volume percentage	Boiling point range (°C)	Paraffins (vol%)	Naphthenes (vol%)	Aromatics (vol%)
Light naphtha	7.9	20-100	89.6	9.5	0.9
Heavy naphtha	6.8	100-150	70.3	21.4	8.3
Kerosene	12.5	150-235	58.0	23.7	18.3
Light gas oil	16.4	235-343	—	—	
Heavy gas oil	26.3	343-565	—	—	
Residual oil	26.8	>565	—	—	

Petroleum refining begins by desalting crude oil via thermal or electrical separations.[7] Contaminants such as sodium, calcium, and magnesium occupy an aqueous phase that is coproduced with the crude oil. These salts must be removed in order to prevent corrosion of pipelines and reactor equipment. Atmospheric distillation (Figure 2) follows removal of inorganic contaminants.[7] The fractionation tower separates light hydrocarbons from heavier gas oils which are subjected to further fractionation at pressures below 1 bar. Side streams of atmospheric distillation, heavy naphtha, kerosene, and light and heavy gas oils, are separated in stripping columns with use of superheated steam. Gas oils and fractions isolated from vacuum distillation are commercially used for lubricating oils and bunker fuels while commodity chemicals are made from atmospheric distillation fractions.[7,8]

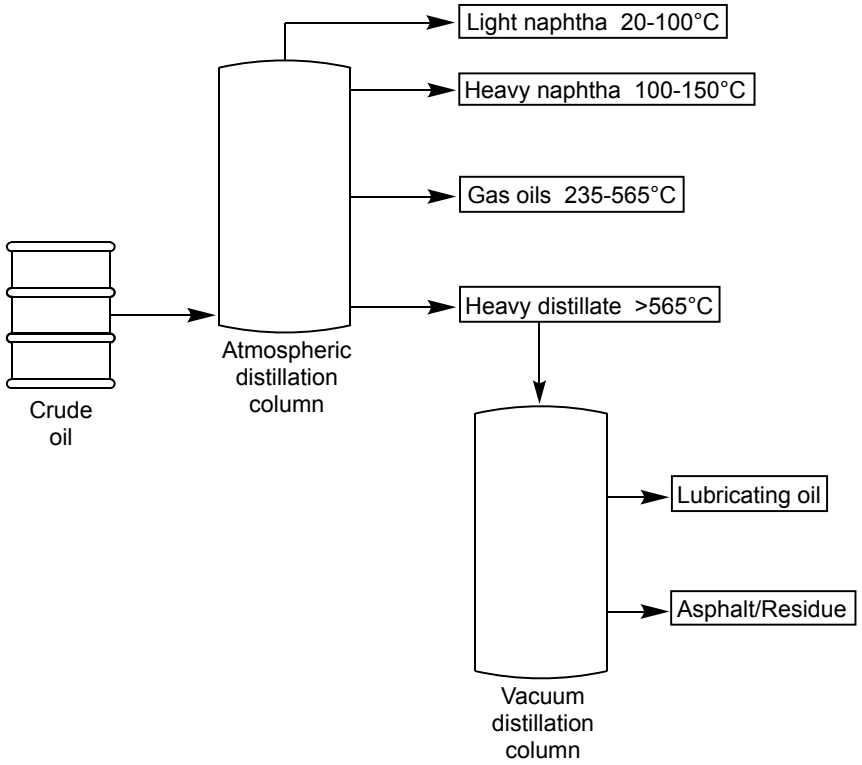

Figure 2. Schematic representation of petroleum fractionation.

Though petroleum and natural gas allow access to a plethora of different hydrocarbons for manufacture of fuels and chemicals, the cost and availability of such resources are subject to substantial and unpredictable variation. Alternative feedstocks must be made available to stabilize costs associated with commodity chemical synthesis. In times of increased petroleum or natural gas prices, synthetic routes involving biobased starting materials are advantageous. Terephthalic acid is an example of a commodity chemical that would greatly benefit from a diverse pool of available feedstocks.

2. Commercial synthesis of terephthalic acid

Since its discovery in 1847,[9] purified terephthalic acid (PTA) has become an important large volume commodity chemical. Nearly all of the 47 million tons consumed globally in 2012 went into the manufacture of poly(ethylene terephthalate) (PET).[10] With applications ranging from clear beverage bottles, molded packaging containers, and polyester films and fibers, PET is widely used and highly valuable.[10]

Current commercial production of PTA relies on the Co^{2+}/Mn^{2+}-catalyzed oxidation of petroleum-derived *para*-xylene developed by the Mid-Century Corporation (Amoco).[11] The xylene isomers, *ortho*-, *meta*-, and *para*- (Figure 3), are dimethylated aromatic compounds which are part of a highly valued cut of petroleum-derived aromatics called BTX (benzene, toluene, xylenes). Products of xylene oxidation are important players in the polymers and plasticizers industry (Figure 3).

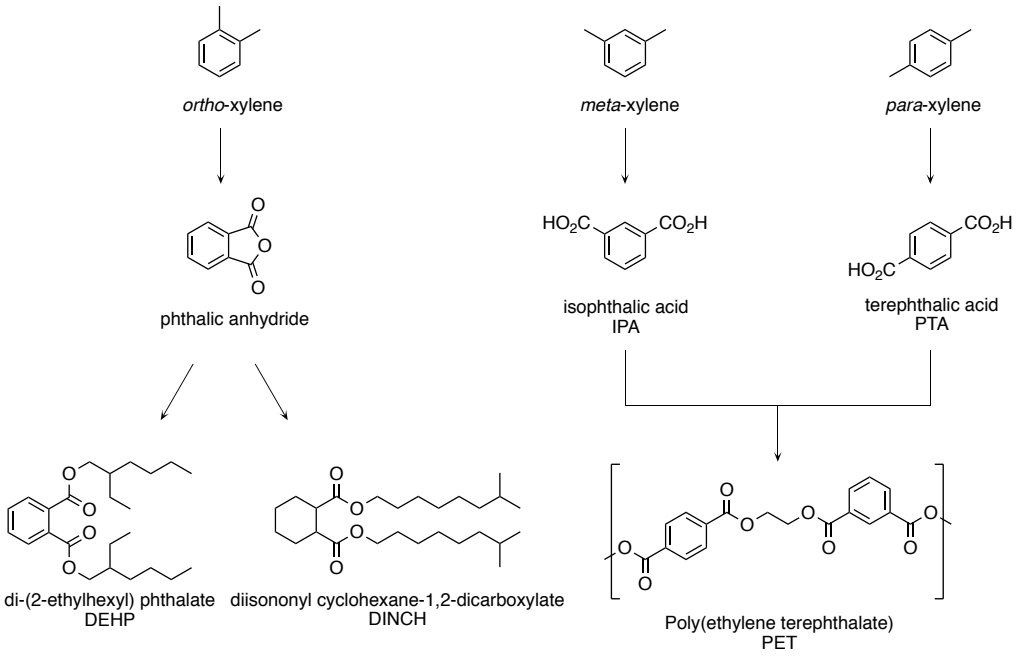

Figure 3. Oxidation of petroleum-derived xylene isomers.

Oxidation of *ortho*-xylene affords phthalic acid (PA) which can be dehydrated to phthalic anhydride. This compound is used as a scaffold for plasticizers such as di-(2-ethylhexyl) phthalate (DEHP) and diisononyl cyclohexane-1,2-dicarboxylate (DINCH) (Figure 3). The products of *meta*- and *para*-xylene oxidation, isophthalic acid (IPA) and terephthalic acid (PTA), respectively, are condensed with ethylene glycol to afford PET. Amoco Mid-Century liquid-phase oxidation of *meta*- and *para*-xylenes is commercially performed in a high pressure reactor charged with substrate and catalyst mixture in acetic acid. The catalyst system is a mixture of cobalt and manganese acetates with a bromine compound such as sodium bromide as a radical chain propagator. The oxidation occurs at pressures of 15-30 bar and temperatures of 175-225°C.[12]

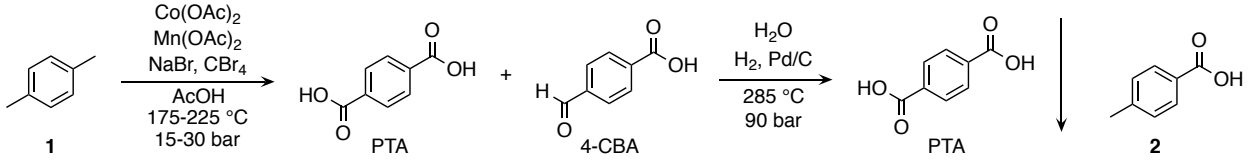

Figure 4. Reaction conditions of Amoco Mid-Century oxidation of *p*-xylene **1** to PTA.

Oxidation of *p*-xylene **1** to PTA (Figure 4) follows the Hammett structure-reactivity relationship (equation 1):

(1) $$\log(k/k_0) = (\sigma)(\rho)$$

where k = the rate constant for the consumption of a compound, k_0 = the rate constant for the consumption of toluene, σ = the characteristic constant for a ring substituent, and ρ = the characteristic constant for a set of reaction conditions. The Hammett equation (eq. 1) describes a linear free-energy relationship relating reaction rates and equilibrium constants for many organic reactions involving benzene derivatives. The equation relates the equilibrium constant (k) for a given reaction with substituent, R, and the equilibrium constant for a reference compound (k_0) where R is a hydrogen atom. Only two parameters are utilized: a substituent constant (σ) which depends only on the specific substituent and the reaction constant (ρ) which depends on the type of reaction but not the substituent used. Reported ρ values for metal/bromine-catalyzed oxidations of aryl methyl groups typically fall in the range of -0.6 to -1.3.[12] Industrial oxidation conditions are conventionally 90% acetic acid solutions in water, which offer ρ values of -0.95.[12] Equation 1 explains why the complete oxidation of one methyl group occurs before the other. Once the first methyl group reaches the carboxylic acid stage, the σ value for the *para*-methyl

group rises from -0.3 to +0.4, thus indicating a reduction in the ring electron density. This reduction causes the second methyl oxidation to proceed 4.9 times slower than the first.[12,13]

Overoxidative burning of *p*-xylene **1** to carbon oxides represents a major challenge associated with the Amoco Mid-Century process. Additional carbon oxides are produced along with methane via Kolbe decomposition of acetic acid (Figure 5).[12,13] These side reactions attendant with radical chain propagation and harsh reaction conditions greatly impact process economics. For every 1000 kg of PTA produced, 165 kg of CO_2 is generated with 60% due to oxidation of acetic acid and 40% due to *p*-xylene **1** overoxidation.[14] Solvent degradation and oxidative burning of crude PTA embody an unnecessary waste of carbon and increase the costs associated with PTA manufacture.

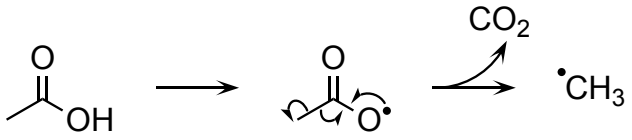

Figure 5. Degradation of acetic acid via Kolbe oxidation.

Ironically, the most problematic contaminant formed during the Amoco Mid-Century oxidation is a product of incomplete oxidation, 4-carboxybenzaldehyde (4-CBA, Figure 4). During the condensation polymerization of IPA, PTA, and ethylene glycol to afford PET, any 4-CBA present in the crude PTA product mixture would serve as a chain terminator, thus inhibiting PET chain growth. As such, significant effort has been expended to eliminate 4-CBA from the product stream. Crude PTA typically containing around 0.3% by weight of 4-CBA is dissolved in water at 285 °C and 90 bar and sent into a trickle-bed reactor. The PTA crude flows down a Pd/C catalyst bed while a gaseous H_2 stream moves upward. Hydrogen reduces 4-CBA to *p*-

toluic acid **2** which has a higher solubility in water than PTA. Terephthalic acid of 99.99% purity precipitates from solution as the aqueous phase exits the reactor while *p*-toluic acid **2** remains in solution.[13]

3. Routes to biobased terephthalic acid

Challenges accompanying Amoco Mid-Century oxidation of aryl methyl groups encourage the development of alternative substrates for PTA production. Synthetic routes involving biobased substrates offer an attractive means to supplement fossil fuel-derived PTA. Synthesis of PTA from alternative feedstocks can be broadly categorized into two groups: those with and those without *p*-xylene **1** intermediacy. Biobased materials including 5-hydroxymethylfurfural (HMF)[15], ethylene **2**,[16,17] isobutanol **3**,[17-21] and sorbitol **4**[22] (Figure 6) offer a means of access to *p*-xylene **1** which are easier to integrate into the current chemical manufacture infrastructure than novel routes to PTA. These routes, however, do not avoid aryl methyl group oxidation. Despite its current utility, the Amoco Mid-Century oxidation requires large amounts of solvent, expensive reactor equipment, arduous purifications, and results in overoxidative burning of the crude product.

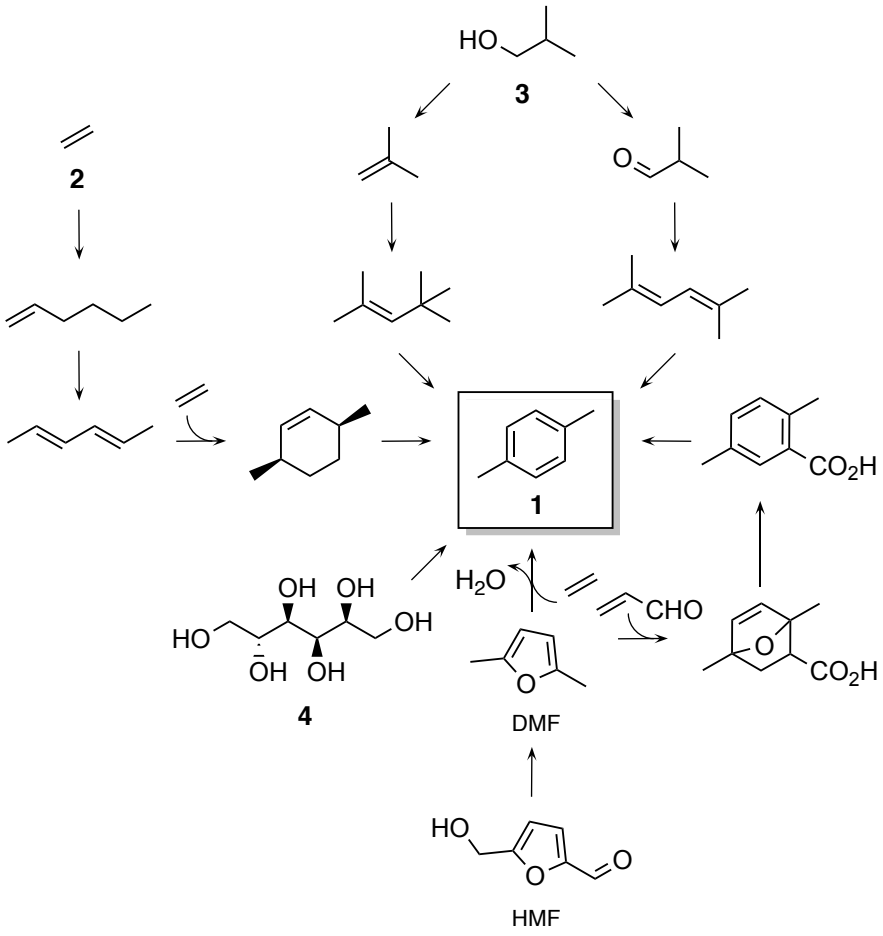

Figure 6. Biobased routes to *p*-xylene **1** from ethylene **2**, isobutanol **3**, sorbitol **4**, and 5-hydroxymethylfurfural.

High yields and selectivities are reported for different steps in many of the syntheses of biobased *p*-xylene **1**. The cycloaddition of ethylene **2** with HMF-derived dimethylfuran (DMF), for example, affords *p*-xylene **1** with >99% conversion and 90% selectivity.[23] Vapor phase dehydration of isobutanol **3** over γ-Al_2O_3 at 450 °C and 4 bar affords isobutylene with >99% conversion with 95% selectivity.[17-20] Currently, no route reports high yields and selectivities for every step of the synthesis. Moreover, pathways from ethylene **2** and sorbitol **4** require expensive catalysts, such as the 10 wt% Pt(Re)/C catalyst used in the conversion of sorbitol **4**[22] to *p*-xylene **1** or the iridium pincer complex used in the second step of the route from biobased

ethylene **2**.[16,17] Industrially viable syntheses should use inexpensive catalysts and afford >90% selectivities. Low conversions could be tolerated assuming any unreacted species are able to be recycled. More development is necessary if any of the routes to biobased *p*-xylene **1** can be considered for commercialization. Even so, Amoco Mid-Century oxidation will be required in order to afford PTA.

Several synthetic routes to biobased PTA have been proposed that do not require *p*-xylene intermediacy and hence avoid the challenges associated with the Amoco Mid-Century process (Figure 7).[24-37] Succinic acid **5**, muconic acid **7**, malonic acid **12**, and 2,5-furandicarboxylic acid (FDCA) already contain the requisite carboxylic acid moieties present in the structure of PTA, thus avoiding the need for aryl methyl group oxidation. Routes from succinic **5**, muconic **7**, and malonic acids **12** require an esterification step to achieve reasonable yields in subsequent cycloadditions. These pathways necessitate hydrolysis of dimethylterephthalate (DMT) to afford PTA. Introducing additional steps makes a synthesis less commercially attractive. Use of limonene as a substrate for PTA synthesis involves an oxidation with stoichiometric potassium permanganate.[36] This reaction would likely by supplanted with an Amoco Mid-Century oxidation as would oxidation of *p*-toluic acid to PTA in the route from isoprene **14** and acrylic acid **15**.[37]

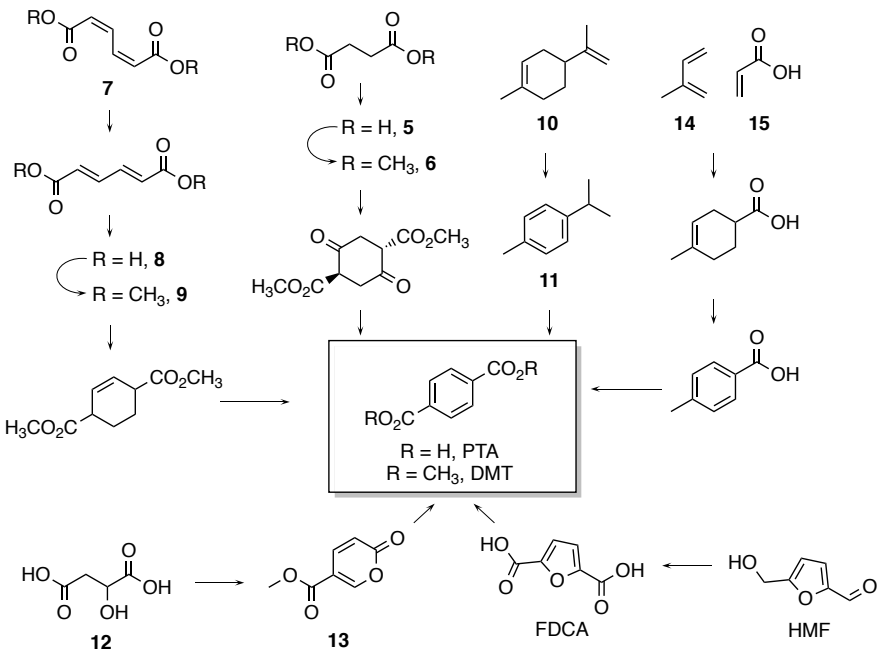

Figure 7. Biobased routes to terephthalic acid from succinic acid **5**, *cis*,*cis*-muconic acid **7**, limonene **10**, malic acid **12**, 5-hydroxymethylfurfural, and isoprene **14** and acrylic acid **15**.

Several challenges must be addressed before PTA production from renewable resources is commercially established. Low conversions and selectivities preclude the viability of most of the proposed routes to biobased PTA. High selectivities may reduce waste if unreacted starting material could be recycled. Without high conversion or selectivity at every step of a synthesis, the likelihood is low that it could be adopted into practice. Stoichiometric use of catalysts such as those employed for limonene **10** and the oxidation of HMF to FDCA are also undesirable for industrial processes.

Finally, there is only one proposed pathway to biobased PTA that addresses the need for 3-5% (w/w) IPA for PET manufacture. Regioselective cycloaddition of isoprene **14** and acrylic acid **15** catalyzed by 2 mol% $TiCl_4$ affords a 24:1 molar ratio of *para*- and *meta*-cycloadducts. After aromatization and oxidation, PTA is produced along with small amounts of IPA which can

be used to manufacture PET. This is a beneficial feature of this particular synthesis, however Amoco Mid-Century oxidation would still be required. A synthetic route to PTA from biobased starting materials that also affords small amounts of IPA allows PET manufacture to remain even if the BTX stream of petroleum refining disappeared. The work reported herein demonstrates biobased 2-hydroxymuconic acid could be converted to mixtures of terephthalic, isophthalic, or phthalic acids without the need for Amoco Mid-Century oxidation, thus establishing a proof-of-concept synthetic strategy that is not reliant on BTX.

PART I

SYNTHESIS OF AROMATIC DIACIDS FROM 2-HYDROXYMUCONIC ACID

1. Overview

Microbe-synthesized 2-hydroxymuconic acid (2-HMA) is an attractive candidate as a precursor to biobased PTA (Figure 8). Cycloaddition with bioethanol **16**-derived ethylene **2** would provide a cyclohexene intermediate that could undergo facile dehydration and aromatization to afford PTA without the need for harsh, wasteful alkyl group oxidations. This is similar to the previously reported synthesis of renewable PTA via reaction of ethylene **2** with biobased muconic acid **7**.[29] A key advantage to using 2-HMA as a synthetic intermediate over muconic acid **7** is its associated intramolecular cyclization reaction leading to 6-carboxy-2-pyrone **19** (Figure 8). A Diels-Alder reaction with methane-derived propiolic acid **18** followed by aromatization affords IPA and PA. All of the products from oxidation of petroleum-derived xylenes could thereby be prepared from 2-HMA obviating the need for the Amoco Mid-Century process. Successful cycloadditions using unprotected carboxylic acids would be highly desirable as they circumvent additional esterification/hydrolysis steps.

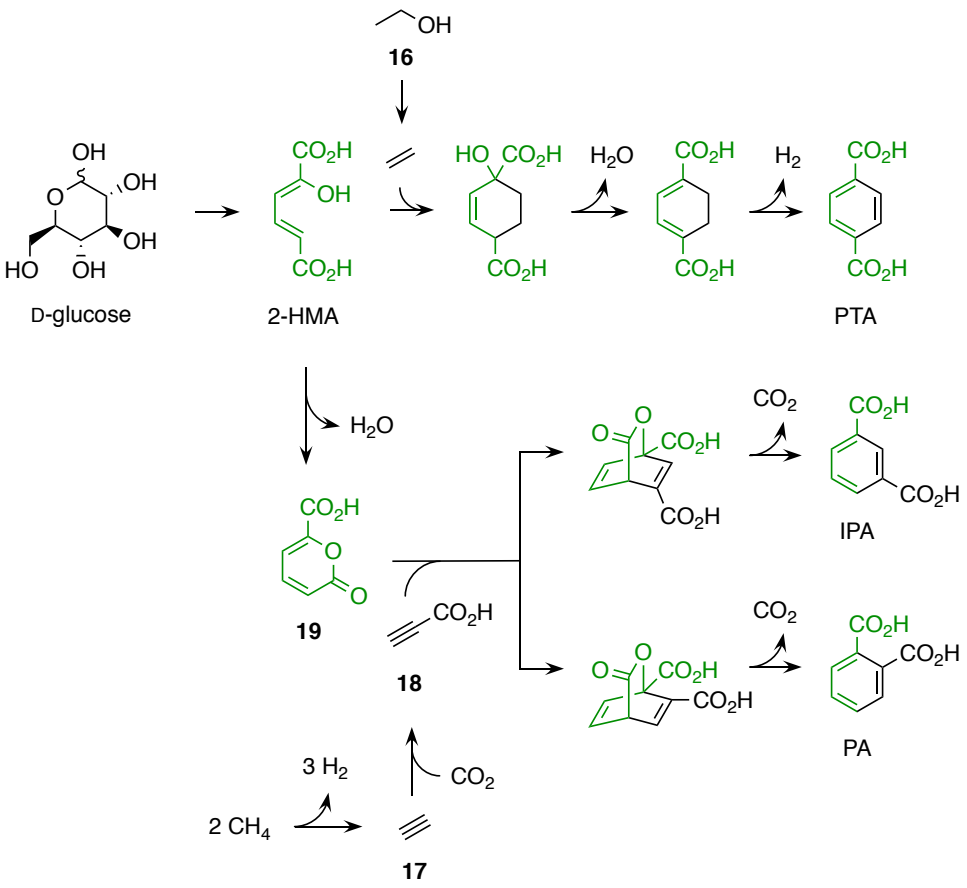

Figure 8. Reaction network to biobased terephthalic acid, isophthalic acid, and phthalic acid via microbe-synthesized 2-hydroxymuconic acid.

2-Hydroxymuconic acid is an intermediate in microbial catabolic pathways of aromatic compounds, such as catechol and protocatechuic acid (PCA). Biocatalytic synthesis of 2-HMA would require a microbe capable of biosynthesis of either catechol or PCA that also expressed the respective degradation pathway enzymes. Both of these aromatics have been previously produced in engineered *E. coli*.[38,39] The lower toxicity of PCA relative to catechol towards *E. coli* makes it a more attractive precursor to 2-HMA. Recently, the PCA 2,3-cleavage pathway was elucidated in *Paenibacillus* sp. JJ-1b[40,41] (Figure 9). Expression of PCA catabolic enzymes would enable the complete biosynthesis of 2-HMA in recombinant *E. coli.*

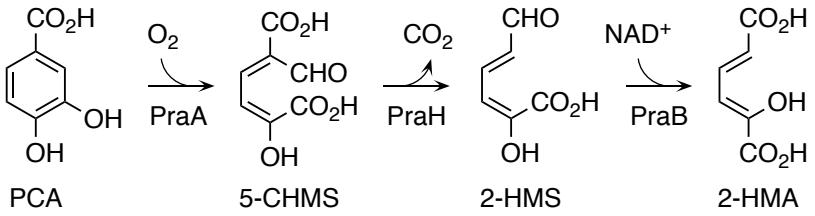

Figure 9. Biosynthesis of 2-hydroxymuconic acid via protocatechuate 2,3-cleavage pathway described in *Paenibacillus* sp. JJ-1b.

2. Chemical synthesis of 2-hydroxymuconic acid and 6-carboxy-2-pyrone

Chemically synthesized 2-HMA and 6-carboxy-2-pyrone **19** were used to develop reactions leading to PTA, IPA, and PA. Condensation of ethyl crotonate **20** with diethyl oxalate **21** affords diethyl 2-hydroxyhexa-2,4-dienedioate **22** (Figure 10). This allows direct access to either 2-HMA or 6-carboxy-2-pyrone **19** upon ester hydrolysis or tandem hydrolysis-lactonization, respectively. Synthesis of 2-hydroxyhexa-2,4-dienedioate **22** likely proceeds via deprotonation of a terminal allylic proton of ethyl crotonate **20** to form a resonance stabilized enolate. Nucleophilic attack upon diethyl oxalate **21** affords a keto intermediate that undergoes rapid deprotonation at the α-carbon to the ketone moiety.

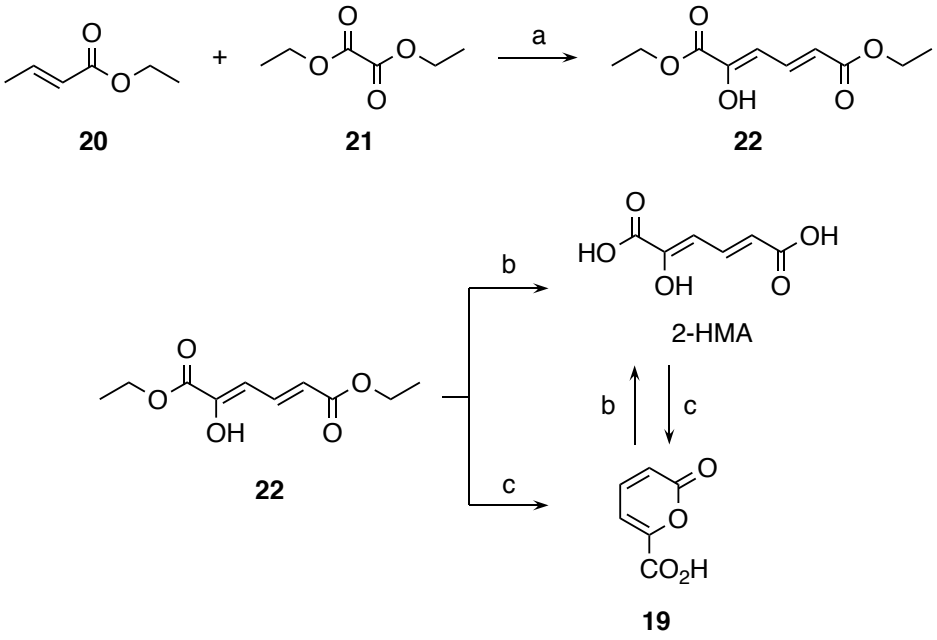

Figure 10. Synthesis of 2-hydroxymuconic acid and 6-carboxy-2-pyrone **19**. (a) K^0, $(CH_3)_3COH$, toluene, 0 °C-rt, 71%; (b) 1. 2 M NaOH, 2. conc. H_2SO_4, 4 °C, 59-64%; (c) H_2SO_4, AcOH, H_2O, 100 °C, 85%.

H_2SO_4 Ethyl crotonate **20** and diethyl oxalate **21** were condensed at 0 °C in dry toluene with freshly prepared $KOC(CH_3)_3$. The reaction was allowed to warm to rt to afford 2-hydroxyhexa-2,4-dienedioate **22** in 71% isolated yield. Ester hydrolysis to 2-HMA was performed in 2 M NaOH followed by treatment with concentrated H_2SO_4 at 4 °C. Acid treatment afforded 2-HMA as a beige precipitate which was washed in hot water and dried. 2-HMA was collected in 59% isolated yield. Lactonization and ester hydrolysis of 2-hydroxyhexa-2,4-dienedioate **22** to afford 6-carboxy-2-pyrone **19** was conducted at 100 °C in a solvent system consisting of 1:4 H_2SO_4:AcOH in water. Extraction into EtOAc followed by solvent removal in vacuo afforded 6-carboxy-2-pyrone **19** in 85% isolated yield. Interconversion of 2-HMA and 6-carboxy-2-pyrone **19** employed the same reaction conditions and achieved similar yields as synthesis via 2-hydroxyhexa-2,4-dienedioate **22**. Isolated products were

characterized by NMR spectroscopy (Figures 11-16) All three products matched previously reported syntheses.[42]

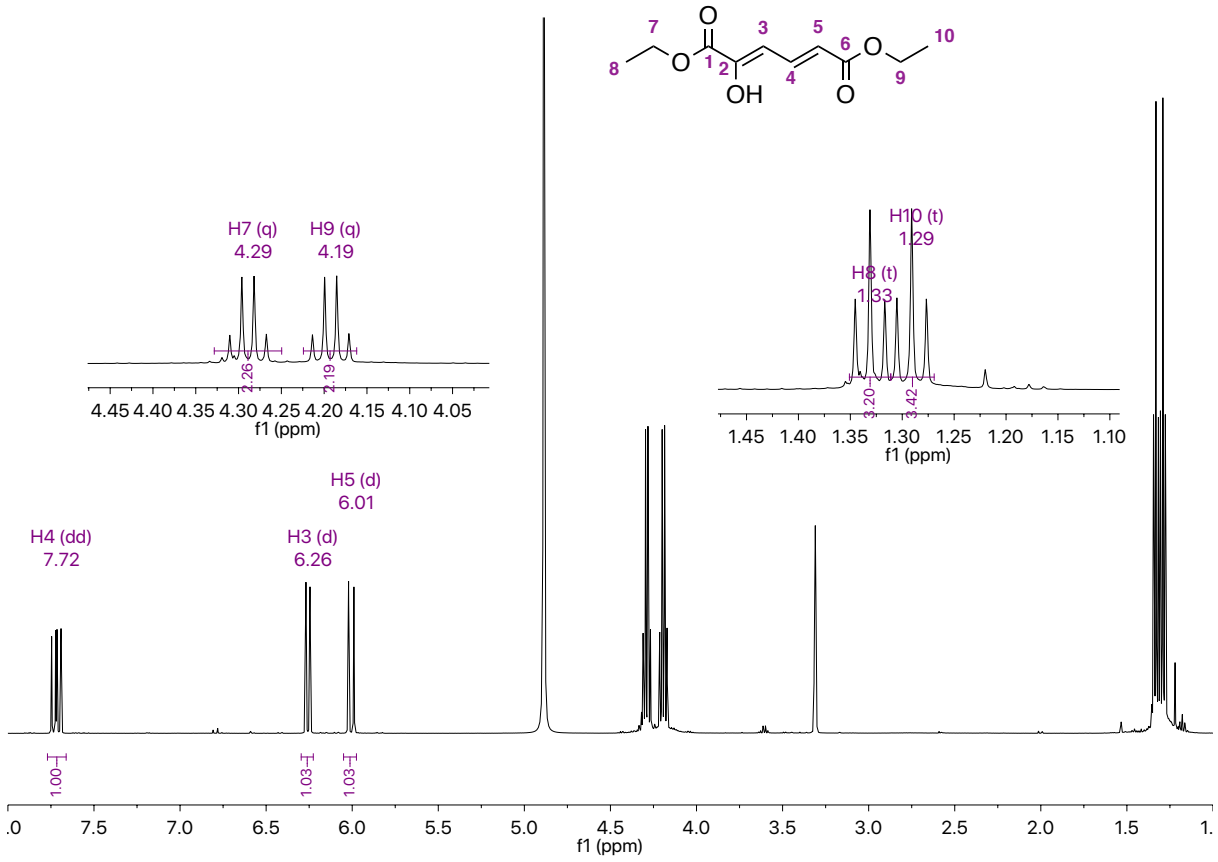

Figure 11. ^{1}H NMR spectrum of 2-hydroxyhexa-2,4-dienedioate **22** (CD_3OD).

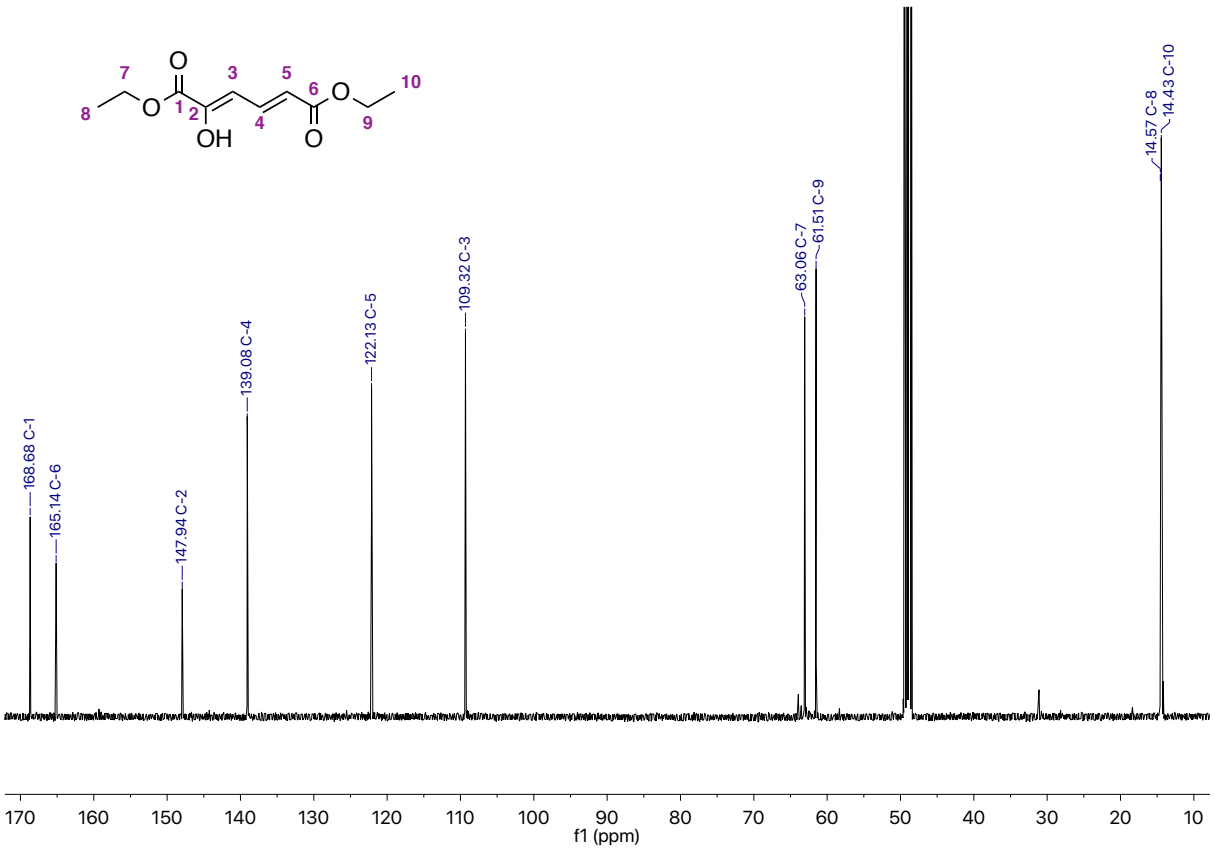

Figure 12. ^{13}C NMR spectrum of 2-hydroxyhexa-2,4-dienedioate **22** (CD_3OD).

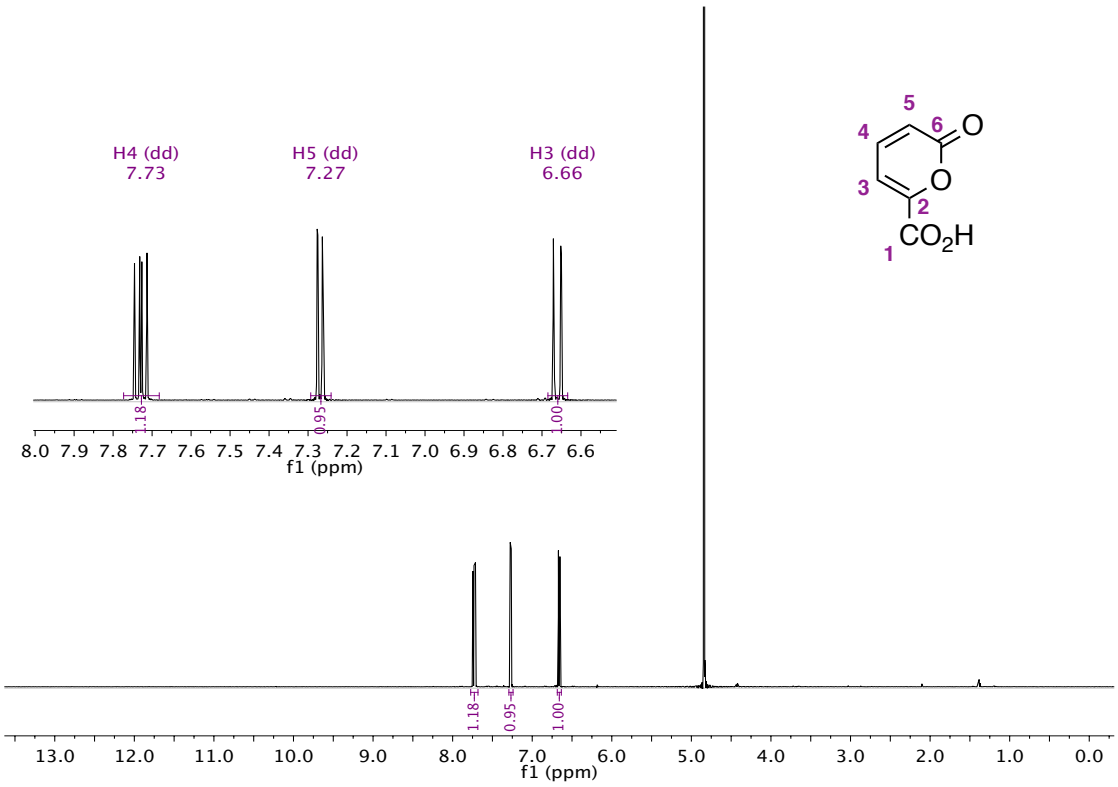

Figure 13. ^{1}H NMR spectrum of 6-carboxy-2-pyrone **19** (D_2O).

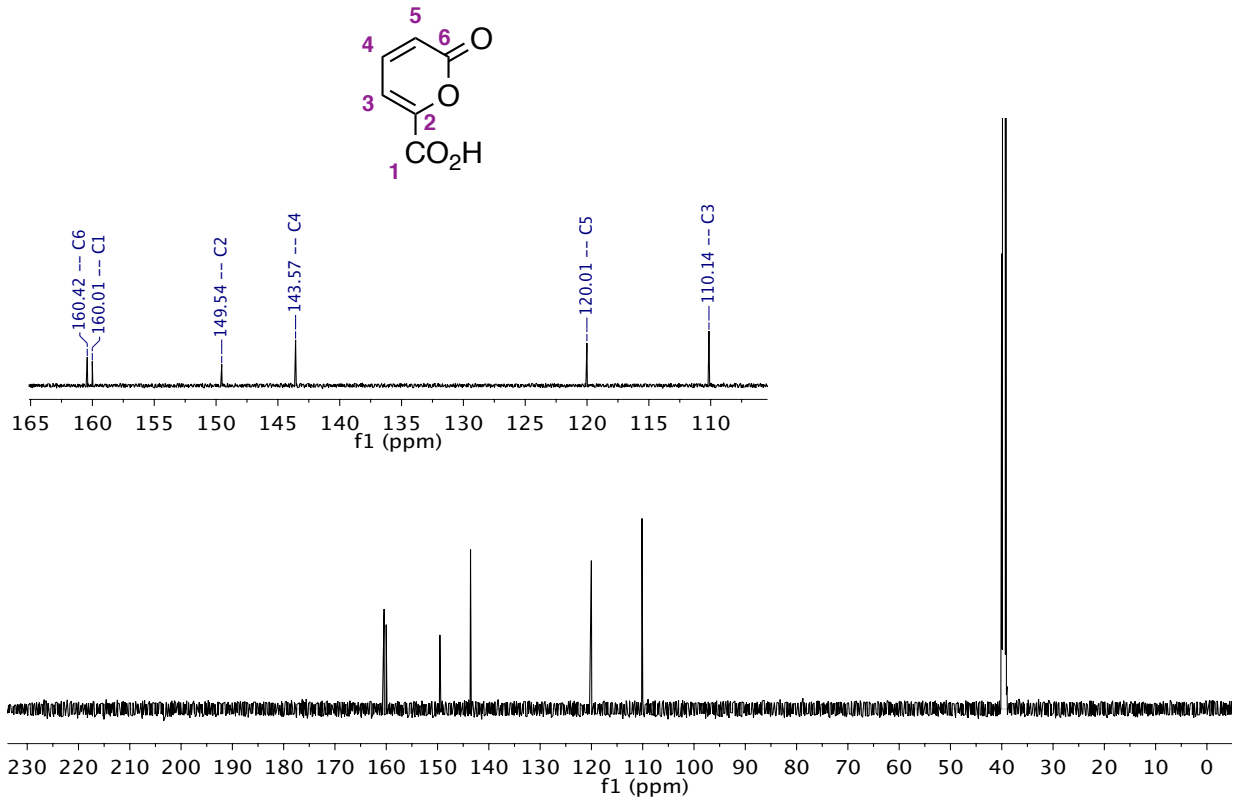

Figure 14. ^{13}C NMR of 6-carboxy-2-pyrone **19** (DMSO-d_6).

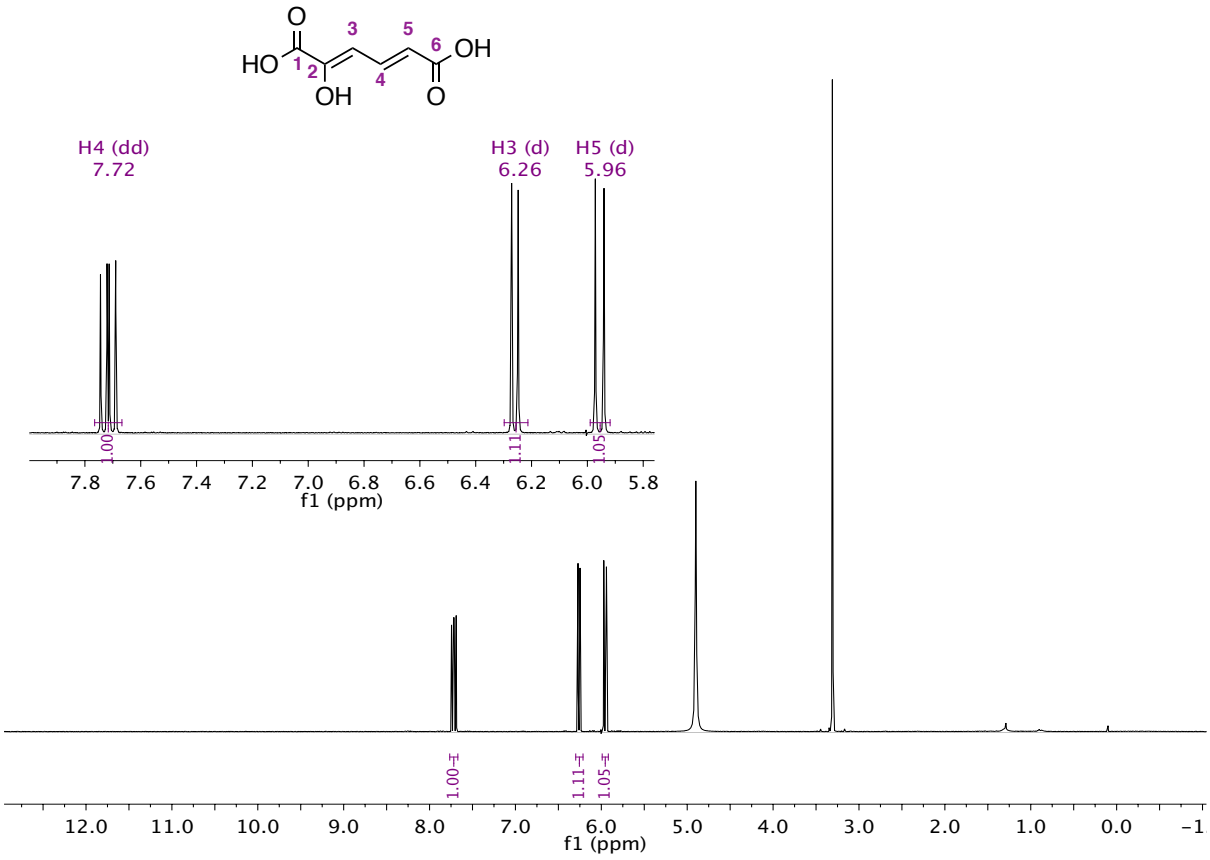

Figure 15. ^{1}H NMR spectrum of 2-hydroxymuconic acid (CD_3OD).

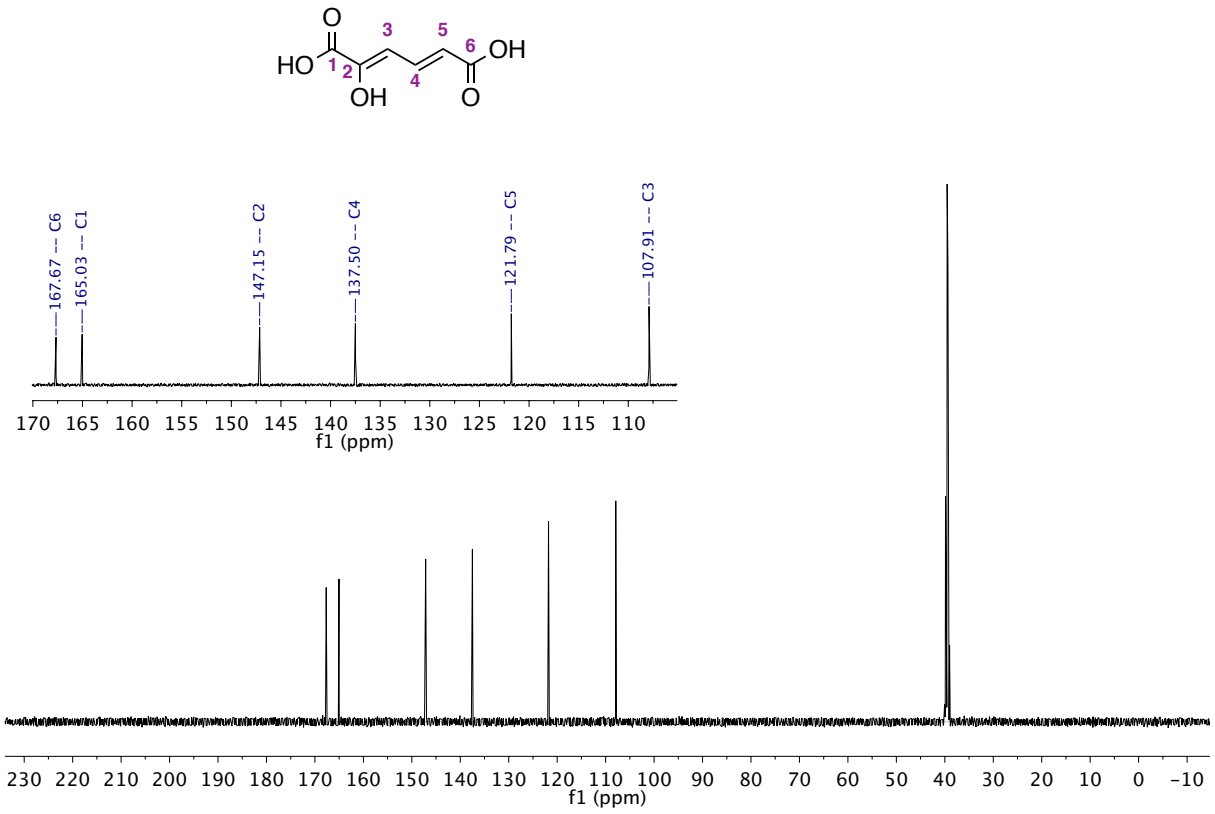

Figure 16. ^{13}C NMR spectrum of 2-hydroxymuconic acid (DMSO-d_6).

3. Synthesis of terephthalic acid via cycloaddition of 2-hydroxymuconic acid and ethylene

To understand the geometry of the conjugated π system in chemically synthesized 2-HMA, NOE (nuclear Overhauser effect) data was collected. This effect results from the transfer of spin polarization from one atom to another via cross-relaxation across interatomic space. Examination of vicinal proton coupling of protons on C-4 and C-5 suggested a *trans*-geometry about the π bond ($J_{3,4}$ = 15.6 Hz). This offered two possible structures for 2-HMA (Figure 17). Transfer of spin polarization in NOE spectroscopy occurs at short interatomic distances. Thus, differentiation between a *2E*- or *2Z*-π bond could be discerned by exciting the proton on C-5. Carboxylic acid protons can be difficult to observe in ^{1}H NMR spectra. To be able to clearly see

any NOE effect of the carboxylate moiety by excitation at C-5, 2-HMA was derivatized to dimethyl 2-hydroxymuconate with trimethylsilyldiazomethane. No NOE effect was observed for the methyl protons on C-1 when C-5 was irradiated indicating that the two proton environments are relatively far away in space. This implies that the π bond between C2 and C3 likely has *Z* stereochemistry.

(*2Z*,*4E*)-2-HMA (*2E*,*4E*)-2-HMA

Figure 17. Possible geometries about the C2-C3 double bond.

HOMO and LUMO energy levels of 2-HMA and ethylene **2** were calculated using Spartan '08 software and Møller-Plesset 6-31+G* basis set from AM1 initial geometry (Figure 18)[104]. The relative energies between the frontier molecular orbitals reveal that a cycloaddition would best proceed from overlap of the HOMO of ethylene **2** and the LUMO of 2-HMA (Figure 18) in an inverse electron demand Diels-Alder (IED DA) reaction.[43] Lewis acid catalysis can modulate the relative orbital energy levels of a substrate, facilitating overlap between the HOMO of one reaction partner and the LUMO of another. Coordination of a Lewis acid to a substrate has two broad effects. Firstly, relative energies of the LUMO and HOMO decrease according to the electron withdrawing strength of the Lewis acid with a concomitant decrease in the gap between the HOMO and LUMO energy levels. An additional effect of Lewis acid coordination is a change in the sizes of the orbital coefficients at each carbon atom. For example, a σ-

complex between the carbonyl oxygen at C-6 of 2-HMA and a classic Lewis acid such as $TiCl_4$ would result in an increase in the LUMO coefficients at C-2, C-4, and C-6, while decreasing the LUMO coefficients at C-1, C-3, and C-5. In asymmetrical reactions, the sizes of the orbital coefficients often influences the regioselectivity of the products.

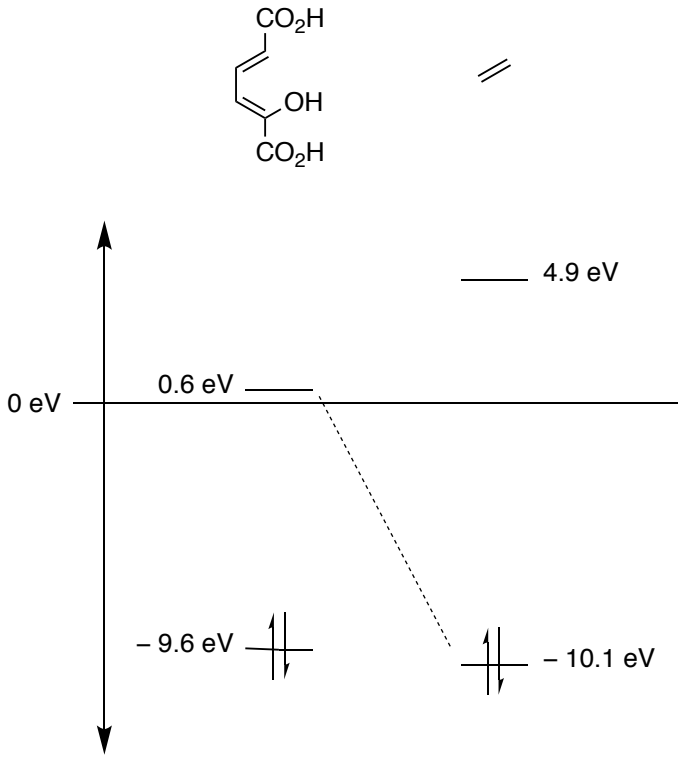

Figure 18. Relative energy levels of the frontier molecular orbitals of 2-hydroxymuconic acid and ethylene **2**.

Catalysis of the reaction between 2-HMA and ethylene **2** could involve either σ- or π-electrophilic Lewis acids.[44] Classic Lewis acids such as BCl_3, $TiCl_4$, and $AlCl_3$ form strong σ-complexes with heteroatoms of carbonyl and imine groups. On the other hand, salts of transition metals can behave as bifunctional Lewis acids, activating either carbon-carbon multiple bonds via π-bonding or forming σ-complexes in the same manner as conventional Lewis acids.

Platinum(II), gold(I), and copper(I) salts, in particular, have high propensities to form π-complexes.[44,45,46] These metals may be able to lower the LUMO energy of ethylene **2** sufficiently to promote reaction with the HOMO of 2-HMA in a normal electron demand Diels-Alder reaction.

2-Hydroxymuconic acid and ethylene **2** were first reacted in the absence of Lewis acid catalysis to determine the effect of thermal cycloaddition (Table 3). Previous reaction conditions for the cycloaddition of *2E*,*4E*-muconic acid and ethylene **2** were initially investigated (Entries 1-3, Table 3).[47] A 20 mL titanium high-pressure reactor was charged with 2-HMA and a solvent. The reactor head was secured and the chamber was flushed with ethylene gas (3x) while stirring. After pressurizing with ethylene **2**, the reactor was heated over a period of 1-2 h to the reaction temperature after which the temperature was held constant. Thermal cycloaddition resulted in low yields likely due to the large difference (10.7 eV) in HOMO-LUMO energy levels of the two substrates. Significant charring was also observed resulting in poor mass balance.

Table 3. Uncatalyzed cycloaddition between 2-hydroxymuconic acid and ethylene **2**.

Entry	Solvent	Reaction time (h)	Temperature (°C)	Ethylene pressure (psi)	Yield PTA (mol %)
1	bis(methoxypropyl) ether	24	150	250	4
2	water	3	200	500	4
3	*m*-xylene	3	150	250	1
4	1,4-dioxane	1	200	500	5
5	acetic acid	24	200	500	1
6	*N*,*N*-dimethylacetamide	24	200	500	1

The uncatalyzed cycloaddition appeared to be complete in 1-3 h as reaction times up to 24 h did not afford substantially improved yields. Solvent choice was the most significant

variable with 1,4-dioxane, bis(methoxypropyl) ether, and water affording >1% yields. Variations of temperature and ethylene **2** pressure had little effect on the yield of PTA.

Several catalysts were screened in the reaction of 2-HMA and ethylene **2** using 1,4-dioxane as a noncomplexing solvent (Table 4). Conventional Lewis acids such as $ScCl_3$ and $TiCl_4$, which is known to catalyze cycloadditions with unprotected carbocylic acids,[37,48-51] afforded only marginal amounts of PTA (Entries 1-2, Table 4). Similarly, $La(OTf)_3$, which has proven to be an effective Diels-Alder catalyst and can be quantitatively recovered and reused upon aqueous workup,[52,53] resulted in minor amounts of PTA (Entry 3). Previous literature reports both $Cu(OTf)_2$- and ammonium zeolite-beta (NH_4-BEA)-catalyzed cycloadditions of ethylene **2** and DMF at 250 °C with conversions of >90% and high selectivity.[23] Copper(II) triflate was the first Lewis acid tested to show appreciable activity in the screen (Entry 5, Table 4). Other base metal triflates such as Fe^{2+} and Fe^{3+} did not exhibit similar catalytic activity (Entries 6 and 7, Table 4).

Table 4. Selected catalysts from screen of catalyzed reaction between 2-hydroxymuconic acid and ethylene **2**.

Entry	Catalyst	Yield PTA (mol %)
1	$ScCl_3$	trace
2	$TiCl_4$	1
3	$La(OTf)_3$	1
4	NH_4-BEA	trace
5	$Cu(OTf)_2$	19
6	$Fe(OTf)_2$	1
7	$Fe(OTf)_3$	1

Lewis acidity can be modulated by altering the ligands surrounding a metal center.[54] Triflate groups are strongly electron withdrawing and produce hard, electrophilic metal atoms.[55]

Attempts to modulate the electrophilicity of the Cu^{2+} metal center were made by varying the counterion of the copper salt. Acetate was selected to provide a softer metal center while $CuCl_2$ was combined with $AgPF_6$ in an effort to generate a harder, electrophilic center. A silver cation would form an insoluble salt with a chloride anion leaving a weakly coordinating hexafluorophosphate anion to complex with the Cu^{2+} ion. Neither catalyst exhibited pronounced activity (Table 5), indicating PTA formation is sensitive to electrophilicity about the Cu^{2+} atom. It is possible that a precise complexation is required between $Cu(OTf)_2$ and 2-HMA which must be strong enough to lower the LUMO energy level but weak enough to allow dissociation and catalyst turnover. Too electrophilic of a Cu^{2+} may not be able to dissociate from the catalyst-substrate complex, while not electrophilic enough would not be able to achieve sufficient LUMO energy level adjustment to promote cycloaddition.

Table 5. Attenuating Cu^{2+} electrophilicity.

Entry	Catalyst	Yield PTA (mol %)
1	$Cu(OAc)_2$	1
2	$CuCl_2 \cdot AgPF_6$	0.5

Alterations of catalyst loading and reaction temperature during $Cu(OTf)_2$-catalyzed cycloadditions resulted in locating an optimal range of reaction conditions (Tables 6 and 7). Temperatures above 100 °C are required for PTA formation however significant decomposition of reaction components at temperatures above 200 °C preclude elevated yields. At 200 °C, the highest yields of PTA were achieved using substoichiometric amounts of catalyst, though catalyst

loading of at least 10% was required. Charring of the reaction mixture was still observed under these conditions.

Table 6. Effects of temperature on yield of PTA.

Entry	Temperature (°C)	Yield PTA (mol %)
1	300	8
2	200	19
3	100	1
4	50	0

Table 7. Effects of catalyst loading on yield of PTA.

Entry	Mol %	Yield PTA (mol %)
1	100	4
2	50	16
3	10	19
4	1	3

The most interesting result from $Cu(OTf)_2$-catalyzed cycloadditions was the effect of a catalytic amount of Brønsted acid (Table 8, Entry 2). Pronounced improvement in yield of PTA was observed when a drop of H_2SO_4 was added to the reaction. Previous research demonstrated that the addition of a small amount of Brønsted acid in $Cu(OTf)_2$-catalyzed benzannulations of alkylacetylenes with *o*-alkynyl(oxo)benzenes suppressed the formation of benzoic acid and benzoic anhydride byproducts and increased yields of desired naphthalene products.[111] The presence of a Brønsted acid in $Cu(OTf)_2$-catalyzed cycloaddition of 2-HMA and ethylene **2** would enhance protonolysis of a Cu-σ-complex and increase catalyst turnover. An acidic

medium would also promote dehydration of the cyclohexene intermediate formed after cycloaddition occurs. A drop of water was added to the $Cu(OTf)_2$-catalyzed reaction as a control which resulted in a substantially decreased yield and the formation of benzoic acid along with a brick-red precipitate.

Table 8. Effect of Brønsted acid on $Cu(OTf)_2$-catalyzed cycloaddition.

Entry	Additive	Yield PTA (mol %)	Yield benzoic acid (mol %)
1	none	19	trace
2	H_2SO_4	26	0
3	H_2O	3	3

The $Cu(OTf)_2$-catalyzed reaction appeared highly sensitive to the presence of oxygen and water. When oxygen was not rigorously excluded, reduced yields were observed in tandem with the formation of a brick-red precipitate visibly similar to Cu_2O. In these reactions, small amounts of benzoic acid were seen as a byproduct. Cuprous aromatic carboxylates readily undergo decarboxylations at temperatures of 150-250 °C.[58,59] Though the mechanism of copper(II) reduction during the cycloaddition of 2-HMA and ethylene **2** was not experimentally verified, it is possible that ethylene **2** reacts with trace amounts of oxygen and water to afford ethylene glycol via ethylene oxide. Heating ethylene glycol in the presence of oxygen affords glycolaldehyde, which is used as a reductant in the synthesis of metal nanoparticles including Pd, Ag, and Cu.[105-108] Incomplete reduction of copper in the presence of oxygen could afford a Cu^{1+} species, catalyzing a protodecarboxylation of either terephthalic acid or a reaction intermediate. The catalytically active Cu^{1+} species could be Cu_2O or another compound that is ultimately converted to Cu_2O. Previous research has demonstrated that Cu^{1+} compounds including Cu_2O,

are effective catalysts for the protodecarboxylation of various aromatic and heteroaromatic carboxylic acids.[60,61] Prior observation of the necessity for unsaturation in the substrate acid, increasing rate with increasing polarizability, and π-complexation propensity of the cuprous ion suggests a mechanism whereby a π-bonded cuprous ion inductively stabilizes the resultant anion which develops as the carbon dioxide is lost.[61]

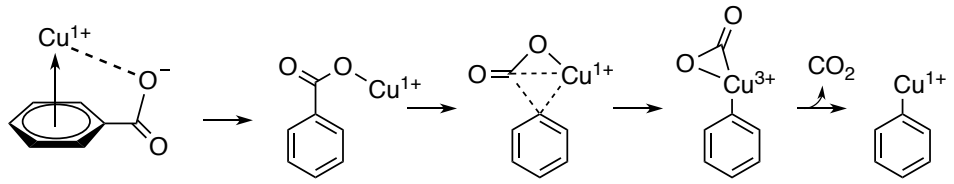

Figure 19. Putative mechanism for copper(I)-catalyzed protodecarboxylation of aromatic carboxylates.

Trapping experiments have suggested a σ-bonded organocopper intermediate, facilitated by the inherent stability of vinyl copper compounds.[62] More recent research suggests complexation of the cuprous ion to the C-CO_2 bond of the carboxylate via π-complexation with the aromatic ring.[60] Oxidative addition would form a ternary copper(III) intermediate[63] which would undergo rapid reductive elimination to the arylcopper species and carbon dioxide (Figure 19). Insertion of copper into the C-C bond would be facilitated by π-backbonding into the σ* orbital of the C-C bond.[60,61] To investigate the possible role of a putative copper(I) species in the cycloaddition of 2-HMA with ethylene **2**, CuOTf was employed in several reactions (Table 9). CuOTf-catalyzed cycloadditions required slightly elevated temperatures relative to $Cu(OTf)_2$-catalyzed reactions to achieve comparable yields. An interesting result of CuOTf-catalyzed reactions was a significant amount of benzoic acid byproduct and accompanying brick-red precipitate. These reactions indicate that protodecarboxylation of either terephthalic acid or

another reaction intermediate likely occurs in the presence of a Cu^{1+} species though the identity of such a species has not been demonstrated.

Table 9. Copper(I)-catalyzed cycloaddition of 2-hydroxymuconic acid and ethylene.

Entry	Catalyst	Temperature (°C)	Yield PTA (mol %)	Yield benzoic acid (mol %)
1	CuOTf	225	11	19
2	CuOTf	175	4	0.5
3	CuOTf/ $Cu(OTf)_2$	200	4	2

Terephthalic acid was heated at 225°C in 1,4-dioxane in the presence of 10 mol% CuOTf to determine whether decarboxylation of terephthalic acid was responsible for the formation of benzoic acid observed during the cycloaddition. Despite the formation of a small amount of brick-red precipitate, no benzoic acid was detected. Therefore, benzoic acid must form as a result of decarboxylation of a reaction intermediate rather than terephthalic acid.

4. Isophthalic acid and phthalic acid from cycloaddition of 6-carboxy-2-pyrone with propiolic acid

Ring closure of 2-HMA provides access to renewable IPA and PA upon reaction with methane-derived propiolic acid **18** (Figure 20). In 2013, annual biogas production was estimated to be 1.2×10^{10} m^3.[64] This represents a massive amount of available carbon. Dehydrodimerization of methane at temperatures of 1500-1900 °C affords acetylene. Carboxylation of acetylene to propiolic acid **18** utilizes copper catalyst in the presence of carbon dioxide.[65,66,67]

Previously established:[65,66,67]

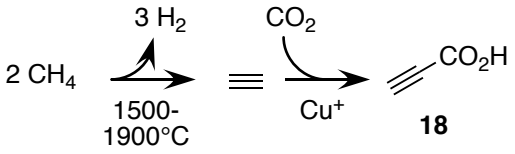

This work:

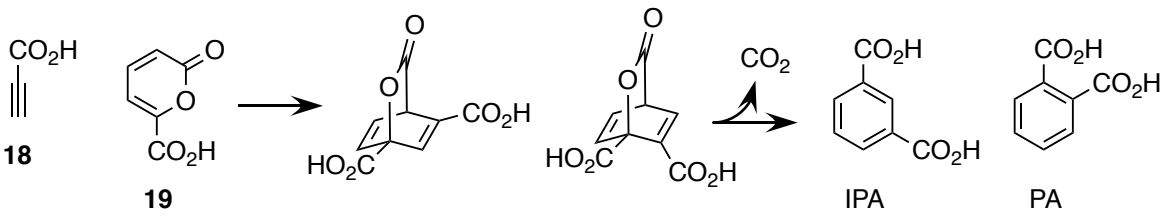

Figure 20. Synthesis of isophthalic acid (IPA) and phthalic acid (PA) from 6-carboxy-2-pyrone **19** and renewable propiolic acid **18**..

Synthesis of aromatic dimethyl dicarboxylates from thermal cycloaddition of the methyl ester of 6-carboxy-2-pyrone **19** with methyl propiolate has been established in the literature.[68] Reflux in mesitylene affords a 1.7:1 ratio of dimethylphthate:dimethylisophthalate in quantitiative yield. No method has been established that utilizes the free acid form of 6-carboxy-2-pyrone **19** and propiolic acid **18**. Nor has selectivity been driven toward the more useful *meta*-substituted IPA. Lewis acid catalysis offers a possible means to achieve each of these features.

Cursory examination of the energy levels of the frontier molecular orbitals of propiolic acid **18** and 6-carboxy-2-pyrone **19** using Spartan '08 software and Møller-Plesset 6-31+G* basis set from AM1 initial geometry,[104] reveals that the closest overlap would result from the LUMO of the propiolic acid **18** dieneophile with the HOMO of the 6-carboxy-2-pyrone **19** diene (Figure 21). This mode of orbital overlap represents a normal electron demand Diels-Alder reaction.

Both $TiCl_4$[37] and BCl_3[69] have been successfully used in catalyzing Diels-Alder cycloadditions with unsaturated carboxylic acid dieneophiles. With precedent established, these Lewis acids were initially investigated for their catalytic propensity in the cycloaddition between 6-carboxy-2-pyrone **19** and propiolic acid **18**.

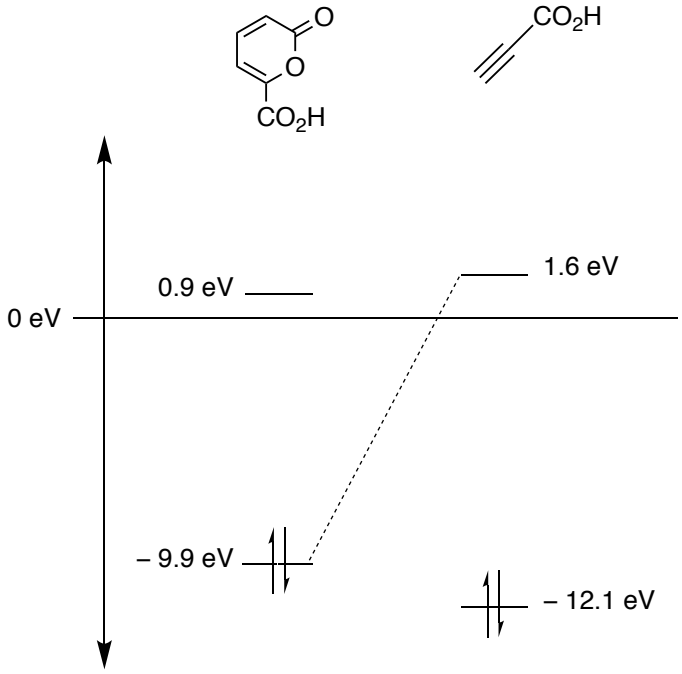

Figure 21. Relative energy levels of the frontier molecular orbitals of 6-carboxy-2-pyrone **19** and propiolic acid **18**.

Refluxing in toluene in the presence of 20 mol% $TiCl_4$ afforded a 2:1 ratio of PA:IPA in a combined yield of 30% mol/mol from 6-carboxy-2-pyrone **19**. Charring resulted in significant amounts of insoluble black solids and low mass balance. These solids were not observed in the BCl_3-catalyzed reaction which appeared to facilitate decomposition of propiolic acid **18** without promoting cycloaddition with the pyrone. The results were disappointing as neither catalyst afforded significant amounts of product and selectivity in the $TiCl_4$-catalyzed reaction favored PA rather than the more useful IPA.

Table 10. Initial Lewis acid-catalyzed reactions between propiolic acid **18** and 6-carboxy-2-pyrone **19** using 1:1 mol:mol ratio propiolic acid **18**:6-carboxy-2-pyrone **19**.

Lewis acid	Remaining 6-carboxy-2-pyrone	Remaining propiolic acid	Yield isophthalic acid (mol %)	Yield phthalic acid (mol %)
$TiCl_4$	10%	0%	10%	20%
BCl_3	95%	2%	2%	0%

Screening of Lewis acid catalysts was performed by another group member. Interesting catalysts were those that exhibited selectivity toward IPA and those that afforded high conversions. Thermal cycloaddition in the presence of a 7:1 molar excess of propiolic acid **18**, resulted in a 1.6:1 ratio of IPA:PA in a combined yield of 49% mol/mol relative to 6-carboxy-2-pyrone **19**. Selectivity was enhanced to a 3.3:1 ratio using 5 mol% $SnCl_4$ in a combined yield of 32%. Interestingly, the copper(II) salts, $CuCl_2$ and $Cu(OTf)_2$, exhibited 100% selectivity toward IPA albeit only in 7% yield.

Charring and decomposition continued to be a challenge for the cycloaddition of propiolic acid **18** and 6-carboxy-2-pyrone **19**, precluding yields above 30-40%. Furthermore, the appearance of phthalic anyhydride in reactions catalyzed by strong Lewis acids suggests facile dehydration of phthalic acid. The water formed during the dehydration may react with the Lewis acid resulting in decreased activity over time. The highest yields of aromatic products were observed with $ZrCl_4$ (81%), phenylboronic acid ($PhB(OH)_2$, 83%), and tetraacetyl diborate ($BOB(OAc)_4$, 90%). However, none of the catalysts affording high yields also achieved high selectivities.

5. Discussion

The results described above demonstrate that 2-HMA can serve as a synthetic precursor to all three aromatic diacids that are currently manufactured via oxidation of petroleum-derived xylenes. The compound is stable as the *2Z*,*4E* stereoisomer as suggested by spin coupling of vicinal protons and nuclear Overhauser effect experiments, which is ideal for a Diels-Alder cycloaddition. At 200 °C in dioxane, 10 mol% $Cu(OTf)_2$ and a catalytic amount of H_2SO_4 affords PTA in a 26% yield with no benzoic acid byproduct.

Interestingly, $Cu(OTf)_2$ was the only catalyst examined to afford appreciable amounts of PTA. Copper(II) triflate has demonstrated high conversions and selectivities in the reaction between ethylene **2** and DMF to afford *p*-xylene **1**. Both in the synthesis of *p*-xylene and in the work reported herein, attenuating the electrophilicity of Cu^{2+} by varying the counterion resulted in decreased yields relative to $Cu(OTf)_2$. This suggests that PTA and *p*-xylene **1** formation via cycloaddition with ethylene **2** is sensitive to the hardness of Cu^{2+}. It is possible that the precise electron density about Cu^{2+} in $Cu(OTf)_2$ allows coordination which is sufficient to lower the LUMO of 2-HMA to promote cycloaddition with ethylene **2** while remaining labile enough for facile protonolysis.

The catalyst screen performed in this work was not exhaustive. A more thorough investigation of different metals and appropriate counterions may succeed in identifying a system with greater catalytic potential than the $Cu(OTf)_2$-H_2SO_4 system presented here. Indeed, such a system would be required before synthesis of PTA from 2-HMA garners commercial interest. Low conversions are acceptable only if unreacted starting material can be recovered and recycled. This cannot currently be done. Charring and decomposition is prevalent throughout 2-

HMA cycloadditions. This is the principal challenge that needs to be solved before any synthesis from 2-HMA becomes industrially viable.

Synthesis of PTA from 2-HMA using $Cu(OTf)_2$ catalysis must be performed in a rigorously oxygen-free environment. Despite drying 1,4-dioxane over Na^0 and preparing the reaction in a glove bag under N_2 atmosphere, trace amounts of O_2 and water are occasionally introduced. In these reactions, decreased yields of PTA are obtained with concomitant formation of a brick red precipitate and benzoic acid. It is likely that these solids are Cu_2O which has been reported to catalyze protodecarboxylation of aromatic carboxylates. Conversion of ethylene **2** to ethylene glycol followed by oxidation affords glycolaldehyde which is a known metal reductant. Reduction of Cu^{2+} to Cu^{1+} generates a species with high propensity for decarboxylation. Whether that species is Cu_2O or a different Cu^{1+} species that is converted to Cu_2O during the reaction is not clear. When CuOTf was added to the reaction instead of $Cu(OTf)_2$, benzoic acid was observed as the major product and significant amounts of red precipitate formed. This supports our hypothesis that the formation of Cu^{1+} initiates decarboxylation of a reaction intermediate. Preventing the introduction of O_2 and water in a $Cu(OTf)_2$-catalyzed cycloaddition should be enough to avoid Cu^{2+} reduction and accompanying decarboxylation.

Cyclization of 2-HMA to afford 6-carboxy-2-pyrone **19** provides access to IPA and PA via Diels-Alder cycloaddition with propiolic acid **18**. The cyclization reaction is performed using Brønsted acid catalysis in good yields (85%). Cycloaddition of 6-carboxy-2-pyrone **19** with propiolic acid requires different catalysis than the reaction of 2-HMA with ethylene. While the HOMO-LUMO energies of 2-HMA and 6-carboxy-2-pyrone **19** are very similar, the frontier molecular orbitals of ethylene **2** and propiolic acid **18** are not. Propiolic acid **18** bears an

electron deficient alkyne and hence has a low energy LUMO, whereas ethylene **2** is more electron rich with higher energy orbitals. This difference in energy delineates a change from an inverse electron demand Diels-Alder reaction in the case of 2-HMA and ethylene **2**, and a normal electron demand Diels-Alder reaction for 6-carboxy-2-pyrone **19** and propiolic acid **18**.

Conventional Lewis acids like BCl_3 and $TiCl_4$ form strong σ-complexes with carbonyl moieties. Because both propiolic acid **18** and 6-carboxy-2-pyrone **19** possess carboxylic acid groups, such a catalyst would likely partition binding between both substrates and thus fail to effectively lower orbital energies for an entire population of a single compound. Softer metals in lower oxidation states such as AuCl or $PtCl_2$ could be used to selectively complex the alkyne group of propiolic acid **18**. These metals are known to form stable π-complexes with alkynes. This mode of binding would be selective towards propiolic acid **18** and could promote sufficient LUMO energy lowering to facilitate the cycloaddition.

High yields of IPA and PA products are observed with $PhB(OH)_2$ (83%), and $BOB(OAc)_4$ (90%) but selectivities are low. Selectivity toward IPA is desired because of its use in PET manufacture. However, developing selectivity in a cycloaddition with 6-carboxy-2-pyrone **19** is challenging due to the similarity in size of the HOMO coefficients about C-3 and C-6. It is a difference in the orbital coefficients that often drives regioselectivity in Lewis acid-catalyzed reactions. When the sizes of the orbital coefficients are similar, other factors such as steric hindrance must influence selectivity.

Though 2-HMA was used to afford PTA, IPA, and PA in cycloadditions with ethylene **2** and propiolic acid **18**, several challenges must be addressed before the proposed route can be of commercial use. Charring and decomposition of reaction mixtures must be prevented. Nearly

all Lewis acids examined for either cycloaddition involved some degree of degradation. This is not sustainable as it precludes attempts to recycle unreacted substrates and requires fresh catalyst for each conversion. Controlling the observed charring would dramatically increase the mass balance for each conversion and enable attempts to recover both catalyst and substrate. Increased yields of PTA and increased selectivity toward IPA are also highly desirable. If a 26% yield was achieved during each conversion, unreacted starting material would need to be recycled over 15 times to reach the same yield of PTA as is currently achieved from a single Amoco Mid-Century oxidation of *p*-xylene **1**.

Despite high yields from $BOB(OAc)_4$-catalyzed reaction of 6-carboxy-2-pyrone **19** with propiolic acid **18**, further development should enhance selectivity toward IPA. While PA is used for manufacture of plasticizers such as DINCH and DINP, it is not manufactured to the same scale as IPA, which is used for the production of PET. Therefore it would be useful to achieve selectivities that match the market value of the products.

Though challenges remain, this work demonstrates that the synthesis of all three aromatic diacids that are currently manufactured from petroleum can be achieved from a single synthetic precursor, 2-HMA. The proposed route does not require Amoco Mid-Century oxidations and does not involve esterification/hydrolysis steps. The catalysts used are relatively inexpensive and all substrates can be prepared from renewable starting materials. Ethylene **2** is synthesized from bioethanol, propiolic acid **18** is produced from biogas methane, and the synthesis of 2-HMA from D-glucose will be discussed in Part II.

PART II

BIOCATALYTIC SYNTHESIS OF 2-HYDROXYMUCONIC ACID FROM D-GLUCOSE

1. Overview

Protocatechuic acid is a central intermediate in several degradation pathways of aromatic compounds including phthalates, hydroxybenzoates, and lignin-derived aromatics. Aromatic ring cleavage catalyzed by one of three distinct dioxygenases, PCA 3,4-dioxygenase,[70] PCA 4,5-dioxygenase,[71] and PCA 2,3-dioxygenase,[72] initiates different degradation pathways. Ring fission catalyzed by PCA 3,4-dioxygenase affords 2-carboxy-*cis*,*cis*-muconic acid which enters the β-ketoadipate pathway reported in several organisms.[70,73] In the 4,5-cleavage pathway, PCA conversion to 4-carboxy-2-hydroxymuconate-6-semialdehyde precedes further degradation which ultimately affords 4-carboxy-4-hydroxy-2-oxoadipate before entering the citric acid cycle.[71a] Prior research identifies PCA 4,5-cleavage in *Sphingomonas*,[71a] *Comamonas*,[74] *Pseudomonas*,[75] and *Arthrobacter*[76] strains.

Paenibacillus sp. JJ-1b (formerly *Bacillus macerans*) exploits 4-hydroxybenzoate (4-HBA) catabolism as a sole source of carbon and energy via the PCA 2,3-cleavage pathway (Figure 22).[72a] In the early stages of the pathway, PCA 2,3-dioxygenase catalyzes extradiol ring cleavage of PCA to (2*E*,4*E*)-5-carboxy-2-hydroxymuconate-6-semialdehyde (5-CHMS). Rapid disappearance of the immediate ring-fission product in cell extracts and accumulation of (2*E*, 4*E*)-2-hydroxymuconate-6-semialdehyde (2-HMS) suggested rapid enzymatic decarboxylation of the former compound. By 1993, only one enzyme, PCA 2,3-dioxygenase, had been purified and characterized (K_{mO_2} = 142 μM, K_{mPCA} = 24 μM, k_{cat} = 210 s^{-1}).[77]

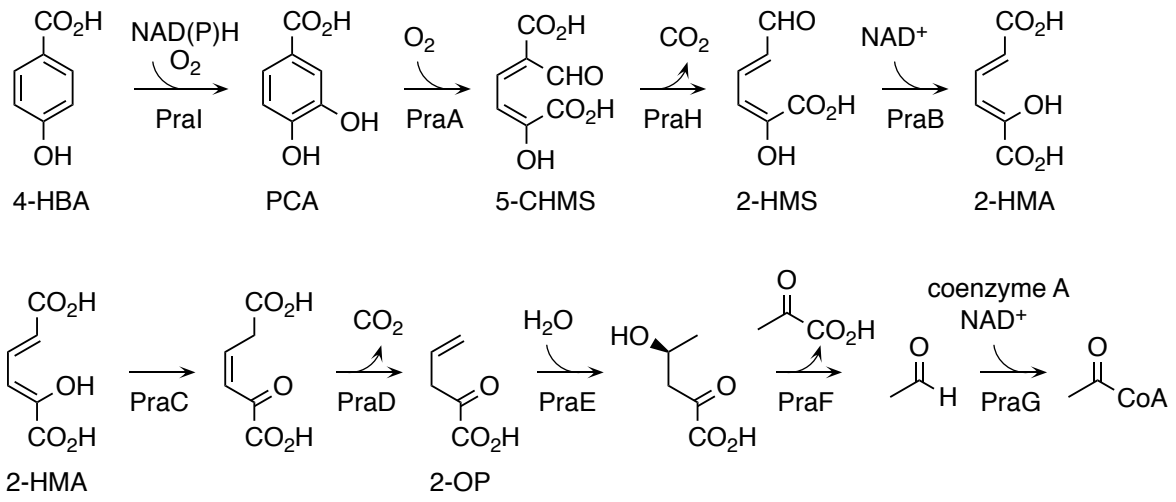

Figure 22. Degradation of 4-hydroxybenzoic acid via the PCA 2,3-cleavage pathway in *Paenibacillus* sp. JJ-1b.

In 2009, all of the genes involved in 4-HBA degradation via the PCA 2,3-cleavage pathway were identified from *Paenibacillus* sp. JJ-1b (Figure 22).[40] Based on *in vitro* experiments using cell extracts of *E. coli* carrying *praI*, *praA*, *praH*, *praB*, *praC*, or *praD* these genes were discovered to encode 4-HBA 3-hydroxylase, PCA 2,3-dioxygenase, 5-carboxy-2-hydroxymuconate-6-semialdehyde decarboxylase, 2-hydroxymuconate-6-semialdehyde dehydrogenase, 4-oxalocrotonate tautomerase, and 4-oxalocrotonate decarboxylase, respectively. Additional genes associated with the *pra* operon were reported to catalyze the degradation of the resultant 2-oxopent-4-enoate (2-OP) to pyruvate and acetyl CoA.

Engineering recombinant *E. coli* for de novo biosynthesis of 2-HMA from D-glucose (Figure 23) requires expression of PCA anabolic and catabolic enzymes. Biosynthesis of PCA via the shikimate pathway has been previously reported using *E. coli* strain WN1.[38,39,47] This strain lacks a catalytically active shikimate dehydrogenase encoded by *aroE* and expresses DHS dehydratase from *Klebsiella pneumoniae* encoded by *aroZ.* Biosynthesis of 2-HMA can be

realized by combining PCA anabolism from WN1 with PCA catabolic enzymes from *Paenibacillus* sp. JJ-1b.

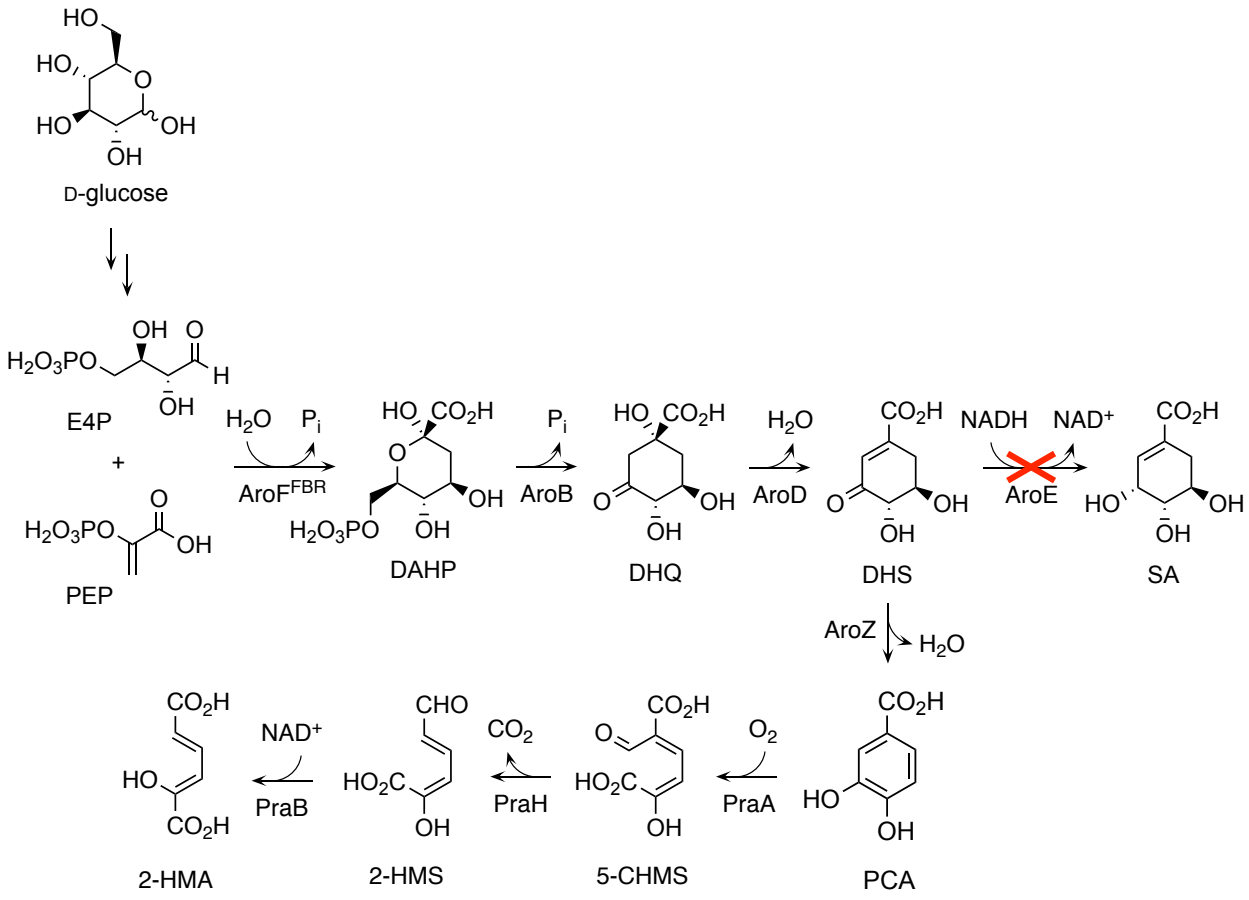

Figure 23. De novo biosynthesis of 2-hydroxymuconic acid combining protocatechuic acid anabolism and catabolism.

2. Host strain

Strains and plasmids used in this work are presented in Table 11. *E. coli* WN1 was used as the host strain for 2-HMA synthesis. The host strain was derived from *E. coli* AB2834 and lacks a catalytically active shikimate dehydrogenase.[79] This mutation prevents hydrogenation of

3-dehydroshikimate (DHS) to shikimate in the common pathway of aromatic amino acid biosynthesis. Further modification of the host genome included homologous recombination of an *aroBaroZ* cassette into the *serA* locus[79] and insertion of a *tktAaroZ* cassette into the *lacZ* locus.[80] Additional genomic copies of *aroB* and *aroZ* prevent the accumulation of 3-deoxy-D-*arabino*-heptulosonate 7-phosphate (DAHP) and DHS, respectively. An additional copy of *tktA* on the genome helps to direct carbon flux from the pentose phosphate pathway into the shikimate pathway and increases the intracellular availability of erythrose 4-phosphate (E4P). Since inactivation of the shikimate dehydrogenase precludes de novo biosynthesis of aromatic amino acids and aromatic vitamins, the growth of all constructs in minimal media required supplementation with L-phenylalanine, L-tryptophan, and L-tyrosine along with *p*-hydroxybenzoic acid, *p*-aminobenzoic acid, and 2,3-dihydroxybenzoic acid.

Table 11. Strains and plasmids used in Chapter 1 of this study.

Strain/plasmid	Relevant characteristics	Source or reference
Escherichia coli DH5α	*F' ϕ80lacZΔM15* Δ(*lacZYA-argF)U169 deoR recA1 endA1 hsdR17*(r_k^-, m_k^+) *phoA* λ^- *supE44 thi-1 gyrA96 relA1*	Invitrogen
Escherichia coli AB2834	*tsx-352 glnV42 aroE353 malT352* λ^-	Coli Genetic Stock Center[78]
Escherichia coli KL7	AB2834 *serA*::*aroBaroZ*	lab[79]
Escherichia coli WN1	KL7 *lacZ*::*tktAaroZ*	lab[80]
Escherichia coli KM1	WN1 *pptA*::FRT	this work
Paenibacillus sp. JJ-1b	source for *praApraBpraH*	ATCC 35889
pBbA1a-RFP	Ap^R, $lacI^q$, P_{trc}*rfp* p15A replicon	Addgene #35334[92]
pWN1.028A	$aroF^{FBR}$ source	lab[80]

Table 11 (cont'd)

pWN1.162A	*serA* source	lab[80]
pMF63A	P_{aroF} source	lab[88]
pKM6.196	P_{trc}*praA* in pBbA1a	this work
pKM6.200	P_{trc}*praB* in pBbA1a	this work
pKM6.201	P_{trc}*praH* in pBbA1a	this work
pKM6.208	P_{trc}*praHpraA* in pBbA1a	this work
pKM6.232	P_{trc}*praBpraHpraA* in pBbA1a	this work
pKM6.240	P_{trc}*serA* in pBbA1a	this work
pKM6.241	$P_{trc}P_{aroF}$ in pBbA1a	this work
pKM6.261	P_{trc}*serA*P_{aroF} in pBbA1a	this work
pKM6.268	P_{trc}*aroF*^{FBR} in pBbA1a	this work
pKM6.274	P_{trc}*aroF*^{FBR}*serA*P_{aroF} in pBbA1a	this work
pKM6.280	P_{trc}*praBpraHpraAaroF*^{FBR}*serA*P_{aroF} in pBbA1a	this work

3. Plasmid construction

2-HMA-synthesizing constructs employed plasmid pKM6.280 (Table 11, Figure 33) which carried *praBpraHpraAaroF*^{FBR}*serA*P_{aroF} under the control of a *trc* promoter. We anticipated that arranging the PCA 2,3-cleavage enzymes in reverse order relative to the reactions they catalyze would ensure carbon is pulled entirely through the pathway. The *serA* gene encodes 3-phosphoglycerate dehydrogenase, which is necessary for biosynthesis of L-serine in *E. coli.* Host strain WN1 possesses a mutated genomic copy of *serA* and is therefore incapable of growth in media lacking L-serine supplementation. The inclusion of a functional *serA* gene on a plasmid restores the ability of the cell to synthesize L-serine, allowing growth in minimal salts medium only if the cell maintains the plasmid. Nutritional rather than antibiotic selection is an extensively used plasmid maintenance strategy.[38,79-87]

Efficient synthesis of PCA from D-glucose requires a mutant isozyme of DAHP synthase, an enzyme which catalyzes the condensation of erythrose-4-phosphate and phosphoenolpyruvate to DAHP.[89] Three DAHP synthase isozymes, AroF, AroG, and AroH, are sensitive to repression by one of three aromatic amino acids, L-tyrosine, L-phenylalanine, or L-tryptophan, respectively. Because of the mutation in *aroE*-encoded shikimate dehydrogenase, the *E. coli* strains used in this study cannot synthesize aromatic amino acids, which necessitated supplementing the culture medium with these compounds. At concentrations above 10 μM, L-tyrosine exhibits noncompetitive inhibition of native *E. coli* AroF with respect to erythrose-4-phosphate and competitive inhibition with respect to phosphoenolpyruvate.[89b] To direct carbon flux into the shikimate pathway, plasmids included $aroF^{FBR}$, encoding a tyrosine feedback resistant isozyme of AroF.[89a] In addition, transcription of $aroF^{FBR}$ is repressed by a complex between the native *E. coli tyrR* gene product and L-tyrosine.[89a] The binding sites for this repressor complex overlap with the *aroF* promoter sequence, P_{aroF}. To mitigate transcriptional repression, an extra copy of P_{aroF} was included on the plasmid.[88] Additional binding sites can titrate away the tyrosine repressor complex and improve transcription of the $aroF^{FBR}$ gene product.[89,90,91]

The construction of pKM6.280 was performed using the BglBrick assembly standard, developed by Anderson and Keasling (Figures 25-33).[92,93] This method of DNA assembly expedites the process of creating the desired construct and facilitates construct modifications such as changing the order of genes in a cassette and the removal or addition of various genetic elements. The creation of BglBrick parts requires genetic elements including, coding sequences for the open reading frames, promoters, and terminators to be individually inserted into a vector with standardized prefix and suffix sequences (Figure 24). These sequences encode specific

restriction enzyme sites. The 5' prefix sequence encodes *Eco*RI and *Bgl*II sites, while the 3' suffix sequence encodes *Bam*HI and *Xho*I restriction sites. Each open reading frame also included a 5' Shine-Dalgarno sequence (AAGGAGG).

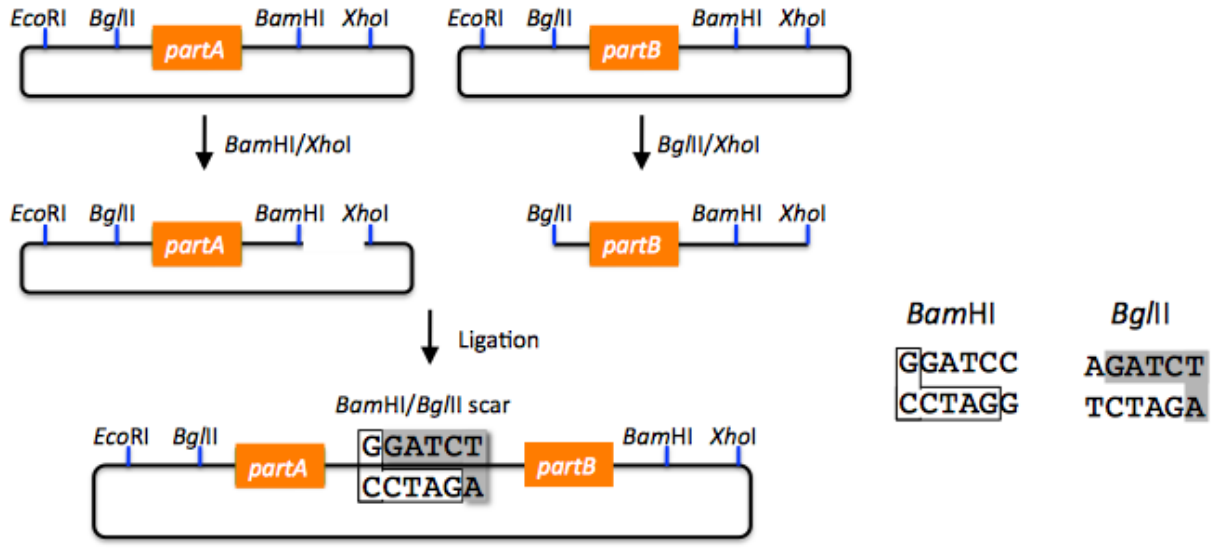

Figure 24. Schematic representation of BglBrick DNA assembly method. Part B is digested with *Bgl*II and *Xho*I restriction enzymes while part A is digested with *Bam*HI and *Xho*I restriction enzymes. Ligation of part B into part A results in a glycine-serine scar sequence and a new part comprising the original parts A and B. This mode of insertion is called suffix-insertion. Figure adapted from reference 109.

The compatible DNA ends of *Bgl*II and *Bam*HI restriction enzymes promotes concatenation of any two genetic elements, creating a glycine-serine scar. Insertion of one part into another generates a new part that retains the original four restriction enzyme sites on the 5' and 3' ends. In this way, assembling an arbitrary number of parts in any desired arrangement is no more difficult than ligating two together. A further advantage of the BglBrick assembly method is that once a genetic element is inserted into the standard vector to create a BglBrick part, there is never a need to PCR-amplify that particular element which eliminates the probability of PCR-derived mutations during a cloning project.[92,93]

The genes, *praA*, *praH*, and *praB*, were PCR amplified from *Paenibacillus* sp. JJ-1b genomic DNA and extended with 5' *Bgl*II and Shine-Dalgarno sequences and 3' *Bam*HI and *Xho*I sites (Figure 25). PCR amplified genes were inserted into the *Bgl*II and *Xho*I sites of BglBrick vector, pBbA1a.[93] The *serA* gene, *aroF*^{FBR} gene, and P_{aroF} sequence were similarly amplified from pWN1.162, pWN1.028A, and pMF63A, respectively (Figures 26-28). Concatenation of *praBpraHpraA* genes resulted in plasmid pKM6.232 (Figure 30) while assembly of *aroF*^{FBR}*serAP*$_{aroF}$ afforded pKM6.274 (Figure 32). Insertion of *praBpraHpraA* into pKM6.274 followed the prefix insertion method to afford pKM6.280 (Figure 33).

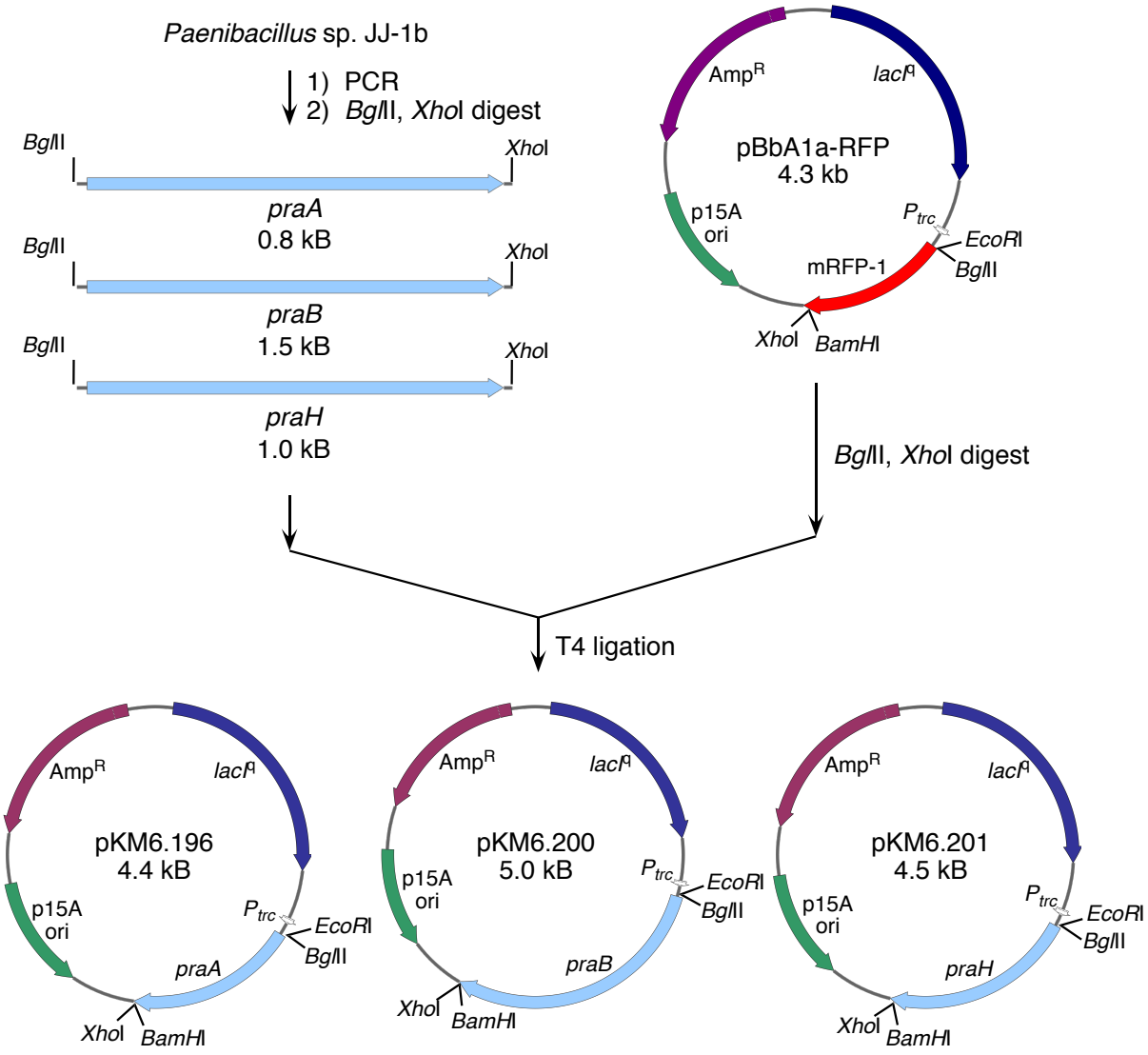

Figure 25. Preparation of *pra* BglBrick parts: plasmids pKM6.196, pKM6.200, and pKM6.201.

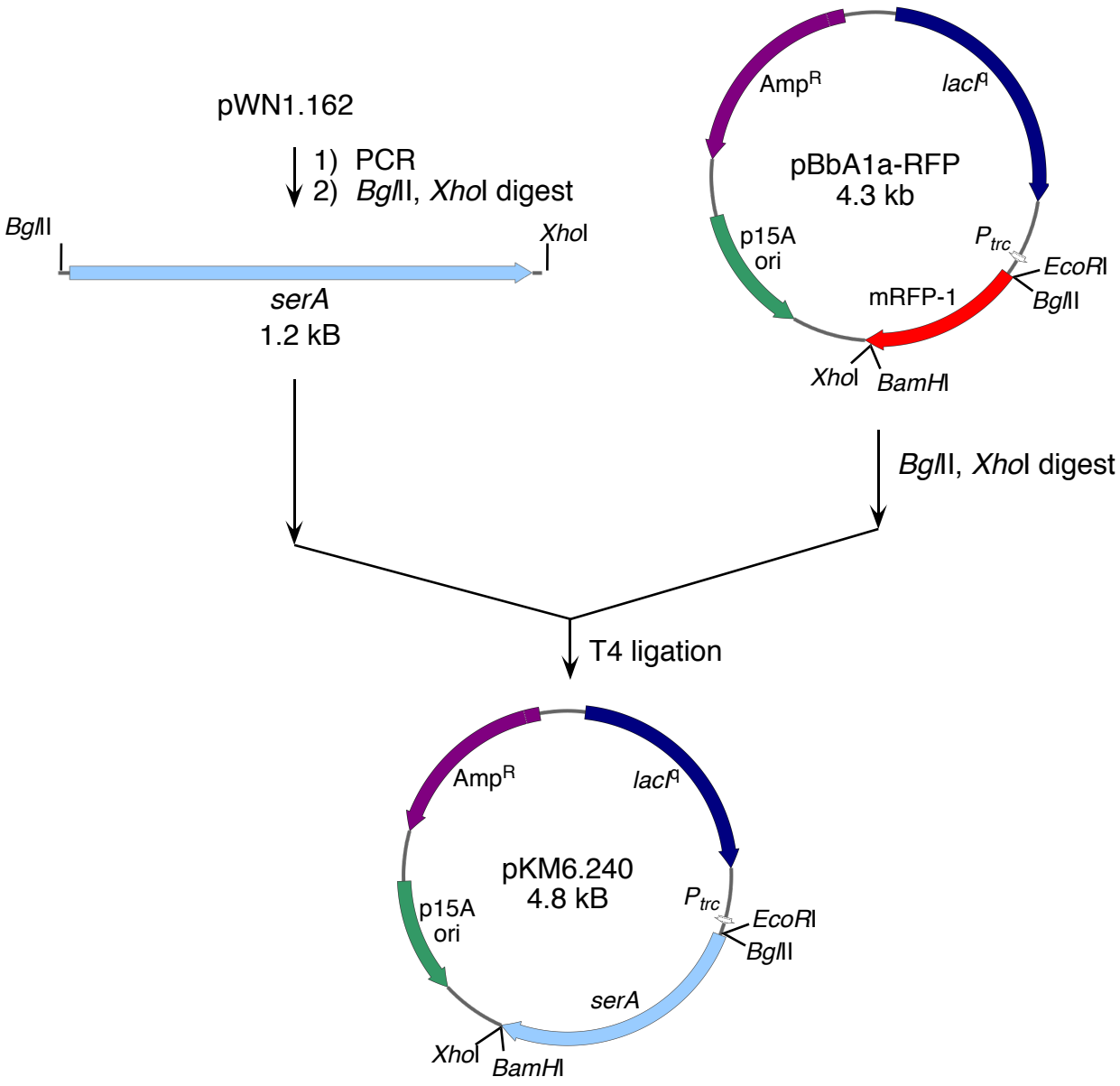

Figure 26. Preparation of *serA* BglBrick part, plasmid pKM6.240.

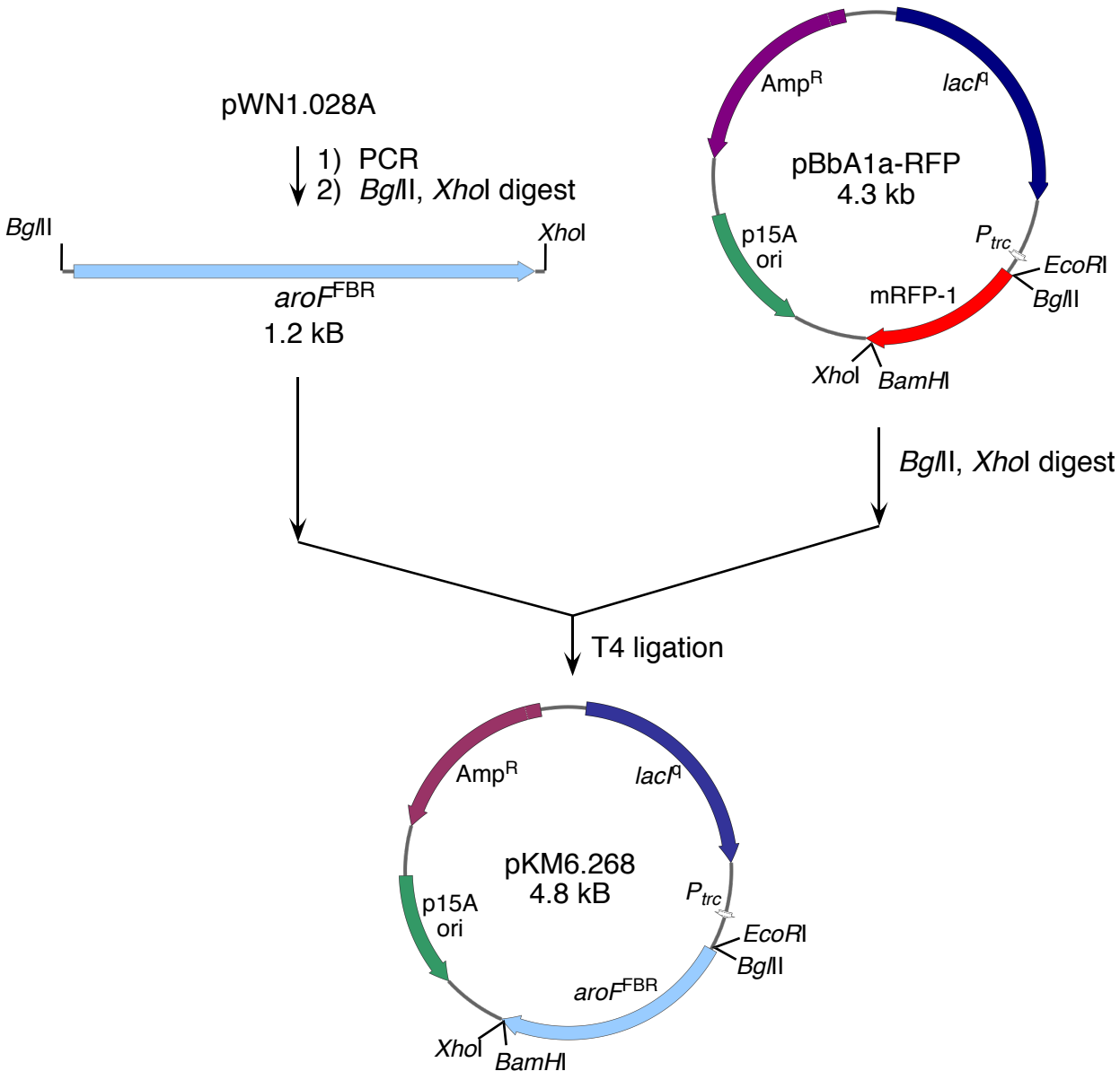

Figure 27. Preparation of *aroF*^{FBR} BglBrick part, plasmid pKM6.268.

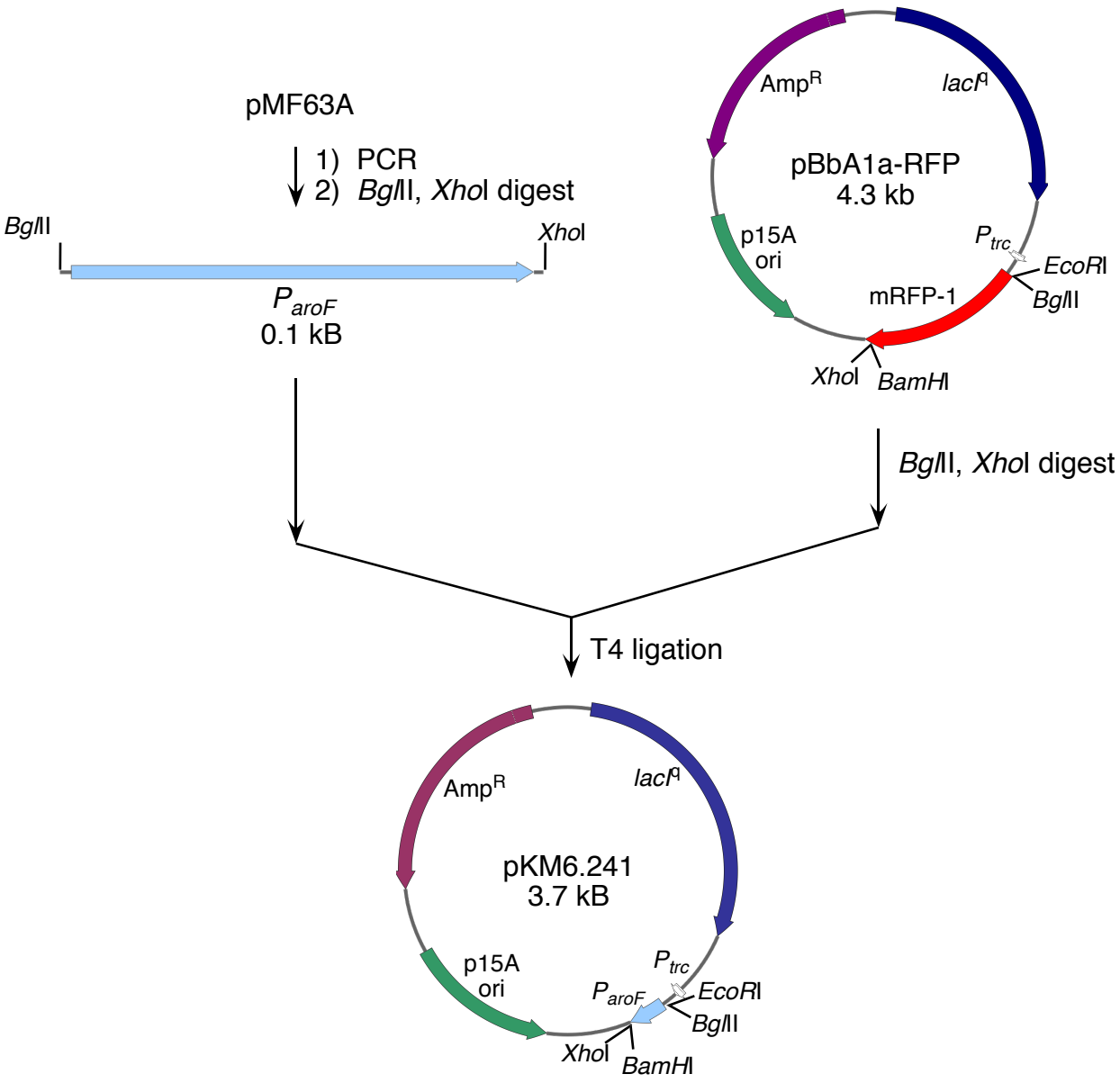

Figure 28. Preparation of P_{aroF} BglBrick part, plasmid pKM6.241.

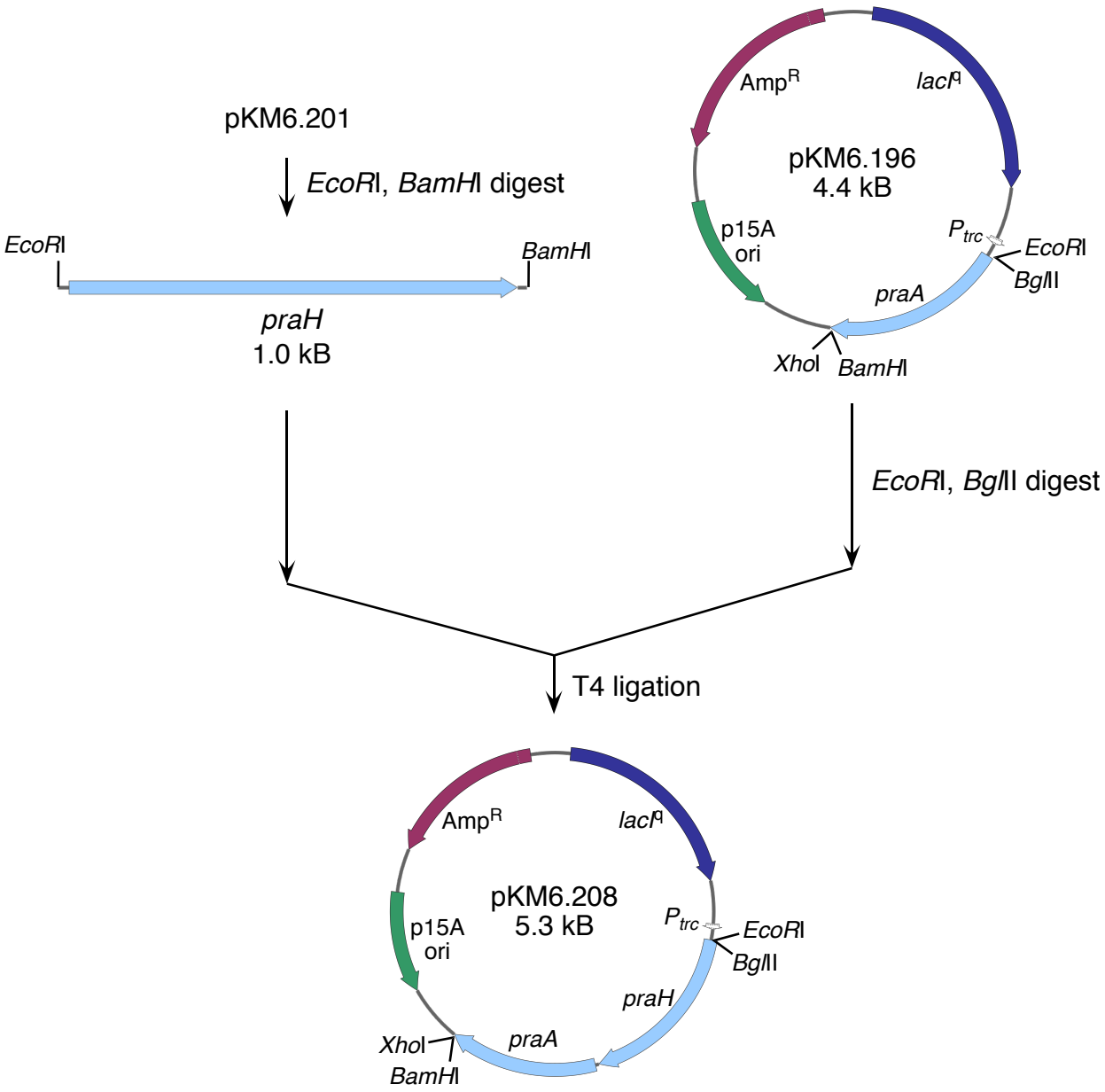

Figure 29. Preparation of plasmid pKM6.208.

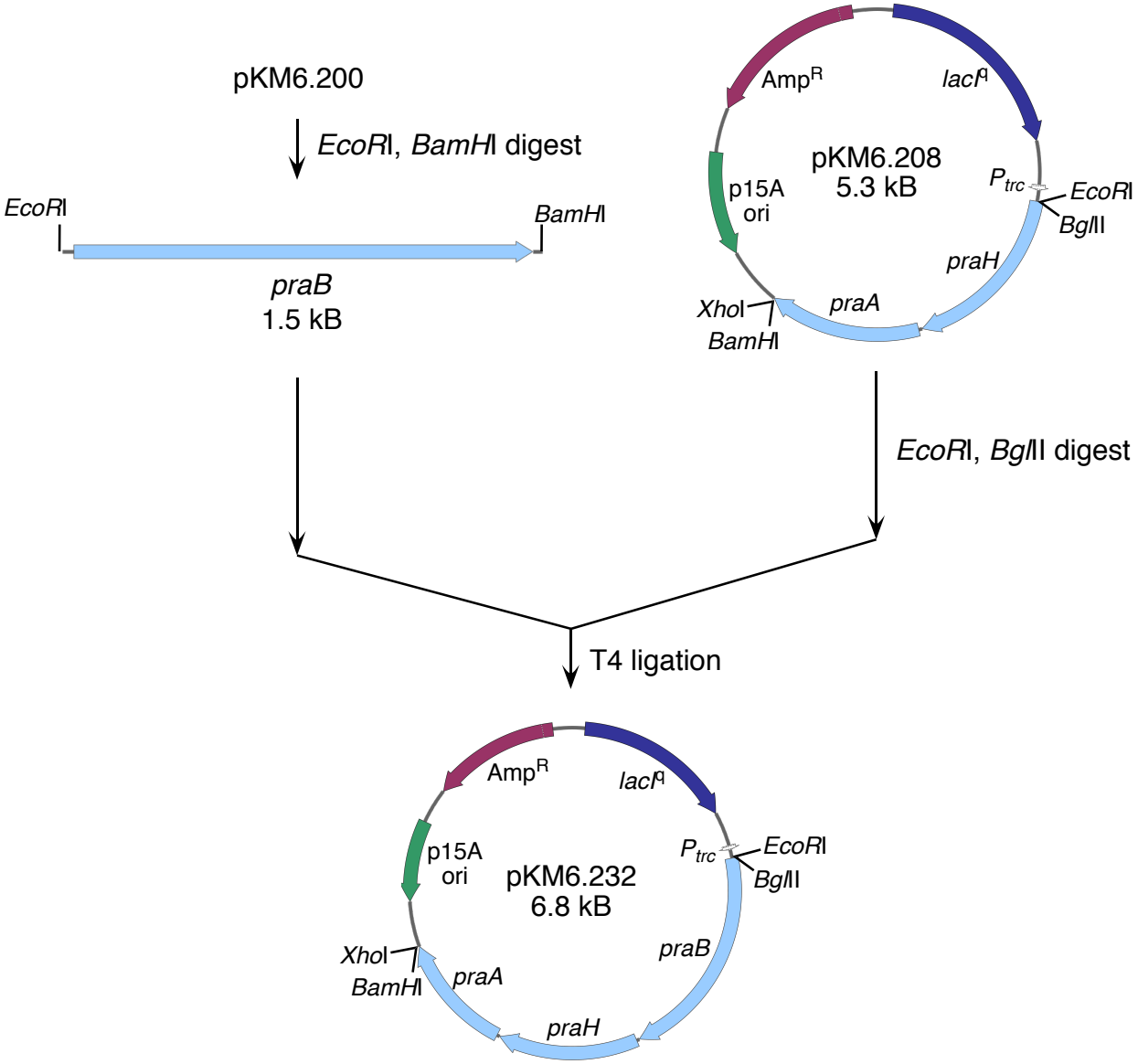

Figure 30. Preparation of plasmid pKM6.232.

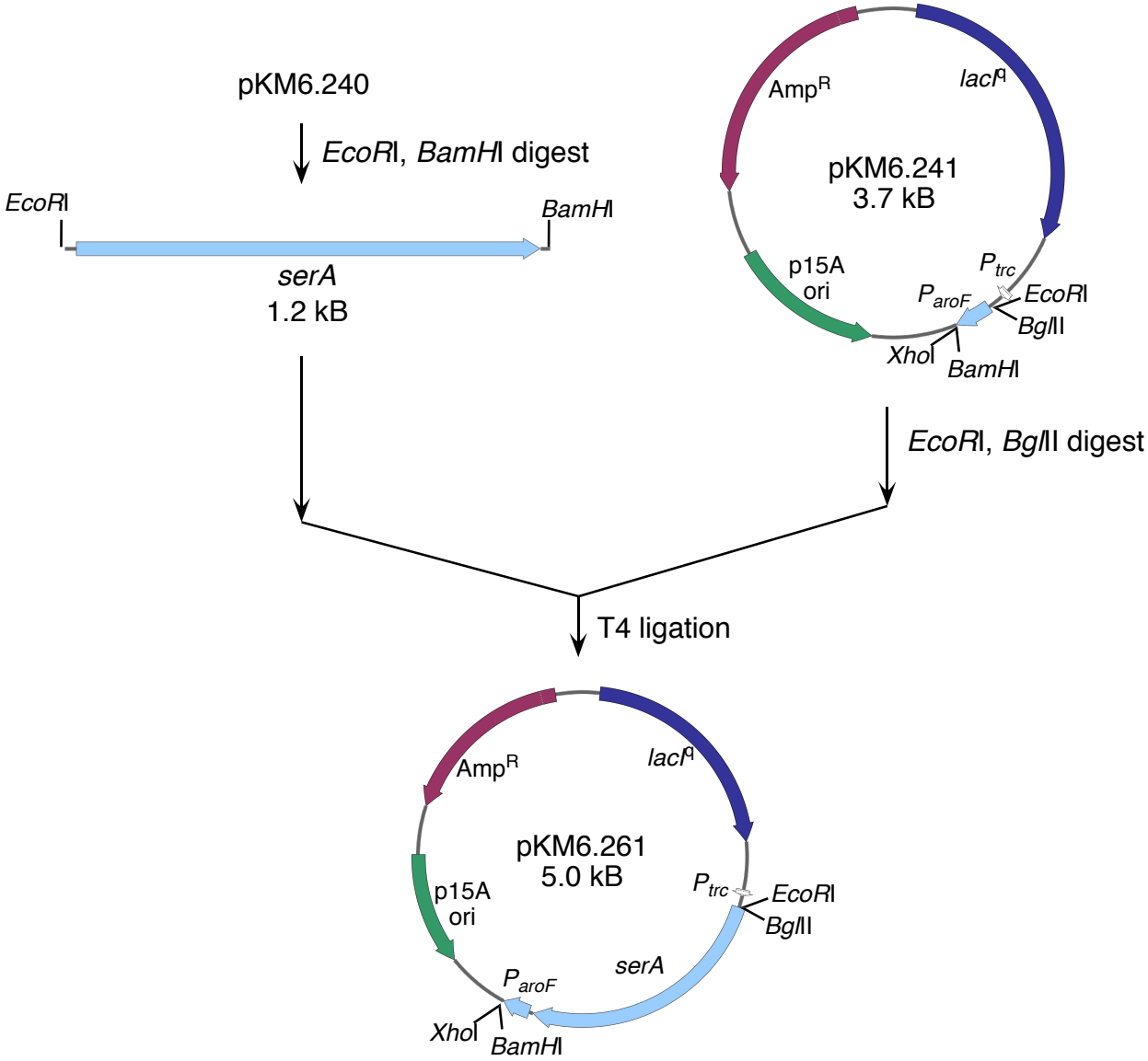

Figure 31. Preparation of plasmid pKM6.261.

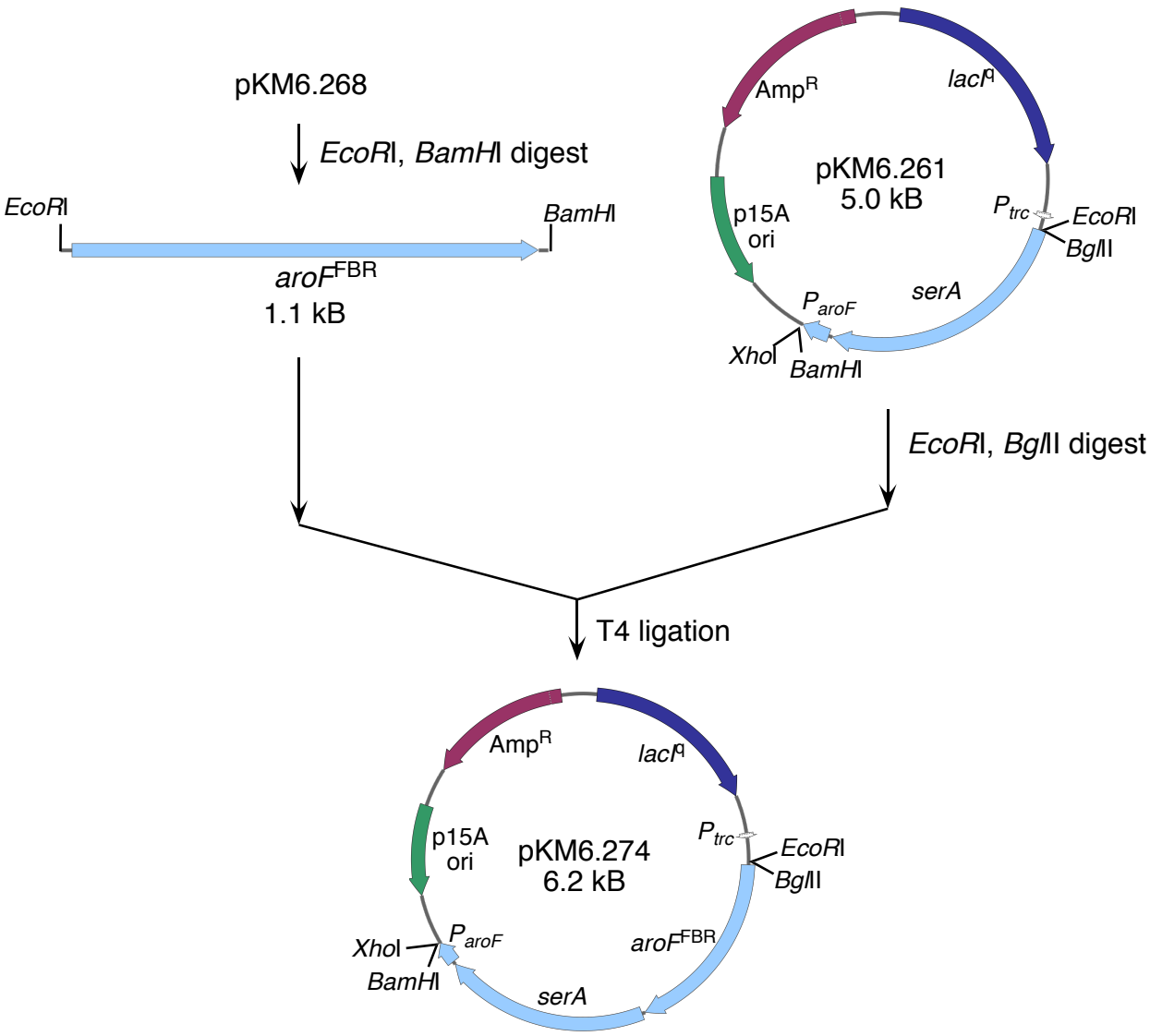

Figure 32. Preparation of plasmid pKM6.274.

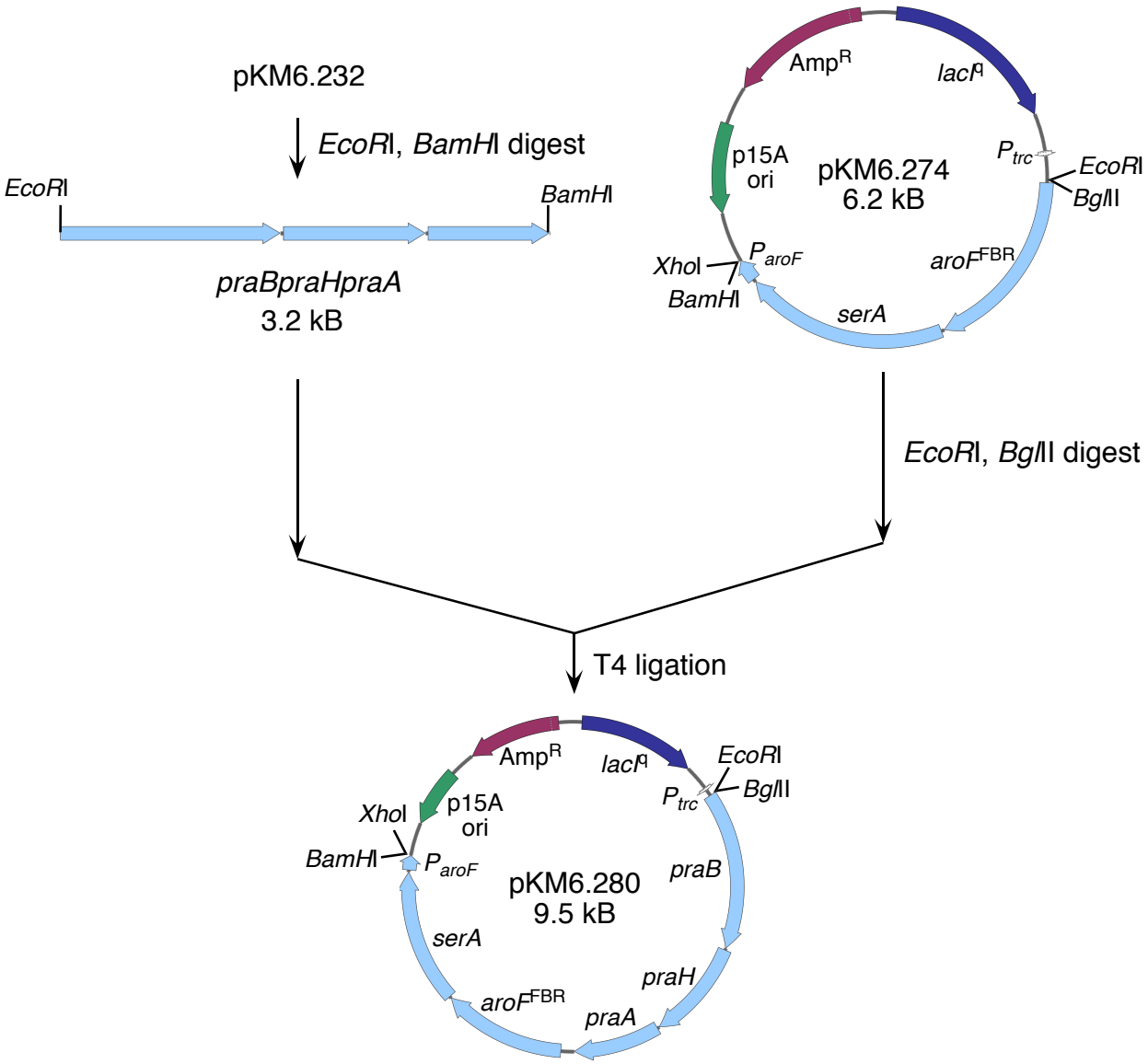

Figure 33. Preparation of plasmid pKM6.280.

4. Fed-batch fermentation conditions

Fed-batch fermentations were performed in a 2 L working volume bench-top bioreactor at 33 °C and pH 7.0. The dissolved oxygen (D. O.) level was maintained at 10% air saturation. Antifoam (Sigma 204) was manually added as needed and pH maintained at 7.0 by addition of NH_4OH and 2 N H_2SO_4. Initial glucose concentrations were 18 g/L for glucose-limited conditions or 25 g/L for glucose-rich conditions.

Fermentation inoculants were initiated by introduction of a single colony into 5 mL of M9 medium and grown at 37 °C with agitation at 250 rpm for 20-24 h. This culture was used to inoculate 100 mL M9 medium to an initial OD_{600} of 0.05 and grown for an additional 6 h at 37 °C and 250 rpm. After reaching an appropriate OD_{600} (1.0-1.5), the inoculant was transferred to the fermentation vessel (t = 0).

4.1. Glucose-rich conditions

Fermentations run under glucose-rich conditions employed an initial glucose concentration of 25 g/L. D-Glucose addition rates were adjusted manually such that the concentration of D-glucose in the medium was maintained in the range of 20-30 g/L. Fermentation runs are divided into three stages, each of which corresponds to a different control procedure for maintaining D. O. levels at 10%. In the first stage, D. O. concentration was maintained by increasing the impeller speed from its initial set point of 50 rpm to a preset maximum of 750 rpm while airflow was held at its initial setting of 0.06 L/L/min. In the second stage, the impeller speed was held constant at 750 rpm while the mass flow controller increased airflow to a preset maximum level of 1.0 L/L/min. In the third stage, D. O. levels were

maintained at 10% by allowing the impeller speed to vary between 400-1800 rpm while the airflow was held constant at 1.0 L/L/min.

4.2. Glucose-limited conditions

Fermentations run under glucose-limited conditions employed an initial glucose concentration of 18 g/L and a steady state concentration of less than 1 g/L of glucose was maintained after the preset maximum levels of airflow (1.0 L/L/min) and impeller speed (850 rpm) were reached. Glucose-limited fermentations involve three stages similar to glucose-rich runs. Indeed, the first two stages are controlled identically. After reaching the preset maximum levels of impeller speed and airflow, oxygen sensor-controlled glucose feeding began, which maintained D. O. levels at 10% throughout the remainder of the run while keeping impeller speed and airflow constant.

5. Biosynthesis of 2-HMA in *E. coli*

5.1. Fermentation of *E. coli* WN1/pKM6.280

Fermentations of *E. coli* WN1/pKM6.280 employed both glucose-rich and glucose-limited conditions. Beginning at 12 h and continuing every 6 h throughout the fermentation run, aliquots of β-D-isopropylthiogalactopyranoside (IPTG, 12 mg, 0.05 mM) were added to induce gene transcription. Glucose-limited fermentations afforded marginally higher titers of 2-HMA than glucose-rich conditions (60 mg/L and 30 mg/L, respectively) (Figures 40 and 41). Unexpectedly, 1-2 g/L of an α-keto acid tautomer, (*E*)-5-oxohex-2-enedioc acid **23**, were

observed in the fermentation broth by ^{1}H NMR. Small amounts (100-500 mg/L) an α-keto tautomer, (*E*)-2-oxohex-3-enedioic acid **24**, were also seen.

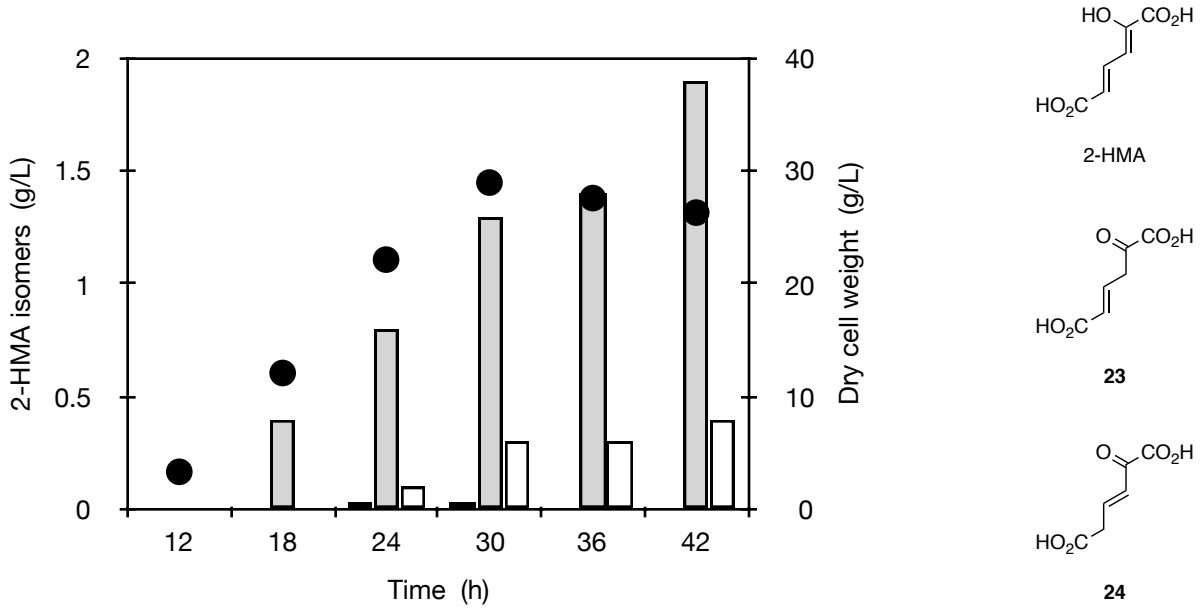

Figure 34. Biosynthesis of 2-hydroxymuconic acid by *E. coli* WN1/pKM6.280 under glucose-rich conditions. Legend: 2-HMA, black columns; tautomer **23**, grey columns; tautomer **24**, open columns; dry cell weight, closed circles.

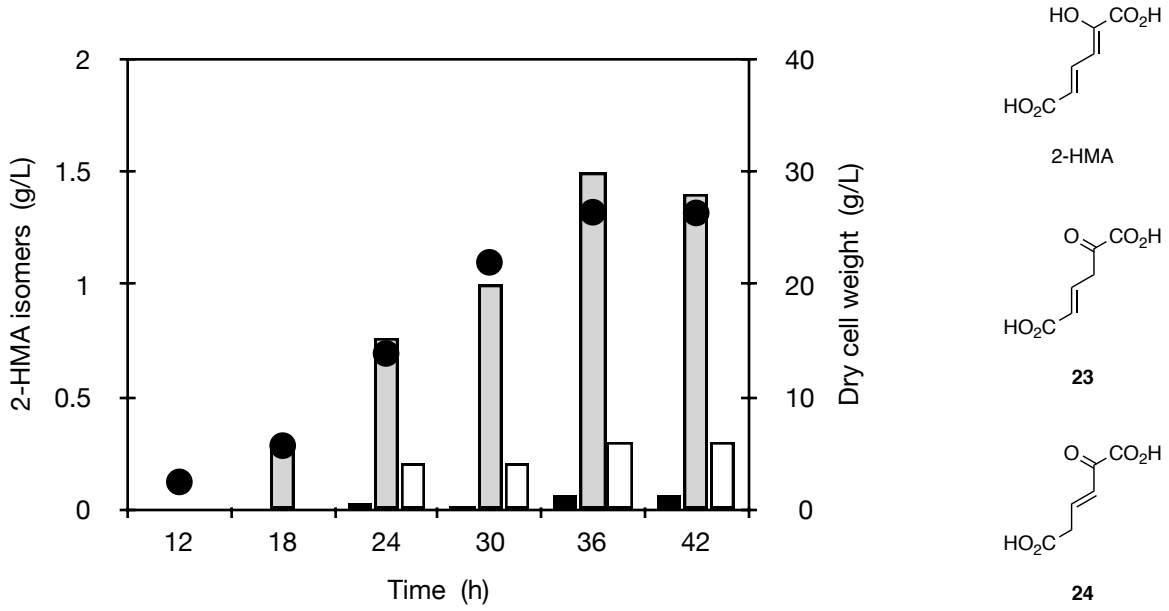

Figure 35. Biosynthesis of 2-hydroxymuconic acid by *E. coli* WN1/pKM6.280 under glucose-limited conditions. Legend: 2-HMA, black columns; tautomer **23**, grey columns; tautomer **24**, open columns; dry cell weight, closed circles.

Alongside 2-HMA isomers, DHS was observed in fermentation broth at concentrations of 2.2 g/L and 1.4 g/L in glucose-rich and glucose-limited runs, respectively. PCA was not observed indicating that any PCA formed was likely consumed by the expressed *pra* enzymes. To examine whether 2-HMA affects PCA anabolism, *E. coli* WN1/pKM6.274 was employed in subsequent fermentations both with and without exogenous 2-HMA.

5.2. An examination of PCA biosynthesis from D-glucose

Plasmid pKM6.274 contains *aroF*^{FBR}*serAP*$_{aroF}$ under the control of a *trc* promoter. Both glucose-rich and glucose-limited fermentations of *E. coli* WN1/pKM6.274 enabled evaluation of PCA biosynthesis productivity in the absence of any PCA cleavage enzymes (Figures 42 and 43).

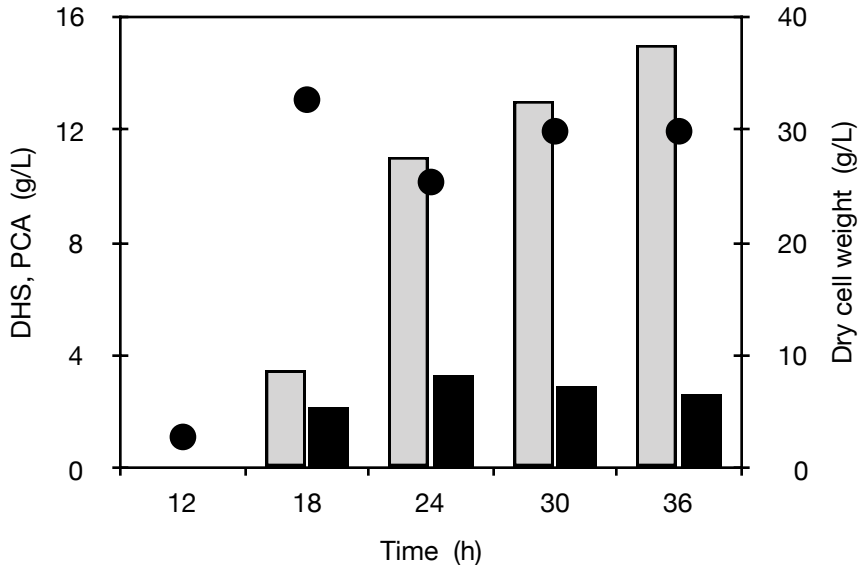

Figure 36. Biosynthesis of PCA by *E. coli* WN1/pKM6.274 under glucose-rich conditions. Legend: protocatechuate (PCA), grey columns; 3-dehydroshikimate (DHS), black columns; dry cell weight, black circles.

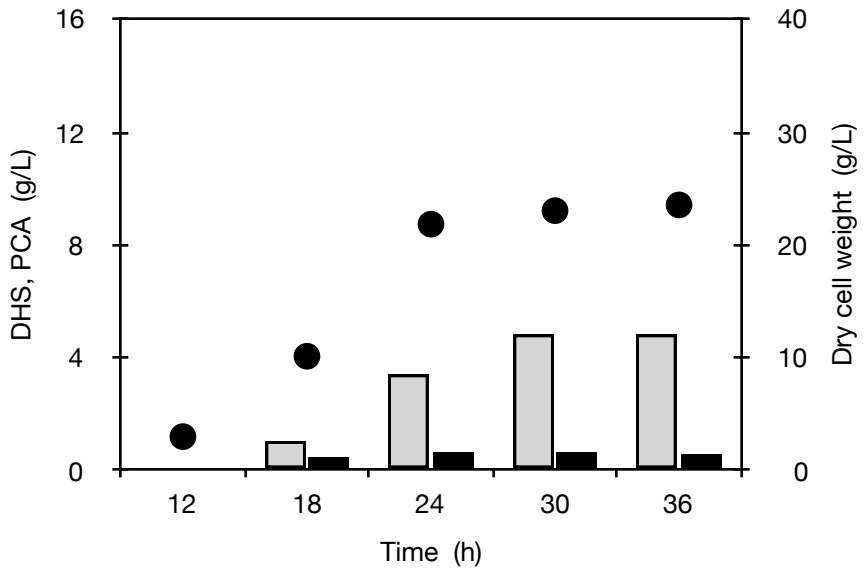

Figure 37. Biosynthesis of PCA by *E. coli* WN1/pKM6.274 under glucose-limited conditions. Legend: protocatechuate (PCA), grey columns; 3-dehydroshikimate (DHS), black columns; dry cell weight, black circles.

Glucose-limited conditions afforded PCA titers of 4.8 g/L while glucose-rich fermentations achieved 15 g/L titers of PCA. Both conditions revealed maximum DHS titers by 24 h. Beyond 24 h, DHS titers slowly decreased throughout the remainder of the fermentation, likely due to either dilution effects or small amounts of cellular uptake.[38] Chemically synthesized 2-HMA was added to exponentially growing WN1/pKM6.274 to determine if 2-HMA accumulation has an effect on PCA production (Figure 38).

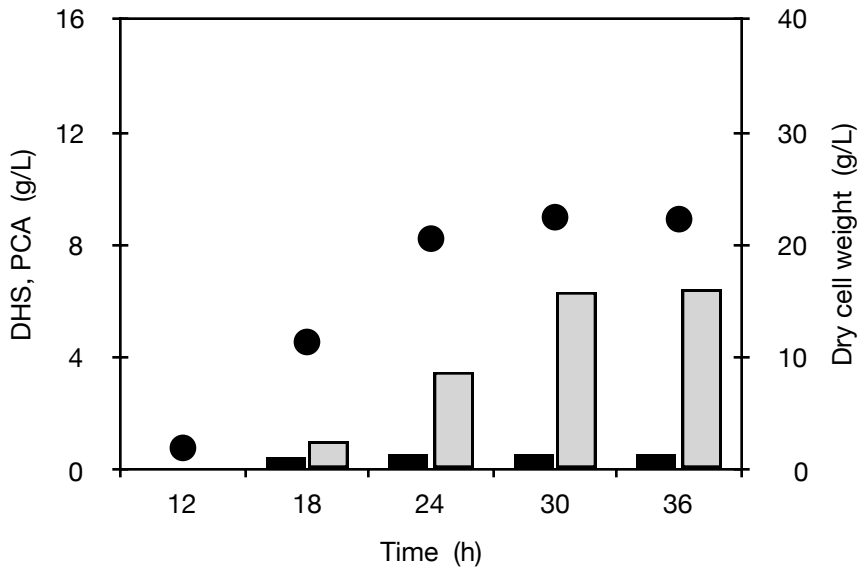

Figure 38. Biosynthesis of PCA and DHS by *E. coli* WN1/pKM6.274 in the presence of externally added 2-HMA (1 g/L). Legend: protocatechuate (PCA), grey columns; 3-dehydroshikimate (DHS), black columns; dry cell weight, black circles.

Once cells reached exponential growth phase (18 h), chemically synthesized 2-HMA was added as a sterile solution in water (pH 7) to a concentration of 1 g/L. Interestingly, no 2-HMA nor either α-keto acid tautomers were observed in the fermentation broth after 6 h following addition. To ensure that the exogenously added 2-HMA does not undergo chemical degradation, a 500 mL baffled flask containing 100 mL fermentation medium and 1 g/L 2-HMA was incubated at 37 °C with agitation at 250 rpm. After 3 h, α-keto acid tautomer **23** predominated in a 9:1 ratio with 2-HMA. This distribution remained unchanged after 24 h. α-Keto acid tautomer **24** did not accumulate. These results indicate the tautomerization of 2-HMA to α-keto acid **23** is facile, but enzyme action is necessary for the production of α-keto acid **24**. All of the mass of the initially added 0.1 g of 2-HMA could be accounted for after 24 h, indicating that chemical degradation does not occur under these conditions. An observed loss of 1 g/L 2-HMA over 6 h during fermentation of WN1/pKM6.274 suggests gradual cellular uptake. Despite apparent

incorporation into the cell, 2-HMA did not appear to have deleterious effects on PCA or DHS biosynthesis. *E. coli* WN1/pKM6.274 achieves similar titers of PCA and DHS both in the presence and absence of 2-HMA. It appears that 2-HMA does not inhibit PCA biosynthesis; however, the possibility of inhibition due to CHMS or 2-HMS remains.

A critical difference between pKM6.280 and pKM6.274 is the location of *aroF*^{FBR} relative to the *trc* promoter. Premature termination of *E. coli* RNA polymerase negatively effects the translation rate of genes placed far away from the promoter sequence.[94] In plasmid pKM6.274, the *aroF*^{FBR} gene is the first gene in the cassette, while in plasmid pKM6.280, it is over 3 kilobases away. The difference in distance of *aroF*^{FBR} away from P_{trc} may lead to a difference in translation rate and a corresponding difference in AroF^{FBR} expression between pKM6.274 and pKM6.280. To determine if there is a difference in AroF^{FBR} expression, DAHP synthase activity was measured in both WN1/pKM6.274 and WN1/pKM6.280.

A comparison of DAHP synthase activities of WN1/pKM6.274 and WN1/pKM6.280 employed a colorimetric assay described by Schoner.[95] Briefly, E4P and phosphoenolpyruvate (PEP) are converted into DAHP during incubation with cellular lysate at 37 °C over 5 min. Aliquots are removed at timed intervals and quenched with 10% trichloroacetic acid. Precipitated protein is removed and a pink chromophore is generated by reaction of DAHP with thiobarbituric acid. Quantification of DAHP proceeded via extraction of the chromophore into cyclohexanone followed by monitoring absorbance at 549 nm (ε = 68,000 M^{-1} cm^{-1}). One unit of DAHP synthase activity was defined as the formation of 1 μmol of DAHP per min at 37 °C.

Four aliquots of cells were taken from glucose-limited fermentation runs with WN1/ pKM6.274 and WN1/pKM6.280 (Tables 12 and 13). Aliquots were taken every 2.5 h beginning

30 min after addition of IPTG. Cells were pelleted, lysed, and assayed for DAHP synthase activity. Steady activity was detected in WN1/pKM6.274 cell-free extracts whereas WN1/ pKM6.280 samples exhibited lower initial DAHP synthase activity that increased over time. After 20 h, DAHP synthase activities for both strains were similar. The reason behind the lower initial activity observed for WN1/pKM6.280 was not proven, but if it is a consequence of premature termination events during transcription of *aroF*^{FBR} by *E. coli* RNA polymerase, insertion of an additional *trc* promoter preceding the *aroF*^{FBR} gene in plasmid pKM6.280 could alleviate this initial lag and improve carbon flow into the shikimate pathway during the early stages of fermentation.

Table 12. Specific activity of DAHP synthase in cellular lysate of WN1/pKM6.274 during glucose-limited fermentation.

Run time	Sp. activity (µmol/min/mg)
12.5 h	12
15 h	9
17.5 h	10
20 h	8

Gene transcription induced by addition of aliquots of IPTG (12 mg, 0.05 mM) at 12 h and 18 h into course of fermentation.

Table 13. Specific activity of DAHP synthase in cellular lysate of WN1/pKM6.280 during glucose-limited fermentation.

Run time	Sp. activity (µmol/min/mg)
12.5 h	1
15 h	2
17.5 h	4
20 h	7

Gene transcription induced by addition of aliquots of IPTG (12 mg, 0.05 mM) at 12 h and 18 h into course of fermentation.

To investigate possible feedback inhibition of AroF^{FBR} by 2-HMA or 2-HMS, DAHP synthase activity of WN1/pKM6.274 cell free lysate was assayed in the presence of these compounds (Table 14). 2-Hydroxymuconic acid was synthesized as described above in Part I and isolated as a dry solid. A known amount of this material was dissolved in water and filtered through a 0.22 μm membrane to generate a stock solution. 2-Hydroxymuconate 6-semialdehyde (2-HMS) was made *in situ* via action of 6xHis-tagged PraA and 6xHis-tagged PraH on PCA prior to addition of DAHP-containing sample. Quantification of 2-HMS was performed by monitoring the increase in absorbance at 375 nm (ε = 35,000 M^{-1} cm^{-1}).[40] Neither compound exhibited inhibition of AroF^{FBR} up to concentrations of 1 mM or 10 mM for 2-HMS or 2-HMA, respectively.

Table 14. Effect of exogenous 2-hydroxymuconic acid and 2-hydroxymuconate 6-semialdehyde on DAHP synthase activity of *E. coli* WN1/pKM6.274. [a] 2-hydroxymuconic acid; [b] 2-hydroxmuconate 6-semialdehyde.

Entry	[HMA] or [HMS] (mM)	Sp. activity (U/mg)
1[a]	0	3
2[a]	10^{-4}	4
3[a]	10^{-3}	3
4[a]	10^{-2}	7
5[a]	10^{-1}	5
6[a]	1	5
7[a]	10	4
8[b]	1	6

5.3. Enzymatic tautomerization of 2-hydroxymuconic acid

After 48 h in glucose-limited fermentation conditions, *E. coli* WN1/pKM6.280 accumulates a product mixture of 2-HMA, α-keto acid **23**, and α-keto acid **24** (Figure 39) is observed. When chemically synthesized 2-HMA was incubated in 100 mL minimal media at 37 °C, isomerization to the β,γ-unsaturated α-keto acid **23** was observed by ^{1}H NMR, however the conjugated α-keto acid **24** was not observed. This indicates that spontaneous tautomerization is selective toward the unconjugated α-keto acid **24** in aqueous solutions. The appearance of predominance of the unconjugated α-keto acid **24** in fermentations of WN1/pKM6.280 must be due to biological activity.

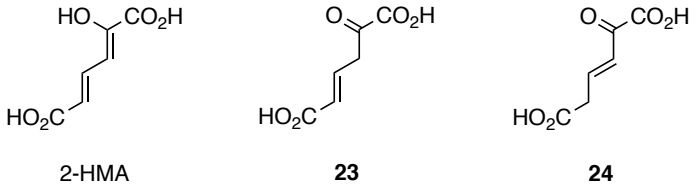

Figure 39. Structures of 2-hydroxymuconic acid (2-HMA) and α-keto acid tautomers.

Enzymatic tautomerization of 2-HMA may be catalyzed by 4-oxalocrotonate tautomerase (4-OT). This enzyme is involved in the lower branch of aromatic hydrocarbon degradation pathways in many organisms including *Pseudomonas putida*, *Bacillus subtilis*, and *Heliobacter pylori*. It catalyzes the π-bond migration of unsaturated α-keto acids via a dienol intermediate (Figure 40).[96-102] The isomerized α-keto acids are then subjected to further enzymatic degradation, ultimately entering the citric acid cycle. In *E. coli*, 4-OT is encoded by *pptA*, and may be at least partly responsible for the low titers observed in fermentations with WN1/

pKM6.280. Homologous recombination was explored to remove the genomic *pptA* locus of WN1 in an effort to increase titers of 2-HMA.

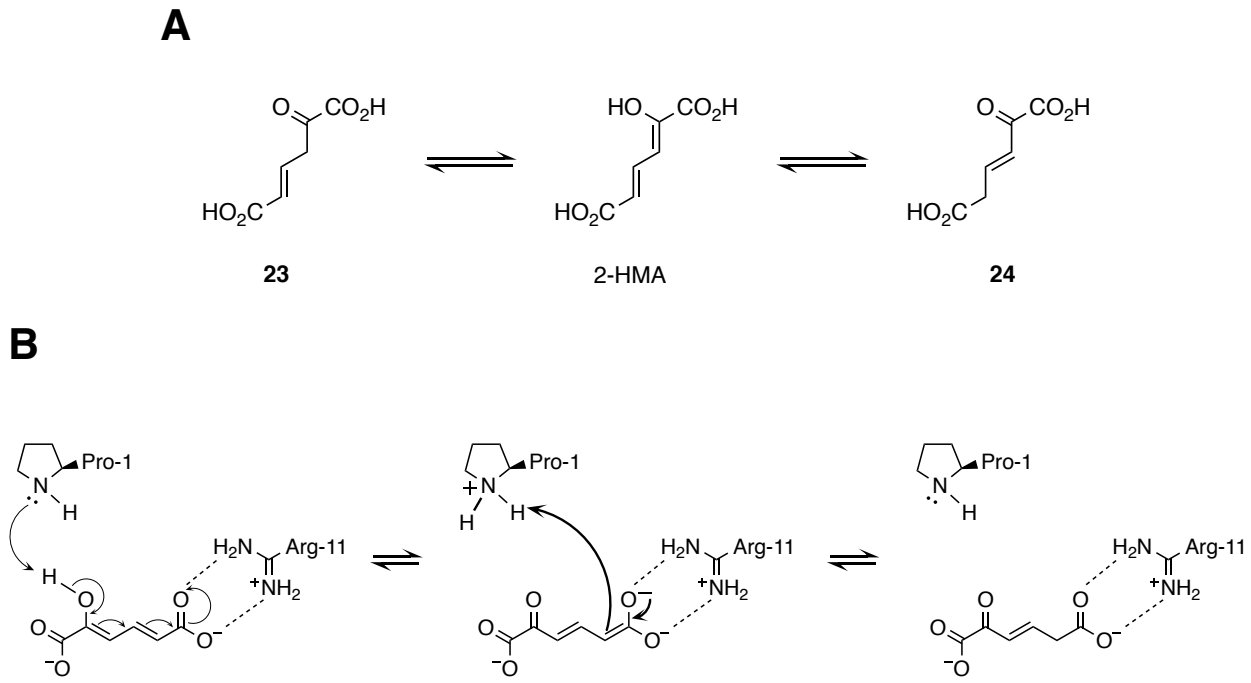

Figure 40. Action of 4-oxalocrotonate tautomerase. **A.** Reactions catalyzed by 4-oxalocrotonate tautomerase on 2-hydroxymuconic acid; **B.** Catalytic mechanism of 4-oxalocrotonate tautomerase demonstrating conversion of 2-hydroxymuconic acid to α-keto acid tautomer **24**.

5.3.1. *Deletion of pptA locus*

Deletion of the *pptA* locus from the genome of *E. coli* WN1 employed the phage λ Red recombinase system.[103] The Red system utilizes three genes: *γ*, *β*, and *exo*, whose products are called Gam, Bet, and Exo, respectively. Gam inhibits the host RecBCD exonuclease V so that Bet and Exo can gain access to ends of linearized DNA and promote recombination.[103] The recombination procedure for deletion of *pptA* involved four steps (Figure 41). A kanamycin resistance gene flanked by FLP recombinase recognition targets (FRT-Kan^R) was PCR amplified

from plasmid pKD4 using primers extended with *pptA*-homologous regions (H1, H2, Fig. 41). The PCR product was transformed into WN1 expressing the λ Red recombinase genes from plasmid pKD46. Growth at 30 °C promotes recombination of FRT-Kan^R into the *pptA* locus of WN1 to afford WN1*pptA::*Kan^R.

Elimination of the kanamycin resistance cassette employed plasmid pCP20 which shows thermal induction of FLP recombinase synthesis and carries ampicillin resistance. After transformation into WN1*pptA::*Kan^R, ampicillin-resistant transformants were selected at 30 °C. These were colony-purified once nonselectively at 43 °C and tested for loss of all antibiotic resistance. Loss of pCP20 and the FRT-flanked Kan^R occurred simultaneously. Deletion of the *pptA* gene from WN1 afforded strain KM1. Successful deletion was verified by PCR using the following primers: A) 5'-CTGGACGTGGTAATGAATGAAGACGACTGC, B) 5'-GTTGCATC ATTTAGGTGCTGGGACGTTTGT, C) 5'-GCCTGCTTGCCGAATATCATGGTGGAAAAT, and D) 5'-GCCATTTTCCACCATGATATTCGGCAAGCA. Primers are represented in Figure 42 as colored squares with the corresponding annealing locations on the genomic DNA of WN1*pptA*::Kan^R, WN1, or KM1. Primers C and D are specific to the kanamycin resistance gene and therefore do not lead to an amplification product using WN1 or KM1 genomic DNA as a template when added to the reaction mixture. The absence of a PCR amplification product in the presence of primers C and D correlate to the absence of the kanamycin resistance gene. In these reactions, a single PCR product was observed by agarose gel electrophoresis corresponding to a 0.6 kb DNA fragment or 0.4 kb fragment, respectively. When WN1*pptA*::KanR genomic DNA was used as a template, three amplification products were obtained which matched the expected

sizes on the basis of the sequence of the kanamycin resistance gene and the genes flanking the *pptA* locus.

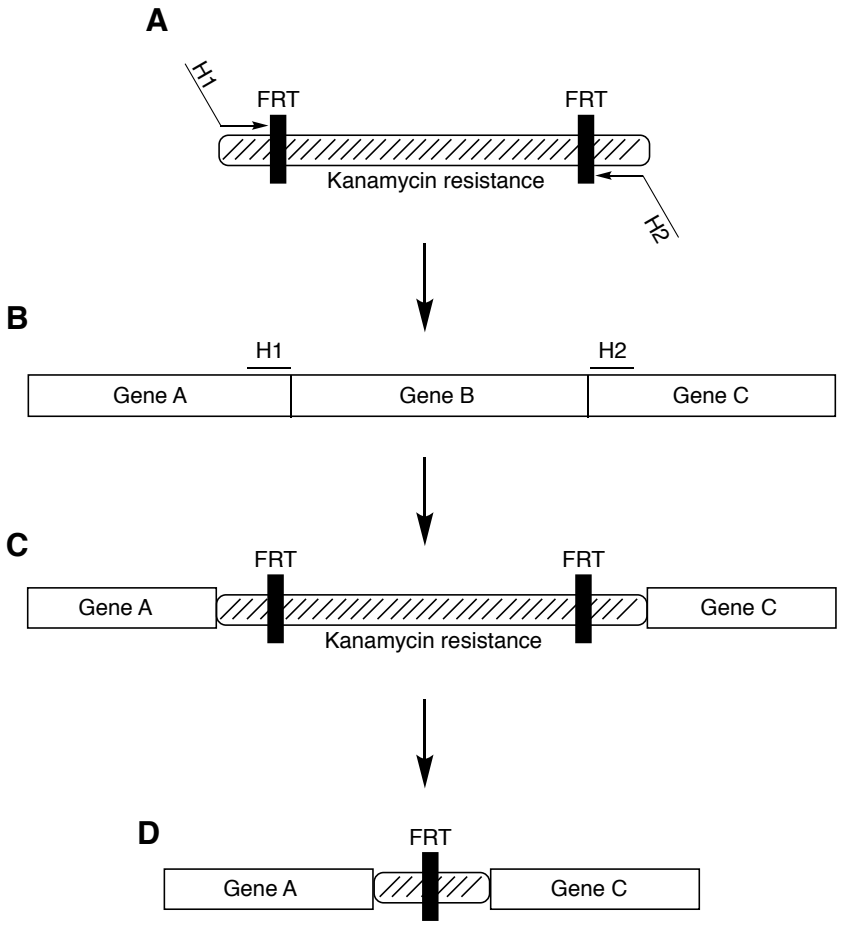

Figure 41. Workflow for homologous recombination using FRT-flanked kanamycin resistance cassette and phage λ Red recombinase system.

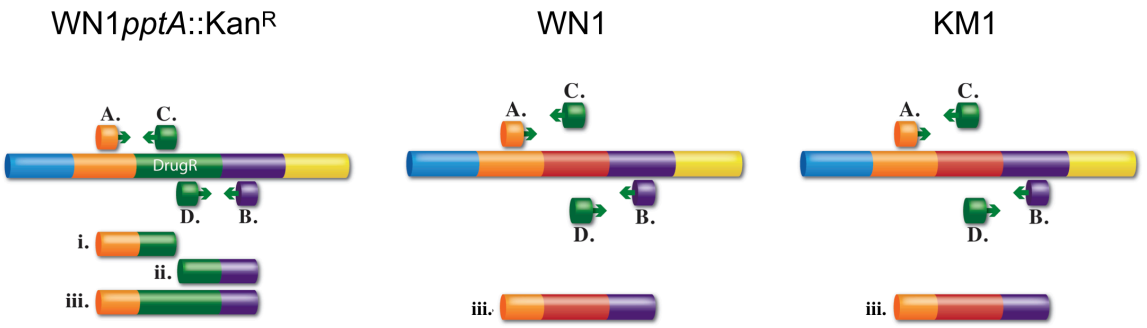

Fragment	Predicted size	Observed band	Predicted size	Observed band	Predicted size	Observed band
i	1311 bp	1.3 kb	none	none	none	none
ii	519 bp	0.5 kb	none	none	none	none
iii	1796 bp	1.8 kb	591 bp	0.6 kb	357 bp	0.4 kb

Figure 42. Verification of *pptA* deletion via PCR. Expected PCR product sizes using genomic DNA from WN1*pptA*::Kan^R, WN1, or KM1 are described below each cartoon. Sizes of DNA fragments observed using agarose gel electrophoresis are also presented.

5.3.2. Fermentations of KM1/pKM6.280

After transformation, *E. coli* KM1/pKM6.280 was examined under glucose-rich and glucose-limited fed-batch fermentor conditions (Figures 43 and 44). The results were encouraging as 2-HMA was the predominant product up to 30 h in glucose-rich fermentation and 36 h in glucose-limited fermentation. The formation of both α-keto acid tautomers **23** and **24** indicates that 4-OT is not solely responsible for 2-HMA tautomerization in *E. coli* KM1. Nonetheless, significant improvement in titers of 2-HMA were achieved. Peak titers in glucose-rich fermentations increased from 30 mg/L to 2.1 g/L while glucose-limited fermentations increased from 60 mg/L to 1.8 g/L of 2-HMA.

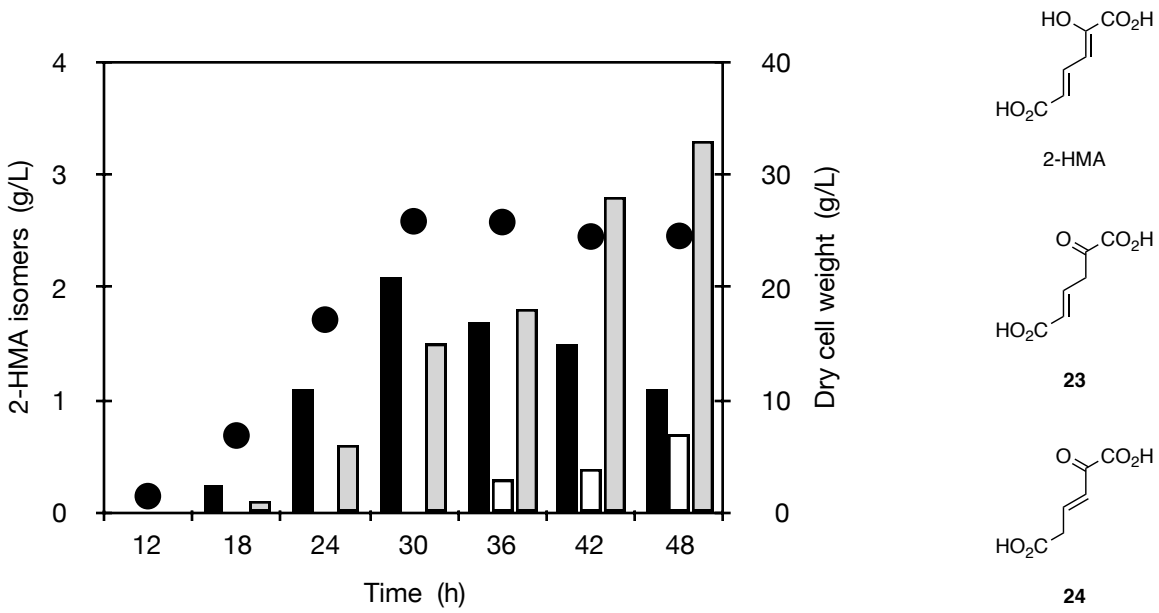

Figure 43. Biosynthesis of 2-hydroxymuconic acid by *E. coli* KM1/pKM6.280 under glucose-rich conditions. Legend: 2-HMA, black columns; tautomer **23**, grey columns; tautomer **24**, open columns; dry cell weight, closed circles.

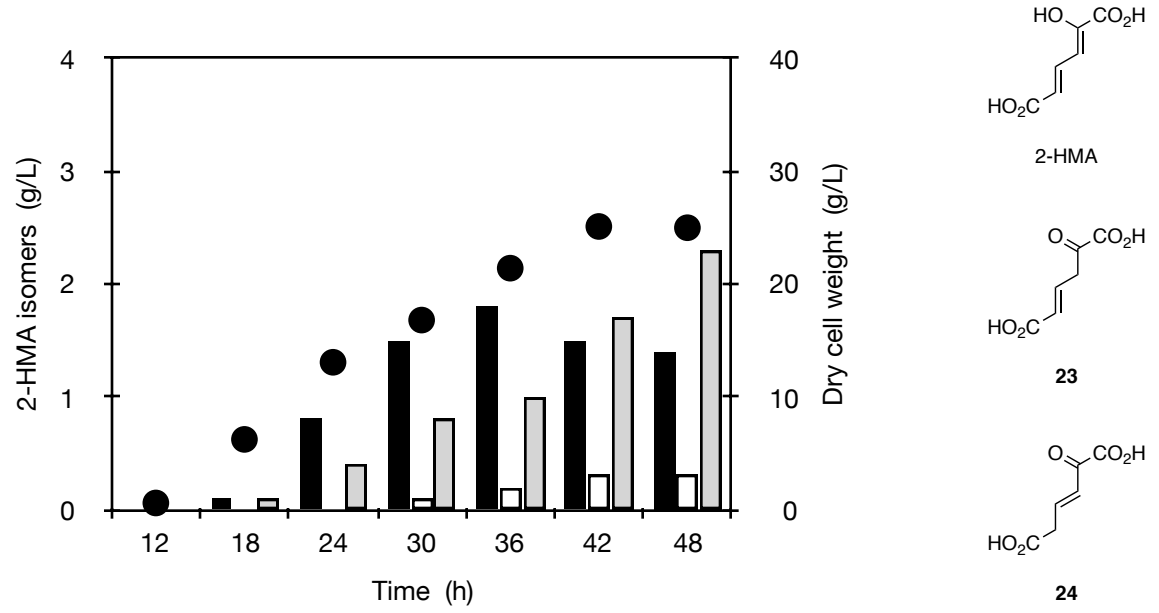

Figure 44. Biosynthesis of 2-hydroxymuconic acid by *E. coli* KM1/pKM6.280 under glucose-limited conditions. Legend: 2-HMA, black columns; tautomer **23**, grey columns; tautomer **24**, open columns; dry cell weight, closed circles.

Deletion of *pptA* resulted in accumulation of 2.1 g/L 2-HMA after 30 h in glucose-rich fermentation, corresponding to a seventy-fold improvement over *E. coli* WN1. After 48 h, the total amount of biosynthesized 2-HMA, tautomer 23, and tautomer 24 reached 5.1 g/L. This corresponds to a two-fold increase over *E. coli* WN1. The gradual decrease in titers of 2-HMA observed with concomitant increase in titers of both α-keto acid isomers **23** and **24** suggests an additional mechanism of tautomerization besides 4-OT. *E. coli* possesses an additional isomerase which may also act upon 2-HMA, called 5-carboxymethyl-2-hydroxymuconate isomerase (5CHMI). Kinetic parameters previously determined for 5CHMI revealed modest activity for the enzyme utilizing 2-HMA rather than its physiological substrate.[102] It is possible that the activity of 5CHMI in KM1/pKM6.280 contributes to the increase of α-keto acid isomers of 2-HMA over the course of fermentations and the continued presence of α-keto acid tautomer **24**, which was not observed during spontaneous tautomerization of 2-HMA.

6. Isolation of 2-hydroxymuconic acid from fermentation broth

Cells were removed from fermentation broth via centrifugation at 8,000 rpm for 20 min. Protein was then removed using a tangential flow apparatus fitted with a 10 kD ultrafiltration cassette (Sartorius). The cell-free/protein-free broth then concentrated to dryness under reduced pressure and redissolved in 1,4-dioxane in preparation for a $Cu(OTf)_2$-catalyzed cycloaddition with ethylene. Only minor amounts of PTA were produced in a 0.5% yield from all three isomers of 2-HMA. Though this result indicates that biobased 2-HMA can be used as a precursor to renewable PTA, the low yield indicates that certain components in the fermentation

broth inhibit the synthesis of PTA. Attempts to isolate 2-HMA from crude cell-free/protein-free fermentation broth were undertaken.

During the chemical synthesis of 2-HMA from 2-hydroxyhexa-2,4-dienedioate **22**, 2-HMA is isolated as a beige-colored solid upon acidification of the reaction mixture at 4 °C. Similar treatment of the 2-HMA-containing fermentation broth did not afford clean material. Organic extraction was explored as the principal strategy of recovering 2-HMA from fermentation broth.

6.1. Organic extraction of 2-hydroxymuconic acid isomers

Various organic solvents were examined for their efficacy in isolating clean 2-HMA. A sample of fermentation broth containing 2 g/L 2-HMA isomers was acidified to pH 2 and concentrated to 1/3 of the original volume under reduced pressure. Aliquots (0.5 mL) were combined with an equal volume of organic solvent and shaken overnight in a rotary incubator. Extraction efficiency was calculated as percent of 2-HMA isomers recovered from the fermentation broth (Table 15).

Table 15. 2-Hydroxymuconic acid extraction solvent screening.

Solvent	Recovery (mol %)
methanol	no separation
ethanol	no separation
n-propanol	no separation
isopropanol	no separation
n-butanol	23%
2-butanol	48%
cyclohexanol	41%
octanol	23%
acetone	no separation
4-methyl-2-pentanone	0%
methyl ethyl ketone	65%

Acetone and the short-chain aliphatic alcohols did not result in distinct separation of aqueous and organic layers. The highest extraction efficiencies were achieved with cyclohexanol, 2-butanol, and methyl ethyl ketone (MEK). As MEK afforded the highest extraction efficiency, it was used in all subsequent extractions. Interestingly, nearly all of α-keto acid tautomer **23** remained in the aqueous layer after treatment with organic solvents.

Pretreatment methods were explored in an attempt to increase recovery of all three isomers of 2-HMA. Iterations of charcoal pretreatment, concentration under reduced pressure, and acidification (pH 2) were employed. Regardless of other treatment methods, acidification proved to be essential for extraction into organic solvents. At neutral pH, carboxylic acid moieties of 2-HMA are deprotonated and would likely form a salt with any available cation. Acidification, therefore, increases organic solubility.

Activated carbon (Sigma, Darco 20-20 mesh) was added to samples of fermentation broth (1 g per 100 mL) which were shaken at 250 rpm at rt for 1 h. Charcoal treated samples did not afford significantly cleaner extracts but did affect the ratio of 2-HMA to α-keto acid tautomers present in the organic extract. Without charcoal pretreatment, both α-keto acids remained in the aqueous layer, whereas charcoal-treated samples afforded higher recoveries of all three isomers. Concentration of the fermentation broth to 1/4 original volume did not have a significant effect on extraction efficiency.

The primary challenge associated with isolation of 2-HMA from fermentation broth is achieving high recovery of all three 2-HMA tautomers. Charcoal pretreatment prior to organic extraction influences the ratio of recovered isomers. Without pretreatment, 2-HMA is recovered in greatest extent with >90% recovery into the organic layer. With charcoal pretreatment, the α-keto acids are predominant in the organic extract. In all cases, over 50% of α-keto acid **23** remains in the aqueous layer regardless of pretreatment methods.

6.2. Conversion to 6-carboxy-2-pyrone and subsequent isolation

Efforts to extract all three tautomers of microbe-synthesized 2-HMA were largely unsuccessful due to the propensity of α-keto acid **23** to remain in the aqueous layer. Recovery of 2-HMA would be easier if the three isomers could be converted to a single structure. No form of chemical treatment was found that could enable conversion of a mixture of 2-HMA tautomers to a single isomer. Attempts to convert 2-HMA to 6-carboxy-2-pyrone **19** in fermentation broth were therefore undertaken with conditions used for conversion of chemically synthesized 2-HMA (1:4 H_2SO_4:AcOH in water, 100 °C). After 3 h, all three isomers of 2-HMA had been fully

consumed however 6-carboxy-2-pyrone **19** was afforded in only 30% yield. The reaction crude had become very dark and slightly more viscous. Evidently, the acidic reaction medium coupled with elevated temperatures resulted in uncontrolled side reactions, consuming much of the initial 2-HMA. Despite the poor yield of 6-carboxy-2-pyrone, higher extraction efficiencies were achieved than extractions of 2-HMA isomers (Table 16).

Table 16. Extraction solvent screening for 6-carboxy-2-pyrone **19** from fermentation broth.

Solvent	Recovery (mol %)
n-butanol	87%
2-butanol	90%
isobutanol	50%
cyclohexanol	67%
octanol	33%
4-methyl-2-pentanone	43%
methyl ethyl ketone	n/a

The primary challenge associated with organic extraction is cleanly isolating the desired product. Solvents with high extraction efficiencies tended to solubilize most of the components within crude fermentation broth. Solvents with lower efficiencies resulted in less contamination but did not effectively recover useful amounts of 2-HMA or 6-carboxy-2-pyrone **19**. Introduction of ion-exchange chromatography into the isolation method either prior to, or following organic extraction may help to provide cleaner extracts. Cleaner material should afford higher yields of PTA with microbe-synthesized 2-HMA.

7. Discussion

This work lays the foundation for the synthesis of renewable aromatic diacids from 2-HMA. Expression of protocatechuate (PCA) 2,3-cleavage enzymes from *Paenibacillus* sp. JJ-1b in *E. coli* WN1 afforded 2.3 g/L of 2-HMA isomers in glucose-rich fed-batch fermentation. However, less than 1% was produced in the conjugated enol form. This is the only isomer with the proper geometry to react with ethylene to afford PTA. The predominance of α-keto acid isomers must therefore be reduced before biobased 2-HMA can be utilized in a cycloaddition.

Deletion of native 4-oxalocrotonase tautomerase (4-OT) activity resulted in a two-fold increase in titer of 2-HMA isomers with a significant prevalence of the enol structure in fermentations of KM1/pKM6.280. The reaction catalyzed by 4-OT results in π-bond migration of an unsaturated α-keto acid via a conjugated enol intermediate prior to degradation through the citric acid cycle. Though titers of 2-HMA improved, product distribution skewed toward α-keto acid tautomers by the end of the fermentation with the continued formation of α-keto acid **23**, indicating that 4-OT activity is not solely responsible for 2-HMA tautomerization. Incubation of chemically synthesized 2-HMA in fermentation medium at 37 °C revealed uncatalyzed tautomerization of 2-HMA to the conjugated α-keto acid **23** to be negligible. This suggests the rate of tautomerization seen in fermentations is likely due to additional biological activity. *E. coli* may possess another isomerase that can utilize 2-HMA as a non-native substrate. 5-Carboxymethyl-2-hydroxymuconate isomerase has been previously shown to catalyze 2-HMA tautomerization in *E. coli* albeit with modest kinetics. Perhaps this, in conjunction with other promiscuous enzymes, contributes to the ultimate predominance of the α-keto acid isomers. The tautomerase superfamily of enzymes is characterized by a catalytic N-terminal proline residue

and a conserved β-α-β motif. Homology searches could help identify additional tautomerases present in the *E. coli* genome. Deletion of genes encoding additional tautomerases via homologous recombination, as was used for deletion of *pptA*, should prevent enzymatic isomerization of 2-HMA.

If genomic modification to remove enzyme-catalyzed tautomerization does not completely prevent the formation of α-keto acid isomers in fermentations, selective adsorption might be employed to remove 2-HMA from fermentation broth as it is produced. This technique has been used with great efficiency in catechol biosynthesis from D-glucose. Selective adsorption may also help alleviate any inhibitory effects from accumulation of 2-HMA or biosynthetic precursors. Inhibition of DAHP synthase was not observed however accumulation of 100-500 mg/L DHS in fermentation broth may indicate a bottleneck due to insufficient *aroZ* activity. Enzyme assays of 6xHis-tagged *aroZ* in the presence of 2-HMA or 2-HMS could indicate whether this repression occurs. There is also a possibility that an α-keto acid isomer is inhibitory to one or more enzymes in the biosynthesis pathway. Selective adsorption may be a way to keep the levels of 2-HMA-associated metabolites low enough to prevent any inhibition.

The primary challenge to be addressed is the isolation of 2-HMA from fermentation broth and subsequent conversion into appreciable quantities of PTA. Attempts to cleanly isolate 2-HMA as a single isomer or via cyclization to 6-carboxy-2-pyrone **19** have been ineffective. The minor amount of PTA produced during $Cu(OTf)_2$-catalyzed cycloaddition of biobased 2-HMA with ethylene **2** indicates pure 2-HMA is necessary. Derivatization to 6-carboxy-2-pyrone **19** is also precluded by impure starting material. Organic extraction affords 2-HMA as a mixture of keto and enol tautomers along with extensive contaminants from fermentation broth. Only the

conjugated enol possesses the appropriate geometry for Diels-Alder cycloaddition with ethylene. Attempts to drive the α-keto acids toward the enol have been unsuccessful. Without isolation of clean 2-HMA from fermentation broth and subsequent conversion to PTA, this route will never be commercially viable.

PART III

CONCLUSIONS

The results described herein demonstrate a proof-of-concept semisynthetic strategy toward renewable terephthalic, isophthalic, and phthalic acids from biobased feedstocks. Current manufacture of aromatic diacids relies exclusively upon subjecting petroleum-derived xylenes to costly and wasteful aryl methyl group oxidation. Materials made from PTA, IPA, and PA are valuable and widely used. It is highly desirable to reduce costs associated with their manufacture by avoiding aryl methyl group oxidation. Biobased compounds are attractive candidates to address this need.

Renewable syntheses of PTA have received the most attention as it is the most highly valued of the aromatic diacids. Many proposed synthetic pathways produce *p*-xylene **1**, thus enabling simple integration into current PTA manufacture architecture. The principal drawback of these routes is their inevitable reliance on the wasteful Amoco Mid-Century oxidation process. Other routes to biobased PTA circumvent the Amoco Mid-Century oxidation by taking advantage of diacid substrates such as malic acid, succinic acid, and muconic acid. All of these syntheses require esterification of the diacid preceding cycloaddition to form the six-membered ring of PTA. Aromatization of the cyclic intermediate affords dimethyl terephthalate (DMT) which must be hydrolyzed to produce PTA. These steps are commercially unattractive as they not only lengthen a synthetic route but involve copious amounts of methanol which is toxic and highly flammable. Industrial facilities which use methanol require fitting of specialty wiring and other precautions to decrease the risk of a fire caused by an inadvertent electrical spark. These

facilities are, of course, highly expensive to build precluding the use of methanol in commodity chemical manufacture.

Only one of the eleven proposed routes to biobased PTA provides access to IPA as well. Poly(ethylene terephthalate) (PET) requires 2-5 wt% IPA to inhibit crystallization and provide a transparent, flexible polymer. Despite stabilizing PTA manufacture costs by diversifying available feedstocks, PET manufacture would still be reliant on petroleum-derived IPA. Thus, a route which allows access to both aromatic components of PET would be highly desirable. Microbe-synthesized 2-hydroxymuconic acid (2-HMA) provides a means to both PTA and IPA along with PA via conversion to 6-carboxy-2-pyrone **19**. Several plasticizers such as diisononyl cyclohexane-1,2-dicarboxylate (DINCH) and di-(2-ethylhexyl)phthalate (DEHP) (Figure 1, Part I), are derived from PA. Access to all regioisomers of aromatic diacids is thereby possible through 2-HMA.

As it stands, use of microbe-synthesized 2-HMA is far from commercial application. Biocatalytic synthesis has been established in *E. coli* and affords modest amounts of 2-HMA. However, not all of the 2-HMA produced is suitable for a cycloaddition with ethylene **2**, and an inability to cleanly isolate any such material precludes its use as a substrate for PTA manufacture. Catalysis of the cycloaddition of 2-HMA with ethylene **2** and the reaction of 6-carboxy-2-pyrone **19** with propiolic acid **18** also needs improvement. Though the latter reaction achieves high yields with $BOB(OAc)_4$, low catalytic selectivity produces IPA and PA in a 1:1 ratio. Desirable selectivities favor IPA, which is more useful in chemicals manufacture. Finally, charring of the reaction mixture during the cycloaddition of 2-HMA with ethylene **2** precludes recovery of unreacted substrate. This challenge, when coupled to a 26% yield per pass,

considerably reduces process efficiency. Optimizing reaction conditions and continued catalyst screening may improve selectivities. Despite lingering challenges, the work presented herein demonstrates that synthesis of PTA, IPA, and PA from a common, biobased starting material is possible.

REFERENCES

REFERENCES

1. Cutler, J. Presented at the West Virginia Marcellus to Manufacturing Conference, Charleston, WV, March 2013.

2. Maps: Exploration, Resources, Reserves, and Production. https://www.eia.gov/maps/maps.htm (accessed March 14, 2018).

3. National Energy Technology Laboratory. Modern Shale Gas Development in the United States: An Update. US Department of Energy, September 2013.

4. Berkowitz, N. *Fossil hydrocarbons: chemistry and technology*; Academic: San Diego, 1997; pp 88-91.

5. King, H. Hydraulic Fracturing of Oil & Gas Wells Drills in Shale. https://geology.com/articles/hydraulic-fracturing/ (Accessed March 11, 2018).

6. Berkowitz, N. *Fossil hydrocarbons: chemistry and technology*; Academic: San Diego, 1997; pp 91-94.

7. Elvers, B. Handbook of Fuels: Energy Sources for Transportation; Wiley-VCH: Weinheim, 2008; pp 29-34.

8. Franck, H.-G.; Stadelhofer, J. W. *Industrial Aromatic Chemistry*; Springer: Berlin, 1988; pp 60-62.

9. Cailliot, A. Etudes sur L'Essence de Terebenthine. Ann. Chim. Phys., 1847, 3, 27-40.

10. Collias, D. I.; Harris, A. M.; Nagpal, V.; Cottrell, I. W.; Schultheis, M. W.; Biobased Terephthalic Acid Technologies: A Literature Review. *Ind. Biotechnol.* **2014**, *10*, 91-105.

11. Saffer, A.; Barker, R. S. Preparation of Aromatic Polycarboxylic Acids. US 2,833,816, 1958.

12. Tomas, R. A. F.; Bordado, J, C. M.; Gomes, J. F. P. *p*-Xylene Oxidation to Terephthalic Acid: A Literature Review Oriented Toward Process Optimization and Development. *Chem Rev.* **2013**, *113*, 7421-7469.

13. Partenheimer, W. Methodology and Scope of Metal/Bromide Autoxidation of Hydrocarbons. *Catal. Today*, **1995**, *23*, 69-158

14. Tibbitt, J. Personal communication.

15. Roman-Leshkov, Y.; Barrett, C. J.; Liu, Z.Y.; Dumesic J.A. Production of Dimethylfuran for Liquid Fuels from Biomass Derived Carbohydrates *Nature*, **2007**, *447*, 982-985.

16. Brookhart, M.; Findlater, M.; Guironnet, D.; Lyons T.W. Synthesis of *para*-Xylene and Toluene US 2013/0237732 A1, 2013

17. Lyons, T.W.; Guironnet, D.; Findlater, M.; Brookhart, M. Synthesis of *para*-Xylene from Ethylene. *J. Am. Chem. Soc.,* **2012**, 134 15708-15711

18. Peters, M. W.; Taylor, J. D.; Jenni, M. M.; Manzer, L. E.; Henton, D. E. Integrated Process to Convert Renewable Isobutanol to *p*-Xylene. US 2011/044243 A1, 2011.

19. Taylor, J. D.; Jenni, M. M.; Peters, M. W. Dehydration of Fermented Isobutanol for the Production of Renewable Chemicals and Fuels. *Top. Catal.* **2010**, *53* (15), 1224–1230.

20. Taylor, T. J.; Taylor, J. D.; Peters, M. W.; Henton, D. E. Variations on Prins-like Chemistry to Produce 2,5-Dimethylhexadiene from Isobutanol. US 8,742,187 B2, 2014.

21. Manzer, L. E.; Kourtakis, K.; Herron, N.; McCarron, E. M.; VerNooy, P. D. Process for the Preparation of *p*-Xylene. US 7,067,708 B2, 2006.

22. Kunkes, E. L.; Simonetti, D. A.; West, R. M.; Serrano-Ruiz, J. C.; Gärtner, C. A.; Dumesic, J. A. Catalytic Conversion of Biomass to Monofunctional Hydrocarbons and Targeted Liquid-Fuel Classes. *Science* **2008**, *322* (5900), 417–421.

23. Chang, C.-C.; Green, S. K.; Luke Williams, C.; Dauenhauer, P. J.; Fan, W. Ultra-Selective Cycloaddition of Dimethylfuran for Renewable *p*-Xylene with H-BEA. *Green Chem.* **2014**, *16* (2), 585–588.

24. Campbell, C. D.; Cole, D. T.; Harold Raymond Taylor, I. Process for the Preparation of Dialkyl Succinylsuccinates. US 5,783,723, 1998.

25. Kruper, W., JR.; Rand, C. L.; Molzahn, D. C. Processes for Producing Terephthalic Acid and Terephthalic Esters. US 2013/0345467A1, 2013.

26. Ashworth, I. W.; Bowden, M. C.; Dembofsky, B.; Levin, D.; Moss, W.; Robinson, E.; Szczur, N.; Virica, J. A New Route for Manufacture of 3-Cyano-1-Naphthalenecarboxylic Acid. *Org. Process Res. Dev.* **2003**, *7* (1), 74–81.

27. Lee, J. J.; Kraus, G. A. One-Pot Formal Synthesis of Biorenewable Terephthalic Acid from Methyl Coumalate and Methyl Pyruvate. *Green Chem.* **2014**, *16* (4), 2111–2116.
28. Lee, J. J.; Kraus, G. A. Divergent Diels–Alder Methodology from Methyl Coumalate toward Functionalized Aromatics. *Tetrahedron Lett.* **2013**, *54* (19), 2366–2368.

29. Frost, J. W.; Miermont, A.; Schweitzer, D.; Bui, R.; Wicks, D. A. Terephthalic and Trimellitic Based Acids and Carboxylate Derivatives Thereof. US 8,367,858 B2, 2013.

30. Miura, T.; Kakinuma, H.; Kawano, T.; Matsuhisa, H. Method for Producing Furan-2,5-Dicarboxylic Acid. US 7,411,078 B2, 2008.

31. Gong, W. H. Terephthalic Acid Composition and Process for the Production Thereof. US 7,385,081 B1.

32 Gong, W. H. Terephthalic Acid Composition and Process for the Production Thereof. US 9,299,278 B2, 2012

33. Hanke, P. D. Enzymatic Oxidation of Hydroxymethylfurfural. US 8,183,020 B2, 2012.

34. Berti, C.; Binassi, E.; Colonna, M.; Fiorini, M.; Kannan, G.; Karanam, S.; Mazzacurati, M.; Odeh, I. Bio-Based Terephthalate Polyesters. 8946472B2.

35. Colonna, M.; Berti, C.; Fiorini, M.; Binassi, E.; Mazzacurati, M.; Vannini, M.; Karanam, S. Synthesis and Radiocarbon Evidence of Terephthalate Polyesters Completely Prepared from Renewable Resources. *Green Chem.* **2011**, *13* (9), 2543–2548.

36. Kamitsou, M.; Panagiotou, G. D.; Triantafyllidis, K. S.; Bourikas, K.; Lycourghiotis, A.; Kordulis, C. Transformation of α-Limonene into *p*-Cymene over Oxide Catalysts: A Green Chemistry Approach. *Appl. Catal. A* **2014**, *474*, 224–229.

37. Miller, K. K.; Zhang, P.; Nishizawa-Brennen, Y.; Frost, J. W. Synthesis of Biobased Terephthalic Acid from Cycloaddition of Isoprene with Acrylic Acid. *ACS Sustainable Chem. Eng.* **2014**, *2* (8), 2053–2056.

38. Li, W.; Xie, D.; Frost, J. W. Benzene-Free Synthesis of Catechol: Interfacing Microbial and Chemical Catalysis. *J. Am. Chem. Soc.* **2005**, *127* (9), 2874–2882.

39. Wang, J.; Shen, X.; Yuan, Q.; Yan, Y. Microbial Synthesis of Pyrogallol Using Genetically Engineered *Escherichia coli*. *Metab. Eng.* **2018**, *45*, 134–141.

40. Kasai, D.; Fujinami, T.; Abe, T.; Mase, K.; Katayama, Y.; Fukuda, M.; Masai, E. Uncovering the Protocatechuate 2,3-Cleavage Pathway Genes. *J. Bacteriol.* **2009**, *191* (21), 6758–6768.

41. *MetaCyc* Pathway: protocatechuate degradation III (*para*-cleavage pathway). https://metacyc.org/META/NEW-IMAGE?type=NIL&object=PWY-6336&redirect=T (Accessed March 14, 2018).

42. Metanis, N.; Keinan, E.; Dawson, P. E. A Designed Synthetic Analogue of 4-OT Is Specific for a Non-Natural Substrate. *J. Am. Chem. Soc.* **2005**, *127* (16), 5862–5868.

43. Boger, D. L.; Patel, M. Chapter 2 - Recent Applications of the Inverse Electron Demand Diels-Alder Reaction. In *Progress in Heterocyclic Chemistry*; Suschitzky, H., Scriven, E. F. V., Eds.; Elsevier, 1989; Vol. 1, pp 30–64.

44. Yamamoto, Y. From Sigma- to Pi-Electrophilic Lewis Acids. Application to Selective Organic Transformations. *J. Org. Chem.* **2007**, *72* (21), 7817–7831.

45. Suzuki, T.; Noble, R. D.; Koval, C. A. Electrochemistry, Stability, and Alkene Complexation Chemistry of Copper(I) Triflate in Aqueous Solution. Potential for Use in Electrochemically Modulated Complexation-Based Separation Processes. *Inorg. Chem.* **1997**, *36* (2), 136–140.

46. Ridlen, S. G.; Wu, J.; Kulkarni, N. V.; Dias, H. V. R. Isolable Ethylene Complexes of Copper(I), Silver(I), and Gold(I) Supported by Fluorinated Scorpionates $[HB\{3\text{-}(CF_3),5\text{-}(CH_3)Pz\}_3]^-$ and $[HB\{3\text{-}(CF_3),5\text{-}(Ph)Pz\}_3]^-$. *Eur. J. Inorg. Chem.* **2016**, *2016* (15-16), 2573–2580.

47. Frost, J. W.; Miermont, A.; Schweitzer, D.; Bui, V. Preparation of *trans, trans*-Muconic Acid and *trans, trans* -Muconates. US 8,426,639 B2, 2013.

48. Miles, W. H.; Cohen, E. M.; Naimoli, B. J. Diels–Alder Reactions of β-Acylacrylic Acids. *Synth. Commun.* **2013**, *43* (14), 1980–1991.

49. Robinson, R.; Fray, G. I. Improved Process for Diels-Alder Additions. GB 835,840, 1960.

50. Robinson, R.; Fray, G. I. Process for the Production of Diels-Alder Adducts. U.S. 3,067,244, 1962.

51 Takenaka, S.; Yamamoto, K.; Nishida, T. Preparation of Cyclohexenecarboxylic Acid. JP S54157546 A, 1979.

52. Kobayashi, S. Lanthanide Trifluoromethanesulfonates as Stable Lewis Acids in Aqueous Media. $Yb(OTf)_3$ Catalyzed Hydroxymethylation Reaction of Silyl Enol Ethers with Commercial Formaldehyde Solution. *Chem. Lett.* **1991**, *20* (12), 2187–2190.

53. Kobayashi, S.; Hachiya, I.; Takahori, T.; Araki, M.; Ishitani, H. Lanthanide Trifluoromethanesulfonates as Reusable Catalysts. Michael and Diels-Alder Reactions. *Tetrahedron Lett.* **1992**, *33* (45), 6815–6818.

54. Pindur, U.; Lutz, G.; Otto, C. Acceleration and Selectivity Enhancement of Diels-Alder Reactions by Special and Catalytic Methods. *Chem. Rev.* **1993**, *93* (2), 741–761.

55. Corey, E. J.; Shibata, T.; Lee, T. W. Asymmetric Diels-Alder Reactions Catalyzed by a Triflic Acid Activated Chiral Oxazaborolidine. *J. Am. Chem. Soc.* **2002**, *124* (15), 3808–3809.

56. Li, P.; Yamamoto, H. Bifunctional Acid Catalysts for Organic Synthesis. In *Bifunctional Molecular Catalysis*; Ikariya, T., Shibasaki, M., Eds.; Springer Berlin Heidelberg: Berlin, Heidelberg, 2011; pp 161–183.

57. Yamamoto, H.; Futatsugi, K. "Designer Acids": Combined Acid Catalysis for Asymmetric Synthesis. *Angew. Chem. Int. Ed.* **2005**, *44* (13), 1924–1942.

58. Cairncross, J. R.; Roland, R. M.; Henderson, W. A.; Sheppard, A. F. J. Am. Chem. Soc. 1970, 92, 3187.

59 a) Shepard, A. F.; Winslow, N. R.; Johnson, J. R. The Simple Halogen Derivatives of Furan. *J. Am. Chem. Soc.* **1930**, *52* (5), 2083–2090. b) Shang, R.; Liu, L. Transition Metal-Catalyzed Decarboxylative Cross-Coupling Reactions. *Sci. China Chem.* **2011**, *54* (11), 1670–1687. c) Gooßen, L. J.; Rodríguez, N.; Gooßen, K. Carboxylic Acids as Substrates in Homogeneous Catalysis. *Angew. Chem. Int. Ed Engl.* **2008**, *47* (17), 3100–3120. d) Gooßen, L. J.; Gooßen, K.; Rodríguez, N.; Blanchot, M.; Linder, C.; Zimmermann, B. New Catalytic Transformations of Carboxylic Acids. *J. Macromol. Sci. Part A Pure Appl. Chem.* **2008**, *80* (8), 2084. e) L. J. Gooßen, K. Gooßen, N. Rodriguez, M. Blanchot, C. Linder, B. Zimmermann, *Pure Appl. Chem*. **2008**, 80, 1725. f) Rodríguez, N.; Gooßen, L. J. Decarboxylative Coupling Reactions: A Modern Strategy for C–C-Bond Formation. *Chem. Soc. Rev* **2011**, *40*, 5030–5048.

60. Cahiez, G.; Moyeux, A.; Gager, O.; Poizat, M. Copper-Catalyzed Decarboxylation of Aromatic Carboxylic Acids: En Route to Milder Reaction Conditions. *Adv. Synth. Catal.* **2013**, *355* (4), 790–796.

61. Cohen, T.; Schambach, R. A. Copper-Quinoline Decarboxylation. *J. Am. Chem. Soc.* **1970**, *92* (10), 3189–3190.

62. Whitesides, G. M.; Casey, C. P. The Stereochemistry of the Thermal Decomposition of Viylic Copper(I) and Silver(I) Organometallic Compounds1. *J. Am. Chem. Soc.* **1966**, *88* (19), 4541–4543.

63. Burdett, J. K.; Sevov, S. Stability of the Oxidation States of Copper. *J. Am. Chem. Soc.* **1995**, *117* (51), 12788–12792.

64. Biogas Potential in the United States; NREL/FS-6A20-60178, National Renewable Energy Laboratory, Energy Analysis: Golden, CO, 2013

65. Bricker, J. C.; Chen, J. Q.; Coughlin, P. K. Production of Oxygenates from a Methane Conversion Process, US 8,933,275, 2015.

66. Bricker, J. C.; Chen, J. Q.; Coughlin, P. K.; Majumder, D. Production of Vinyl Chloride from a Methane Conversion Process, US 9,308,513, 2015.

67. Gooßen, L. J.; Garrido, N. R.; Costa, F. M.; Lange, P. P. Process for Preparing a Propiolic Acid or Derivative Thereof, US 9,073,844, 2015.

68. Effenberger, F.; Ziegler, T. Diels-Alder-Reaktionen Mit 2H-Pyran-2-Onen: Reaktivität Und Selektivität. *Chem. Ber.* **1987**, *120* (8), 1339–1346.

69. Zhang, P.; Kriegel, R. M.; Frost, J. W. B–O–B Catalyzed Cycloadditions of Acrylic Acids. *ACS Sustainable Chem. Eng.* **2016**, *4* (12), 6991–6995.

70. Harwood, C. S.; Parales, R. E. The Beta-Ketoadipate Pathway and the Biology of Self-Identity. *Annu. Rev. Microbiol.* **1996**, *50*, 553–590.

71. a) Masai, E.; Katayama, Y.; Fukuda, M. Genetic and Biochemical Investigations on Bacterial Catabolic Pathways for Lignin-Derived Aromatic Compounds. *Biosci. Biotechnol. Biochem.* **2007**, *71* (1), 1–15. b) Noda, Y.; Nishikawa, S.; Shiozuka, K.; Kadokura, H.; Nakajima, H.; Yoda, K.; Katayama, Y.; Morohoshi, N.; Haraguchi, T.; Yamasaki, M. Molecular Cloning of the Protocatechuate 4,5-Dioxygenase Genes of Pseudomonas Paucimobilis. *J. Bacteriol.* **1990**, *172* (5), 2704–2709.

72. a) Crawford, R. L.; Bromley, J. W.; Perkins-Olson, P. E. Catabolism of Protocatechuate by Bacillus Macerans. *Appl. Environ. Microbiol.* **1979**, *37* (3), 614–618. b) Wolgel, S. A.; Lipscomb, J. D. Protocatechuate 2,3-Dioxygenase from Bacillus Macerans. *Methods Enzymol.* **1990**, *188*, 95–101.

73.Harayama, S.; Rekik, M.; Ngai, K. L.; Ornston, L. N. Physically Associated Enzymes Produce and Metabolize 2-Hydroxy-2,4-Dienoate, a Chemically Unstable Intermediate Formed in Catechol Metabolism via *meta*-Cleavage in *Pseudomonas putida*. *J. Bacteriol.* **1989**, *171* (11), 6251–6258.

74. Providenti, M. A.; Mampel, J.; MacSween, S.; Cook, A. M.; Wyndham, R. C. Comamonas Testosteroni BR6020 Possesses a Single Genetic Locus for Extradiol Cleavage of Protocatechuate. *Microbiology* **2001**, *147*, 2157–2167.

75. Maruyama, K.; Shibayama, T.; Ichikawa, A.; Sakou, Y.; Yamada, S.; Sugisaki, H. Cloning and Characterization of the Genes Encoding Enzymes for the Protocatechuate Meta-Degradation Pathway of Pseudomonas Ochraceae NGJ1. *Biosci. Biotechnol. Biochem.* **2004**, *68* (7), 1434–1441.

76. Eaton, R. W. Plasmid-Encoded Phthalate Catabolic Pathway in *Arthrobacter keyseri* 12B. *J. Bacteriol.* **2001**, *183* (12), 3689–3703.

77. Wolgel, S. A.; Dege, J. E.; Perkins-Olson, P. E.; Jaurez-Garcia, C. H.; Crawford, R. L.; Münck, E.; Lipscomb, J. D. Purification and Characterization of Protocatechuate 2,3-Dioxygenase from Bacillus Macerans: A New Extradiol Catecholic Dioxygenase. *J. Bacteriol.* **1993**, *175* (14), 4414–4426.

78. Pittard, J.; Wallace, B. J. Distribution and Function of Genes Concerned with Aromatic Biosynthesis in *Escherichia coli*. *J. Bacteriol.* **1966**, *91* (4), 1494–1508.

79. Li, K.; Frost, J. W. Synthesis of Vanillin from Glucose. *J. Am. Chem. Soc.* **1998**, *120* (40), 10545–10546.

80. Niu, W.; Draths, K. M.; Frost, J. W. Benzene-Free Synthesis of Adipic Acid. *Biotechnol. Prog.* **2002**, *18* (2), 201–211.

81. Draths, K. M.; Knop, D. R.; Frost, J. W. Shikimic acid and quinic acid: replacing isolation from plant sources with recombinant microbial biocatalysis. *J. Am. Chem. Soc.* **1999**, *121*, 1603-1604.

82. Knop, D. R.; Draths, K. M.; Chandran, S. S.; Barker, J. L.; von Daeniken, R.; Weber, W.; Frost, J. W. Hydroaromatic equilibration during biosynthesis of shikimic acid. J. *Am. Chem. Soc*. **2001**, *123*, 10173-10182.

843. Chandran, S. S.; Yi, J.; Draths, K. M.; von Daeniken, R.; Weber, W.; Frost, J. W. Phosphoenolpyruvate availability and the biosynthesis of shikimic acid. *Biotechnol. Prog*. **2003**, *19*, 808-814.

84. Dell, K. A.; Frost, J. W. Identification and removal of impediments to biocatalytic synthesis of aromatics from D-glucose: Rate-limiting enzymes in the common pathway of aromatic amino acid biosynthesis. *J. Am. Chem. Soc*. **1993**, *115*, 11581-11589.

85. Li, K.; Mikola, M. R.; Draths, K. M.; Worden, R. M.; Frost, J. W. Fed-batch fermentor synthesis of 3-dehydroshikimic acid using recombinant *Escherichia coli*. *Biotechnol. Bioeng.* **1999**, *64,* 61-73.

86. Draths, K. M.; Pompliano, D. L. Conley, D. L.; Frost, J. W.; Berry, A.; Disbrow, G. L.; Staversky, R. J.; Lievense, J. C. Biocatalytic synthesis of aromatics from D-glucose: The role of transketolase. *J. Am. Chem. Soc*. **1992**, *114*, 3956-3962.

87. Kambourakis, S.; Draths, K. M.; Frost, J. W. Synthesis of Gallic Acid and Pyrogallol from Glucose: Replacing Natural Product Isolation with Microbial Catalysis. *J. Am. Chem. Soc.* **2000**, *122* (37), 9042–9043.

88. Farabaugh, M. A. Biocatalytic Production of Aromatics from D-glucose. Master of Science, Michigan State University, 1996.

89. a) Garner, C. C.; Herrmann, K. M. Operator Mutations of the *Escherichia coli aroF* Gene. *J. Biol. Chem.* **1985**, *260* (6), 3820–3825. b) Schoner, R.; Herrmann, K. M. 3-Deoxy-D-*arabino*-Heptulosonate 7-Phosphate Synthase. Purification, Properties, and Kinetics of the Tyrosine-Sensitive Isoenzyme from *Escherichia coli*. *J. Biol. Chem.* **1976**, *251* (18), 5440–5447.

90. Cobbett, C. S.; Delbridge, M. L. Regulatory Mutants of the *aroF-tyrA* Operon of *Escherichia coli* K-12. *J. Bacteriol.* **1987**, *169* (6), 2500–2506.

91. Li, K.; Mikola, M. R.; Draths, K. M.; Worden, R. M.; Frost, J. W. Fed-Batch Fermentor Synthesis of 3-Dehydroshikimic Acid Using Recombinant *Escherichia coli*. *Biotechnol. Bioeng.* **1999**, *64* (1), 61–73.

92. Anderson, J.; Dueber, J. E.; Leguia, M.; Wu, G. C.; Goler, J. A.; Arkin, A. P.; Keasling, J. D. BglBricks: A Flexible Standard for Biological Part Assembly. *J. Biol. Eng.* **2010**, *4* (1), 1.

93. Lee, T. S.; Krupa, R. A.; Zhang, F.; Hajimorad, M.; Holtz, W. J.; Prasad, N.; Lee, S. K.; Keasling, J. D. BglBrick Vectors and Datasheets: A Synthetic Biology Platform for Gene Expression. *J. Biol. Eng.* **2011**, *5*, 12.

94. Mischo, H. E.; Proudfoot, N. J. Disengaging Polymerase: Terminating RNA Polymerase II Transcription in Budding Yeast. *Biochim. Biophys. Acta* **2013**, *1829* (1), 174–185.

95. Schoner, R.; Herrmann, K. M. 3-Deoxy-D-*arabino*-Heptulosonate 7-Phosphate Synthase. Purification, Properties, and Kinetics of the Tyrosine-Sensitive Isoenzyme from *Escherichia coli.* *J. Biol. Chem.* **1976**, *251* (18), 5440–5447.

96. Lian, H.; Czerwinski, R. M.; Stanley, T. M.; Johnson, W. H.; Watson, R. J.; Whitman, C. P. The Contribution of the Substrate's Carboxylate Group to the Mechanism of 4-Oxalocrotonate Tautomerase. *Bioorg. Chem.* **1998**, *26* (3), 141–156.

97. Whitman, C. P. The 4-Oxalocrotonate Tautomerase Family of Enzymes: How Nature Makes New Enzymes Using a Beta-Alpha-Beta Structural Motif. *Arch. Biochem. Biophys.* **2002**, *402* (1), 1–13.

98. Almrud, J. J.; Kern, A. D.; Wang, S. C.; Czerwinski, R. M.; Johnson, W. H.; Murzin, A. G.; Hackert, M. L.; Whitman, C. P. The Crystal Structure of YdcE, a 4-Oxalocrotonate Tautomerase Homologue from *Escherichia coli*, Confirms the Structural Basis for Oligomer Diversity,. *Biochemistry* **2002**, *41* (40), 12010–12024.

99. Wang, S. C.; Johnson, W. H.; Czerwinski, R. M.; Whitman, C. P. Reactions of 4-Oxalocrotonate Tautomerase and YwhB with 3-Halopropiolates: Analysis and Implications. *Biochemistry* **2004**, *43* (3), 748–758.

100. Whitman, C. P.; Aird, B. A.; Gillespie, W. R.; Stolowich, N. J. Chemical and Enzymic Ketonization of 2-Hydroxymuconate, a Conjugated Enol. *J. Am. Chem. Soc.* **1991**, *113* (8), 3154–3162.

101. Huddleston, J. P.; Burks, E. A.; Whitman, C. P. Identification and Characterization of New Family Members in the Tautomerase Superfamily: Analysis and Implications. *Arch. Biochem. Biophys.* **2014**, *564*, 189–196.

102. Whitman, C. P.; Hajipour, G.; Watson, R. J.; Johnson, W. H.; Bembenek, M. E.; Stolowich, N. J. Stereospecific Ketonization of 2-Hydroxymuconate by 4-Oxalocrotonate Tautomerase and 5-(Carboxymethyl)-2-Hydroxymuconate Isomerase. *J. Am. Chem. Soc.* **1992**, *114* (26), 10104–10110.

103. Datsenko, K. A.; Wanner, B. L. One-Step Inactivation of Chromosomal Genes in *Escherichia coli* K-12 Using PCR Products. *Proc. Natl. Acad. Sci. U. S. A.* **2000**, *97* (12), 6640–6645.

104.Velders, G. J. M.; Feil, D. Comparison of the Hartree-Fock, Møller-Plesset, and Hartree-Fock-Slater Method with Respect to Electrostatic Properties of Small Molecules. *Theor. Chim. Acta* **1993**, *86* (5), 391–416.

105. Samiee, L.; Dehghani, M. M.; Karami, R.; Ayazi, M. Developing of Ethylene Glycol as a New Reducing Agent for Preparation of Pd-Ag/PSS Composite Membrane for Hydrogen Separation. **2012**.

106.Skrabalak, S. E.; Wiley, B. J.; Kim, M.; Formo, E. V.; Xia, Y. On the Polyol Synthesis of Silver Nanostructures: Glycolaldehyde as a Reducing Agent. *Nano Lett.* **2008**, *8* (7), 2077–2081.

107. Guzman, A.; Arroyo, J.; Verde, L.; Rengifo, J. Synthesis and Characterization of Copper Nanoparticles/Polyvinyl Chloride (Cu NPs/PVC) Nanocomposites. *Procedia Materials Science* **2015**, *9*, 298–304.

108. Asao, N.; Nogami, T.; Lee, S.; Yamamoto, Y. Lewis Acid-Catalyzed Benzannulation via Unprecedented [4+2] Cycloaddition of O-Alkynyl(oxo)benzenes and Enynals with Alkynes. *J. Am. Chem. Soc.* **2003**, *125* (36), 10921–10925.

109. *The BioBrick approach*. https://j5.jbei.org/j5manual/pages/21.html (Accessed 20 Aug. 2018).

CHAPTER TWO: HETEROLOGOUS EXPRESSION OF KANOSAMINE BIOSYNTHESIS PATHWAYS IN *ESCHERICHIA COLI*

INTRODUCTION

Soil-borne plant pathogens are responsible for causing many plant diseases.[1] Widespread crop infection can result in significant economic losses. Bacteria angatonistic to these pathogens have been isolated from the rhizosphere and used either alone or in conjunction with chemical biocontrol agents to control major crop diseases caused by pathogenic fungi and bacteria.[1-18] In particular, microbes of the genus *Bacillus* have been of interest for use in biocontrol strategies. *Bacillus* species are attractive candidates for biocontrol agents in agricultural applications due to their ability to produce a wide variety of bio-active compounds (Figure 45) and tendency to induce plant defense and growth.

The many compounds produced and exported by members of the genus *Bacillus*, some of which are depicted in Figure 45, have various modes of action. Some lipopeptides directly inhibit fungal growth, such as iturin A[17] against *Rhizoctonia solani*, while others including surfactin[8,9] and fengycin[8] induce systemic resistance in plants. In bean and tomato plants, surfactin and fengycin induce plant cells to activate lipoxygenase and lipid hydroperoxidase enzymes. These enzymes are crucial for degradation of linolenic and linoleic acids to biologically active small molecules.

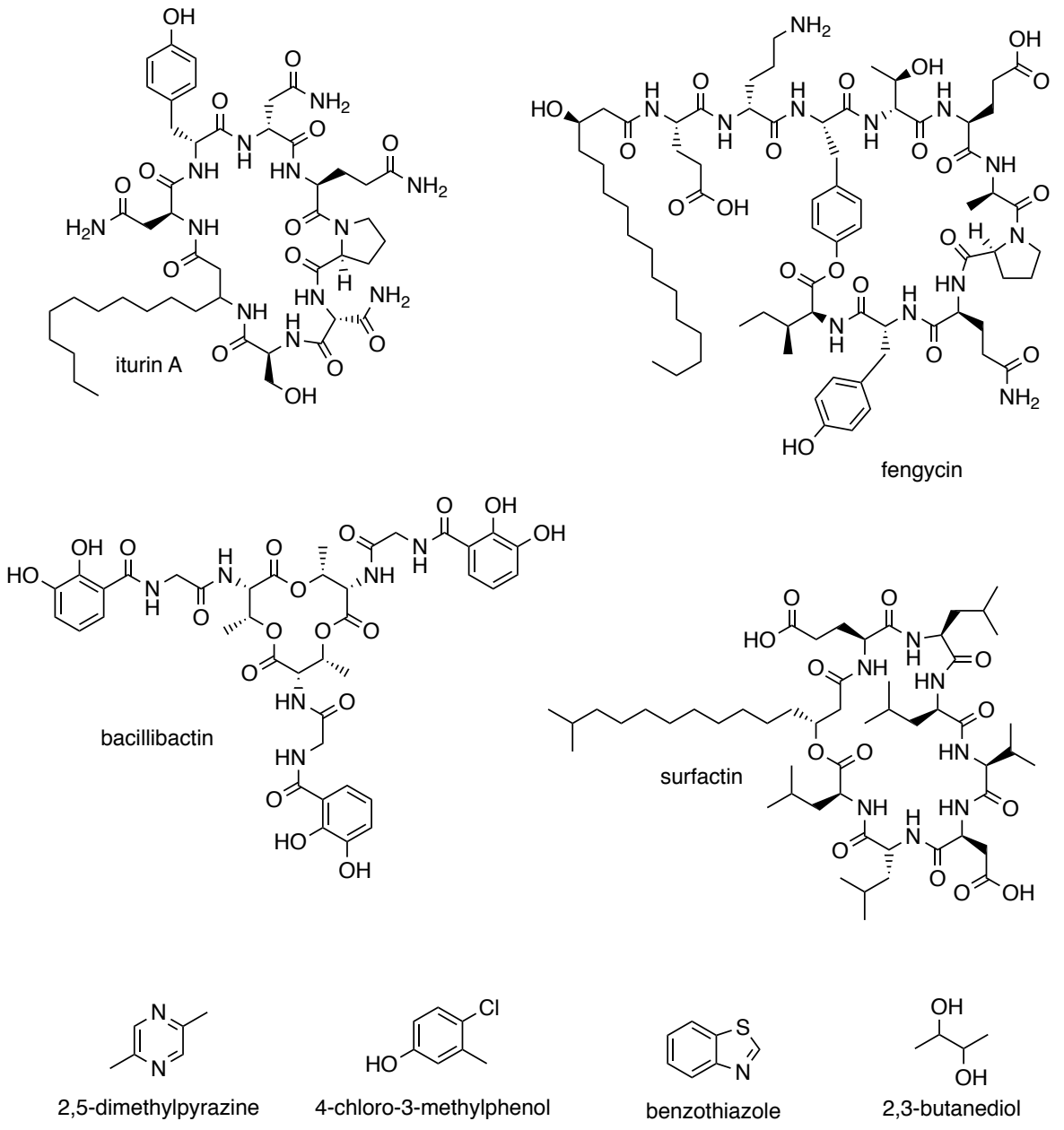

Figure 45. Biologically active lipopeptides, siderophores, and volatile organic compounds produced by *Bacillus* spp.

Organic compounds produced by *Bacillus* spp., including 2,5-dimethylpyrazine, benzothiazole, 4-chloro-3-methylphenol, directly inhibit growth of pathogenic fungi[17] but may possess additional bioactivity. For example, 2,3-butanediol imparts resistance to *Erwinia carotovora* via an ethylene-dependent pathway and also induces growth responses in certain

strains of the mustard plant, *Arabidopsis thaliana*.[15] Siderophores and phytohormones produced by *Bacillus* spp. have been found to impact the growth of various plants. For example, red peppers treated with bacillibactin, a catecholic siderophore, grew 27-54% taller, bore fruit that was 37% heavier, and flowered 17 days sooner than untreated plants. Treated pepper also had reduced instance of *Fusarium* wilt (12-57%) relative to untreated plants.[16] Products based on *Bacillus* spp. currently commercialized by phytopharmaceutical companies include EcoGuard® by Novozymes[11] (*Bacillus lichenformis* isolate SB3086), Serenade® by Bayer[12] (*Bacillus subtilis* isolate QST30002), and Kodiak® by Gustafson[13] (*Bacillus subtilis* isolate GB03).

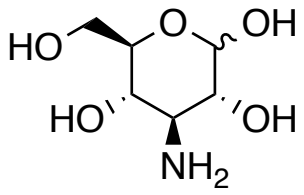

kanosamine

Figure 46. Structure of kanosamine (3-amino-3-deoxy-D-glucose).

Among the biologically active compounds produced and exported by *Bacillus* spp. is kanosamine (3-amino-3-deoxy-D-glucose, Figure 46). Unlike other aminosugars of natural origin which are produced as a structural component of larger compounds, kanosamine is the only aminosugar to be exported in a free, monomeric form.[19] Like the compounds described above, kanosamine also displays important biological activity in the environment. For example, kanosamine inhibits the growth of the oomycete *Phytophthora medicaginis*, a fungus-like eukaryote responsible for damping-off disease in alfalfa, as well as select phytopathogenic fungi including *Venturia inaequalis* (apple scab) and *Ustilago maydis* (corn smut).[20] Minimal

inhibitory concentrations of kanosamine against many bacteria and yeasts are high (Table 17), but in combination with other antibiotics produced by *Bacillus* spp. such as zwittermycin A, kanosamine displays additive or synergistic activity.[23,24] Equipping crops with the genes required for kanosamine biosynthesis or incorporating a kanosamine-overproducing organism into soil alongside *Bacillus* spp. could serve as biocontrol strategies that both enhance plant resistance to pathogenic fungi and strengthen the inhibitory effects of antibiotic compounds produced by *Bacillus* spp. currently utilized for biocontrol of phytopathogens

Table 17. Minimal inhibitory concentrations of kanosamine against various bacteria and yeast.

Organism	MIC (μg/mL)	Reference
Staphylococcus aureus FDA 209P	50	21
S. aureus FDA 209P JC-1	100	21
S. aureus FS-1227 (penicillin resistant)	100	21
Sarcina lutea PCI 1001	100	21
Cytophaga johnsonae	300	21
Escherichia coli NIHJ JC-2	>800	21
Salmonella typhimurium	>800	21
Pseudomonas aeruginosa P-3	>800	21
Candida albicans ATCC 26278	1,250	22
Escherichia coli IAM 1253	>2,000	30
Saccharomyces cerevisiae ATCC 9763	2,500	22

Two pathways have been elucidated for kanosamine biosynthesis in different *Bacillus* strains. In *Bacillus subtilis* (Figure 47) kanosamine is biosynthesized from D-glucose-6-phosphate through a pathway beginning with dehydrogenation to afford 3-keto-D-glucose-6-

phosphate. The C-3 keto functionality is converted to an amine by an L-glutamate-dependent aminotransferase, followed by hydrolysis of the phosphate monoester of kanosamine-6-phosphate. This pathway was first discovered in 2013 from *in vitro* experiments using purified Ntd proteins.[25] The *ntdC*, *ntdA*, and *ntdB* genes of *B. subtilis* encode, respectively, D-glucose-6-phosphate 3-dehydrogenase, 3-keto-D-glucose-6-phosphate:L-glutamate aminotransferase, and kanosamine-6-phosphate kinase. Crystal structures of NtdA[26] and kinetic studies of NtdC have been published.

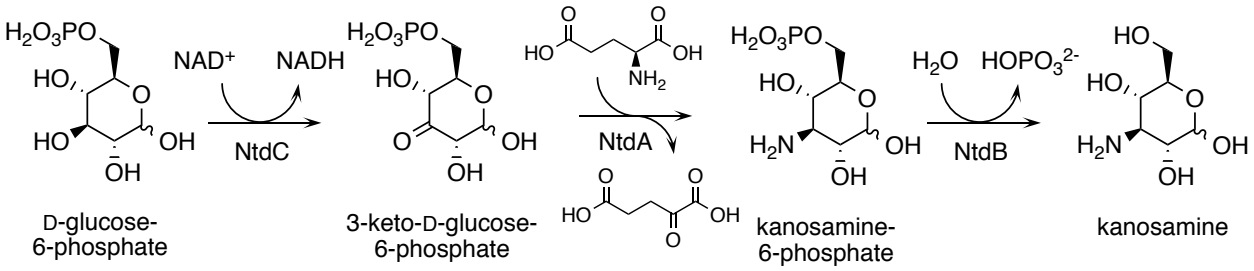

Figure 47. Kanosamine biosynthesis from D-glucose-6-phosphate described in *Bacillus subtilis*.

An alternate pathway was described in *Bacillus cereus*[28] and *Bacillus pumilus*.[29] The pathway (Figure 48) begins with UDP-D-glucose, which undergoes a similar reaction sequence of oxidation, transamination, and hydrolysis to afford kanosamine. This pathway was first described in 1967 based on in vitro experiments using cell-free extracts of *B. pumilus*.[30] Using a reaction mixture consisting of cell-free extract, uniformly labeled D-[U-^{14}C]-glucose, $MgSO_4$, NAD^+, L-glutamine, ATP, and UTP in phosphate buffer the total radioactivity of the kanosamine produced was 2,800 counts per minute (cpm). This value fell to 215 cpm if both ATP and UTP

were omitted from the reaction mixture. The observed requirement for ATP and UTP led to the proposed pathway shown in Figure 48.[30]

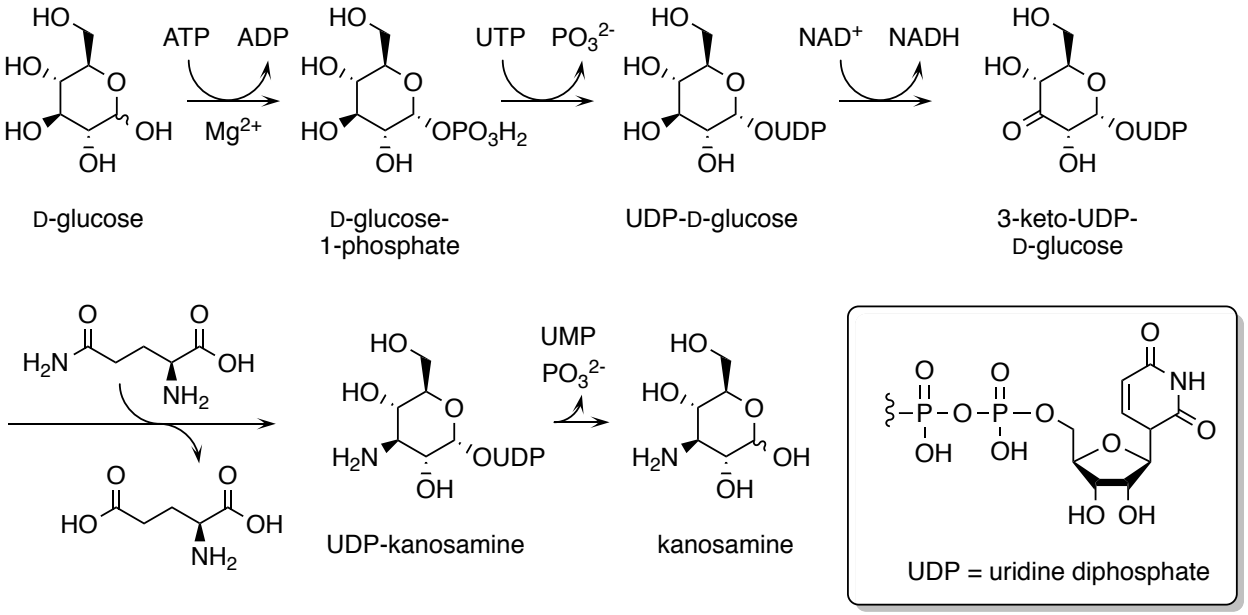

Figure 48. Kanosamine biosynthesis pathway via UDP-D-glucose as proposed by Umezawa.[30]

In other bacterial species, kanosamine serves as a biosynthetic precursor to 3-amino-5-hydroxybenzoic acid (AHBA), which serves as a core for the ansamycins, including the rifamycins, and the mitomycin families of antibiotics (Figure 49).[31] AHBA produced via the aminoshikimate pathway (Figure 50) is required in the biosynthesis of a variety of secondary metabolites with biological activity.[31] .

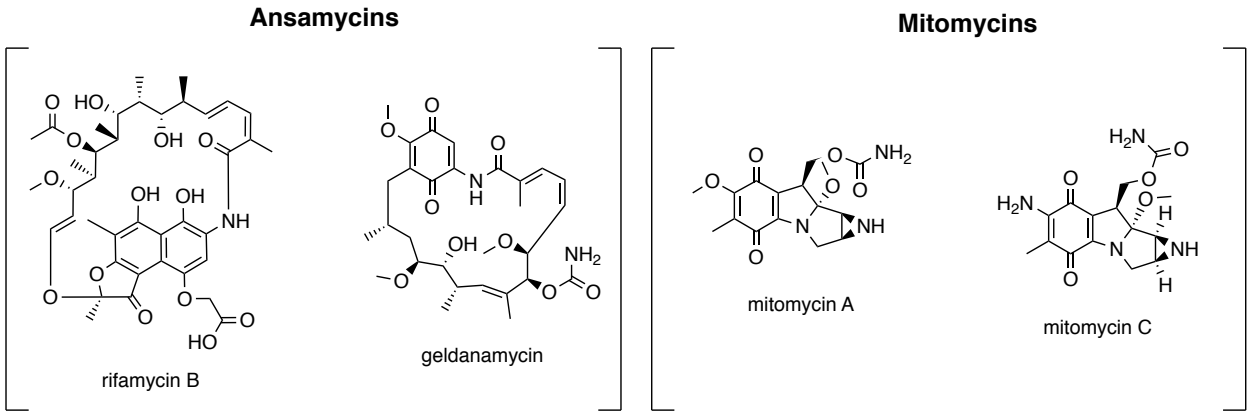

Figure 49. Representative members of the ansamycin and mitomycin families of antibiotics.

The AHBA biosynthesis gene cluster was described in the rifamycin-producing organism, *Amycolatopsis mediterranei*, which is a Gram positive bacteria of the family *Actinobacteria* distinguished by their high genomic G+C content ranging from 51% to over 70% G+C.[32] The functions of many AHBA biosynthesis enzymes were assigned using feeding experiments with a variety of labeled precursors and genetic mutants.[33,34] The origin of 3-amino-3-deoxy-D-*arabino*-heptulosonate-7-phosphate (aminoDAHP) biosynthesis remained unknown for several years following sequencing of the AHBA biosynthesis gene cluster. Progress was made following the discovery of an essential transketolase-encoding gene, *orf15AB*, within the AHBA biosynthesis genes, suggesting that aminoDAHP may be produced from condensation of phosphoenolpyruvate (PEP) and a nitrogen-containing analog of erythrose-4-phosphate (E4P).[34]

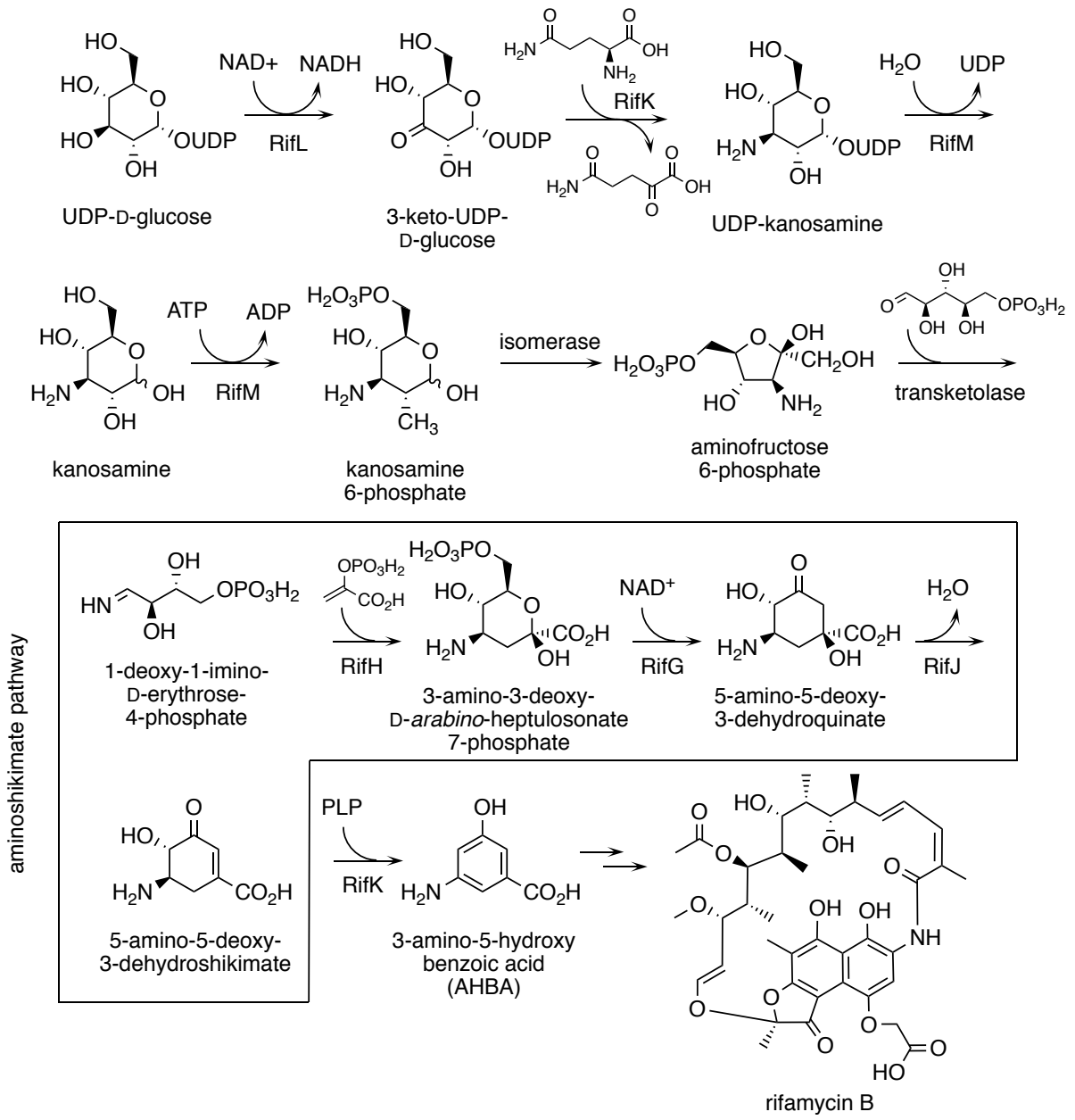

Figure 50. Synthesis of kanosamine from UDP-D-glucose and the formation of 3-amino-5-hydroxybenzoic acid via the aminoshikimate pathway in *Amycolatopsis mediterranei.*

This hypothesis was proven when incubation of 3-amino-3-deoxyfructose-6-phosphate (aminoF6P), PEP, and ribose-5-phosphate with purified *rifH*-encoded aminoDAHP synthase afforded aminoDAHP in 2% yield and DAHP in 35% yield.[36] An *E. coli* transketolase-catalyzed reaction of 3-[^{15}N]-6,6-[$^{2}H_2$]-aminoF6P demonstrated that the framework and nitrogen atom of

aminoF6P is incorporated into aminoDAHP.[35] The origin of aminoF6P in the aminoshikimate pathway was confirmed following incubation of kanosamine-6-phosphate, ribose-5-phosphate, and PEP with *E. coli tktA*-encoded transketolase, yeast phosphoglucose isomerase, and *rifH*-encoded aminoDAHP synthase.[37] Isomerization of kanosamine-6-phosphate to aminoF6P catalyzed by yeast phosphoglucose isomerase during the reaction resulted in accumulation of aminoDAHP and DAHP in 2% and 30% yields, respectively. Repeating the incubation of kanosamine-6-phosphate with *A. mediterranei* cell-free extract in place of *E. coli tktA*-encoded transketolase, yeast phosphoglucose isomerase, and purified *rifH*-encoded aminoDAHP synthase afforded aminoDAHP and DAHP in 6% and 20% yields, respectively, along with AHBA (2% yield), tyrosine (3% yield), and phenylalanine (2% yield).[37]

In this work, genes encoding kanosamine biosynthetic enzymes from *B. subtilis*, *A. mediterranei*, and *B. pumilus* are expressed in *Escherichia coli* to determine whether heterologous expression results in kanosamine accumulation and if the system can be manipulated to maximize kanosamine production. Recombinant *E. coli* are evaluated in fed-batch fermentation at 2 L scale using two substrate feeding regimes. Kanosamine does not inhibit growth of *E. coli* strains used in the fermentations and can be isolated from fermentation broth. Recombinant *E. coli* expressing genes from *B. subtilis* 168 produces 12.7 ± 0.6 g/L kanosamine in a 4.4 ± 0.4% mol/mol yield from D-glucose via the D-glucose-6-phosphate 3-dehydrogenation-pathway described above. Kanosamine yields were increased to 18 ± 1% mol/mol by blocking the Embden-Meyerhoff-Parnas pathway through a mutation in *pgi*-encoded phosphoglucose isomerase. *Amycolatopsis mediterranei* S699 enzymes prove to be challenging to express efficiently in *E. coli* and did not result in kanosamine accumulation via UDP-D-

glucose in fermentation broth. In light of this, *B. pumilus* was examined as a source of kanosamine biosynthesis genes in order to evaluate kanosamine production from UDP-D-glucose. Expression of *B. pumilus* SH-B11 genes in *E. coli* results in 6.3 g/L kanosamine titers in 4.4% mol/mol yield from D-glucose in glucose-limited fermentations. Surprisingly, our results indicate that *B. pumilus* does not utilize UDP-D-glucose but rather D-glucose-6-phosphate, which suggests a departure from what is in the literature regarding kanosamine production in *Bacillus pumilus*.

PART I

KANOSAMINE PRODUCTION VIA EXPRESSION OF *BACILLUS SUBTILIS* GENES

1. Variations in gene arrangement and promoter strength

Bacillus subtilis 168 is a common strain employed during studies of biocontrol methods on various plants. Kanosamine biosynthesis in *B. subtilis* has been reported to proceed via D-glucose-6-phosphate in a sequence of three reactions catalyzed by *ntdC*-encoded D-glucose-6-phosphate 3-dehydrogenase, *ntdA*-encoded 3-keto-D-glucose-6-phosphate:L-glutamate aminotransferase, and *ntdB*-encoded kanosamine-6-phosphate phosphatase (Figure 46).[25] For expression of these enzymes in *E. coli*, the BglBrick assembly standard of cloning was used to build a plasmid which harbored *ntdC*, *ntdA*, and *ntdB*, as well as *serA*. All bacterial strains and plasmids used in this Chapter are presented in Table 18. As described in Chapter 1, *E. coli* strains used in this study carry a mutation in the *serA* locus of the genome which prevents the synthesis of L-serine. Plasmid-localized *serA* serves as the basis of plasmid maintenance when cells are cultured in a defined minimal media.

Table 18. Strains and plasmids used in Chapter 2 of this work.

Strain/plasmid	Relevant characteristics	Source or reference
Escherichia coli DH5α	*F' ϕ80lacZΔM15* Δ(*lacZYA-argF)U169 deoR recA1 endA1 hsdR17*(r_k^-, m_k^+) *phoA* λ^- *supE44 thi-1 gyrA96 relA1*	Invitrogen
Escherichia coli AB2834	*tsx-352 glnV42 aroE353 malT352* λ^-	Coli Genetic Stock Center[58]
Escherichia coli KL3	AB2834 *serA*::*aroB*	lab[54]
Escherichia coli W3110	F^- *IN(rrnD-rrnE)1* λ^- *rph1*	
Escherichia coli RB791*serA*	W3110 *lacL8*I^q *serA*	lab[40]

Table 18 (cont'd)

Escherichia coli RB791*serA*(DE3)	RB791*serA λ(DE3)*	lab[56]
Escherichia coli RB791*serA pgi*::Kan^R	RB791*serA pgi*::*Kan*^{R}	lab[46]
Bacillus subtilis 168	source for *ntdA*^{sub}*ntdB*^{sub}*ntdC*^{sub}	ATCC 23857
pBbA1a-RFP	Ap^R, *lacI*^{q}, P_{trc}*rfp* p15A replicon	Addgene #35334[57]
pBbA7k-RFP	Kan^R, *lacI*^{q}, P_{T7}*rfp*, p15A replicon	Addgene #35318[57]
pKM6.240	P_{trc}*serA* in pBbA1a	Chapter 1
pSN1.294	P_{trc}*ntdC*^{sub}	lab (described herein)
pSN1.295	P_{trc}*ntdB*^{sub}	lab (described herein)
pSN1.296	P_{trc}*ntdA*^{sub}	lab (described herein)
pSN1.119	P_{trc}*ntdC*^{sub}*ntdA*^{sub} in pBbA1a	lab (described herein)
pSN1.139	P_{trc}*ntdC*^{sub}*ntdA*^{sub}*ntdB*^{sub} in pBbA1a	lab (described herein)
pSN1.292	P_{trc}*ntdC*^{sub}*ntdA*^{sub}*ntdB*^{sub}*serA* in pBbA1a	lab (described herein)
pJG7.246	Ap^R, P_{T5}, His$_6$, *lacI*^{q}, ColE1 replicon	lab[49]
pKM9.279C	P_{T5}His$_6$-*ntdC*^{sub} in pJG7.246	this work
pKM10.82A	P_{T7}*ntdC*^{sub}*ntdA*^{sub}*ntdB*^{sub}*serA* in pBbA7k	this work
pKM10.204A	P_{trc}*ntdA*^{sub}*serA* in pBbA1a	this work
pKM10.204B	P_{trc}*ntdB*^{sub}*serA* in pBbA1a	this work
pKM10.204C	P_{trc}*ntdC*^{sub}*serA* in pBbA1a	this work
pKM10.214CA	P_{trc}*ntdC*^{sub}*ntdA*^{sub}*serA* in pBbA1a	this work
pKM10.214CB	P_{trc}*ntdC*^{sub}*ntdB*^{sub}*serA* in pBbA1a	this work
pKM10.214AB	P_{trc}*ntdA*^{sub}*ntdB*^{sub}*serA* in pBbA1a	this work
pKM10.214BC	P_{trc}*ntdB*^{sub}*ntdC*^{sub}*serA* in pBbA1a	this work
pKM10.220ABC	P_{trc}*ntdA*^{sub}*ntdB*^{sub}*ntdC*^{sub}*serA* in pBbA1a	this work
pUCIDT(Kan)-rifK	Kan^R, P_{lac}, codon optimized *rifK*, ColE1 replicon	IDT
pUCIDT(Kan)-rifL	Kan^R, P_{lac}, codon optimized *rifL*, ColE1 replicon	IDT
pUCIDT(Kan)-rifM	Kan^R, P_{lac}, codon optimized *rifM*, ColE1 replicon	IDT

Table 18 (cont'd)

pKM10.254K	P_{trc}*rifK* in pBbA1a	this work
pKM10.254L	P_{trc}*rifL* in pBbA1a	this work
pKM10.254M	P_{trc}*rifM* in pBbA1a	this work
pKM10.268K	P_{trc}*rifKserA* in pBbA1a	this work
pKM10.268L	P_{trc}*rifLserA* in pBbA1a	this work
pKM10.268M	P_{trc}*rifMserA* in pBbA1a	this work
pKM10.278KM	P_{trc}*rifKrifMserA* in pBbA1a	this work
pKM10.284L	P_{T5}His$_6$-*rifL* in pJG7.246	this work
pKM11.9	P_{trc}*rifLrifKrifMserA* in pBbA1a	this work
pKM11.46	P_{T7}*rifLrifKrifMserA* in pBbA7k	this work
pUCIDT(Kan)-ntdA	Kan^R, P_{lac}, *ntdA*^{pum}, ColE1 replicon	IDT
pUCIDT(Kan)-ntdB	Kan^R, P_{lac}, *ntdB*^{pum}, ColE1 replicon	IDT
pUCIDT(Kan)-ntdC	Kan^R, P_{lac}, *ntdC*^{pum}, ColE1 replicon	IDT
pKM11.121A	P_{trc}*ntdA*^{pum} in pBbA1a	this work
pKM11.121B	P_{trc}*ntdB*^{pum} in pBbA1a	this work
pKM11.121C	P_{trc}*ntdC*^{pum} in pBbA1a	this work
pKM11.125	P_{trc}*ntdB*^{pum}*serA* in pBbA1a	this work
pKM11.130	P_{trc}*ntdC*^{pum}*ntdA*^{pum} in pBbA1a	this work
pKM11.135	P_{trc}*ntdC*^{pum}*ntdA*^{pum}*ntdB*^{pum}*serA* in pBbA1a	this work

The *ntd* genes were PCR-amplified (Figure 51) from *B. subtilis* 168 genomic DNA with 5' *Eco*RI and *Bgl*II and 3' *Bam*HI and *Xho*I sites. Each gene was first inserted into the *EcoRI* and *Xho*I sites of plasmid pBbA1a to afford a BglBrick part (Figure 51). These parts were used in the BglBrick assembly standard by iteratively inserting one gene in front of another using a routine sequence of digestion and ligations. Firstly, each *ntd* gene was inserted upstream of *serA* by digesting the BglBrick part containing *serA*, pKM6.240 (Figure 51), with *Eco*RI and *Bgl*II to create a double-stranded break upstream of *serA*. Digestion of the *ntd*-containing BglBrick parts, pSN1.294, pSN1.295, and pSN1.296 (Figure 51), with *Eco*RI and *Bam*HI followed by ligation of

the digested DNA afforded pSN1.288, pKM10.204A, and pKM10.204C. During the ligation, the *Eco*RI site was reformed and the complementary cohesive *Bam*HI and *Bgl*II digested DNA ends created a glycine-serine scar sequence between *ntdB* and *serA*. Importantly for the BglBrick assembly standard, all four restriction sites (*Eco*RI, *Bgl*II, *Bam*HI, *Xho*I) that were originally present in the pKM6.240 recipient plasmid remain in the new plasmid. This allows repeated cycles of digesting the vector plasmid with *Eco*RI and *Bgl*II, digesting the plasmid containing the desired insert with *Eco*RI and *Bam*HI, and using T4 DNA ligase to reform the *Eco*RI site and create a glycine-serine scar sequence between the newly inserted gene and the gene at the 5' end of the operon. Using this method, *ntdC* was inserted upstream of *ntdA* in plasmid pSN1.296 to afford pSN1.119 (Figure 52) which contained a P_{trc}*ntdCntdA* cassette. The *trc* promoter is encoded on the original BglBrick vector, pBbA1a, and is optimally positioned for expression of the inserted genes. The *ntdCntdA* fragment was inserted upstream of *ntdB* in plasmid pSN1.295 to afford pSN1.139, which contained a P_{trc}*ntdCntdAntdB* cassette (Figure 53). Finally, the *ntdCntdAntdB* gene fragment was inserted upstream of *serA* in plasmid pKM6.240 to afford plasmid pSN1.292, containing a P_{trc}*ntdCntdAntdBserA* cassette (Figure 54). Similarly, a plasmid was created that contained a P_{trc}*ntdAntdBntdCserA* cassette by inserting *ntdB* from pSN1.295 into pKM10.204C (Figure 55) to afford pKM10.214BC (Figure 56), followed by insertion of *ntdA* from pSN1.296 into pKM10.214BC to afford pKM10.220ABC, containing the full set of *ntd* genes (Figure 57).

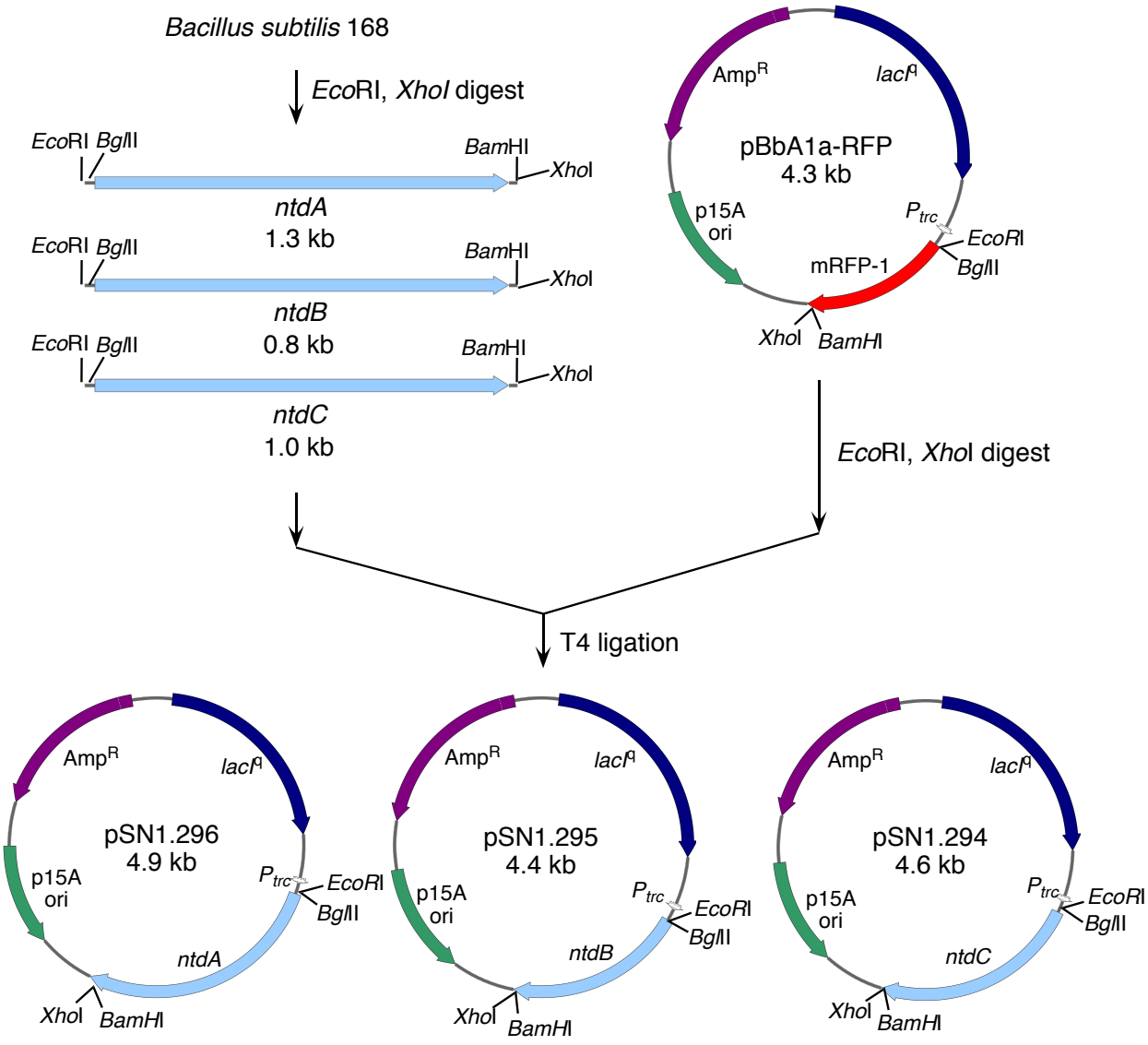

Figure 51. Construction of *ntd* BglBrick parts: plasmids pSN1.296, pSN1.295, and pSN1.294

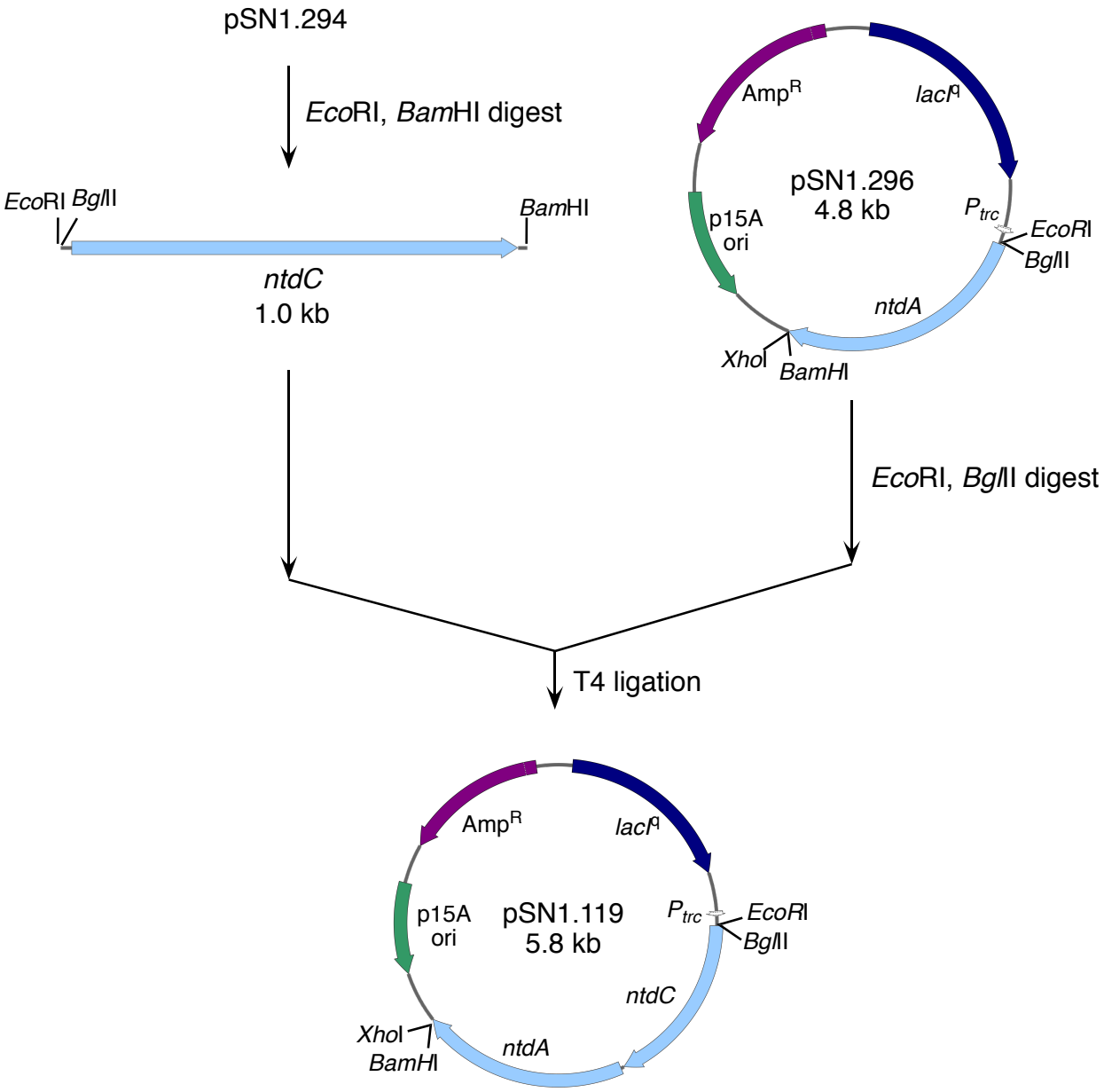

Figure 52. Construction of plasmid pSN1.119.

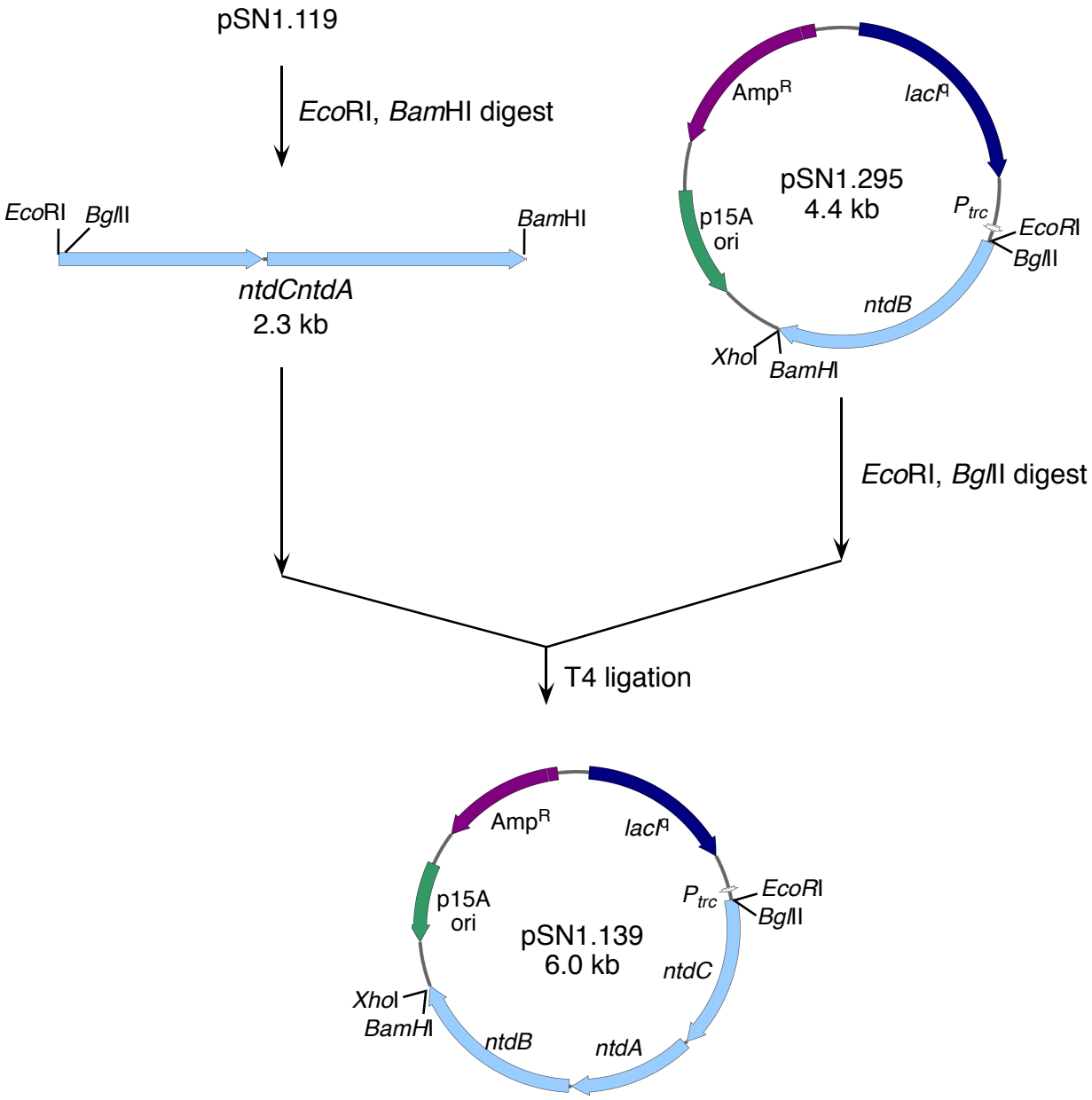

Figure 53. Construction of plasmid pSN1.139.

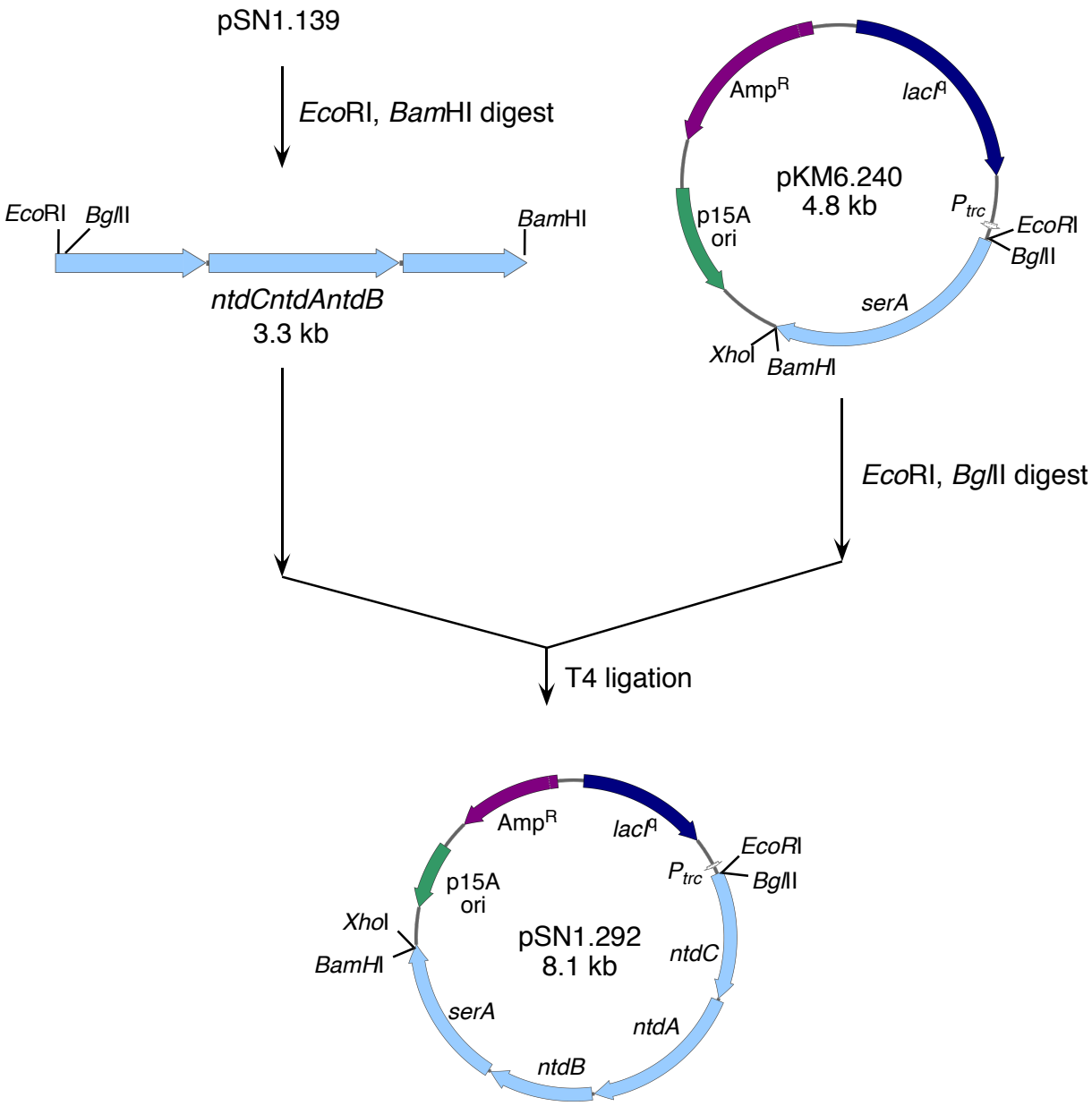

Figure 54. Construction of plasmid pSN1.292.

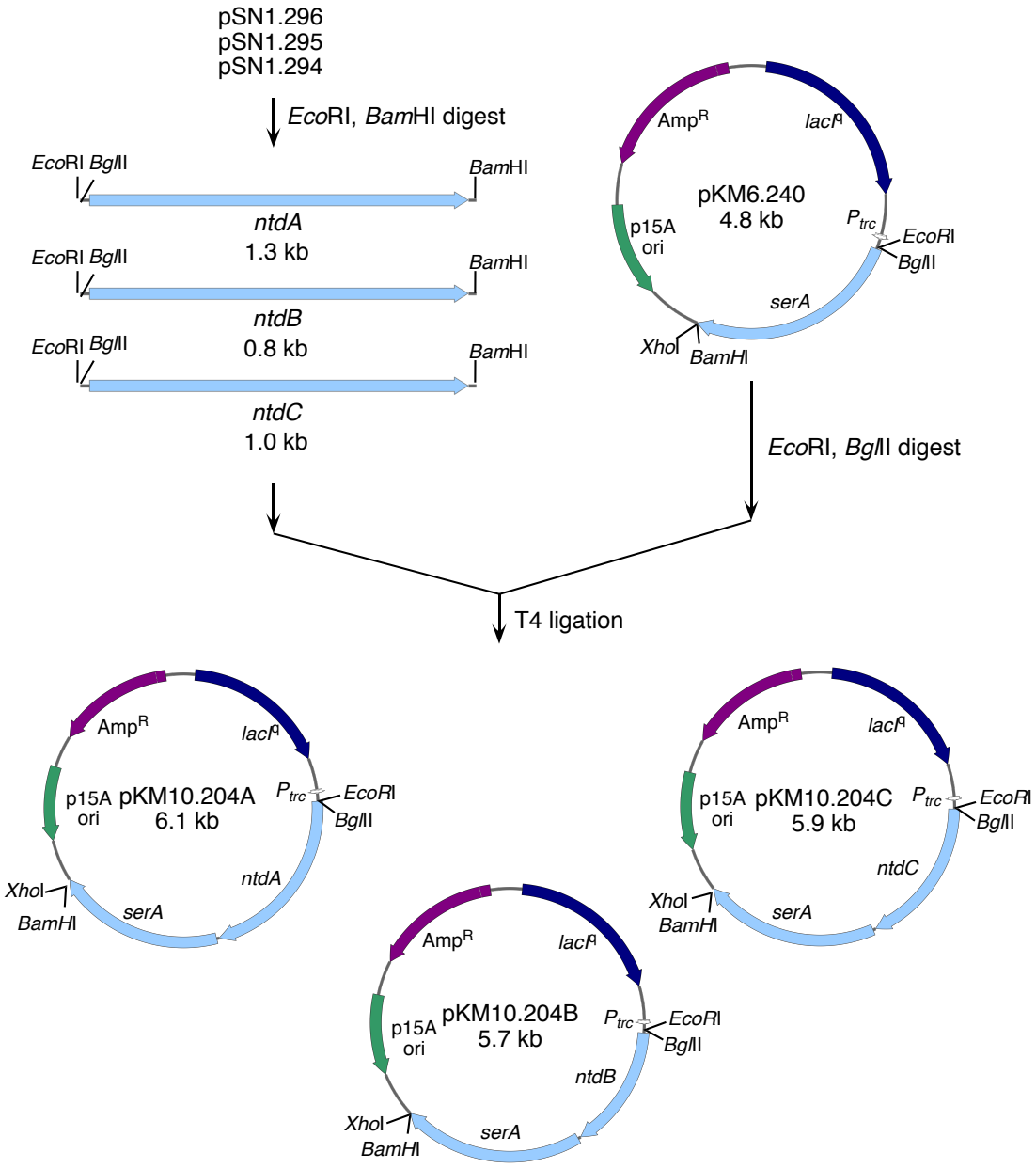

Figure 55. Construction of plasmids pKM10.204A, pKM10.204B, and pKM10.204C.

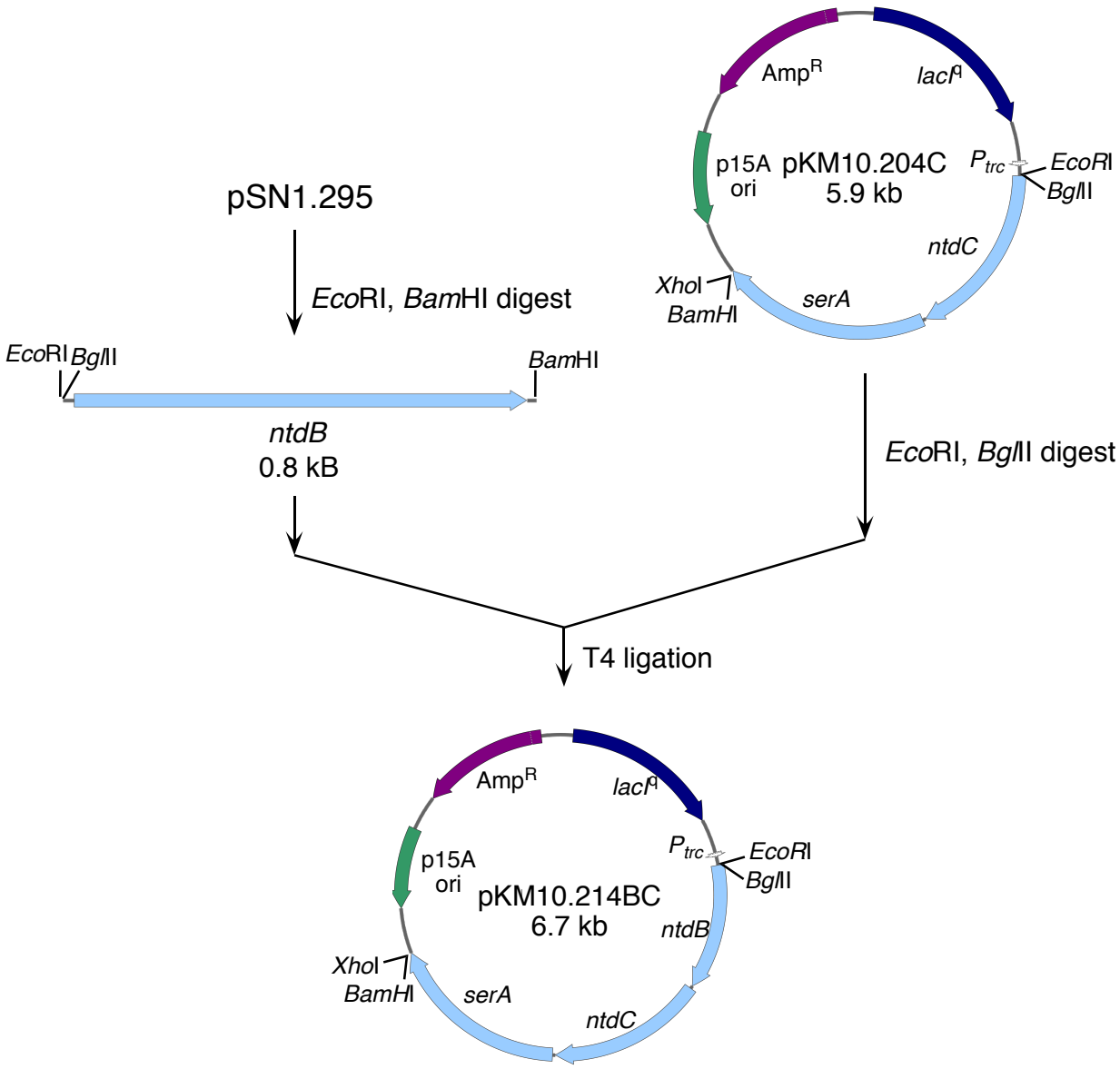

Figure 56. Construction of plasmid pKM10.214BC.

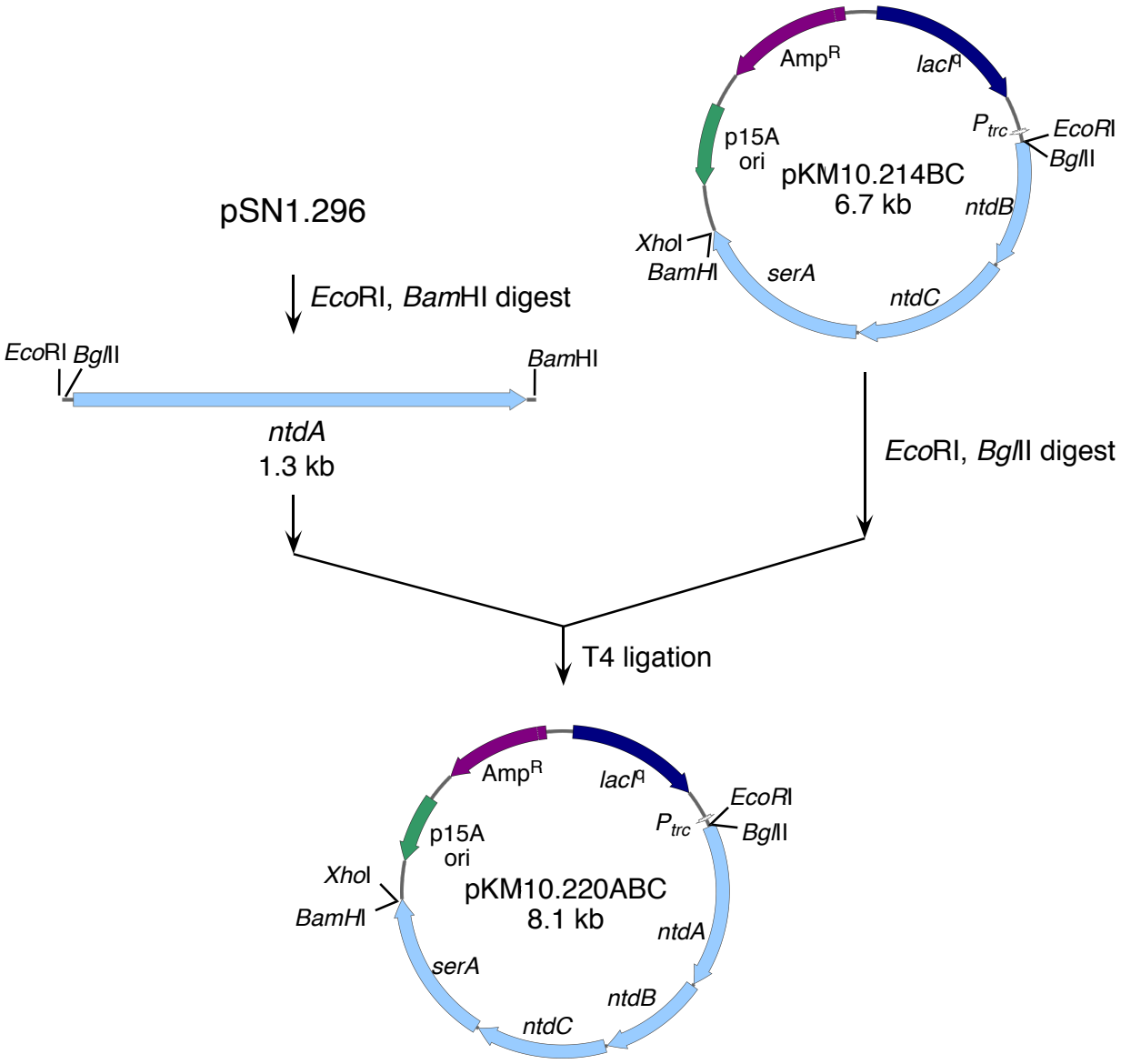

Figure 57. Construction of pKM10.220ABC.

Fed-batch fermentation of RB791*serA* constructs were conducted as described in Chapter 1 following either glucose-rich or glucose-limited conditions. Glucose-rich conditions maintain an excess (20-30 g/L) of D-glucose in the culture throughout the course of a fermentation run. Initial glucose was added to the fermentation vessel prior to inoculation at a concentration of 30 g/L. This concentration was chosen to ensure that the amount of D-glucose present in the culture medium at the end of the batch phase (approximately 12 h after inoculation) and before D-glucose feeding began, did not fall below 20 g/L. Glucose-rich fermentations used three staged methods to maintain the dissolved oxygen (D.O.) concentration at 10% air saturation. The first stage maintained airflow at an initial setting of 0.06 L/L/min and increased impeller speed from an initial set point of 50 rpm to a preset maximum of 750 rpm. This maximum was reached approximately 9 h after inoculation. With an impeller speed maintained at 750 rpm, the second stage began in which the mass flow controller maintained D.O. concentration by increasing airflow from 0.06 L/L/min to a preset maximum of 1.0 L/L/min. Approximately 3 h were needed to reach maximum airflow which coincided with cells beginning exponential growth phase. Between 11-12 h into a fermentation run after the maximum set points for airflow and stir rate were reached, the third stage of the fermentation was entered in which D-glucose (60% w/v) was added at a rate sufficient to maintain D-glucose concentration of 20-30 g/L throughout the run. The start of D-glucose feeding corresponded to the beginning of exponential growth phase for RB791*serA* constructs. At 12 h, isopropyl β-D-1-thiogalactopyranoside (IPTG, 12 mg unless otherwise stated) was added to induce transcription of plasmid-localized *ntd* genes. After initial addition of IPTG at 12 h, addition occurred every 6 h until the end of the

fermentation run. Yields of metabolites from D-glucose were calculated based on observed amount of glucose added to the fermentation culture.

Glucose-limited fermentation conditions utilized oxygen-sensor-controlled glucose feeding to maintain D-glucose concentrations well below 1 g/L throughout the course of a fermentation. Precise concentrations were not be measured as D-glucose levels were too low to detect using a GlucCell™ meter or to be detected by ^{1}H NMR. Initial glucose was added to the fermentation medium prior to inoculation at a concentration of 20 g/L. This concentration was selected to ensure the complete consumption of D-glucose corresponded to cells entering exponential growth phase and the beginning of D-glucose feeding. Three staged methods were used during glucose-limited fermentations to ensure D.O. concentration was maintained at 10% air saturation. The first two stages were similar to those described for glucose-rich fermentations with a different preset maximum impeller speed. With airflow maintained at 0.06 L/L/min, impeller speed was allowed to increase during the first stage from 50 rpm to a preset maximum of 850 rpm. This maximum value was reached approximately 9 h after inoculation of the fermentation vessel. The second staged method maintained impeller speed at 850 rpm while increasing airflow to a preset maximum of 1.0 L/L/min. Approximately 1 h was required after the maximum airflow was reached for the initial glucose to be completely consumed. This was marked by a sudden increase in D.O. levels and a corresponding decrease of airflow. As soon as the D.O. spike was observed, oxygen-sensor-controlled glucose feeding was initiated. Impeller speed and airflow was manually set to the maximum levels of 850 rpm and 1.0 L/L/min, respectively, while the mass flow controller adjusted glucose feeding rate to maintain D.O. concentration at 10% air saturation. As in glucose-rich fermentations, IPTG (12 mg unless

otherwise stated) was added beginning at 12 h and continued every 6 h until the end of a fermentation run.

Kanosamine concentrations were calculated by ^{1}H NMR analysis of cell-free fermentation broth. Integrals corresponding to the α-anomeric proton (4.73 ppm, d, J = 7.2 Hz) and the β-anomeric proton (5.27 ppm, d, J = 3.6 Hz) were summed to estimate the molar concentration of kanosamine in the NMR sample. This value was used to calculate the kanosamine concentration in the fermentation sample using a calibration curve with sodium 3-(trimethylsilyl)propionate-*2*,*2*,*3*,*3*-d_4 (TSP) as an internal standard and a response factor of 1.013. The calibration curve was generated using D-glucosamine hydrochloride (>98%, Alfa Aesar), which is a 2-amino regioisomer of kanosamine. The longitudinal relaxation time (T_1) for D-glucosamine calculated via an inversion-recovery experiment was found to be the same as kanosamine (5.2 s for the β-anomeric proton). A relaxation delay of 26 s was used to acquire ^{1}H NMR spectra.

The precise relationship between the arrangement of genes that comprise an operon and expression of those genes is not completely understood. However, it was recently demonstrated using synthetic operons in *E. coli* that the expression of a given gene increases with the length of the operon and as its position moves closer to the promoter.[38] The authors suggested that the increased distance from the start of a given gene to the end of the operon provides more time for translation to occur during transcription, leading to increased expression. To evaluate whether the arrangement of plasmid-localized *ntd* genes between the *trc* promoter and *rrnB* transcription terminator affects kanosamine production in RB791*serA*, two plasmids were utilized in fed-batch fermentations with different arrangements of the same *B. subtilis ntd* genes. Plasmid

pKM10.220ABC contains an *ntdAntdBntdCserA* cassette behind P_{trc} to match the order of genes observed in the *B. subtilis* genome while plasmid pSN1.292 carries a P_{trc}*ntdCntdAntdBserA* cassette. This second arrangement places the genes in a "reaction sequence order" with the *ntdC*-encoded D-glucose-6-phosphate 3-dehydrogenase placed closest to P_{trc} and the *ntdB*-encoded kanosamine-6-phosphate phosphatase placed furthest away. These two plasmids were utilized to determine if the particular arrangement of *ntd* genes has an impact on kanosamine production in fed-batch fermentations in *E. coli*.

Fed-batch fermentations of RB791*serA*/pSN1.292 resulted in 12.7 ± 0.6 g/L kanosamine (4.4 ± 0.4% mol/mol yield from D-glucose) under glucose-rich conditions (Figure 58) and 8.5 ± 1.4 g/L kanosamine (6.2 ± 2.2% mol/mol yield from D-glucose) under glucose-limited conditions (Figure 59). Glucose-rich conditions led to much higher cell-densities (40-50 g/L dry cell weight) compared to glucose-limited conditions (20-30 g/L dry cell weight). This increased biomass is a result of excess available carbon present in the culture media. Glucose-rich conditions also contribute to greater D-glucose consumption during a 48 h fermentation run than glucose-limited conditions. After 48 h, an average of 293 g (1.64 mol) D-glucose was consumed during glucose-rich fermentations while an average of 144 g (0.80 mol) D-glucose was consumed during glucose-limited fermentations. This difference in D-glucose consumption results in higher yields of kanosamine in glucose-limited fermentations despite lower overall titers.

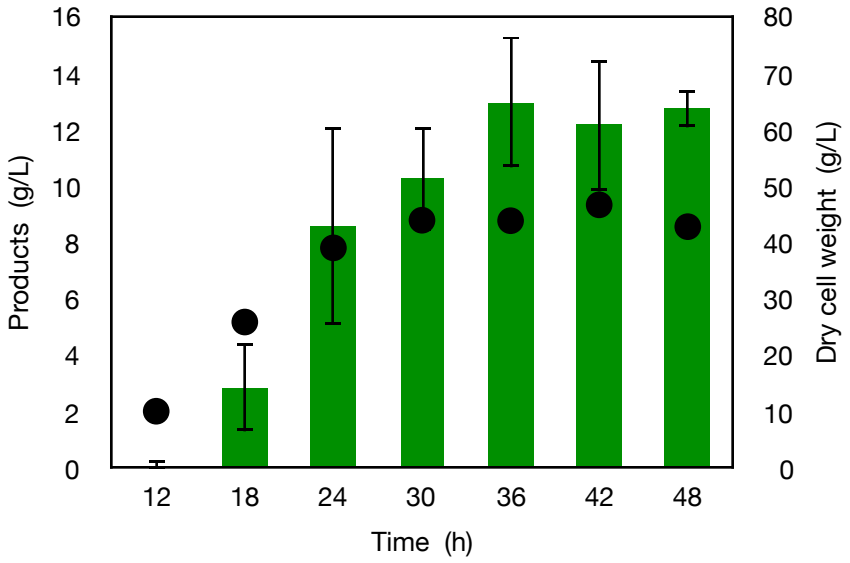

Figure 58. Kanosamine production by *E. coli* RB791*serA*/pSN1.292 under glucose-rich conditions. Legend: kanosamine, green columns; dry cell weight, black circles. Error bars represent one standard deviation away from the mean across triplicate runs.

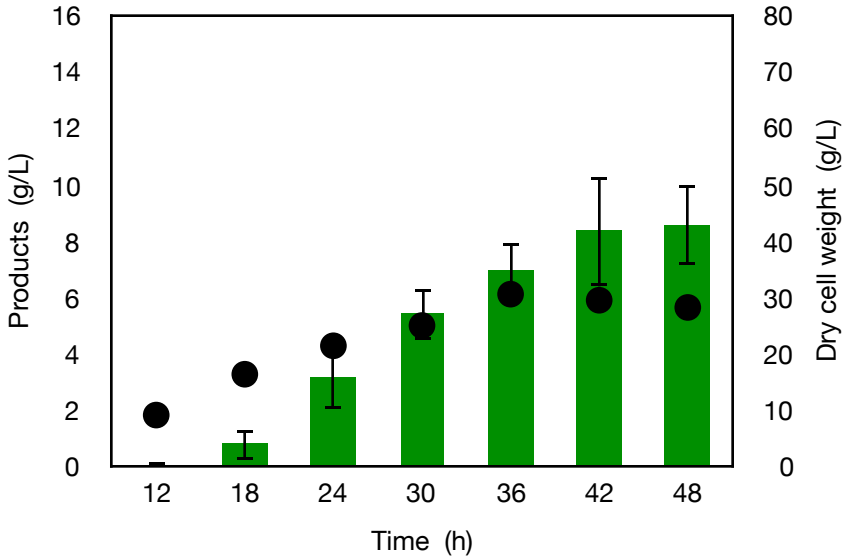

Figure 59. Kanosamine production by *E. coli* RB791*serA*/pSN1.292 under glucose-limited conditions. Legend: kanosamine, green columns; dry cell weight, black circles. Error bars represent one standard deviation away from the mean across quadruplicate runs.

A decrease in rate of kanosamine accumulation appears to correlate with stationary growth phase in both glucose-rich (Fig. 58) and glucose-limited (Fig. 59) fermentations of RB791*serA*/pSN1.292. As cell growth slows, so does kanosamine production which may reflect

the lower metabolic rates for *E. coli* in stationary phase relative to exponential phase.[38] This feature of both glucose-rich and glucose-limited fermentations has an impact on the yields from D-glucose reported here. During stationary phase, kanosamine production slows yet D-glucose continues to be taken in by the cells. The highest yields of kanosamine would result from halting D-glucose feeding at the moment kanosamine production slows. However, as this would lead to lower titers than those observed herein, D-glucose feeding continued into stationary phase for both glucose-rich and glucose-limited fermentations.

Fed-batch fermentations of RB791*serA*/pKM10.220ABC (Figure 60 and Figure 61) afforded similar titers and yields of kanosamine relative to RB791*serA*/pSN1.292. In glucose-rich conditions, RB791*serA*/pKM10.220ABC achieved kanosamine titers of 13.7 g/L in 4.9% mol/mol yield from D-glucose while RB791*serA*/pSN1.292 achieved titers of 12.7 ± 0.6 g/L in 4.4 ± 0.4% mol/mol yield from D-glucose. During glucose-limited fermentations, RB791*serA*/pKM10.220ABC produced 7.9 g/L kanosamine in 5.6% mol/mol yield from D-glucose while RB791*serA*/pSN1.292 produced 8.5 ± 1.4 g/L kanosamine in 6.2 ± 2.2% mol/mol yield. The similarities between fermentations employing the two constructs suggest that the particular arrangement of *ntd* genes behind P_{trc} does not have a great impact on kanosamine production with RB791*serA*. Based on these results, alternate gene permutations were not explored and the "reaction sequence order" arrangement of *ntdCntdAntdB* was used for further experiments.

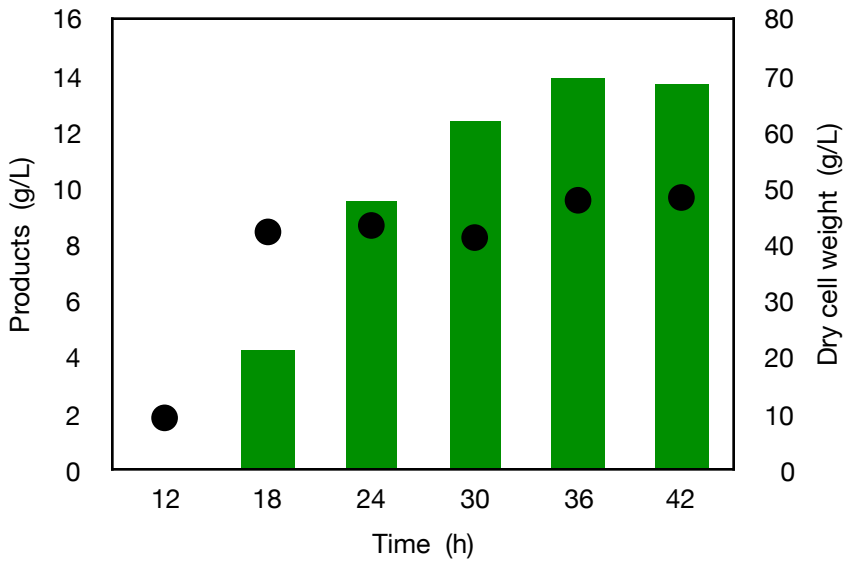

Figure 60. Kanosamine production by *E. coli* RB791*serA*/pKM10.220ABC under glucose-rich conditions. Legend: kanosamine, grey columns; dry cell weight, black circles.

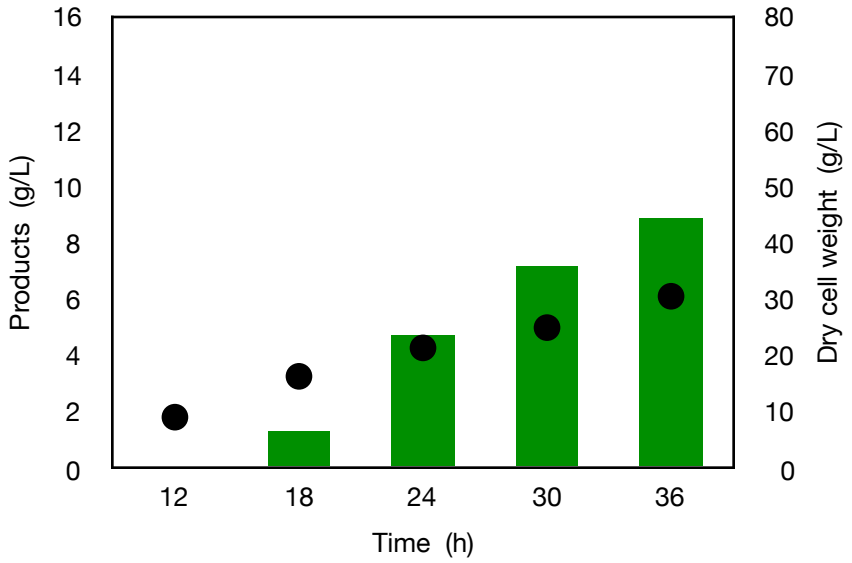

Figure 61. Kanosamine production by *E. coli* RB791*serA*/pKM10.220ABC under glucose-limited conditions. Legend: kanosamine, grey columns; dry cell weight, black circles.

Such experiments included placing the *ntdCntdAntdBserA* cassette from pSN1.292 behind a T7 promoter, which is not recognized by native *E. coli* RNA polymerase. Kanosamine production was therefore evaluated in RB791*serA*(DE3), previously engineered by Hansen and

Frost.[40] The DE3 designation indicates the respective strain contains the λ prophage DE3 lysogen. The λDE3 lysogen carries the gene for T7 RNA polymerase under control of an IPTG-inducible lacUV5 promoter. Strength of a promoter is determined by the relative frequency of transcription initiation, which is mainly affected by the affinity of the promoter sequence for RNA polymerase. The bacteriophage λ T7 RNA polymerase has a high frequency of initiation and is not easily subject to early termination events. These features result in transcription rates approximately five-fold higher than *E. coli* RNA polymerase.[41] To build the T7 expression plasmid, the 4.5 kb *ntdCntdAntdBserA* fragment from pSN1.292 was liberated by digestion with *Eco*RI, *Bam*HI double-digestion and inserted immediately behind P_{T7} into the *Eco*RI, *Bam*HI sites of BglBrick vector, pBbA7k to afford pKM10.82A (Figure 62). Plasmid pKM10.82A carries a kanamycin resistance gene and a p15A origin of replication. The orientation of the *ntdCntdAntdBserA* cassette was in the same direction as the T7 promoter. Transformation of pKM10.82A into RB791*serA*(DE3) was followed by evaluation of kanosamine production in both glucose-rich (Figure 63) and glucose-limited fed-batch fermentation (Figure 64).

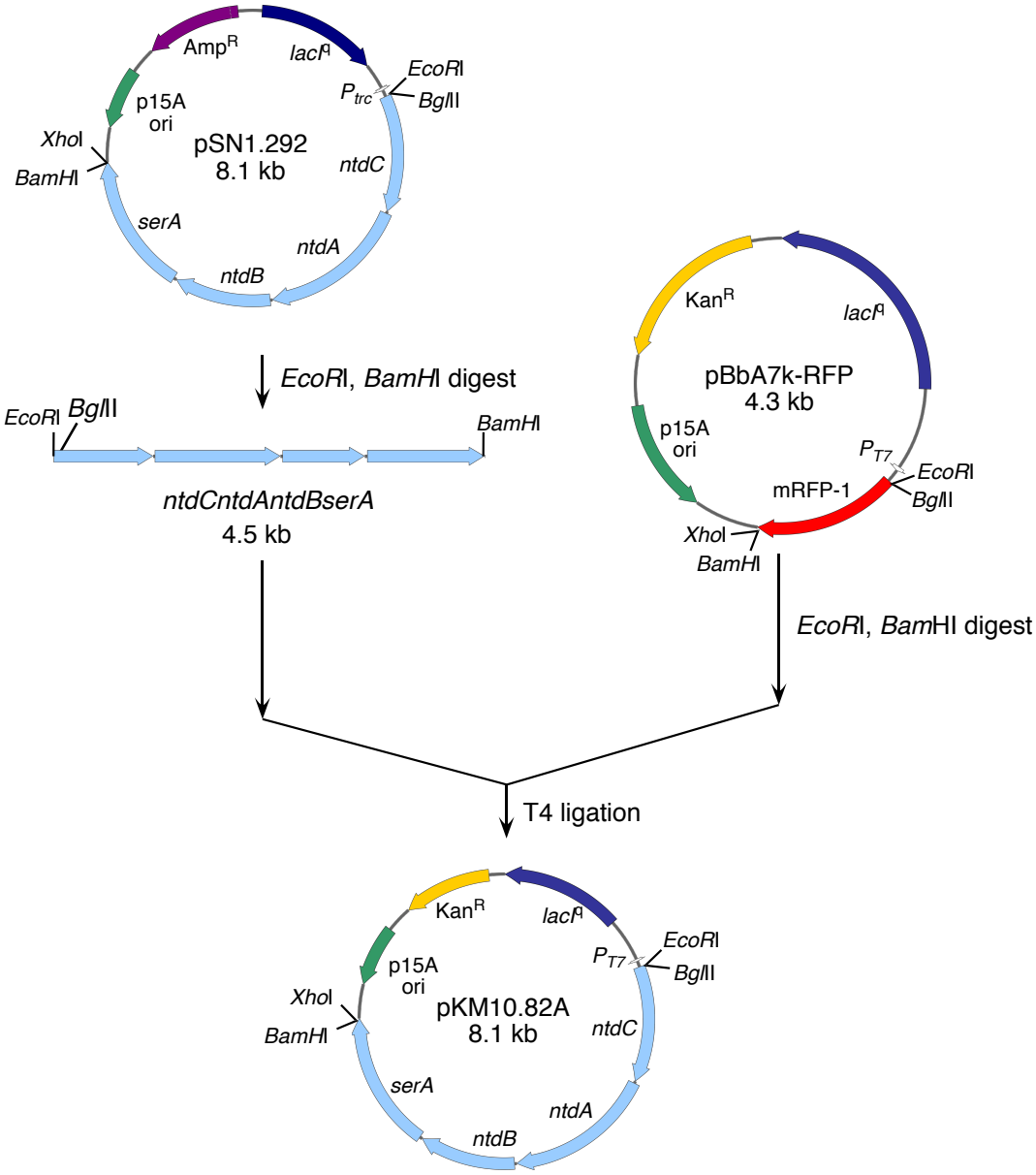

Figure 62. Construction of plasmid pKM10.82A.

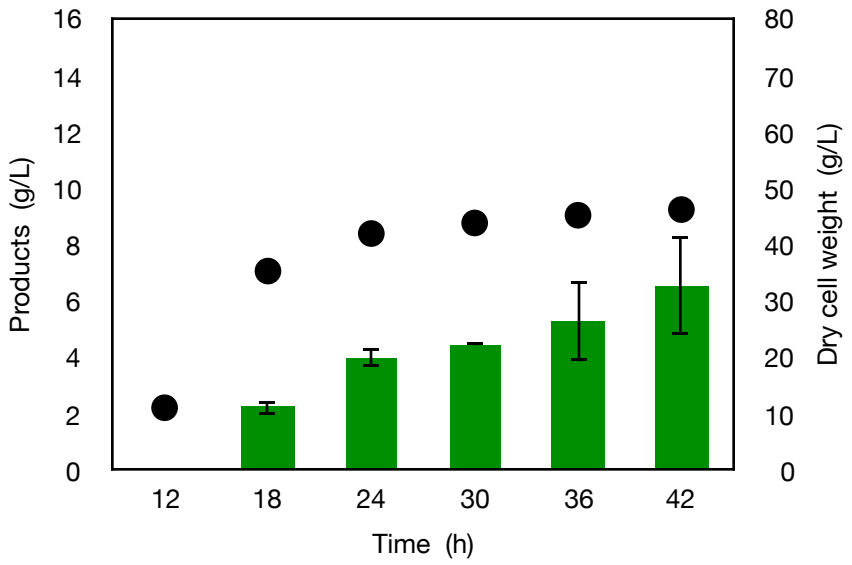

Figure 63. Kanosamine production by *E. coli* RB791*serA*(DE3)/pKM10.82A under glucose-rich conditions. Legend: kanosamine, green columns; dry cell weight, black circles. Error bars represent one standard deviation away from the mean across duplicate runs.

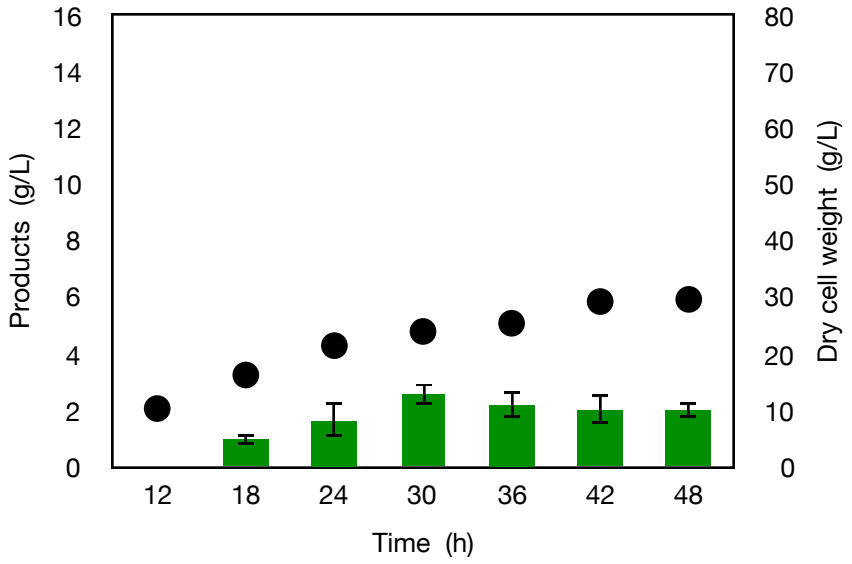

Figure 64. Kanosamine production by *E. coli* RB791*serA*(DE3)/pKM10.82A under glucose-limited conditions. Legend: kanosamine, green columns; dry cell weight, black circles. Error bars represent one standard deviation away from the mean across duplicate runs.

Fermentation results shown in Fig. 63 and Fig. 64 utilized 12 mg IPTG added every 6 h beginning at 12 h. This is in the same manner as fermentations of RB791*serA*/pSN1.292, which carried the *ntd* genes under the control of P_{trc}. Lower titers and yields of kanosamine were

observed using P_{T7} expression relative to P_{trc} using the same method of induction, affording 7.4 ± 0.6 g/L (2.6 ± 0.3% mol/mol yield from D-glucose) under glucose-rich conditions and 2.0 ± 0.3 g/L (1.4 ± 0.2% mol/mol yield from D-glucose) under glucose-limited conditions. This corresponds to a 1.7-fold and 4.2-fold decrease in kanosamine titers relative to P_{trc} expression under glucose-rich and glucose-limited conditions, respectively.

Titrating IPTG concentration resulted in improved kanosamine production using P_{T7} gene expression in *E. coli* RB791*serA*(DE3)/pKM10.82A (Table 19). Repeated IPTG additions every 6 h throughout a fermentation run resulted in better yields and higher titers relative to fermentations which involved a single addition of IPTG at the beginning of exponential growth phase (12 h after inoculation). Decreasing IPTG concentration from 12 mg (0.05 mM) to either 6 mg (0.025 mM) or 2.4 mg (0.01 mM) resulted in improved titers and slightly improved yields of kanosamine. It appeared that 6 mg IPTG added every 6 h resulted in marginally improved kanosamine production as compared to 2.4 mg IPTG addition, however, as these were singleton experiments, the difference may not be statistically significant. Even with the improvements resulting from decreasing IPTG concentration from 12 mg to 6 mg, the T7 expression system, RB791*serA*(DE3)/pKM10.82A, did not achieve the same titers and kanosamine yields as when the *B. subtilis ntd* genes were under control of P_{trc} in either RB791*serA*/pKM10.220ABC or RB791*serA*/pSN1.292.

Table 19. Kanosamine production in fed-batch fermentation of *E. coli* RB791*serA*(DE3)/pKM10.82A.

Entry	Glucose conditions	Amount IPTG	Addition frequency	[Kanosamine] (g/L)	Yield (mol/mol)
1	Rich	12 mg [0.05mM]	Every 6 h	7.4 ± 0.6	2.6 ± 0.3%
2	Limited	12 mg [0.05mM]	Every 6 h	2.0 ± 0.3	1.4 ± 0.2%
3	Rich	6 mg [0.025mM]	Every 6 h	10.5	4.2%
4	Rich	6 mg [0.025mM]	Once at 12 h	1.2	0.6%
5	Rich	2.4 mg [0.01mM]	Every 6 h	9.1	3.5%
6	Rich	2.4 mg [0.01mM]	Once at 12 h	6.2	2.1%

The requirement for each of the *B. subtilis ntd* genes for kanosamine production in *E. coli* was evaluated by fed-batch fermentation of RB791*serA* with one of three different plasmids. Each plasmid contained two of the three kanosamine biosynthesis *ntd* genes and was constructed as described above using the BglBrick assembly standard. Plasmid pKM10.214CA was constructed by inserting *ntdC* from plasmid pSN1.294 upstream of *ntdA* in plasmid pKM10.204A (Figure 65). Insertion of *ntdA* from plasmid pSN1.296 upstream of *ntdB* in plasmid pSN10.204B afforded plasmid pKM10.214AB (Figure 66). Construction of plasmid pKM10.214CB followed insertion of *ntdC* from pSN1.294 upstream of *ntdB* in plasmid pSN10.204B (Figure 66).

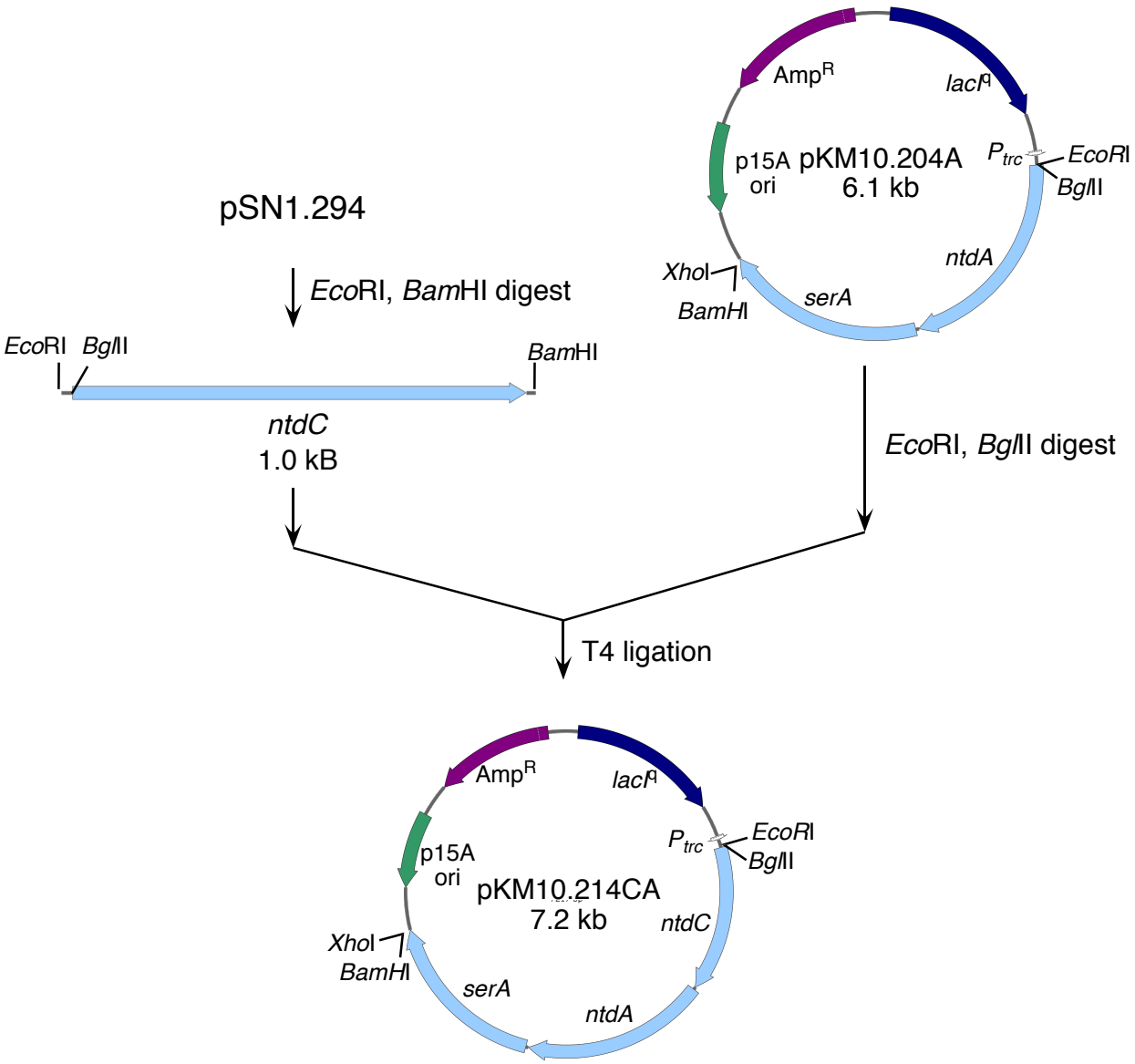

Figure 65. Construction of plasmid pKM10.214CA.

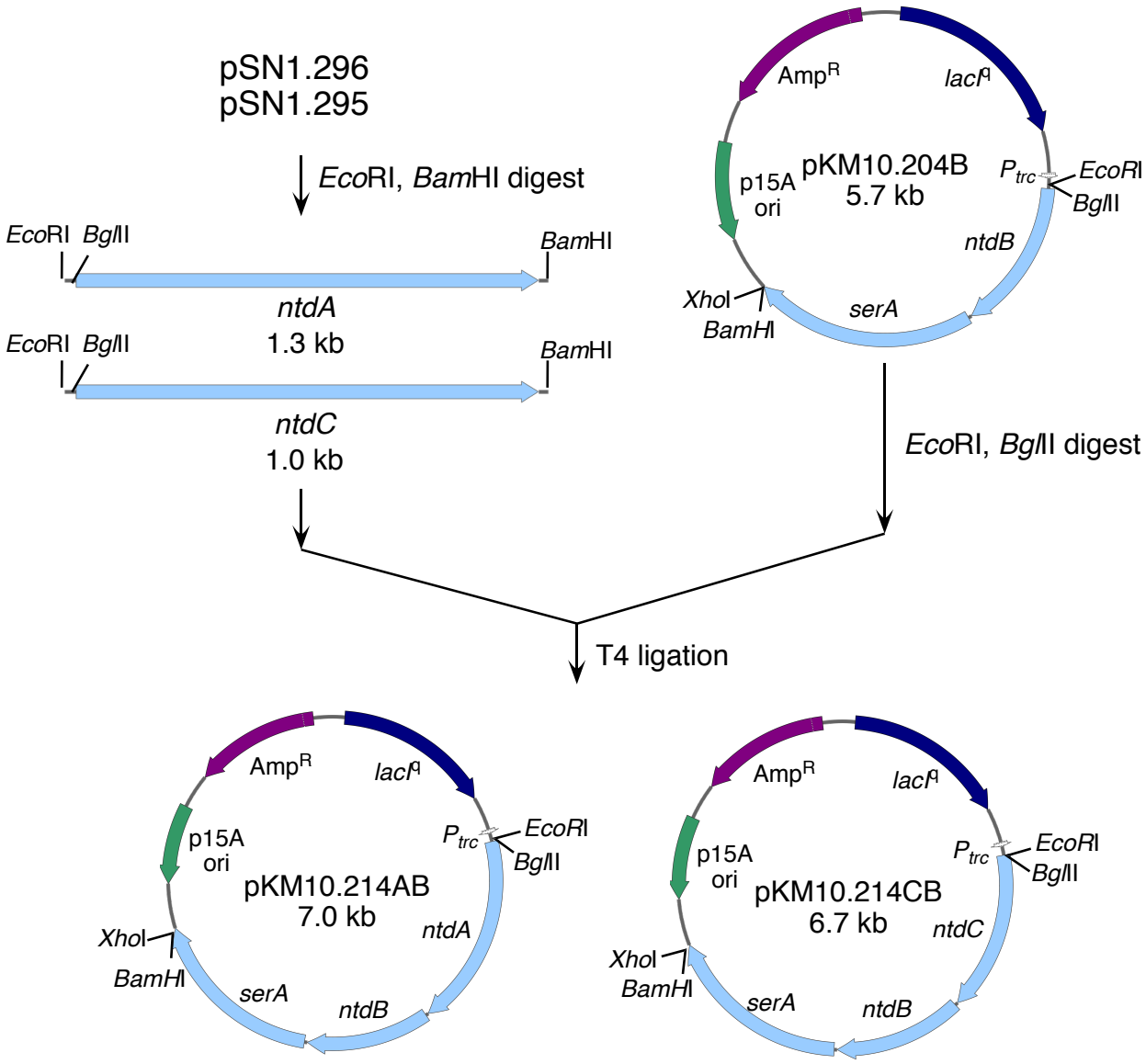

Figure 66. Construction of plasmids pKM10.214AB and pKM10.214CB.

Results from fermentations of RB791*serA* constructs transformed with pKM10.214CA, pKM10.214AB, or pKM10.214CB are summarized in Table 20. Plasmid pKM10.214CA did not carry the *ntdB*-encoded kanosamine-6-phosphate phosphatase. Fed-batch fermentation of RB791*serA*/pKM10.214CA revealed whether a native *E. coli* phosphatase had sufficient promiscuity to accumulate kanosamine in fermentation broth. Kanosamine concentrations did not exceed 0.11 ± 0.03 g/L, corresponding to a 0.04% mol/mol yield from D-glucose. While the small amount of kanosamine observed indicates that RB791*serA* does possess some native promiscuous phosphatase activity, the titers and yields are far from those achieved with any of the previously described constructs expressing a dedicated kanosamine-6-phosphate phosphatase encoded by *ntdB*.

Table 20. Kanosamine production with incomplete constructs.

Entry	Plasmid	[Kanosamine] (g/L)	Yield (mol/mol)
1	pKM10.214CA	0.11 ± 0.03	0.04 ± 0.01%
2	pKM10.214AB	0	0%
3	pKM10.214CB	0	0%

Error represents one standard deviation away from the mean across duplicate runs.

Promiscuous D-glucose-6-phosphate 3-dehydrogenase activity in *E. coli* was examined in fed-batch fermentation of RB791*serA*/pKM10.214AB while promiscuous aminotransferase activity was evaluated in fermentations of RB791*serA*/pKM10.214CB. Neither of these constructs resulted in any observable amounts of kanosamine in either glucose-rich or glucose-

limited fermentations. These results indicate that kanosamine biosynthesis in *E. coli* requires expression of all three *B. subtilis* enzymes.

Regardless of the *E. coli* strain used, glucose-rich fermentations consistently resulted in higher final cell-densities and greater byproduct accumulation than glucose-limited fermentations. Figure 67 and Figure 68 compare biomass and byproduct formation between glucose-rich and glucose-limited fermentations of RB791*serA*/pSN1.292 using P_{trc} expression of *B. subtilis ntd* genes. Approximately 15-20 g/L more biomass was generated in glucose-rich fermentations than glucose-limited conditions while the most abundant byproduct observed was acetic acid. Pyruvic acid and lactic acid were also observed in glucose-rich fermentations.

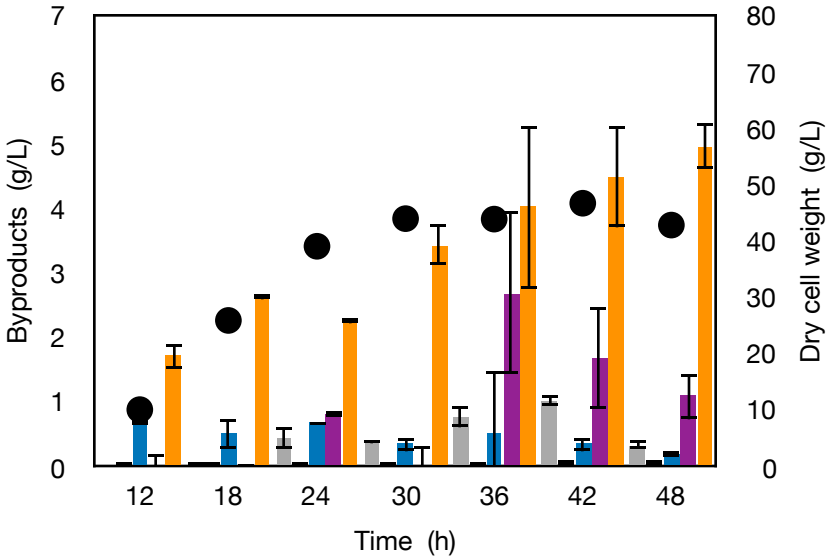

Figure 67. Byproducts formed during fermentation of *E. coli* RB791*serA*/pSN1.292 under glucose-rich conditions. Legend: acetic acid, orange columns; formic acid, grey columns; pyruvic acid, red columns; lactic acid, blue columns; D-glucosamine, purple columns; dry cell weight, black circles.

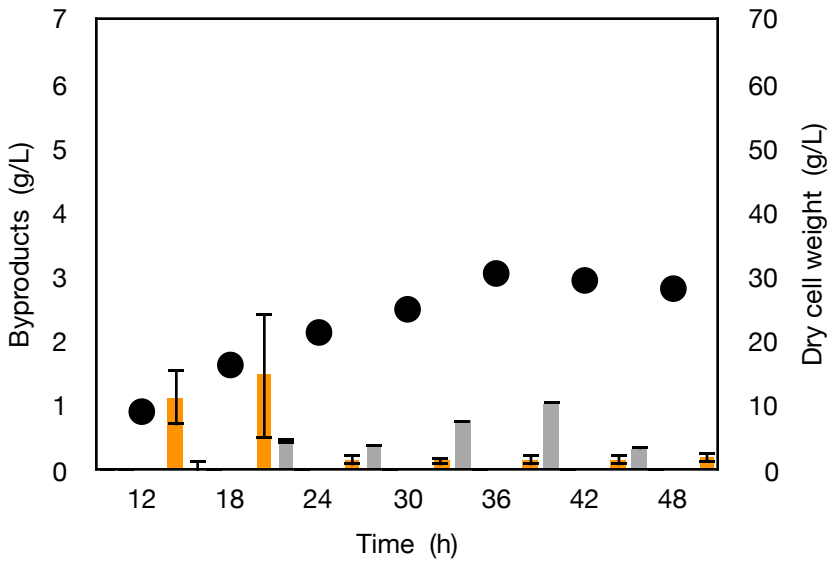

Figure 68. Byproducts formed during fermentation of *E. coli* RB791*serA*/pSN1.292 under glucose-limited conditions. Legend: acetic acid, orange columns; formic acid, grey columns; dry cell weight, black circles.

Glucose-rich fermentations of RB791s*erA*/pKM10.220ABC and RB791*serA*/pSN1.292 resulted in formation of D-glucosamine alongside the organic acid byproducts. Resonances for D-glucosamine became more clear upon partial purification of kanosamine-containing fermentation broth (Figure 69) by cation exchange chromatography. A mass spectrometry analysis conducted by another group member revealed a single molecular ion peak at 180 m/z, corresponding to the molecular mass of both kanosamine and D-glucosamine. Though complete separation of D-glucosamine and kanosamine could not be achieved by ion exchange chromatography, partial purification of kanosamine-containing fermentation broth by cation exchange chromatography (Dowex 50WX8, H^+-form) afforded a sample with which the identity of D-glucosamine could be confirmed. The partially purified sample containing a mixture of the two aminosugars was analyzed by ^{1}H and ^{13}C NMR and then spiked with >98% pure D-glucosamine hydrochloride (Alfa Aesar) (Figure 69). Prior to this experiment, a calibration curve was generated using sodium (trimethylsilyl)-*2*,*2*,*3*,*3*-d_4-propionate (TSP, $\delta = 0.00$ ppm) as

an internal standard. Comparing the relative integrations of the signal corresponding to TSP and the β-anomeric proton peak of D-glucosamine (5.42 ppm, 0.6 H, J = 3.6 Hz) in samples containing D-glucosamine hydrochloride across a range of concentrations (0.5-100 mM), a calibration curve was calculated: [mM sample] = 1.013(1H × mM TSP) + 0.16 (r^2 = 0.99).

This calibration curve was used to determine the concentration of D-glucosamine in a partially purified sample of RB791*serA*/pSN1.292 fermentation broth by ^{1}H NMR (19.6 mM, "without D-glucosamine spike," Fig. 69). An aliquot (21 μL) of 0.47 mM D-glucosamine in D_2O was added to the NMR sample in order to increase the amount of D-glucosamine by 10 mM. The concentration of D-glucosamine in this spiked sample was also determined by ^{1}H NMR (31.4 mM). Thus, the observed increase peak size corresponding to the β-anomer was observed to be proportional to the amount of D-glucosamine added to the sample. No new peaks were observed. Increasing the amount of added D-glucosamine to 300 mM allowed previously masked peaks to become apparent (Figure 69). Furthermore, ^{13}C NMR analysis of the unspiked sample and sample with 300 mM D-glucosamine added did not reveal the presence of new peaks when D-glucosamine was added (Figure 70). These results provide strong evidence that D-glucosamine is produced alongside kanosamine in glucose-rich fermentations.

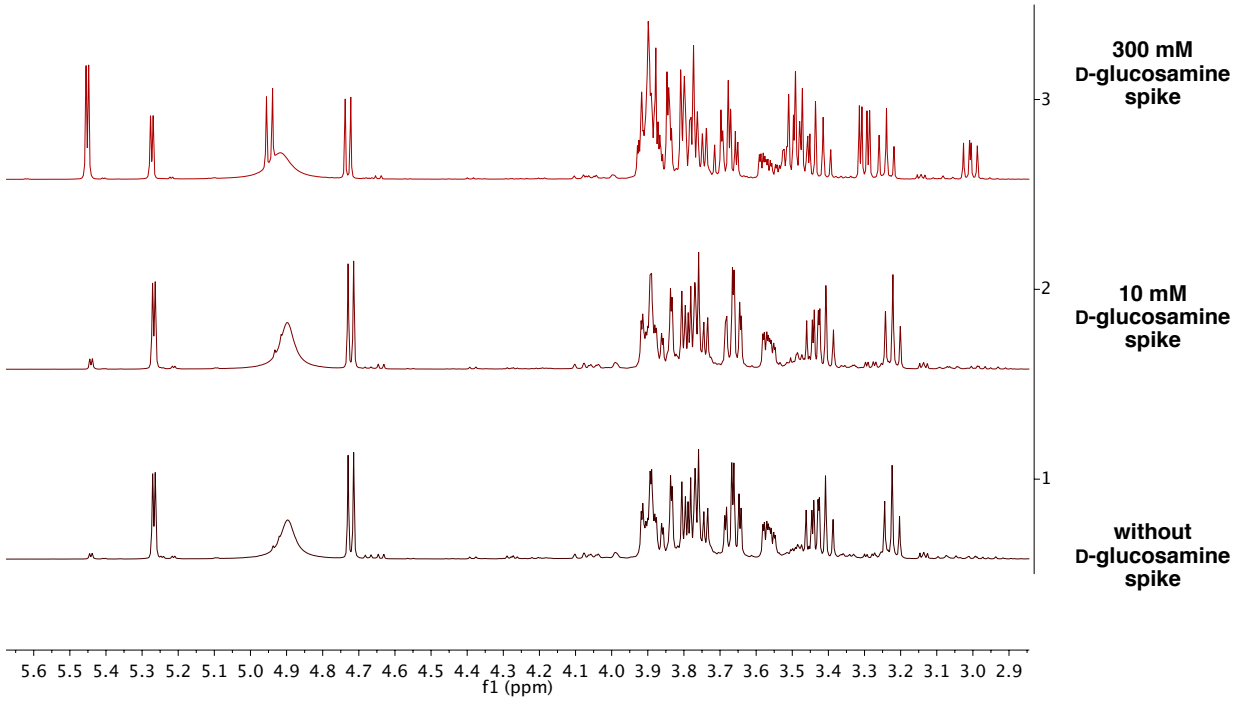

Figure 69. Stacked ^{1}H NMR spectra of partially purified kanosamine with increasing amounts of added D-glucosamine.

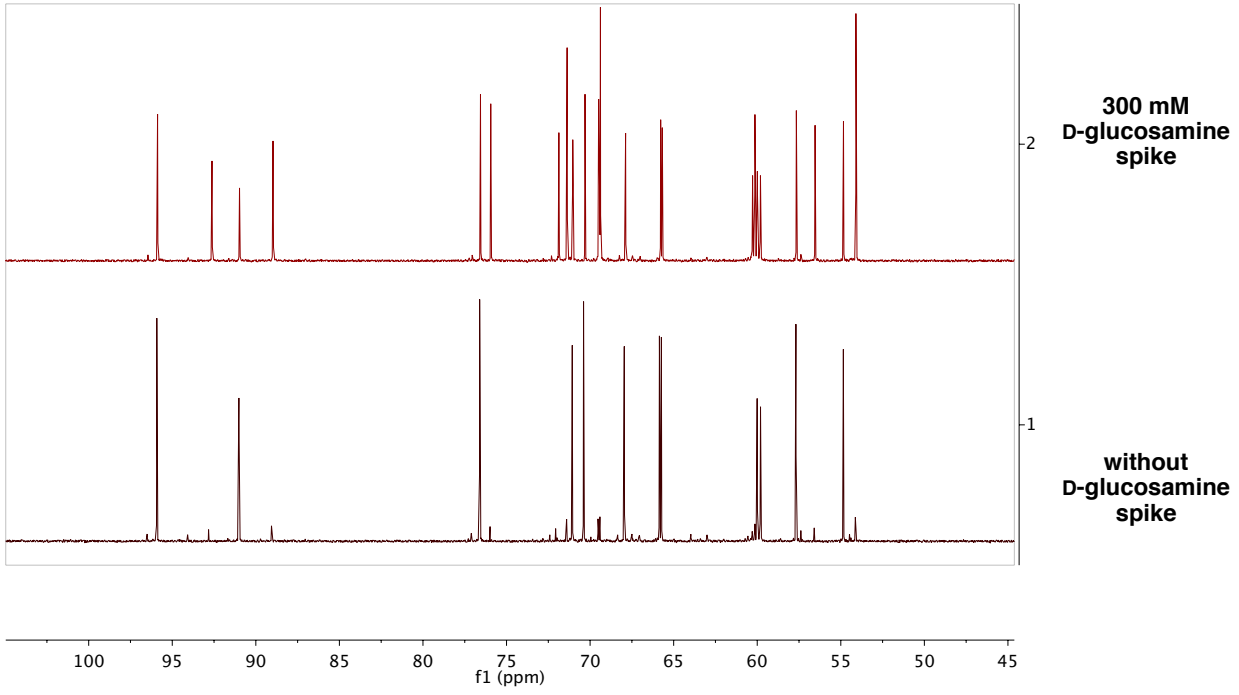

Figure 70. Stacked ^{13}C NMR spectra corresponding to partially purified kanosamine with and without added D-glucosamine.

The lack of D-glucosamine formation in glucose-limited fermentations of RB791*serA*/pSN1.292 and RB791*serA*/pKM10.220ABC implies that D-glucosamine is not formed as a result of promiscuous isomerase or aminotransferase activity in *E. coli* but is more likely due to D-glucose availability. Evidence from fermentations of RB791*serA pgi::*Kan^R in which kanosamine is produced without D-glucosamine accumulation under glucose-rich conditions with either a D-glucose or D-glucose/D-fructose mixed feed (described in a later section) offers further support to this hypothesis.

D-Glucosamine is produced in *E. coli* upon hydrolysis of D-glucosamine-6-phosphate, in turn formed from β-D-fructose-6-phosphate by action of *glmS*-encoded L-glutamine:D-fructose-6-phosphate aminotransferase (Figure 71). The smaller relative amount of D-glucosamine produced during glucose-rich (0.33 ± 0.2 g/L) fermentations of RB791*serA*/pSN1.292 compared to other glycolytic byproducts such as acetic acid (5.0 ± 2.3 g/L), likely reflects competition between GlmS and the 6-phosphofructokinase enzymes, PfkA and PfkB, which convert β-D-fructose-6-phosphate into β-D-fructose-1,6-bisphosphate for further degradation through glycolysis. Additional competition results from expression of *B. subtilis* kanosamine biosynthesis genes which compete with glycolysis for D-glucose-6-phosphate. Blocking the D-glucosamine biosynthesis pathway through a mutation in *glmS* may help reduce byproduct formation during kanosamine biosynthesis in *E. coli*, however increased kanosamine production may more effectively come from increasing D-glucose-6-phosphate availability.

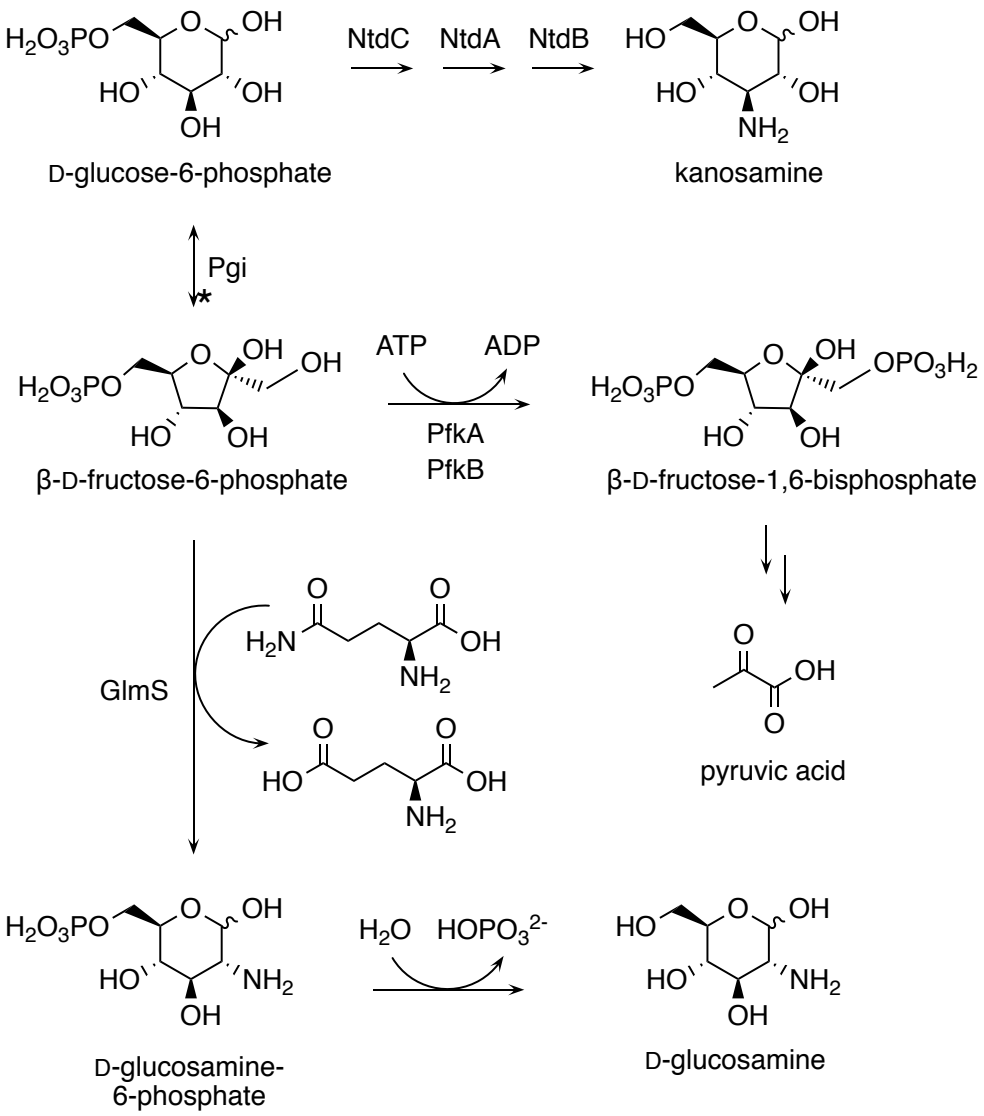

Figure 71. D-Glucosamine synthesis from D-glucose-6-phosphate through transamination of D-fructose-6-phosphate catalyzed by *glmS*-encoded L-glutamine:D-fructose-6-phosphate aminotransferase followed by phosphate ester hydrolysis. GlmS must compete with phosphofructokinase isozymes, PfkA and PfkB, for substrate availability.

2. Competition with glycolysis for D-glucose-6-phosphate availability

2.1. Activity of D-glucose-6-phosphate 3-dehydrogenase

During fermentative metabolism in *E. coli*, D-glucose is concomitantly transported and phosphorylated by the phosphoenolpyruvate-dependent phosphotransferase system. The resulting D-glucose-6-phosphate is metabolized via the Embden-Meyerhof-Parnas pathway and the

pentose phosphate pathway, affording ATP, reducing equivalents, and organic compounds for biosynthesis. Under oxygen-limiting conditions, *E. coli* converts most of the D-glucose-6-phosphate to a mixture of organic acids and carbon dioxide, which are largely generated from pyruvate.[42] The observation of several products of fermentative metabolism (i.e., acetic acid, formic acid, and lactic acid) alongside pyruvic acid in glucose-rich fermentations with various RB791*serA* constructs suggests that the glycolysis pathways compete for D-glucose-6-phosphate with kanosamine biosynthesis. This competition results in low yields of kanosamine from D-glucose (e.g., 4.4 ± 0.4% mol/mol in glucose-rich fermentation of RB791*serA*/pSN1.292). Kanosamine yields are slightly improved in glucose-limited conditions
which afford reduced accumulation of fermentative byproducts and lower final cell-densities relative to glucose rich conditions (Fig. 67, Fig. 68). Glucose-limited fermentations of RB791*serA*/pSN1.292 achieve 6.2 ± 2.2% mol/mol yields of kanosamine from D-glucose.

Kanosamine biosynthesis and glycolysis both utilize D-glucose-6-phosphate as a substrate. In order for kanosamine production to compete with glycolysis pathways for D-glucose-6-phosphate availability in fed-batch fermentation of RB791*serA* constructs, *E. coli* must be able to express active Ntd enzymes. Cell samples withdrawn from glucose-limited fermentation of RB791*serA*/pSN1.292 every 12 h throughout the course of the fermentation were lysed and assayed for *ntdC*-encoded D-glucose-6-phoshpate 3-dehydrogenase activity.

Table 21. D-glucose-6-phosphate 3-dehydrogenase specific activity

Entry	Time point	Specific activity (μmol min^{-1} mg^{-1})
1	12 h	0.003
2	24 h	0.27
3	36 h	0.34
4	48 h	0.33

Fed-batch fermentation samples from glucose-limited run with *E. coli* RB791*serA* /pSN1.292.

The activity of *ntdC*-encoded D-glucose-6-phosphate 3-dehydrogenase was assayed in cell-free extracts of RB791*serA*/pSN1.292 during incubation with NAD^+ and D-glucose-6-phosphate in 100 mM 2-amino-2-methyl-1-propanol (AMP) buffer, pH 9.5. The rate of the NtdC-catalyzed dehydrogenation has been previously reported[27] to increase up to pH 9.5 before sharply falling at pH ≥ 10. The absorbance at 340 nm was monitored for 5 min at ambient temperature and NtdC specific activity was calculated from the increase in absorbance due to formation of NADH (Table 21). Because enzyme activity is determined by monitoring cofactor reduction, which is not enzyme-specific, the small amount of observed enzyme activity at 12 h before the first aliquot of IPTG had been added is likely due background activity by one or more native *E. coli* enzymes present in the cell-free extract. After induction, *ntdC*-encoded D-glucose-6-phosphate 3-dehydrogenase activity increased to 0.27 μmol/min/mg (U/mg) and remained steady throughout the course of the fermentation.

Specific activities are reported as a function of amount of total protein (mg^{-1}) and are therefore a reflection of enzyme purity. Activities around 0.3 U/mg match those reported for other D-glucose-6-phosphate dehydrogenases assayed in cell-free extracts, such as the wild-type

D-glucose-6-phosphate 1-dehydrogenase from *Pseudomonas fluorecens* (0.31 U/mg).[43] These assay results imply good *in vivo* activity of NtdC following induction of transcription with IPTG, which remains stable during a fermentation.

2.2. Improving product yields by blocking glycolysis pathway

One possible strategy to improve kanosamine production from expression of *B. subtilis* Ntd enzymes would be to block a competing pathway. The presence of acetic acid, lactic acid, formic acid, and pyruvic acid in fermentation broth as major byproducts indicate that glycolysis pathways compete with kanosamine biosynthesis for D-glucose-6-phosphate availability. Prior research has demonstrated that D-glucose fermentation of an *E. coli* mutant with an inactive *pgi*-encoded phosphoglucose isomerase results in increased intracellular availability of D-glucose-6-phosphate relative to wild-type strains.[44] Deletions in *pgi* have previously been used to achieve increased titers of compounds such as 2-deoxy-*scyllo*-inosose[45] from D-glucose.

To evaluate whether a *pgi*-deficient mutant would lead to greater kanosamine accumulation, pSN1.292 was transformed into RB791*serA pgi*::Kan^R, a strain previously engineered by Amy Dean in the Frost group.[46] The resulting strain was evaluated in fed-batch fermentations under glucose-rich conditions. The phosphoglucose isomerase mutation resulted in unsustained growth when utilizing D-glucose as the sole carbon source and produced minor amounts of kanosamine (Figure 72). Loss of an active phosphoglucose isomerase significantly alters the structure of the metabolic network in *E. coli* by disabling the upper pathway of glycolysis.[47] Prior research has shown this reduces the growth rate to <20% of wild-type levels in minimal media. *E. coli* remains viable because D-glucose metabolism is rerouted through the

pentose phosphate pathway. This introduces a redox imbalance as excess NADPH is produced which contributes to the growth characteristics of *pgi* mutants.[47]

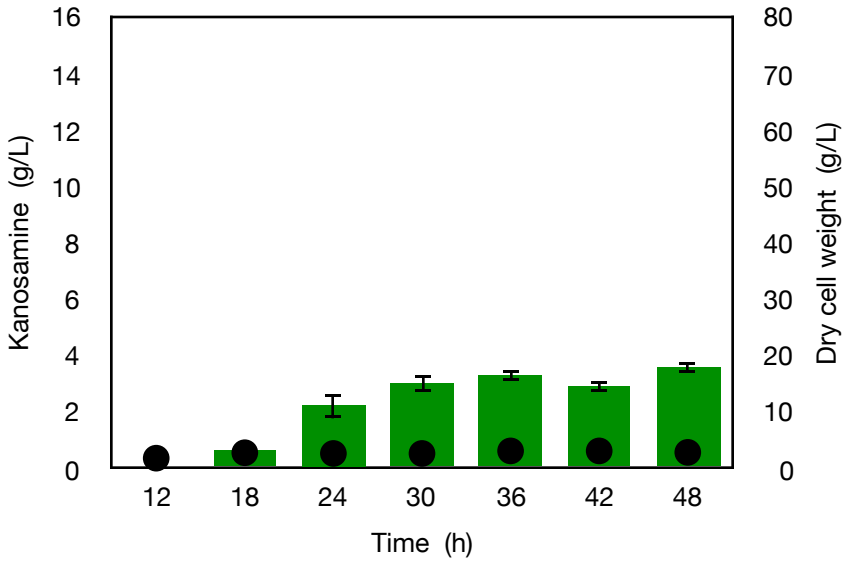

Figure 72. Kanosamine production by *E. coli* RB791*serA pgi*::Kan^R/pSN1.292 under glucose-rich conditions with a D-glucose-only feed. Legend: kanosamine, green columns; dry cell weight, black circles. Error bars represent one standard deviation away from the mean across duplicate runs.

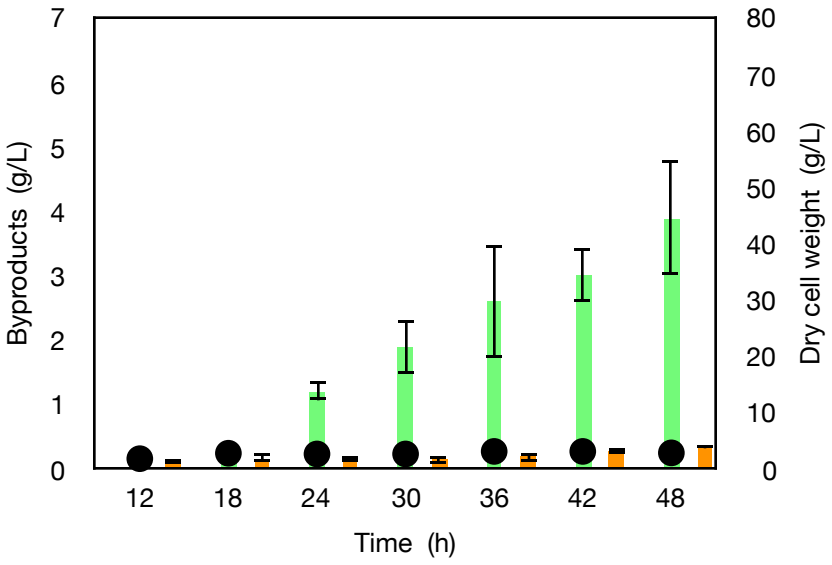

Figure 73. Byproducts formed in fed-batch fermentation of *E. coli* RB791*serA pgi*::Kan^R/pSN1.292 under glucose-rich conditions with a D-glucose-only feed. Legend: acetic acid, orange columns; L-glutamic acid, bright green columns; dry cell weight, black circles. Error bars represent one standard deviation away from the mean across duplicate runs.

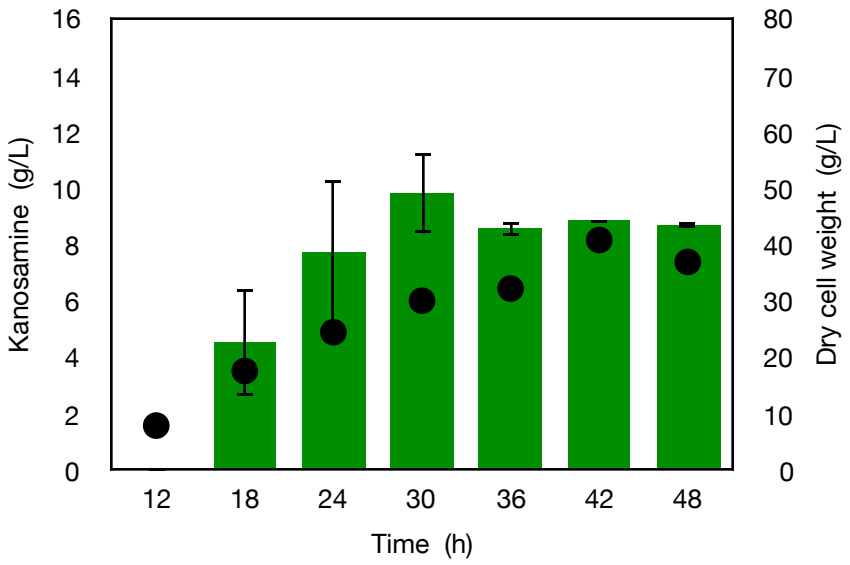

Figure 74. Kanosamine production by *E. coli* RB791*serA pgi*::Kan^R/pSN1.292 under glucose-rich conditions with a mixed feed of D-glucose/D-fructose (1:1 mol/mol). Legend: kanosamine, green columns; dry cell weight, black circles. Error bars represent one standard deviation away from the mean across duplicate runs.

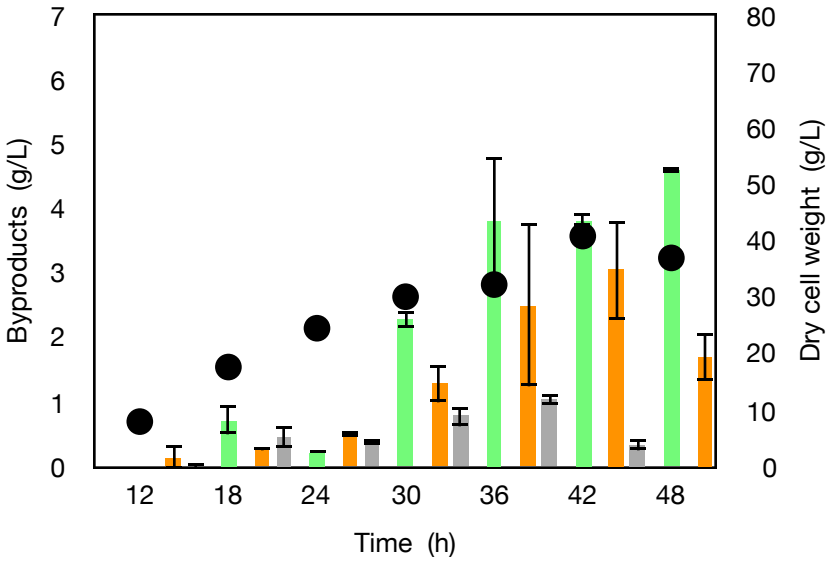

Figure 75. Byproducts formed in fed-batch fermentation of *E. coli* RB791*serA pgi*::Kan^R/pSN1.292 under glucose-rich conditions with a D-glucose-only feed. Legend: acetic acid, orange columns; formic acid, grey columns; L-glutamic acid, bright green columns; formic acid, grey columns; dry cell weight, black circles. Error bars represent one standard deviation away from the mean across duplicate runs.

Fermentation of RB791*serA pgi*::Kan^R/pSN1.292 on a D-glucose-only feed resulted in the highest yields of kanosamine observed thus far. Kanosamine titers reached 3.6 ± 0.2 g/L in an 18

± 1% mol/mol yield from D-glucose (Figure 72). These fermentations resulted in a 14.7-fold decrease in biomass formation (2.9 ± 1.4 g/L dry cell weight) relative to RB791*serA*/pSN1.292 with wild-type phosphoglucose isomerase in glucose-rich fermentations (42.8 ± 1.7 g/L dry cell weight). Furthermore, only 20 g of D-glucose was consumed during these runs as opposed to 296 g in glucose-rich fermentations of RB791*serA*/pSN1.292. Though growth was inhibited by the mutation in phosphoglucoisomerase, kanosamine yield from D-glucose implies that more D-glucose-6-phosphate was availabile to the kanosamine biosynthesis enzymes relative to fermentations of RB791*serA*/pSN1.292 or RB791*serA*/pKM10.220ABC.

Cell growth was restored and D-glucose consumption increased with the use of a feed consisting of equimolar amounts of D-glucose and D-fructose. Upon transport into the cell, D-fructose is phosphorylated to D-fructose-6-phosphate, which is catabolized through the Embden-Meyerhoff-Parnas pathway of glycolysis. Thus, a feed containing D-fructose was used to supplement levels of D-fructose-6-phosphate that would have otherwise been supplied by phosphoglucose isomerase-catalyzed isomerization of D-glucose-6-phosphate to D-fructose-6-phosphate. Final cell densities reached 37 ± 2.4 g/L dry cell weight with 150 g D-glucose consumed. Kanosamine titers reached 8.7 ± 0.08 g/L in 5.9 ± 0.6% mol/mol yield (Figure 74), enabled by the increased D-glucose consumption relative to RB791*serA pgi*::Kan^R/pSN1.292 grown on a D-glucose-only feed. Though the observed titers are lower than glucose-rich fermentations of RB791*serA*/pSN1.292 (12.7 ± 0.6 g/L, 4.4 ± 0.4% mol/mol yield), the overall yield from D-glucose is higher. Fermentations of RB791*serA pgi*::Kan^R/pSN1.292 also resulted in reduced formation of the acetic acid and pyruvic acid relative to RB791*serA*/pSN1.292 fermentations (Figure 73 and Figure 75). Acetic acid concentration decreased from 5.0 ± 2.5 g/L

to 1.7 ± 0.4 g/L and the concentration of pyruvic acid decreased from 0.7 ± 0.2 g/L to 0.05 ± 0.02 g/L. These results indicate that blocking glycolysis may be an effective strategy to increase kanosamine production, but strain or feed conditions must be optimized to balance kanosamine production with cell viability.

An unexpected observation during these fermentations was the appearance of L-glutamic acid in the fermentation broth. Both the D-glucose-only feed and the mixed D-glucose/D-fructose feed led to L-glutamic acid accumulation with 2.9 ± 0.7 g/L L-glutamic acid produced with a D-glucose-only feed (Fig. 73) and 3.9 ± 0.9 g/L L-glutamic acid produced during fermentations of a 1:1 D-glucose:D-fructose feed (Fig. 75). Accumulation of L-glutamic acid is likely a result of a metabolic network imbalance due to the *pgi* mutation. Previous reports have demonstrated that the glyoxylate shunt of the Krebs cycle (Figure 76) is more active in Δ*pgi* mutant strains of *E. coli* than wild type.[47] Routing flux through the glyoxylate shunt rather than the full Krebs cycle avoids exacerbating the redox imbalance caused by increased carbon flux through the pentose phosphate pathway, as NADH biosynthesis normally arising from conversion of 2-ketoglutarate to succinyl-CoA would not occur.[47] This increased flux through the glyoxylate shunt may result in an increased intracellular concentration of 2-ketoglutarate, which is converted to L-glutamic acid by *gdhA*-encoded glutamate dehydrogenase (Figure 77). It is possible that the kanosamine production observed in fermentations of RB791*serA pgi*::Kan^R/pSN1.292 are at least partially due to increased intracellular L-glutamate levels as more substrate would be available for the transamination of 3-keto-D-glucose-6-phosphate to kanosamine-6-phosphate.

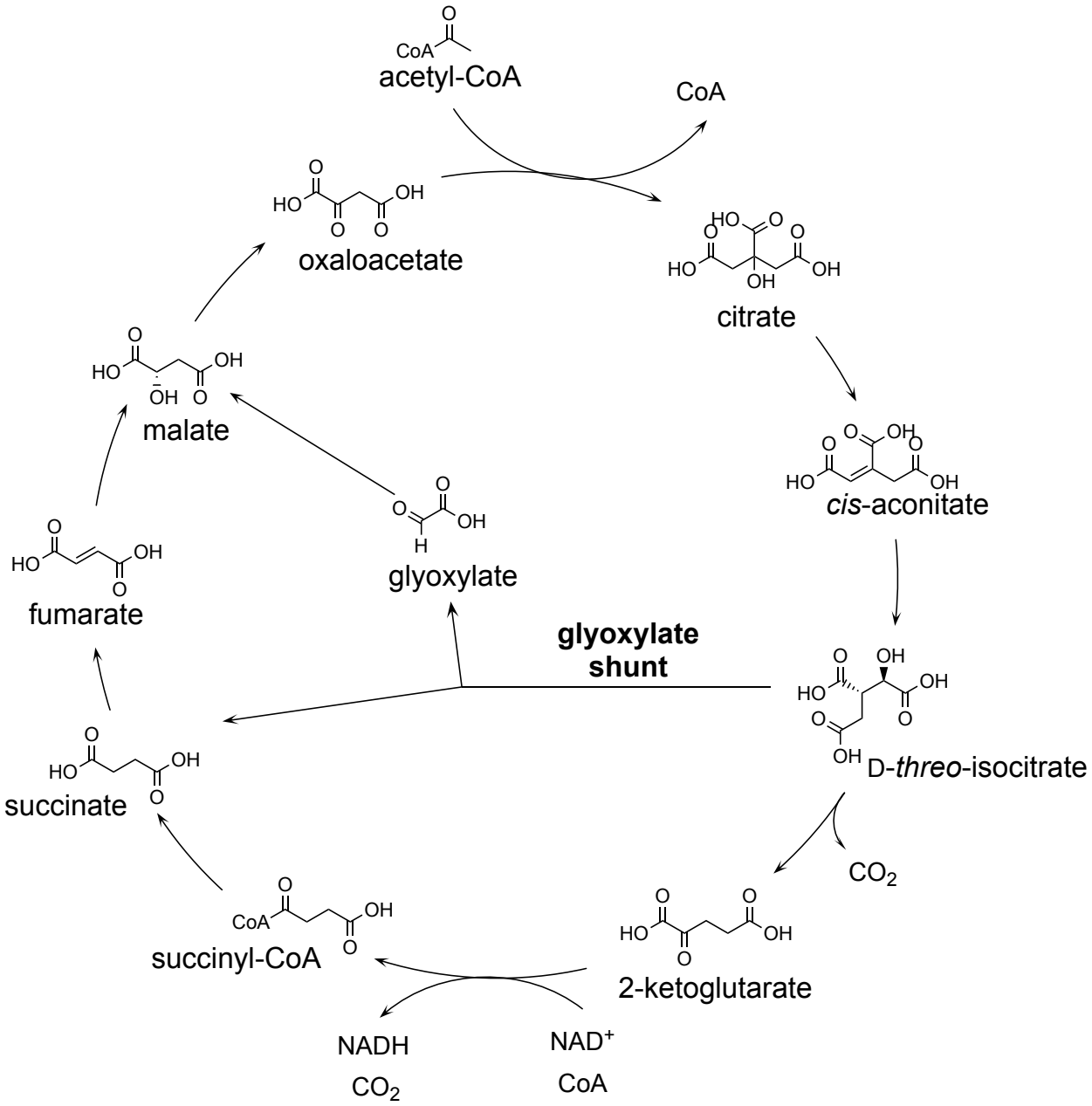

Figure 76. The Krebs cycle indicating the glyoxylate shunt from D-*threo*-isocitrate to glyoxylate.

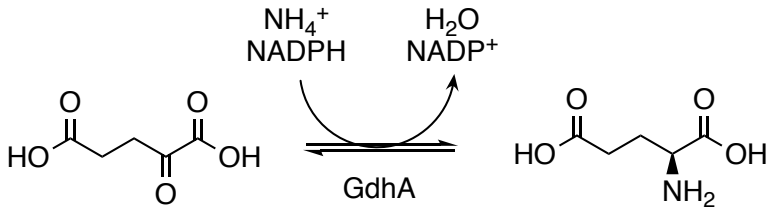

Figure 77. Glutamate dehydrogenase-catalyzed transamination of 2-ketoglutarate to L-glutamic acid.

Increased intracellular L-glutamic acid may explain the lack of D-glucosamine production in the fermentation broth in fermentations of RB791*serA pgi*::Kan^R/pSN1.292. Transamination of β-D-fructose-6-phosphate by action of *glmS*-encoded L-glutamine:D-fructose-6-phosphate aminotransferase affords L-glutamate as a byproduct. Increased L-glutamate levels relative to wild type concentrations would drive the equilibrium position of the *glmS*-encoded transamination (Figure 71) in the reverse direction, resulting in reduced D-glucosamine production. This provides additional support to the hypothesis that D-glucosamine is not derived directly from kanosamine but rather forms as a result of carbon flux through glycolysis and action of native *E. coli* enzymes such as GlmS.

The observation of D-fructose remaining in the fermentation broth after 48 h while D-glucose was not detected indicates that the two carbohydrates were not metabolized at equal rates. Carbon catabolite repression is well documented and often observed during fermentations of mixed carbohydrate feeds.[48] Because D-glucose is the preferred carbon source for *E. coli*, it is preferentially metabolized in the presence of alternative carbon sources. A mutation in *zwf*-encoded D-glucose-6-phosphate 1-dehydrogenase in addition to a mutation in *pgi*-encoded phosphoglucose isomerase has been shown to block carbon catabolite repression during fermentation of *E. coli* on a D-glucose/D-xylose mixed feed. Cells were shown to grow

exclusively on D-xylose while utilizing D-glucose for biosynthesis of D-glucaric acid.[48] An RB791*serA* Δ*pgi* Δ*zwf* double-mutant may result in an additional increase in kanosamine yield from D-glucose while achieving the good growth and high kanosamine titers that were absent during fermentation of RB791*serA pgi*::Kan^R/pSN1.292.

2.3. Media supplementation

The increased kanosamine yields observed in fermentations of RB791*serA pgi*::Kan^R, especially in the case of a D-glucose-only feed, in conjunction with accumulation of L-glutamic acid, a substrate for *ntdA*-encoded 3-keto-D-glucose-6-phosphate:L-glutamate aminotransferase, may suggest that increased L-glutamate availability may have a beneficial effect on kanosamine production in *E. coli*. Therefore, external L-glutamate (10 g/L) was added during glucose-limited runs (Table 22) of RB791*serA*/pSN1.292. Surprisingly, these fermentations resulted in greatly reduced D-glucose consumption relative to glucose-limited fermentation of RB791*serA*/ pSN1.292 in the absence of additional supplements (63 g relative to 145 ± 17.9 g). The decrease in D-glucose metabolism led to lower titer and yield of kanosamine (2.3 g/L, 3.7% mol/mol yield relative to 8.5 ± 1.4 g/L, 6.2 ± 2.2% mol/mol yield).

Table 22. Nitrogen supplementation during fed-batch fermentation of *E. coli* RB791*serA*/pSN1.292

Entry	Glucose conditions	Glucose consumed (g)	Nitrogen supplementation[a]	[Kanosamine] (g/L)	Yield (mol/mol)
1	limited	145 ± 17.9	none	8.5 ± 1.4	6.2 ± 2.2%
2	rich	296 ± 6.9	none	12.7 ± 0.6	4.4 ± 0.4%
3	limited	63	L-glutamate	2.3	3.1%
4	limited	155	soy flour	2.8	1.6%
5	rich	300	soy flour	9.9	5.3%

[a]Nitrogen supplements added prior to inoculation at 10 g/L final concentration. Error represents one standard deviation away from the mean across triplicate (glucose-rich) or quadruplicate (glucose-limited) runs.

Previous reports indicate that single amino acids such as L-proline, L-arginine, and L-glutamate are poor nitrogen sources.[49] Saturating levels of one of these amino acids lead to an increase in intracellular levels of α-ketoglutarate. Nitrogen and carbon assimilation pathways are linked at a branch point in which α-ketoglutarate serves as a regulatory molecule. Under nitrogen-limiting conditions, carbon flux is directed out of the citric acid cycle and into amino acid biosynthesis, affording a rise in α-ketoglutarate levels. Increased concentrations of α-ketoglutarate create a feedback signal for carbon assimilation at the level of adenylate cyclase which catalyzes synthesis of cAMP. As a regulatory molecule involved in D-glucose transport into the cell, reduced levels of cAMP lead to repression of D-glucose uptake.[49] Previous research by Jintao Guo in the Frost group demonstrated that soy flour supplementation at 10 g/L increased the amount of kanosamine produced in fed-batch fermentations of *Bacillus pumilus* by four-fold.[50] We then tested soy flour as a complex media supplement and source of extra nitrogen at 10 g/L under both glucose-rich and glucose-limited fermentations of RB791*serA*/pSN1.292 (Table 22). Under these conditions, D-glucose consumption was restored to levels matching

those of RB791*serA*/pSN1.292 without additional supplementation. However, kanosamine production under glucose-rich conditions (9.9 g/L, 5.3% mol/mol yield from D-glucose) was not enhanced beyond levels reached without an external nitrogen source (Table 22), suggesting that nitrogen is not the limiting factor in kanosamine production. Though exogenous L-glutamate supplementation did not lead to an enhancement of kanosamine biosynthesis, it is possible that an engineered *E. coli* with overexpressed L-glutamate biosynthesis enzymes could be more effective at improving kanosamine production than external media additives.

3. Kanosamine isolation from fermentation broth and inhibitory affects on RB791*serA*

Kanosamine displays antibiotic activity against a variety of different organisms with varying effectiveness (Table 17). To determine whether it is toxic to RB791*serA*, kanosamine was isolated from fermentation broth and added to shake-flask cultures of RB791*serA*/pSN1.292 in minimal media. Kanosamine was isolated as the hydrochloride salt using a procedure involving activated charcoal treatment, ion-exchange chromatography, and selective solubilization of kanosamine to separate contaminating salts. Cell-free, protein-free fermentation broth was treated with activated charcoal (10 g/L) at 37°C for 1 h and filtered through a layer of Celite 545. The clear, colorless filtrate was loaded onto a cation exchange column (Dowex 50WX8, H^+-form) and washed with four column-volumes of water. Kanosamine hydrochloride was eluted with a linear gradient of HCl (0-0.5 N). Fractions containing kanosamine were pooled and brought to pH 7.0 with 5 N KOH. Water was removed under reduced pressure and the pale yellow solids were dissolved into methanol. Insoluble salts were removed by filtration. The filtrate was evaporated under reduced pressure to afford kanosamine hydrochloride as an

off-white solid. Isolated material was characterized by ^{1}H, ^{13}C and two-dimensional NMR (Figures 78-80).

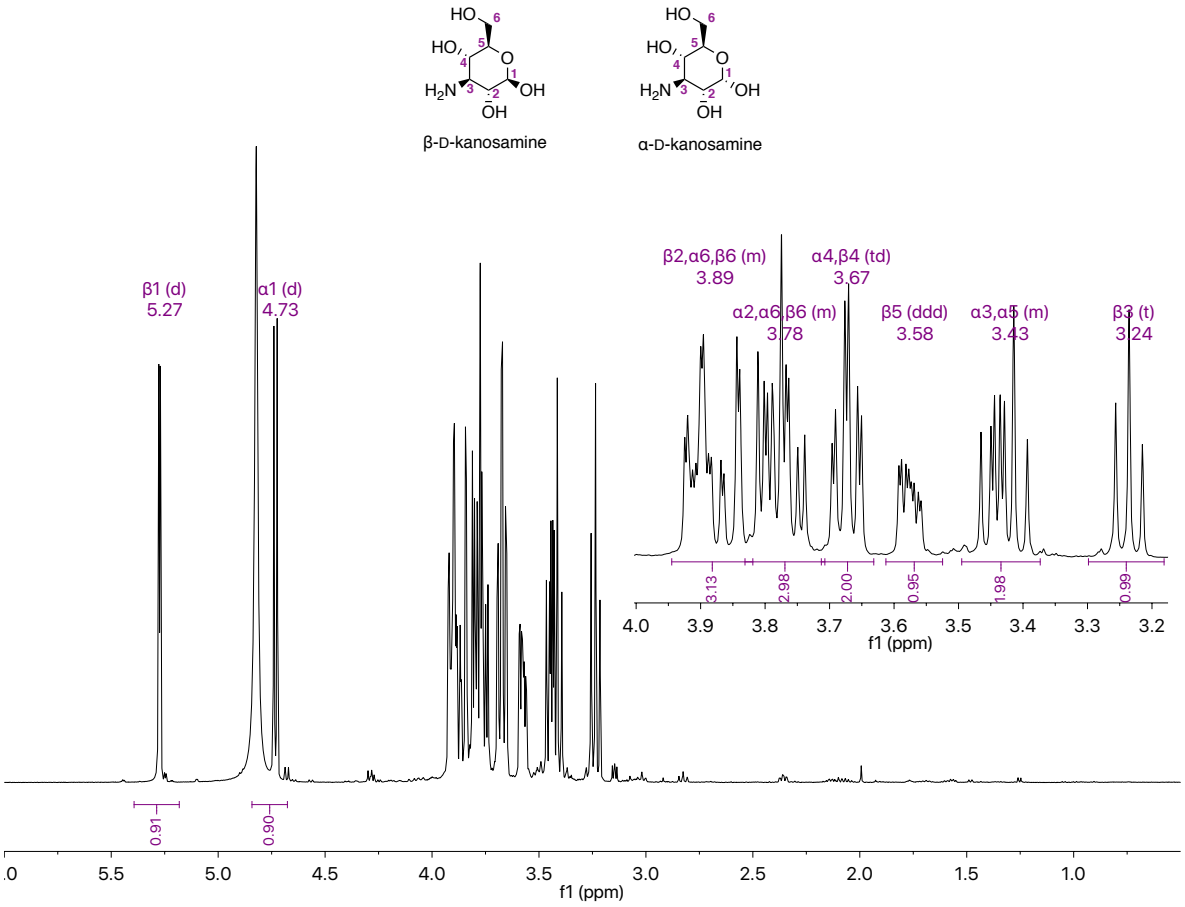

Figure 78. ^{1}H NMR spectrum of kanosamine isolated from fermentation broth.

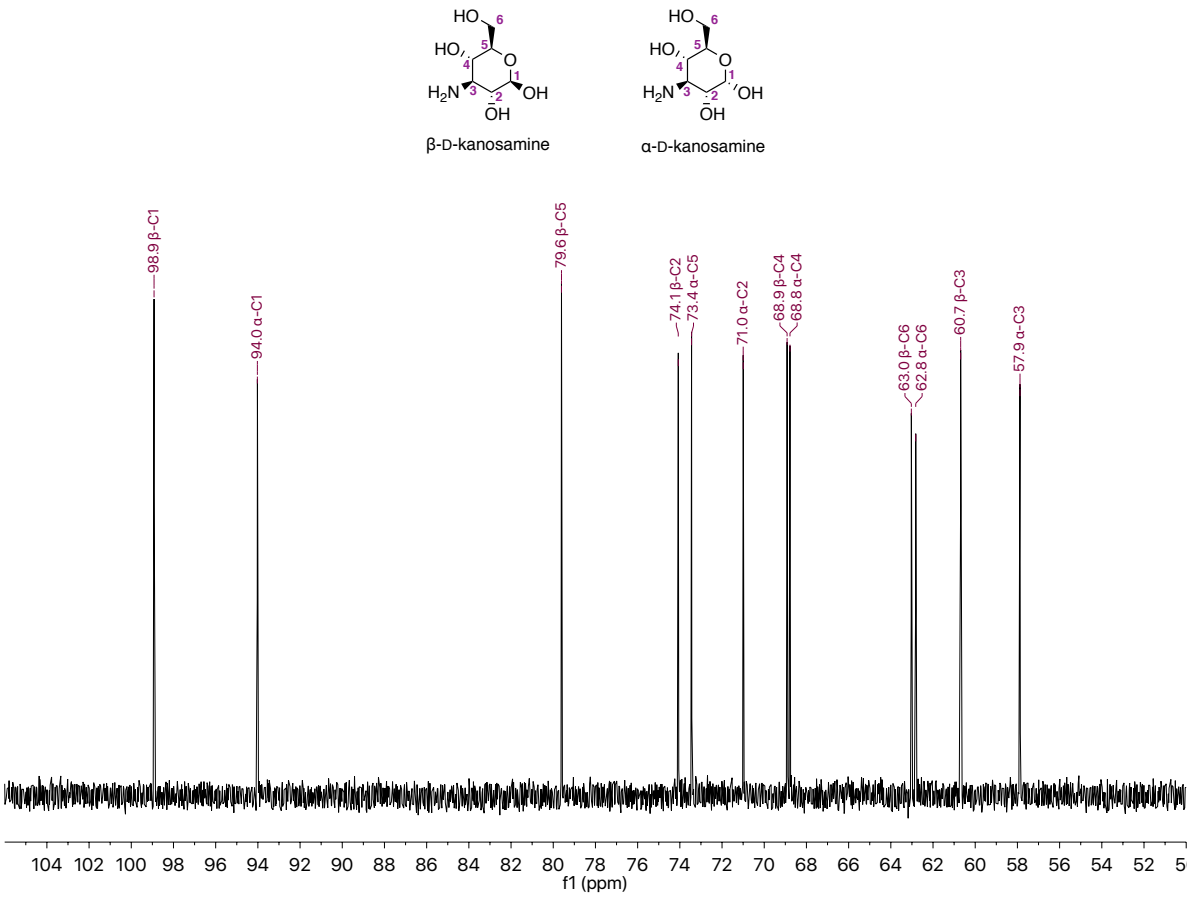

Figure 79. ^{13}C NMR spectrum of kanosamine isolated from fermentation broth.

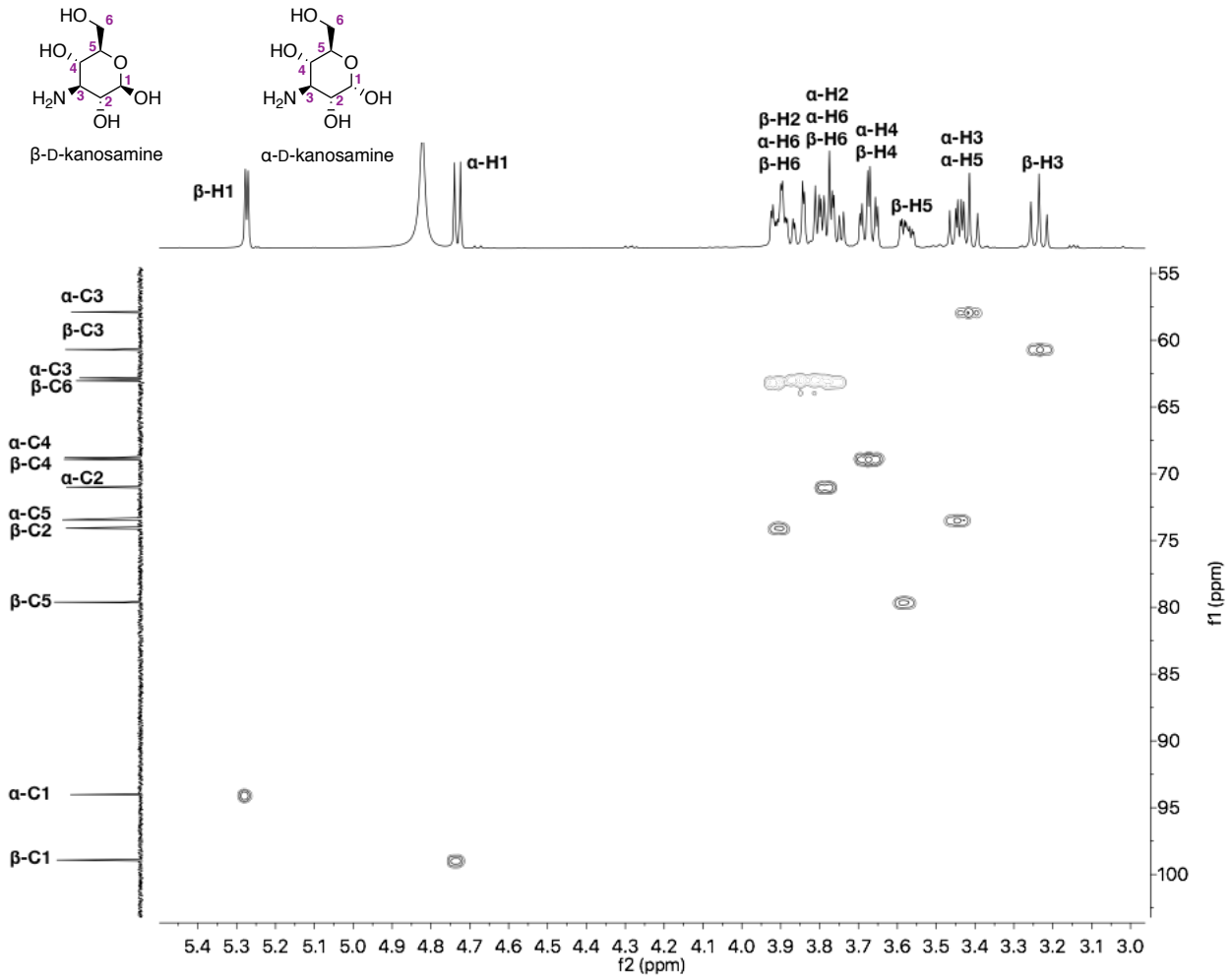

Figure 80. HSQC NMR spectrum of kanosamine isolated from fermentation broth.

To investigate potential inhibitory effects of kanosamine on RB791*serA*/pSN1.292, kanosamine isolated from fermentation broth was added to exponentially growing cells. A 5 mL culture of RB791*serA*/pSN1.292 in minimal media was grown overnight at 35°C with agitation at 250 rpm. This culture was used to inoculate 20 mL of the same media to an initial optical density (OD_{600}) of 0.05. Cells were grown at 35°C with agitation at 250 rpm to an OD_{600} = 0.4 marking the beginning of exponential growth phase, after which an aqueous solution of kanosamine (pH 8.0) was added to a final concentration of 25 mM (4.5 g/L) and 50 mM (9.0 g/

L). The optical density of each culture was measured at 1 h intervals during mid-exponential growth phase. These values were used to calculate the number of cells per milliliter of culture in order to determine growth rate of each culture (Figure 81). Conversion of optical density at 600 nm (OD_{600}) to number of cells per milliliter utilized the following conversion formula: $OD_{600}(1.0) = 1\times10^8$ cells/mL. The logarithm of the cellular concentration was plotted and the growth rates for each culture compared based on the slopes of the log curves. Exogenously added kanosamine did not inhibit growth of RB791*serA*/pSN1.292 at the concentrations tested, evidenced by growth rates similar to a culture of RB791*serA*/pSN1.292 without added kanosamine. This is supported by previous results reporting poor antibiotic activity of kanosamine on *E. coli* strains.

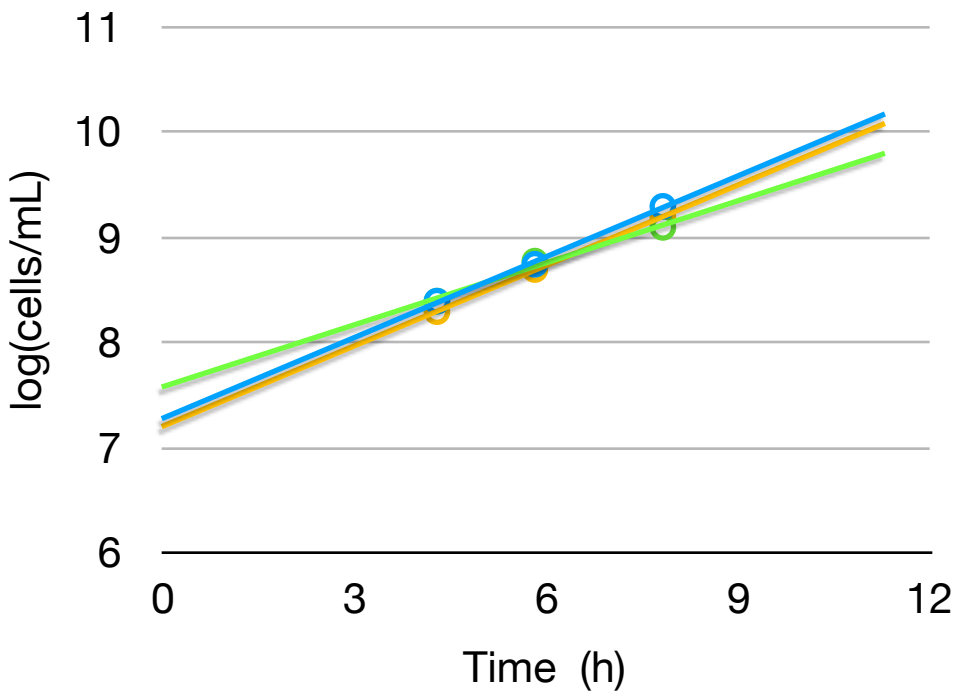

Figure 81. Exponential phase growth of RB791*serA*/pSN1.292 with exogenously added kanosamine at 0 mM (blue), 25 mM (green), and 50 mM (orange).

PART II

KANOSAMINE BIOSYNTHESIS FROM UDP-D-GLUCOSE

1. Overview

Two pathways of kanosamine biosynthesis have been reported in the literature (Figure 82). The pathway beginning with UDP-D-glucose (Pathway B, Fig. 82) has been implicated in kanosamine production both *Bacillus cereus*[28] and *Bacillus pumilus*,[29] as well as organisms such as *Amycolatopsis mediterranei*.[33,34] In *A. mediterranei*, kanosamine is a biosynthetic precursor to 3-amino-5-hydroxybenzoic acid (AHBA) via the aminoshikimate pathway. The key enzymes in this pathway responsible for kanosamine biosynthesis, *rifL*-encoded UDP-D-glucose 3-dehydrogenase, *rifK*-encoded 3-keto-UDP-D-glucose:L-glutamine aminotransferase, and *rifM*-encoded UDP-kanosamine phosphatase, have been assigned largely based on circumstantial evidence and sequence homology.[51] For instance, RifK, in addition to its well established role as AHBA synthase, has been assigned a second role in the aminoshikimate pathway as a 3-keto-UDP-D-glucose:L-glutamine aminotransferase. This assignment was based on structural similarities between RifK and the family of aspartate transaminases. The roles of RifL and RifM were assigned based on structural homology to known oxidoreductases and phosphatases, respectively.[51]

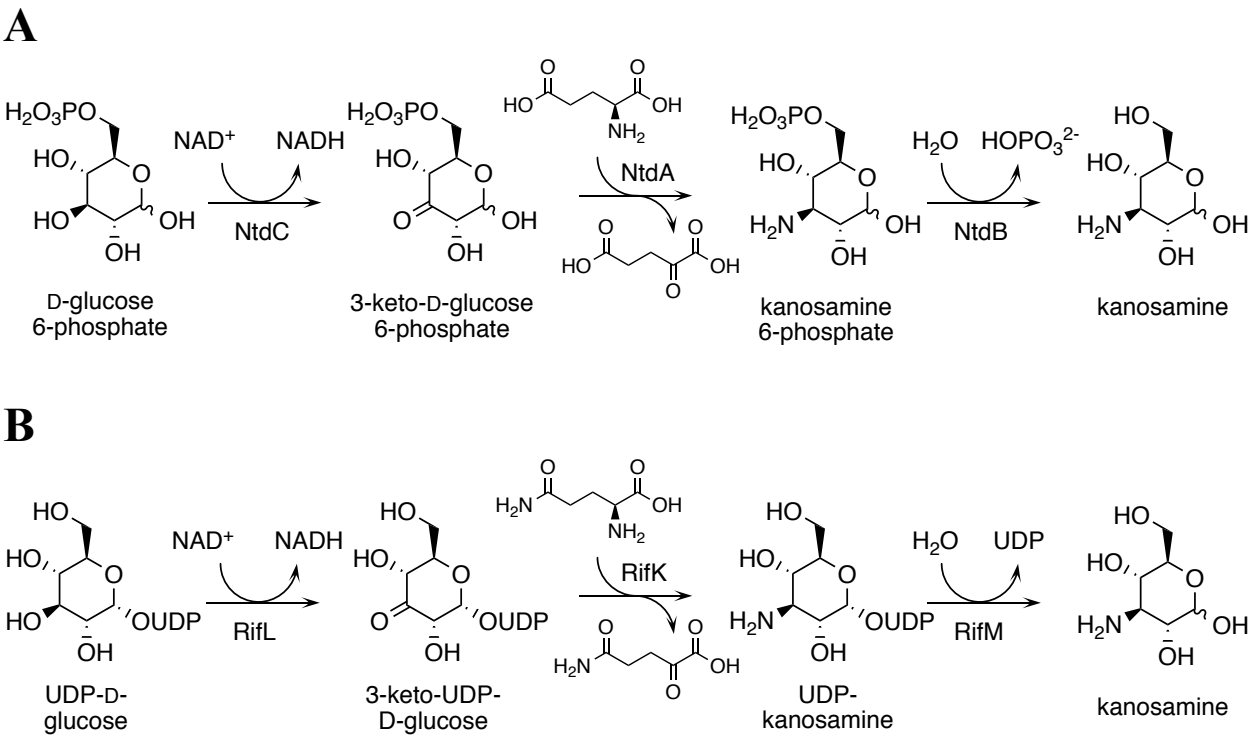

Figure 82. Kanosamine biosynthesis pathways reported in the literature. Pathway A described in *Bacillus subtilis*; Pathway B described in *B. pumilus*, *B. cereus*, and *A. mediterranei.*

2. Kanosamine production in fed-batch fermentation of *E. coli* constructs carrying *Amycolatopsis mediterranei* kanosamine biosynthetic genes

Kanosamine production resulting from expression of *Amycolatopsis mediterranei* gene expression in *E. coli* was evaluated in fed-batch fermentations following glucose-rich and glucose-limited conditions as described above. Because of the phylogenetic gap between *A. mediterranei* and *E. coli* and the difference in genomic G+C content, codon-optimized genes were utilized. Gene sequences encoding *rifL*, *rifK*, and *rifM* from *Amycolatopsis mediterranei* S699 were optimized for expression in *E. coli* using the web service OPTIMIZER®.[52] Optimized genes were synthesized by Integrated DNA Technologies, Inc. (IDT, Coralville, IA),

and inserted by IDT into a pUC18 vector with a 5' *Bgl*II restriction site and 3' *Bam*HI and *Xho*I restriction sites. The restriction sites flanking synthetic *rif* genes facilitated BglBrick assembly of two plasmids containing a *rifLrifKrifMserA* cassette either behind P_{trc} (pKM11.9, Figure 86) or P_{T7} (pKM11.46, Figure 87).

Each gene was first inserted into the *Bgl*II and *Xho*I sites of plasmid pBbA1a to afford a BglBrick part (Figure 83). Next, each *rif* gene was inserted upstream of *serA* by digesting the BglBrick part containing *serA*, pKM6.240 (Figure 84), with *Eco*RI and *Bgl*II to create a double-stranded break upstream of *serA*. Digestion of the *rifM*-containing BglBrick part, pKM10.254M (Figure 84), with *Eco*RI and *Bam*HI followed by ligation of the digested DNA afforded plasmid pKM10.268M. The *rifK* gene from pKM10.254K was then inserted upstream of *rifM* in plasmid pKM10.268M to afford plasmid pKM10.278KM (Figure 85). Finally, *rifL* from plasmid pKM10.254L was inserted upstream of *rifM* in plasmid pKM10.278KM to afford plasmid pKM11.9 containing a P_{trc}*rifLrifKrifMserA* cassette (Figure 86). Another plasmid was created that contained a P_{T7} cassette by inserting the *rifLrifKrifMserA* fragment from pKM11.9 into pBbA7k to afford pKM11.46 (Figure 87).

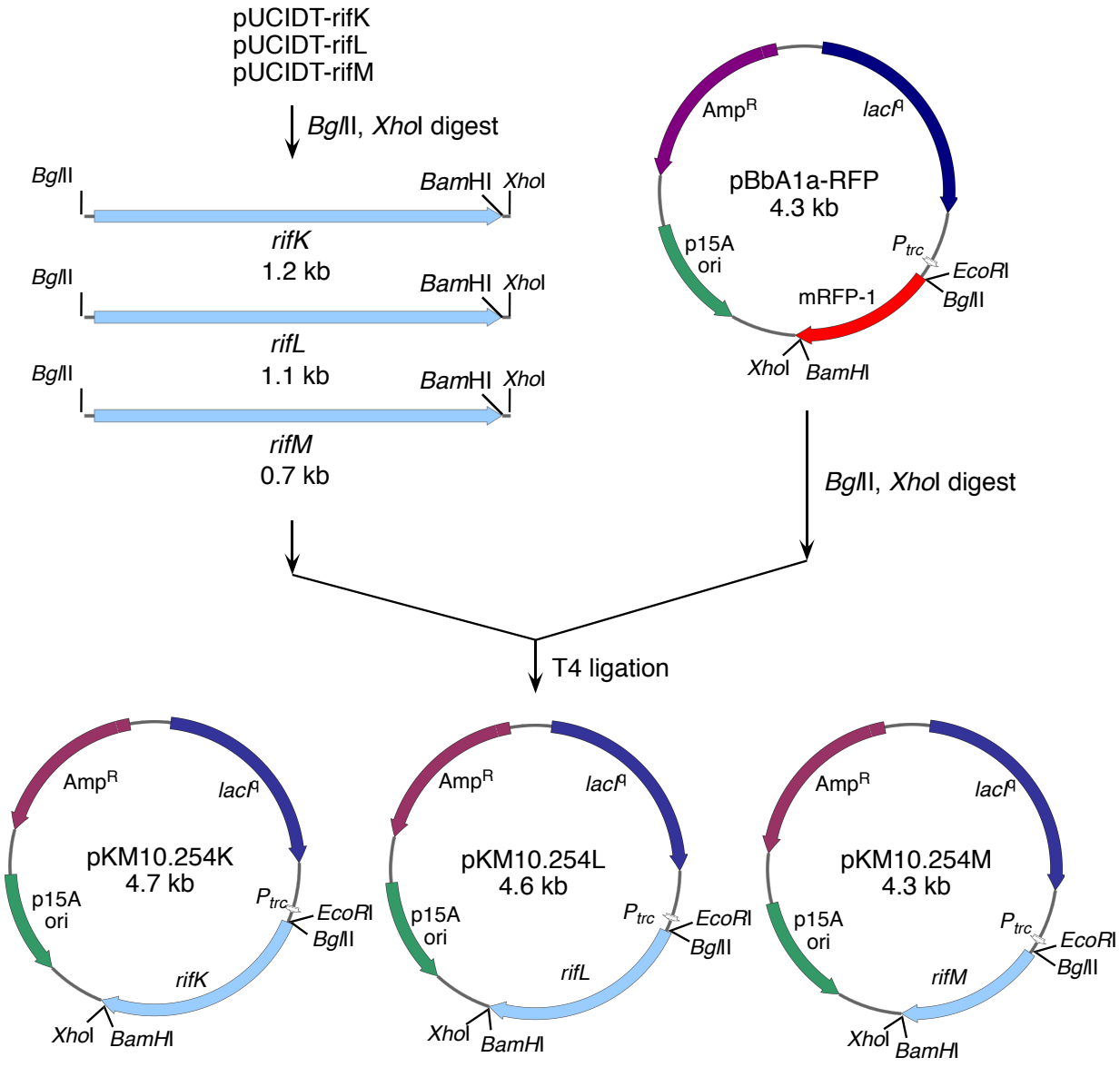

Figure 83. Construction of *rif* BglBrick parts: plasmids pKM10.254K, pKM10.254L, and pKM10.254L.

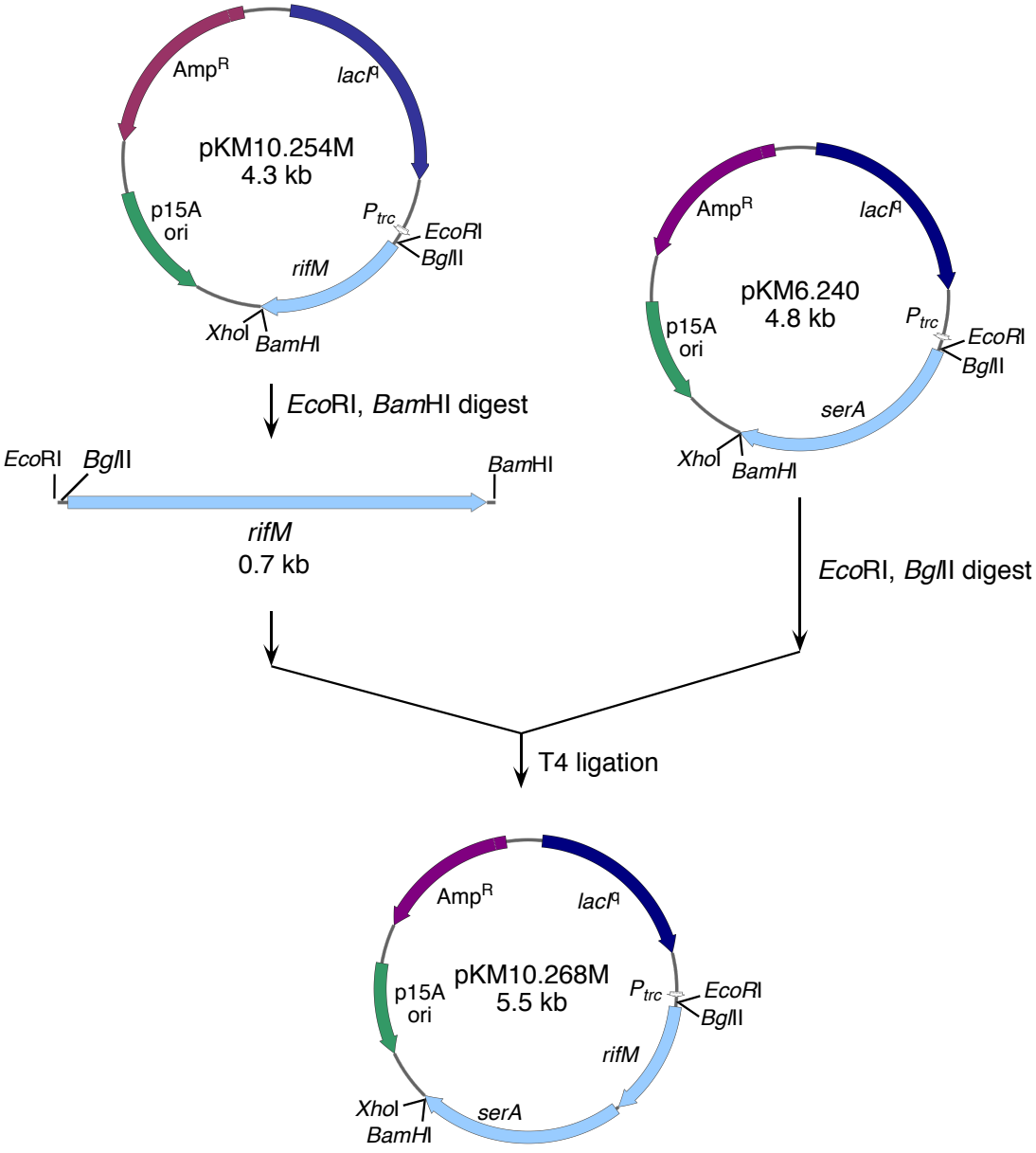

Figure 84. Construction of plasmid pKM10.268M.

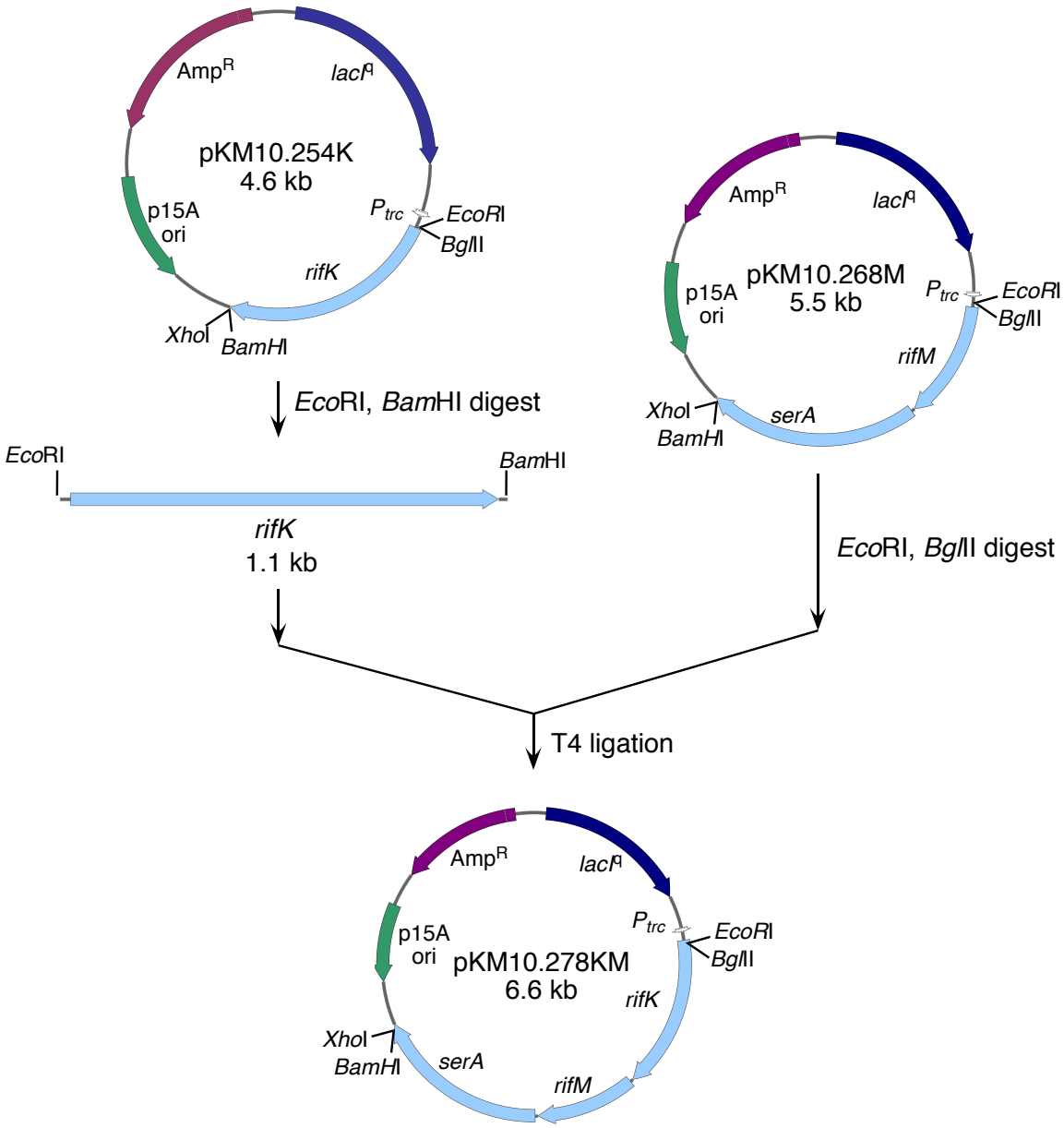

Figure 85. Construction of plasmid pKM10.278KM.

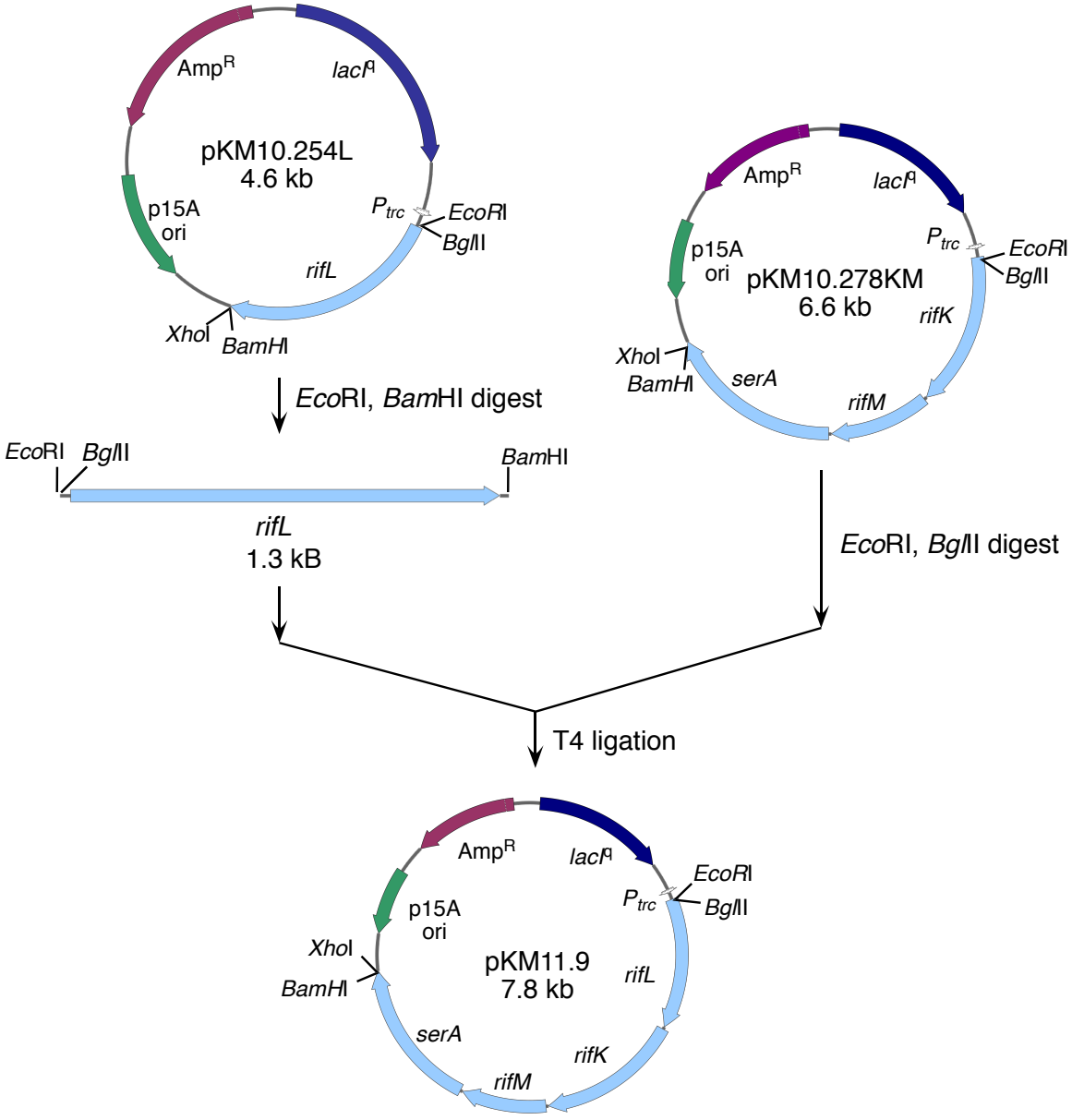

Figure 86. Construction of plasmid pKM11.9.

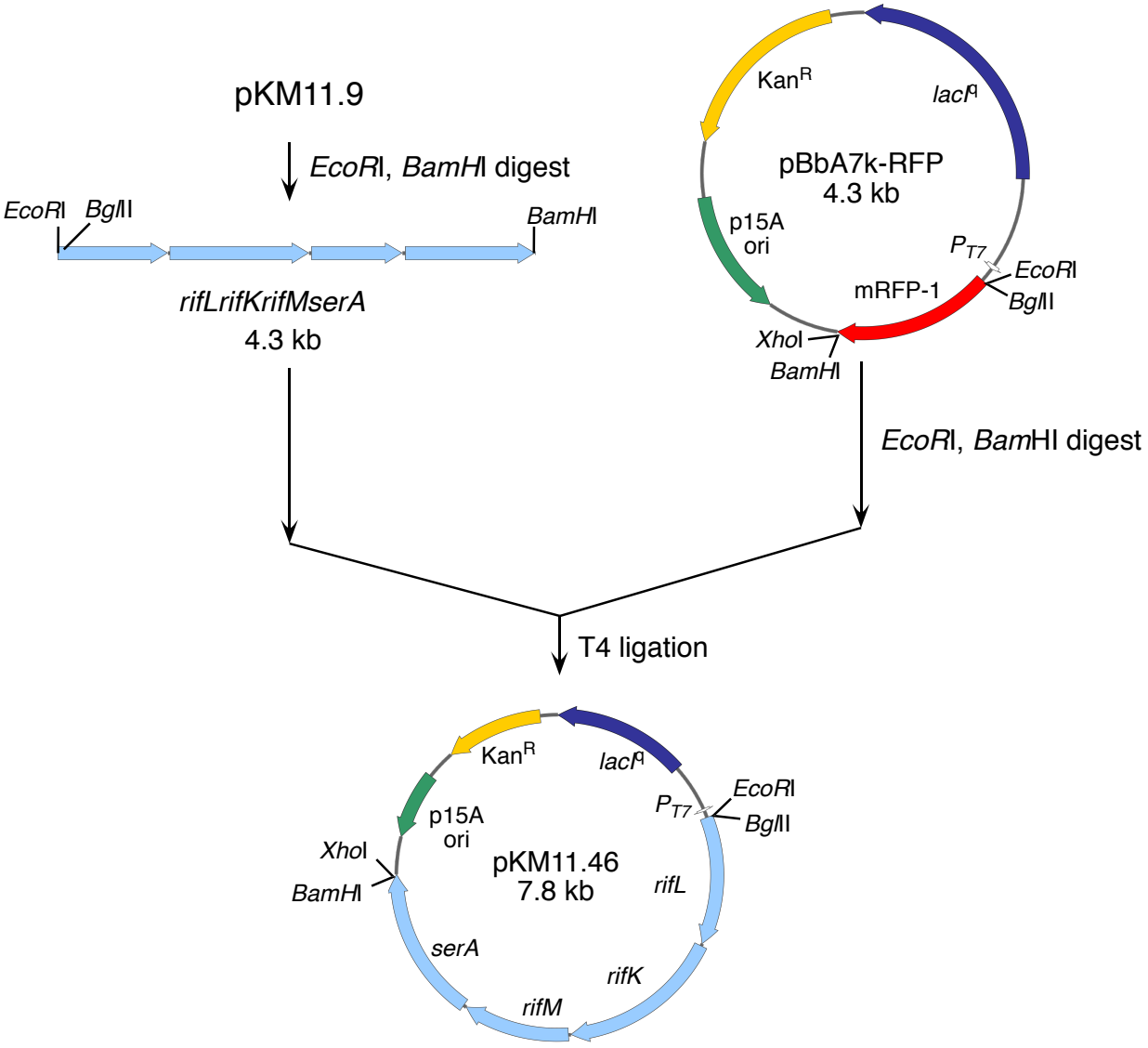

Figure 87. Construction of plasmid pKM11.46.

Plasmid pKM11.9 was transformed into RB791*serA* and kanosamine production was examined in glucose-rich (Figure 88) and glucose-limited conditions (Figure 89). Rather than accumulating kanosamine as was anticipated, glucose-rich conditions afforded substantial amounts (46 g/L) of acetic acid. Formic acid, pyruvic acid, and lactic acid were also observed at

concentrations of 0.75 g/L, 0.35 g/L, and 0.26 g/L, respectively. Glucose-limited fermentation of RB791*serA*/pKM11.9 (Figure 89) resulted in small amounts of acetic acid (0.09 g/L), formic acid (0.07 g/L), pyruvic acid (0.04 g/L), and lactic acid (0.05 g/L).

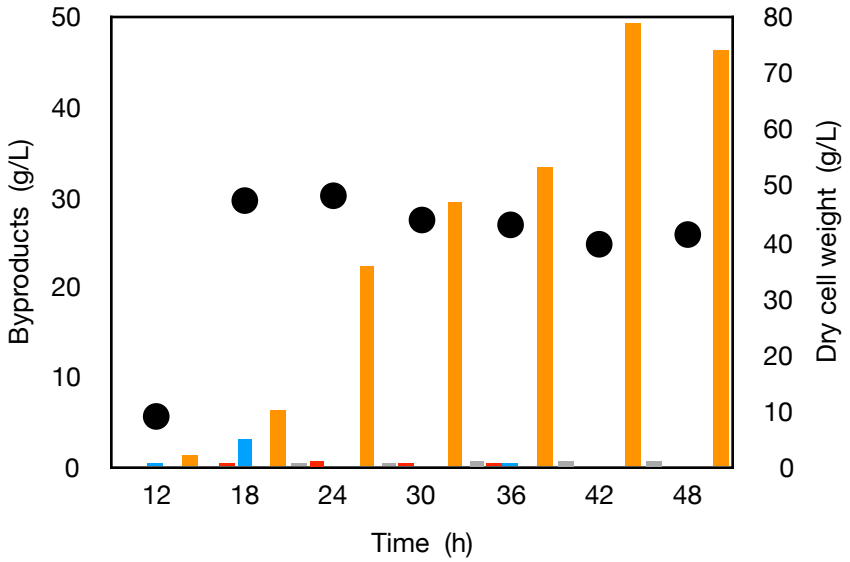

Figure 88. Products formed in fed-batch fermentation of *E. coli* RB791*serA*/pKM11.9 under glucose-rich conditions. Legend: acetic acid, orange columns; formic acid, grey columns; lactic acid, blue columns; dry cell weight, black circles.

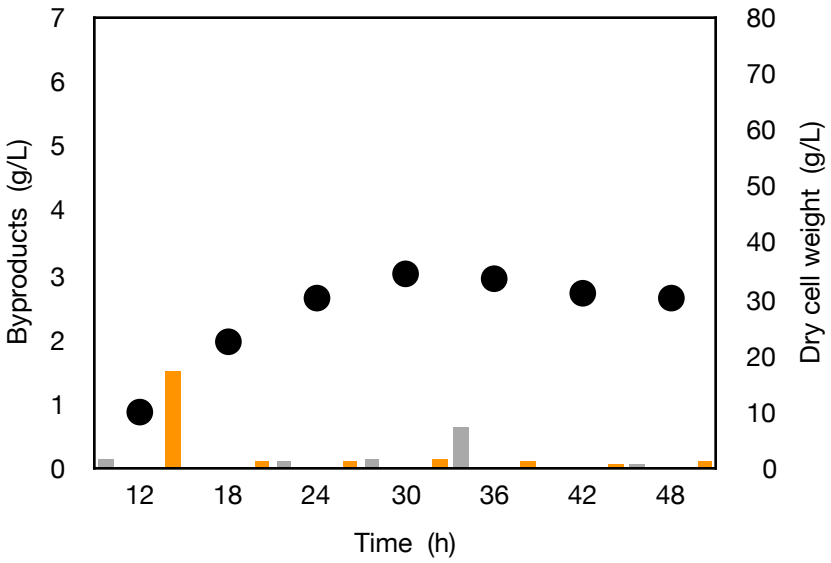

Figure 89. Products formed in fed-batch fermentation of *E. coli* RB791*serA*/pKM11.9 under glucose-limited conditions. Legend: acetic acid, orange columns; formic acid, grey columns; dry cell weight, black circles.

It was thought that the lack of kanosamine production in RB791*serA*/pKM11.9 which contained *rifLrifKrifMserA* under the control of P_{trc} was due to pyrimidine starvation. Previous research reports *E. coli* K-12 wild type strains, W3110 and MG1655, suffer pyrimidine starvation when cultured in minimal media.[53] As RB791*serA* is a derivative of W3110, uracil was added at 20 mg/L in glucose-rich fermentation of RB791*serA*/pKM11.9 and at 200 mg/L in glucose-limited fermentation of RB791*serA*(DE3)/pKM11.46, which carried the *rif* genes under control of P_{T7}. Neither set of conditions resulted in kanosamine accumulation (Figure 90 and Figure 91).

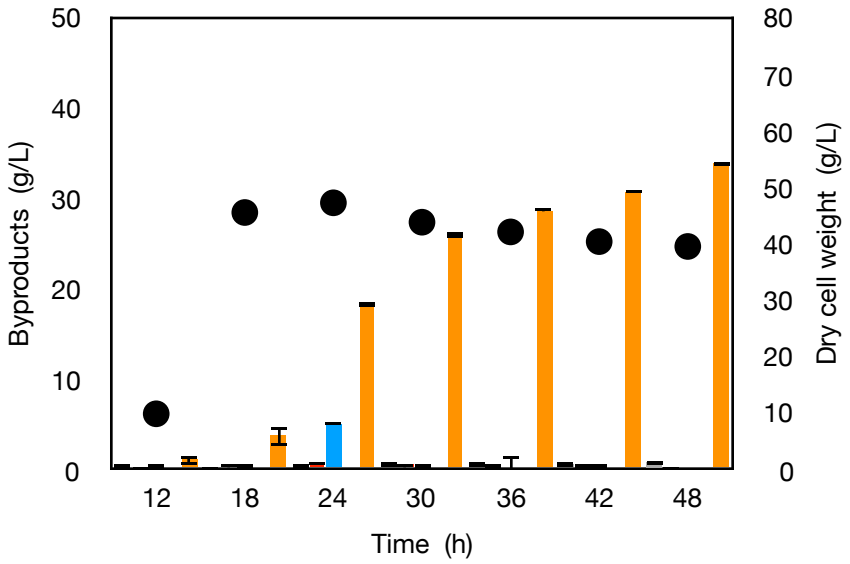

Figure 90. Products formed in fed-batch fermentation of *E. coli* RB791*serA*/pKM11.9 with 20 mg/L uracil supplementation under glucose-rich conditions. Legend: acetic acid, orange columns; formic acid, grey columns; lactic acid, blue columns; dry cell weight, black circles.

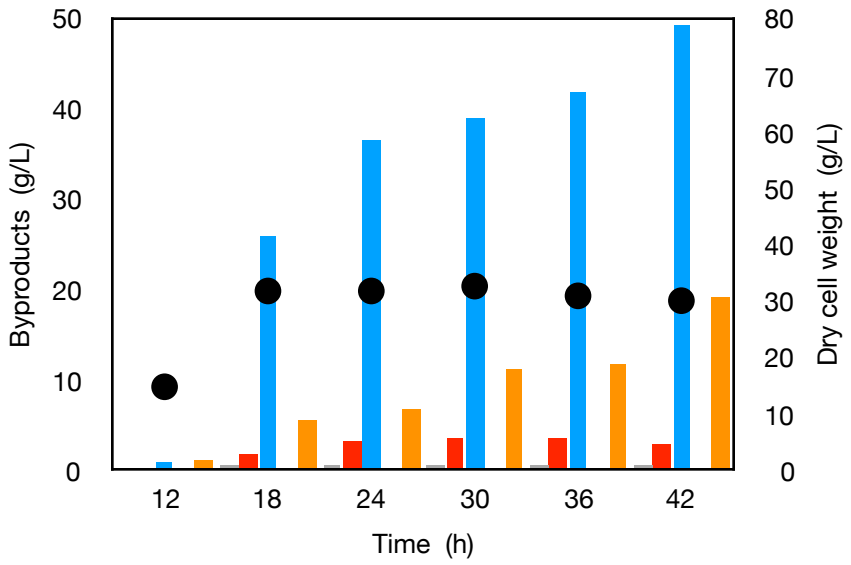

Figure 91. Products formed in fed-batch fermentation of *E. coli* RB791*serA*(DE3)/pKM11.46 with 200 mg/L uracil supplementation under glucose-limited conditions. Legend: acetic acid, orange columns; formic acid, grey columns; lactic acid, blue columns; dry cell weight, black circles.

Kanosamine production was then evaluated using *E. coli* KL3, which is not known to suffer pyrimidine starvation. *E. coli* KL3 is a derivative of AB2834 and contains a mutation in *aroE* encoding shikimate dehydrogenase.[54] Because of this mutation, it is unable to synthesize aromatic amino acids and aromatic vitamins. To ensure viability in minimal media, L-tryptophan, L-phenylalanine, L-tyrosine, 2,3-dihydroxybenzoic acid, 4-hydroxybenzoic acid, and 4-aminobenzoic acid were added to all culture and fermentation media when utilizing KL3. Transformation of plasmid pKM11.9, which contained a P_{trc}*rifLrifKrifMserA* cassette, into KL3 was followed by both glucose-rich and glucose-limited fermentations (Figure 92 and Figure 93).

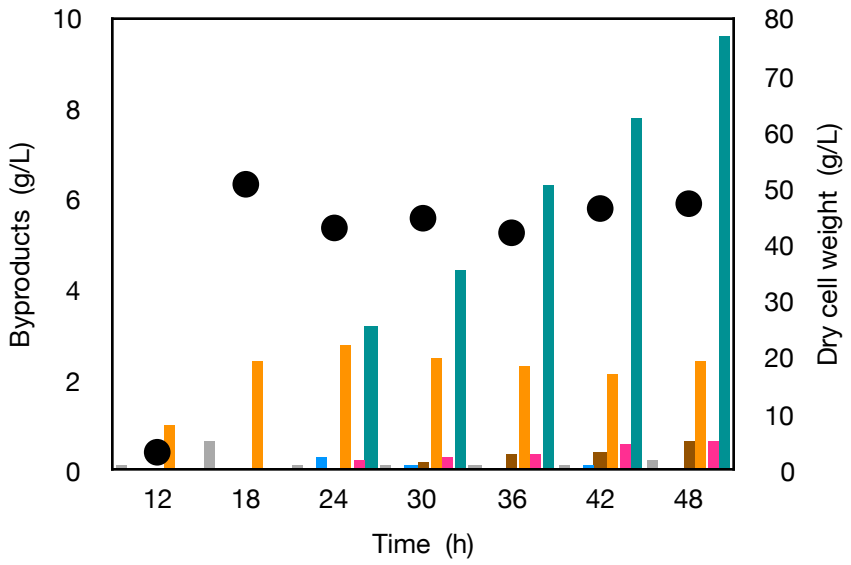

Figure 92. Products formed in fed-batch fermentation of *E. coli* KL3/pKM11.9 glucose-rich conditions. Legend: acetic acid, orange columns; formic acid, grey columns; lactic acid, blue columns; gallic acid, brown columns; 3-dehydroquinic acid, pink columns; 3-dehydroshikimic acid, teal columns; dry cell weight, black circles.

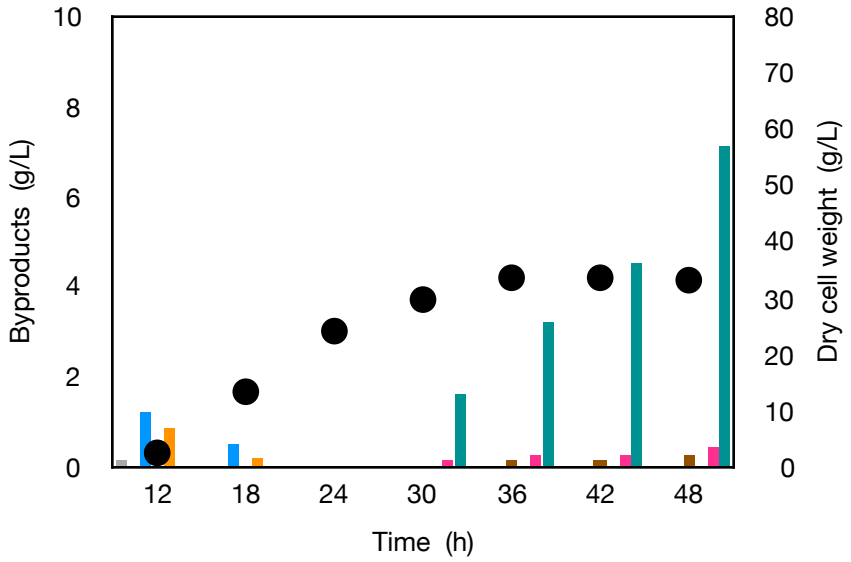

Figure 93. Products formed in fed-batch fermentation of *E. coli* KL3/pKM11.9 glucose-limited conditions. Legend: acetic acid, orange columns; formic acid, grey columns; lactic acid, blue columns; gallic acid, brown columns; 3-dehydroquinic acid, pink columns; 3-dehydroshikimic acid, teal columns; dry cell weight, black circles.

As was observed in fermentations of RB791*serA*/pKM11.9 and RB791*serA*(DE3)/ pKM11.46, kanosamine did not accumulate in fermentation broth. Acetic acid production was

substantially lower with KL3/pKM11.9 (2.4 g/L and 0.03 g/L under glucose-rich and glucose-limited conditions, respectively) than with RB791*serA*/pKM11.9 either in the presence (33.9 g/L) or absence (46.3 g/L) of exogenously added uracil. The major product observed in fermentations of KL3/pKM11.9 was 3-dehydroshikimic acid which accumulated in both glucose-rich and glucose-limited fermentations at a concentration of 7.1 g/L. 3-Dehydroquinic acid and gallic acid were also observed in both glucose-rich and glucose-limited conditions. Accumulation of shikimate pathway metabolites is due to the mutation in *aroE*-encoded shikimate dehydrogenase.

3. Activity of UDP-D-glucose 3-dehydrogenase

A possible reason for lack of kanosamine production in fermentations of *E. coli* transformed with codon-optimized *rif* genes could be due to an inability of *E. coli* to express the enzymes in active forms. Cell-free extracts of samples withdrawn from fermentation of RB791*serA*/pKM11.9 and His_6-tagged UDP-D-glucose 3-dehydrogenase encoded by *rifL* were assayed for activity by monitoring absorbance at 340 nm due to formation of NADH during the dehydrogenation of UDP-D-glucose in 10 mM sodium phosphate buffer, pH 7.0 at ambient temperature (Figure 94). Enzyme activity was not observed in the cell-free extract with either UDP-D-glucose. Activity of 0.4 U/mg was measured in incubations of UDP-D-glucose with His_6-RifL, which had been purified by Ni-NTA metal-affinity chromatography on an ÄKTA FPLC (GE Life Sciences) (Table 23). Though an observed activity of 0.4 U/mg would be expected using cell-free extracts, observed activity of a given enzyme is proportional to the purity of that enzyme. Therefore, an activity of 0.4 U/mg of Ni-NTA purified protein suggests

low inherent catalytic activity. The lack of activity in cell-free extracts and the small amount of activity observed with His_6-tagged protein suggests a difficulty in expressing active enzyme in *E. coli*. Assays using D-glucose-6-phosphate were conducted as a negative control.

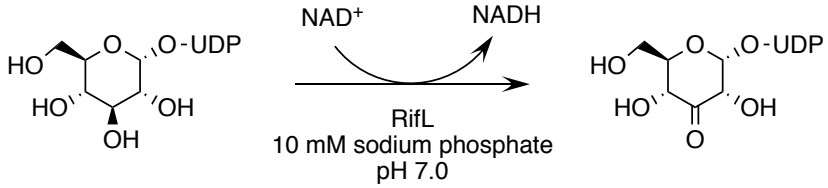

Figure 94. Assay conditions for RifL-catalyzed conversion of UDP-D-glucose to 3-keto-UDP-D-glucose.

Floss and coworkers report similar challenges associated with expression the kanosamine biosynthesis enzymes from *Amycolatopsis mediterranei* in *E. coli*.[51] The authors were unable to observe phosphatase activity using His_6-RifM and report a lack of His_6-RifK-catalyzed aminotransferase activity using a variety of pseudosubstrates in either the forward or reverse direction. They further describe expression of RifL in *E. coli* resulted only in formation of insoluble protein aggregates.[50] An organism that is more closely related to *A. mediterranei*, such as *Streptomyces* spp. may be better suited for Rif enzyme expression.

Table 23. Specific activity of UDP-D-glucose 3-dehydrogenase in cell-free extract and with purified protein.

Enzyme source[a]	Sp. activity (µmol/min/mg) (UDPGlc)	Sp. activity (µmol/min/mg) (G6P)
His_6-RifL	0.41	not tested
12 h cell lysate	n.d.	n.d.
24 h cell lysate	n.d.	n.d.
36 h cell lysate	n.d.	n.d.
48 h cell lysate	n.d.	n.d.

[a] His_6-tagged protein purified by Ni-NTA chromatography; cell lysates collected from glucose-limited fermentation of RB791*serA*/pKM11.9. n.d. = not detected.

4. *Bacillus pumilus* as source of kanosamine biosynthetic genes

The lack of kanosamine accumulation in fermentation of *E. coli* harboring plasmid-localized, codon-optimized *rif* genes from *Amycolatopsis mediterranei* and the poor catalytic activity associated with *rifL*-encoded UDP-D-glucose 3-dehydrogenase in *in vitro* assays prompted a search for an alternative source of kanosamine biosynthesis genes. *Bacillus pumilus* was the first microbe reported to accumulate kanosamine in batch fermentations in a media consisting of D-glucose (1.0 wt%), soybean meal (1.5 wt%), and NaCl (0.3 wt%), at 34°C for 76 h.[29] When fed universally labelled D-[U-^{14}C]-glucose, fermentation of *Bacillus pumilus* resulted in universially labelled [U-^{14}C]-kanosamine. The same feeding experiment was performed using D-[1-^{14}C]-glucose, D-[2-^{14}C]-glucose, and D-[6-^{14}C]-glucose, which resulted in the production of the associated ^{14}C-labelled kanosamine. In vitro conversion of D-[U-^{14}C]-glucose catalyzed by a *B. pumilus* cell-free extract resulted in greater amounts of isotopically labelled kanosamine when both ATP and UTP were present in the reaction mixture. When these cofactors were absent, a 92% reduction of kanosamine production was observed. These observations ultimately led to the proposed pathway presented in Figure 95.[30]

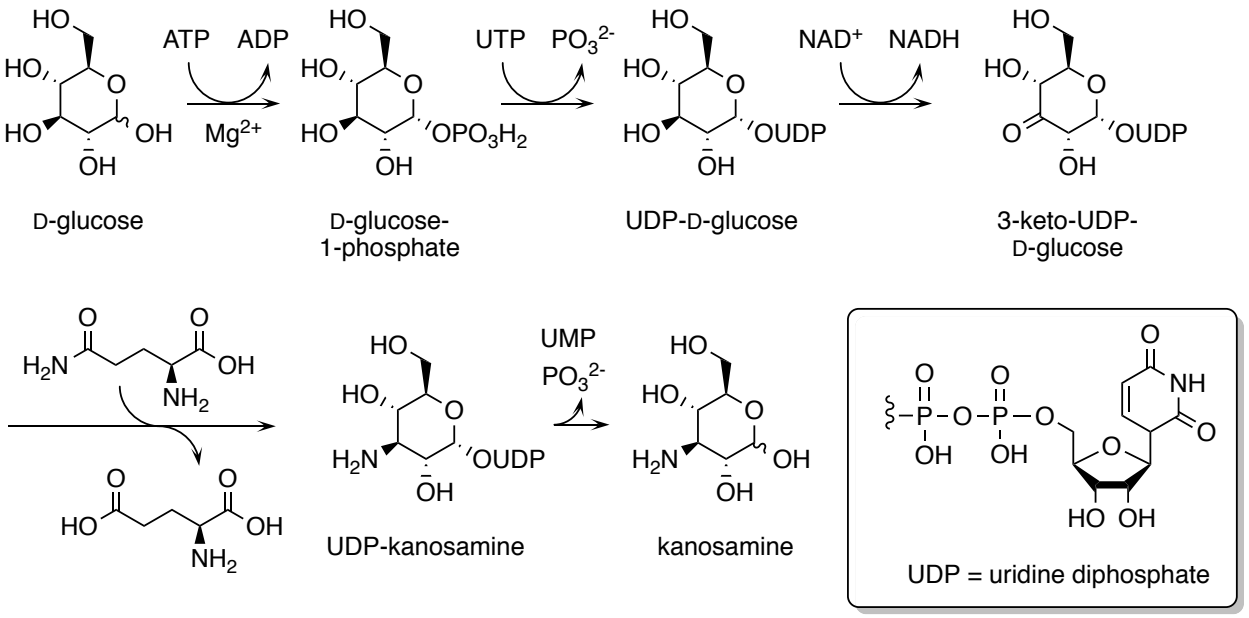

Figure 95. Kanosamine biosynthesis pathway via UDP-D-glucose as proposed by Umezawa.[30]

A Basic Local Alignment Search Tool (BLAST) query of Rif proteins against protein sequence data reported for *Bacillus pumilus* (Taxonomy ID: 1408) did not identify highly similar Rif analogs in *Bacillus pumilus*. The taxonomy ID 1408 group encompasses all *Bacillus pumilus* strains derived from type strain *B. pumilus* Meyer and Gottheil 1901 and is assigned by the National Center for Biotechnology Information (NCBI). Protein sequence data in the reference protein (ref_seq) database was used and proteins were determined to be highly similar if sequences contained >30% alignment with an expect-threshold value $<10^{-6}$. The expect-threshold (*E*) is used to estimate statistical significance and represents the amount of positive alignments one "expects" to see by chance when searching a database. In other terms, this value represents random background noise. Lower expect-thresholds indicate higher degrees of significant alignment. A threshold of 10^{-6} indicates that one in one million alignments may be a random positive alignment.

Protein BLAST queries did reveal sequences for an oxidoreductase, aminotranferase, and a phosphatase present in multiple strains of *Bacillus pumilus* (Taxonomy ID: 1408) with a high degree of similarity and statistical significance to the Ntd protein sequences from *Bacillus subtilis*. The oxidoreductase protein sequence had 57% identity (78% similar) to *B. subtilis* NtdC ($E = 2e^{-142}$) over 91% of the 348 amino acid sequence. The aminotransferase contained 58% identity (75% similar) to *B. subtilis* NtdA ($E = 0.0$) over 99% of the 441 amino acid sequence. Lastly, the phosphatase sequence had 55% identity (75% similar) to *B.* subtilis NtdB ($E = 3e^{-110}$) over 96% of the 288 amino acid sequence. Based on these highly similar sequences we wondered if *Bacillus pumilus* contains putative *ntd* genes that encode kanosamine biosynthesis enzymes which might utilize the D-glucose-6-phosphate-dependent pathway described above for *B. subtilis*.

Several strains of *B. pumilus* have complete genome sequence data. These include *B. pumilus* ATCC 7061, *B. pumilus* SH-B11, *B. pumilus* SAFR-032, and *B. pumilus* NCTC 10337, among others. All of these strains are catalogued by NCBI under the Taxonomy ID 1408 and were found to contain genes that encode the putative Ntd proteins discovered by BLAST queries. The putative *ntd* gene sequences from the *B. pumilus* SH-B11 genome were submitted to IDT for gene synthesis without prior codon optimization. Codon optimization was not utilized in order to make a direct comparison between expression of *B. pumilus* genes in *E. coli*, and the previously described expression of *B. subtilis* genes, which had been PCR-amplified from the *B. subtilis* 168 genome and therefore not codon-optimized.

To distinguish between genes and enzymes native to *B. subtilis* and those native to *B. pumilus*, superscript descriptors, sub or pum, will be hereafter included in the name of a gene or

protein. For example, *ntdC*^{sub} will indicate the gene encoding D-glucose-6-phosphate 3-dehydrogenase native to *B. subtilis*, while *ntdC*^{pum} will indicate the gene encoding D-glucose-6-phosphate-3-dehydrogenase native to *B. pumilus*.

The synthetic *ntd*^{pum} genes were received from IDT in separate pUC18 vectors with a 5' *Bgl*II restriction site and 3' *Bam*HI and *Xho*I restriction sites. Each vector was digested with *Bgl*II and *Xho*I and inserted into the *Bgl*II and *Xho*I sites of plasmid pBbA1a to create BglBrick parts for each *ntd*^{pum} gene (Figure 96). A complete plasmid was constructed by using prefix insertion of one BglBrick part in front of another. To begin, the BglBrick part containing *ntdB*^{pum} (plasmid pKM11.121B) was digested with *Eco*RI and *Bam*HI while the *serA*-containing BglBrick part (plasmid pKM6.240) was digested with *Eco*RI and *Bgl*II (Figure 97). Ligation of the digested DNA with T4 DNA ligase resulted in plasmid pKM11.125 which contained *ntdB*^{pum} upstream of *serA*. The *Eco*RI site was reformed in plasmid pKK11.125 while the *Bgl*II and *Bam*HI compatible DNA ends were joined to afford a glycine-serine scar sequence between *ntdB*^{pum} and *serA*. Plasmid pKM11.125, contains the same restriction sites as plasmid pKM6.240, which allows iterative gene insertion without need to use varying cut sites or enzymes. This method of gene insertion was repeated to insert *ntdC*^{pum} upstream of *ntdA*^{pum} affording plasmid, pKM11.130 (Figure 98), which carried a P_{trc}*ntdC*^{pum}*ntdA*^{pum} cassette. Finally, *ntdC*^{pum}*ntdA*^{pum} was inserted into pKM11.125 upstream of *ntdB*^{pum} to afford plasmid pKM11.135 (Figure 99), which contained the complete operon: P_{trc}*ntdC*^{pum}*ntdA*^{pum}*ntdB*^{pum}*serA*.

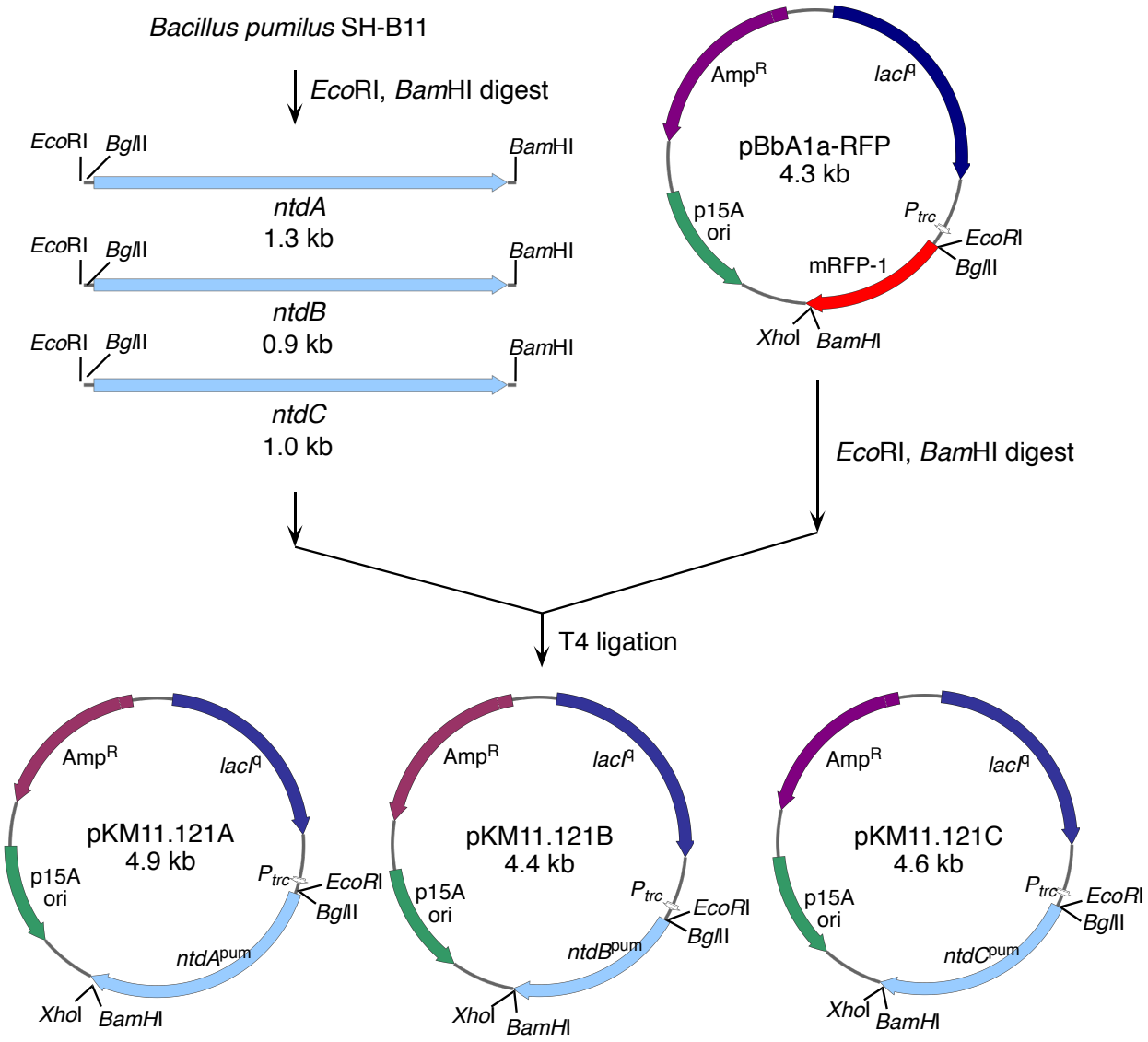

Figure 96. Construction of *ntd* BglBrick parts: plasmids pKM11.121A, pKM11.121B, and pKM11.121C.

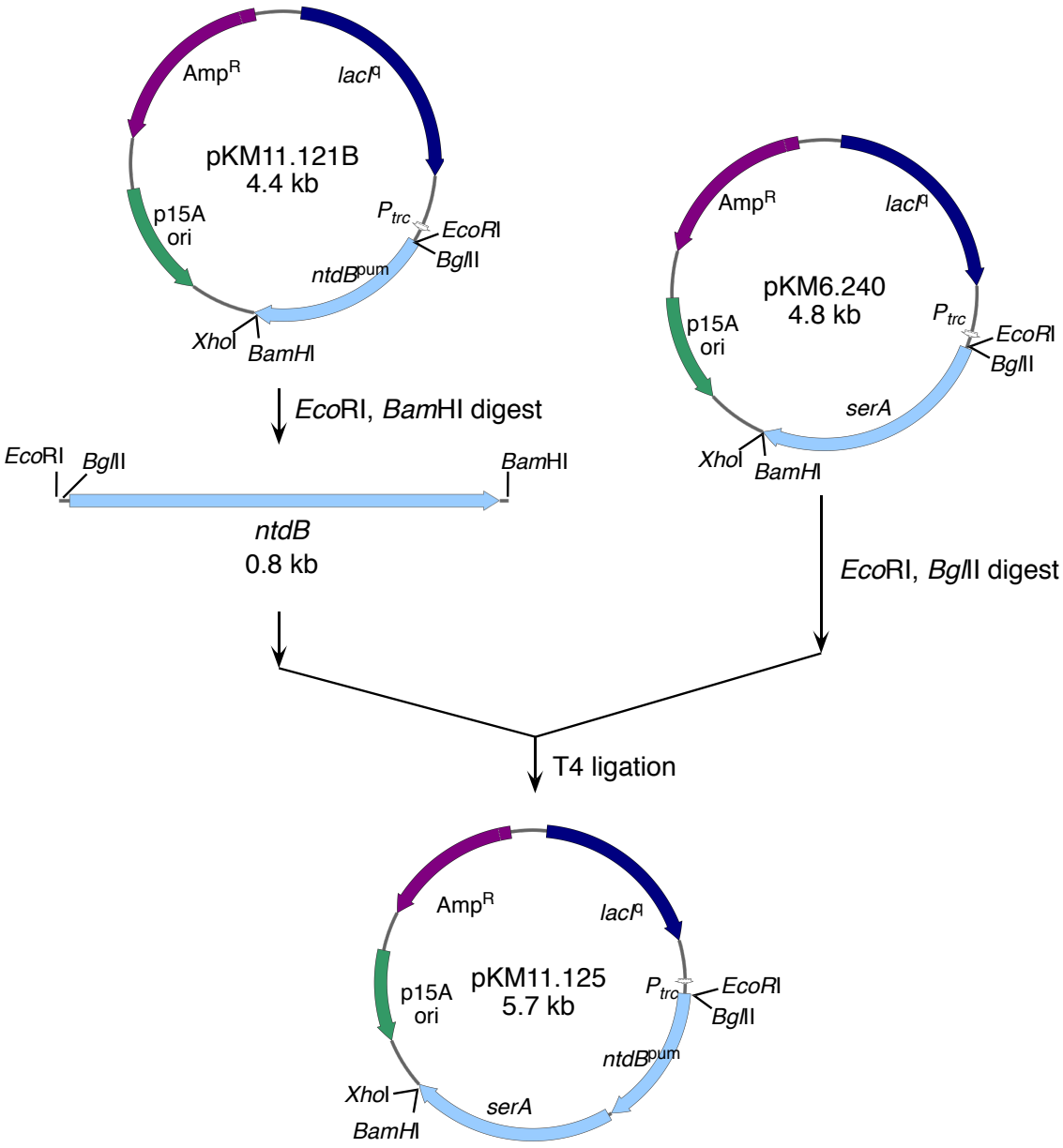

Figure 97. Construction of plasmid pKM11.125.

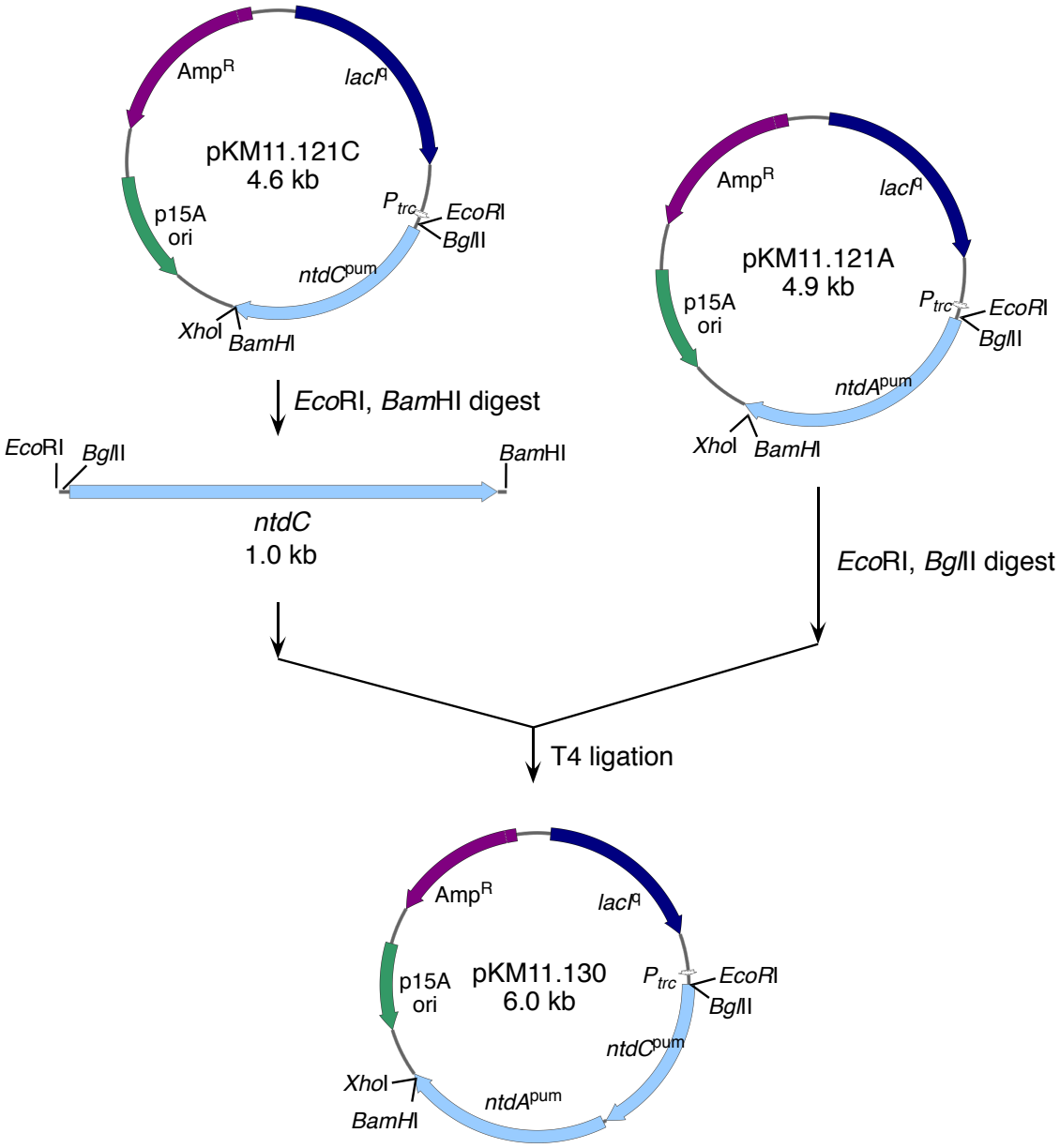

Figure 98. Construction of plasmid pKM11.130.

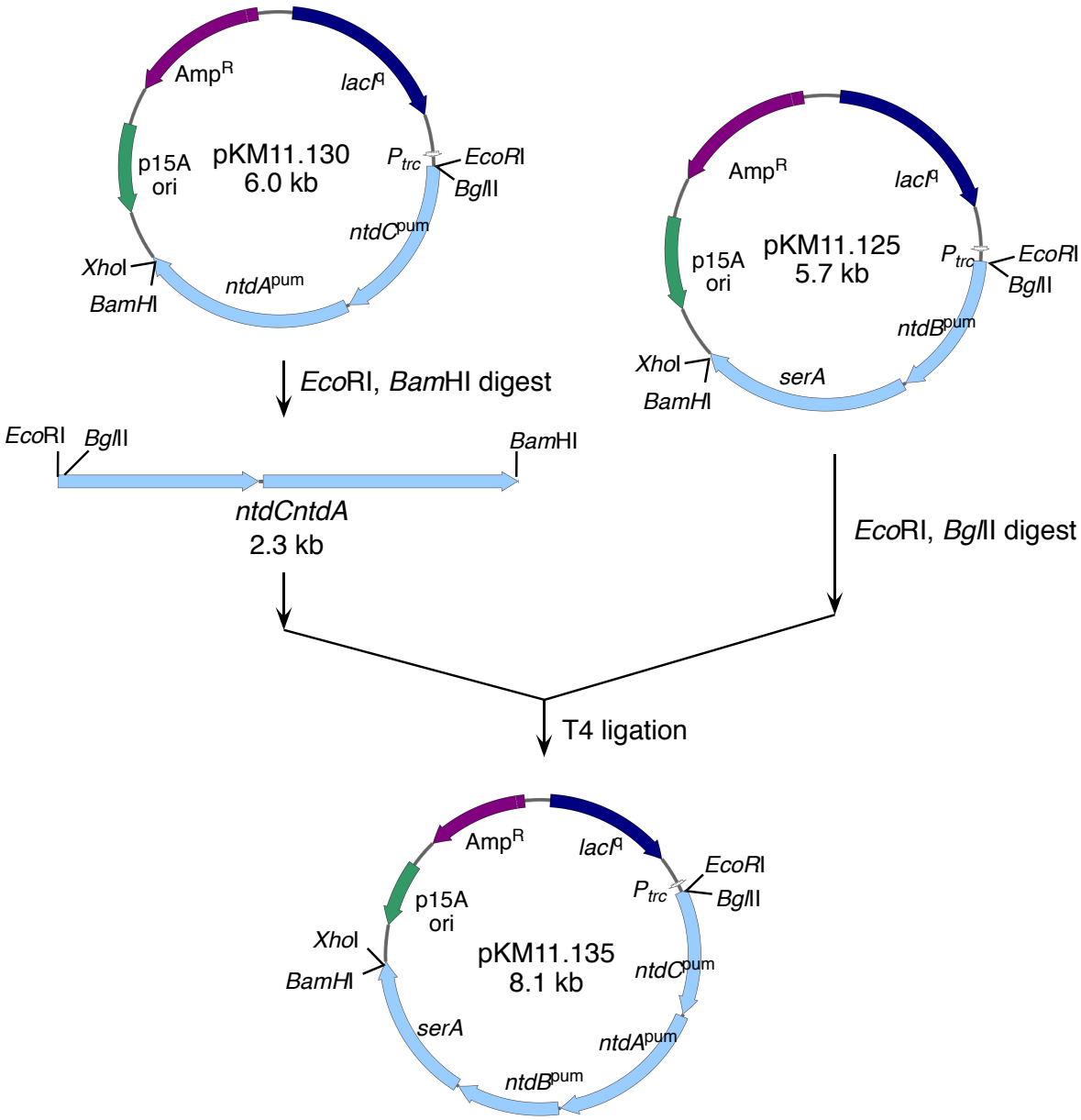

Figure 99. Construction of plasmid pKM11.135.

Kanosamine production resulting from expression of *ntd*^{pum} genes in *E. coli* was evaluated in glucose-rich (Figure 100) and glucose-limited (Figure 101) fed-batch fermentation of RB791*serA*/pKM11.135. As was the case during fermentations of RB791*serA*/pSN1.292 and RB791*serA*/pKM10.220ABC which carried plasmid-localized *ntd*^{sub} genes, 12 mg IPTG was added every 6 h throughout the course of a fermentation beginning at 12 h.

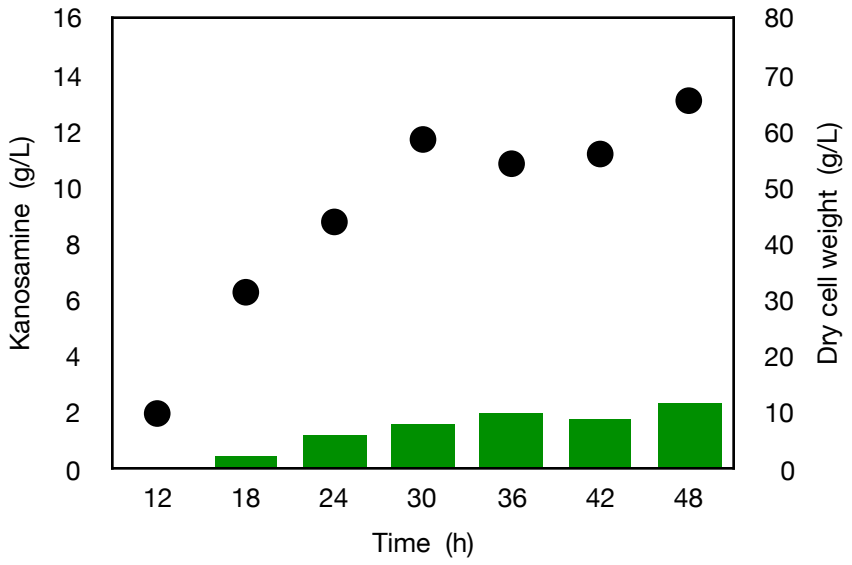

Figure 100. Kanosamine production by *E. coli* RB791*serA*/pKM11.135 under glucose-rich conditions. Legend: kanosamine, green columns; dry cell weight, black circles.

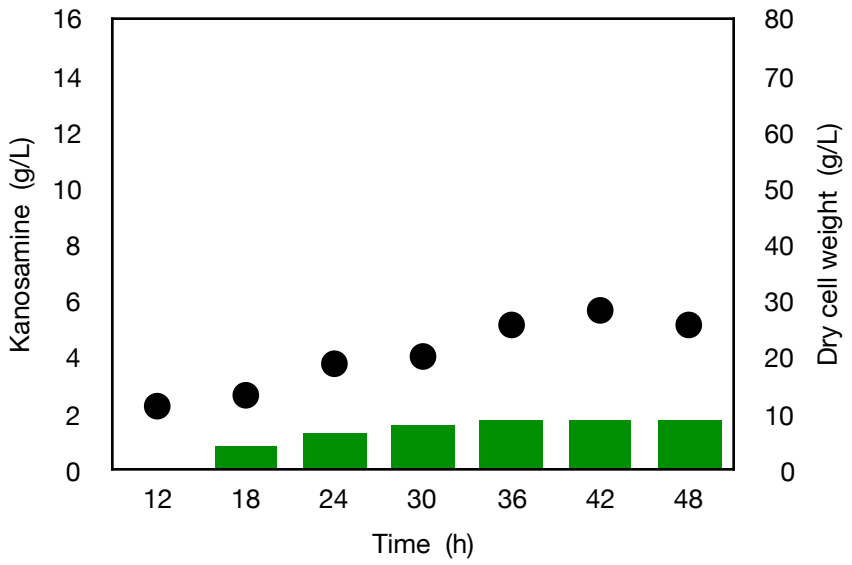

Figure 101. Kanosamine production by *E. coli* RB791*serA*/pKM11.135 under glucose-limited conditions. Legend: kanosamine, green columns; dry cell weight, black circles.

Glucose-rich fermentation of RB791*serA*/pKM11.135 resulted in 2.4 g/L kanosamine in a 0.6% mol/mol yield from D-glucose. This is a seven-fold decrease in titer and yield relative to glucose-rich fermentation of RB791*serA*/pSN1.292 which harbored kanosamine biosynthetic *ntd*^{sub} genes. Glucose-limited fermentation also resulted in reduced kanosamine production relative to RB791*serA*/pSN1.292 fermentation, affording 1.8 g/L kanosamine after 48 h in 1.2% mol/mol yield from D-glucose. No new byproducts were observed by ^{1}H NMR in the fermentation broth of RB791*serA*/pKM11.135 relative to RB791*serA*/pSN1.292 or RB791*serA*/pKM10.220ABC, with acetic acid, pyruvic acid, formic acid, and lactic acid forming in both glucose-rich and glucose-limited fermentations (Figure 102 and Figure 103). The overall amount of organic acid byproducts was reduced but an increase in final cell density was observed in fermentation of RB791*serA*/pKM11.135 relative to RB791*serA*/pSN1.292. These observations may reflect a difference in the fate of acetyl-CoA between the two constructs. Described in the

literature as "overflow metabolism"[55] acetyl-CoA can convert to acetic acid during fermentation of *E. coli* on D-glucose. This appears less pronounced in RB791*serA*/pKM11.135 than RB791*serA*/pSN1.292. Instead of conversion to acetic acid, acetyl-CoA may be more effectively channelled into the Krebs cycle resulting in greater biomass production in fermentation of RB791*serA*/pKM11.135 relative to RB7981*serA*/pSN1.292. This hypothesis has not been explored and is offered as a possible explanation for the observed differences between the two constructs regarding cell-densities and organic acid accumulation.

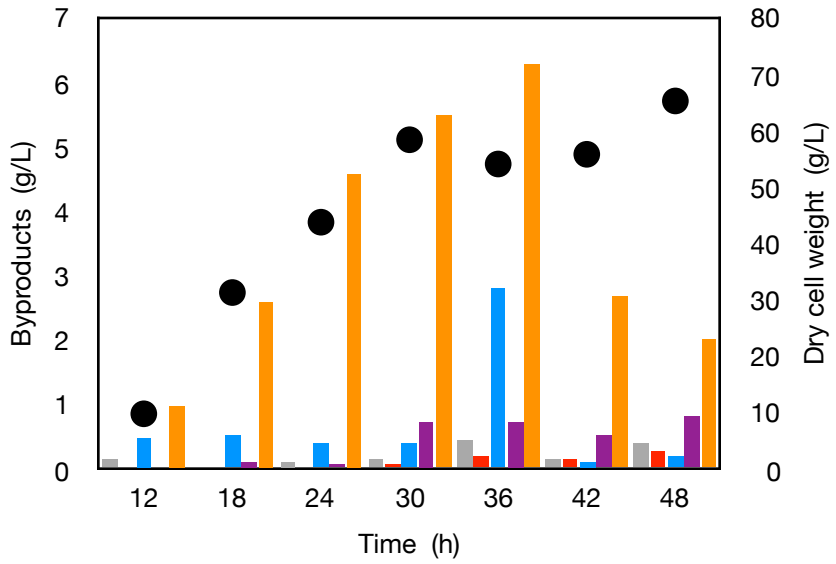

Figure 102. Byproducts formed during fermentation of *E. coli* RB791*serA*/pKM11.135 under glucose-rich conditions. Legend: acetic acid, orange columns; formic acid, grey columns; pyruvic acid, red columns; lactic acid, blue columns; D-glucosamine, purple columns; dry cell weight, black circles.

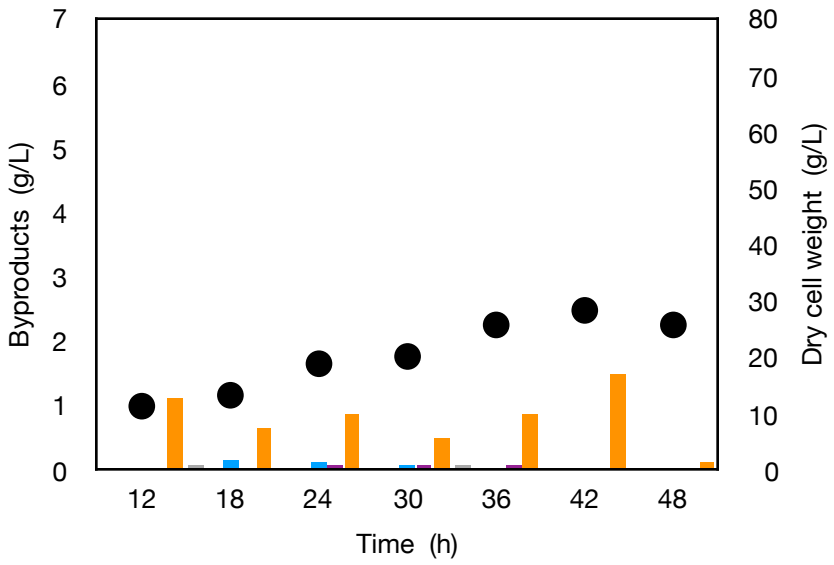

Figure 103. Byproducts formed during fermentation of *E. coli* RB791*serA*/pKM11.135 under glucose-limited conditions. Legend: acetic acid, orange columns; formic acid, grey columns; pyruvic acid, red columns; lactic acid, blue columns; D-glucosamine, purple columns; dry cell weight, black circles.

A 3.6-fold improvement in kanosamine production was observed in glucose-limited conditions following a reduction of IPTG added every 6 h from 12 mg to 6 mg. Kanosamine titers reached 6.3 g/L in a 4.4% mol/mol yield from D-glucose (Figure 104). This yield matches those observed during glucose-rich fermentations of RB791*serA*/pSN1.292 which carried *ntd*^{sub} genes also under control of P_{trc}. (4.4 ± 0.4% mol/mol) though falls short of yields achieved in RB791*serA*/pSN1.292 glucose-limited fermentations (6.2 ± 2.2% mol/mol). Unexpectedly, decreasing the amount of IPTG added every 6 h throughout a fermentation from 12 mg to 6 mg did not greatly impact kanosamine production under glucose-rich conditions (Figure 104). Kanosamine titers reached 3.0 ± 0.7 g/L in a 1.1 ± 0.3% mol/mol yield from D-glucose.

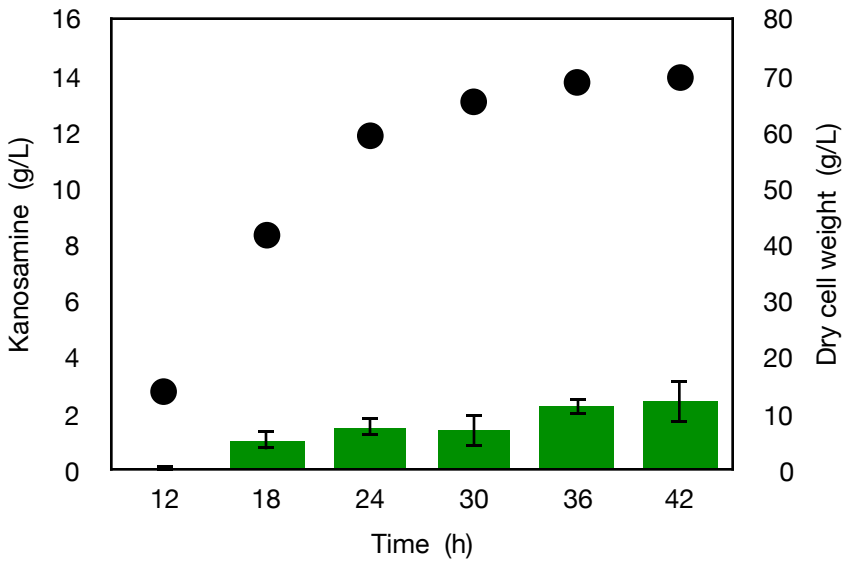

Figure 104. Kanosamine production in fed-batch fermentation of RB791*serA*/pKM11.135 in glucose-rich conditions with 6 mg IPTG addition every 6 h beginning at 12 h into the fermentation run. Legend: kanosamine, green bars; cell dry weight, black circles. Error bars represent one standard deviation away from the mean across duplicate runs.

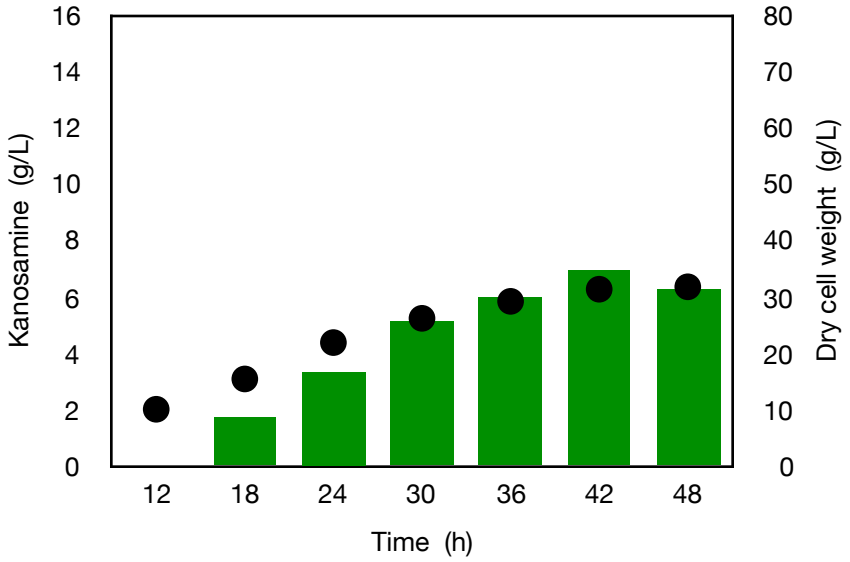

Figure 105. Kanosamine production in fed-batch fermentation of RB791*serA*/pKM11.135 in glucose-limited conditions with 6 mg IPTG addition every 6 h beginning at 12 h into the fermentation run. Legend: kanosamine, green bars; cell dry weight, black circles.

4.1. Substrate specificity of NtdC^{pum}

Bacillus pumilus was first examined as a source of kanosamine biosynthesis enzymes as a result of challenges associated with heterologous expression of *A. mediterranei* proteins, with the goal of achieving kanosamine biosynthesis from UDP-D-glucose in *E. coli*. Examination of protein sequences using the Basic Local Alignment Search Tool revealed three proteins, an oxidoreductase, an aminotransferase, and a phosphatase, with a high degree of similarity to the Ntd^{sub} proteins native to *Bacillus subtilis*, which have been reported to synthesize kanosamine from D-glucose-6-phosphate. Expression of *ntd*^{pum} and *ntd*^{sub} genes in *E. coli* RB791*serA* have led to kanosamine accumulation of 6.3 g/L (4.6% mol/mol from D-glucose) and 8.5 ± 1.4 g/L kanosamine (6.2 ± 2.2% mol/mol yield from D-glucose) under glucose-limited conditions. Both fermentation results and protein sequence alignments imply *B. subtilis* and *B. pumilus* contain functionally homologous kanosamine biosynthesis enzymes.

Evidence supporting homology between *B. subtilis* and *B. pumilus* kanosamine biosynthesis enzymes was found by examining the D-glucose-6-phosphate 3-dehydrogenation reaction catalyzed by NtdC^{pum} and NtdC^{sub}. Cell samples were withdrawn from a glucose-limited fermentation of RB791*serA*/pSN1.292 carrying plasmid-localized *ntd*^{sub} genes, as well as a glucose-limited fermentation of RB791*serA*/pKM11.135, harboring *ntd*^{pum} genes and achieving 6.3 g/L kanosamine titers. Samples were taken at 12, 24, 36, and 48 h and were lysed and centrifuged to afford cell-free extracts. These extracts were used to determine whether the oxidoreductase encoded by *ntdC* from both *B. subtilis* and *B. pumilus* was expressed in an active form and if so, whether it acts upon D-glucose-6-phosphate (G6P) or UDP-D-glucose (UDPGlc) (Table 24). The results demonstrate that both enzymes act upon D-glucose-6-phosphate and have

no significant activity with UDP-D-glucose. The minor amount of observed activity is likely due to the use of crude cell-free extract which may contain one or more native *E. coli* oxidoreductases that acted upon the NAD^+ used in the assay. The lower relative titers and yields observed in fermentation of RB791*serA*/pKM11.135 compared to RB791*serA*/pSN1.292 is likely due to the gradual observed loss of enzyme activity (Table 24). Improving kanosamine production in RB791*serA*/pKM11.135 might be achieved through further alteration of IPTG additions, performing the fermentation at different temperatures, or synthetic evolution of the $NtdC^{pum}$ protein.

From the results presented herein, it is reasonable to conclude that based on sequence homology, kanosamine production in fed-batch fermentation, and NtdC substrate specificities, that both *Bacillus subtilis* and *Bacillus pumilus* utilize the same pathway for kanosamine biosynthesis via D-glucose-6-phosphate. These results are a departure from the literature regarding the nature of kanosamine biosynthesis in *Bacilus pumilus.*

Table 24. Activity of D-glucose-6-phosphate 3-dehydrogenase from *B. subtilis* and *B. pumilus* when expressed in *E. coli*.

	***Bacillus pumilus* NtdC**		***Bacillus subtilis* NtdC**	
Run time (h)	**Sp. activity(G6P) (µmol/min/mg)**	**Sp. activity(UDPGlc) (µmol/min/mg)**	**Sp. activity(G6P) (µmol/min/mg)**	**Sp. activity(UDPGlc) (µmol/min/mg)**
12	n.d.	n.d.	n.d.	n.d.
24	0.20	n.d.	0.27	n.d.
36	0.14	n.d.	0.34	n.d.
48	0.091	n.d.	0.33	n.d.

Reaction mixture (1 mL) consisted of cell-free extract (0.05-0.5 mg as protein), D-glucose-6-phosphate (5 mM) or UDP-D-glucose (5 mM), NAD^+ (5 mM), AMP-HCl (100 mM, pH 9.5). n.d. = not detected.

PART III

CONCLUSIONS

This work sought to address two questions: 1. Can *E. coli* produce kanosamine via expression of one or both reported biosynthesis pathways? 2. Can modifications be made to improve kanosamine production from D-glucose? The answer to the first question is clear. *E. coli* RB791*serA* accumulates kanosamine in both glucose-rich and glucose-limited fermentations when transformed with a plasmid carrying either *B. subtilis* or *B. pumilus* biosynthesis genes. A surprising discovery was that both species of *Bacillus* appear to synthesize kanosamine via a common pathway. It had been previously reported that *B. subtilis* utilizes D-glucose-6-phosphate while *B. pumilus* utilizes UDP-D-glucose to biosynthesize kanosamine. However, highly similar homologues to the Ntd enzymes native to *B. subtilis* were found across multiple strains of *Bacillus pumilus* (taxonomy ID: 1408) using the BLAST tool provided by NCBI. When the Ntd homologues from *Bacillus pumilus* SH-B11 were expressed in *E. coli* RB791*serA*, 6.3 g/L kanosamine was produced in 4.6% mol/mol from D-glucose in glucose-limited fermentation. Though the titers are lower, yields are similar to those achieved in fermentations of RB791*serA*/pSN1.292, which carried the *ntd*^{sub} genes (12.7 ± 0.6 g/L, 4.4 ± 0.4% mol/mol in glucose-rich fermentations; 8.5 ± 1.4 g/L, 6.2 ± 2.2% mol/mol in glucose-limited fermentations). The strongest piece of evidence to support a common pathway between *B. subtilis* and *B. pumilus* came from in vitro assays using cell-free extracts obtained from fermentations of RB791*serA*/pKM11.135, expressing *B. pumilus* genes under control of P_{trc}, and RB791*serA*/pSN1.292, expressing *B. subtilis* genes under control of P_{trc}. Monitoring absorption at 340 nm due to

formation of NADH from NAD^+ revealed good activity (0.2-0.3 U/mg) using D-glucose-6-phosphate and cell-free extract taken at 24 h during a fermentation run, but only trace activity with UDP-D-glucose. The amount of observed activity using UDP-D-glucose is most likely due to presence of native *E. coli* oxidoreductase(s) in the cell-free extract that convert NAD^+ to NADH. The combination of sequence data, kanosamine production in fed-batch fermentation, and the common substrate specificity of the oxidoreductase from *B. subtilis* and *B. pumilus* indicate that both *Bacillus subtilis* and *Bacillus pumilus* synthesize kanosamine from D-glucose-6-phosphate and present a correction to the literature regarding *Bacillus pumilus*.

Kanosamine did not accumulate during fed batch fermentation of *E. coli* harboring plasmid-localized kanosamine biosynthesis *rif* genes from *Amycolatopsis mediterranei*. Previous research demonstrates that *A. mediterranei* utilizes kanosamine as a nitrogenous precursor to 3-amino-5-hydroxybenzoic acid (AHBA) during the biosynthesis of aminoglycoside antibiotics.[31,33,36,37] The kanosamine biosynthesis enzymes in *A. mediterranei* were reported to require UDP-D-glucose as a substrate. It was initially thought that the lack of kanosamine accumulation was due to an inherent pyrimidine starvation of RB791*serA*, but neither uracil supplementation nor a strain of *E. coli* not known to starve for pyrimidine led to detectable amounts of kanosamine in fermentation broth.

Cell-free extracts of cell samples taken during fermentation of *E. coli* containing plasmid-localized, codon-optimized *rif* genes were incubated with NAD^+ and UDP-D-glucose in phosphate buffer to detect UDP-D-glucose-3-dehydrogenase activity. Only a minor increase in absorbance at 340 nm due to formation of NADH was observed. This was also seen when D-glucose-6-phosphate was used in place of UDP-D-glucose, indicating that the absorbance

increase is not due to kanosamine biosynthetic enzymes but is merely background activity resulting from native *E. coli* oxidoreductase. In vitro assays of purified His_6-tagged protein resulted in low activity (0.41 U/mg) for the *rifL*-encoded UDP-D-glucose 3-dehydrogenase. It appears that despite codon-optimization of *rif* genes, expression of active enzymes is difficult in *E. coli*. This is supported by reports by the Floss group[51] who first sequenced the AHBA biosynthesis gene cluster in *A. mediterranei* that neither the *rifM*-encoded UDP-D-kanosamine phosphatase nor the *rifK*-encoded dual-functional 3-keto-UDP-D-glucose:L-glutamine aminotransferase/AHBA synthase exhibited any activity when expressed in *E. coli*. The challenges associate with expression of catalytically active kanosamine biosynthesis enzymes from *A. mediterranei* may be avoided if an alternative host organism is employed. *Streptomyces coelicolor* has been previously used to produce rifamycin via expression of *A. mediterranei* genes and might be a suitable candidate for kanosamine production as well.

Despite unsuccessful attempts to accumulate kanosamine via expression of enzymes reported to utilize UDP-D-glucose as a substrate in *E. coli*, this work demonstrates that kanosamine biosynthesis in *E. coli* is viable when utilizing *Bacillus* genes. The second question to be addressed by this report is whether kanosamine biosynthesis in *E. coli* can be improved to maximize production in fed-batch fermentation. Progress has been made in that direction but further work is necessary to achieve substantial improvements.

The highest titers of kanosamine are observed during fermentation of RB791*serA* constructs expressing *B. subtilis* genes in glucose-rich conditions: 12.7 ± 0.6 g/L (4.4 ± 0.4% mol/mol yield) using a plasmid carrying a P_{trc}*ntdCntdAntdBserA* cassette (pSN1.292) and 13.7 g/L (4.9% mol/mol yield) using a plasmid carrying a P_{trc}*ntdAntdBntdCserA* cassette

(pKM10.220ABC). These fermentations result in accumulation of acetic acid, formic acid, pyruvic acid, and lactic acid, which are a result of carbon flux through glycolysis and have been attributed to an abundance of D-glucose in fermentation broth. D-Glucosamine was also observed in glucose-rich conditions and is likely due to D-glucose availability, as it is not observed in glucose-limited fermentations nor those utilizing RB791*serA pgi*::Kan^R. Kanosamine yields above 4.9% are achieved by restricting D-glucose availability in glucose-limited fermentations. Titers of 8.5 ± 1.4 g/L kanosamine are observed in a 6.2 ± 2.2% mol/mol yield from D-glucose.

Because the major byproducts observed in fermentation of RB791*serA*/pSN1.292 are result from carbon flow through glycolysis, a mutant strain was utilized in which the Embden-Meyerhoff-Parnas pathway of glycolysis was blocked at *pgi*-encoded phosphoglucose isomerase. This was in effort to increase the intracellular availability of D-glucose-6-phosphate for kanosamine biosynthesis. The mutant strain, RB791*serA pgi*::Kan^R, was transformed with pSN1.292 and kanosamine production was examined using a D-glucose-only feed or a mixed feed consisting of equimolar amounts of D-glucose and D-fructose. The highest yields of kanosamine observed thus far were achieved using a feed consisting of only D-glucose. Kanosamine titers reached 3.6 ± 0.2 g/L in an 18 ± 1% mol/mol yield from D-glucose. These fermentations resulted in only transient growth of RB791*serA pgi*::Kan^R/pSN1.292 with final cell densities reaching 2.9 ± 1.4 g/L dry cell weight. Furthermore, only 20 g of D-glucose was consumed during these runs. Growth was restored and D-glucose consumption increased with the use of a feed consisting of equimolar amounts of D-glucose and D-fructose. Final cell

densities reached 37 ± 2.4 g/L dry cell weight with 150 g D-glucose consumed. Kanosamine titers reached 8.7 ± 0.08 g/L in 5.9 ± 0.6% mol/mol yield.

It appears that maximizing kanosamine production by blocking a major glycolysis pathway must be balanced with deleterious growth effects when feeding D-glucose. A mixed carbohydrate feed restored cell viability but did not result in high titers or yields of kanosamine. A substantial amount of D-fructose was observed at the completion of the fermentations of RB791*serA pgi*::Kan^{R}/pSN1.292 while D-glucose had been completely consumed. This is indicative of carbon catabolite repression, whereby D-glucose is consumed by the cell preferentially over other carbohydrates.

Previous research has demonstrated high yields of D-glucaric acid from D-glucose by indroducing a mutation in *zwf*-encoded D-glucose-6-phosphate dehydrogenase to a Δ*pgi* mutant *E. coli*.[48] With both major pathways of glycolysis blocked, the redox imbalance leading to reduced cell viability in Δ*pgi E. coli* was not observed, nor was competing carbon catabolite repression when cells were cultured on a mixed D-glucose/D-xylose feed. It was shown that cells grew exclusively on D-xylose while using most of the available D-glucose for D-glucaric acid biosynthesis. This could be a possible strategy to achieve kanosamine yields of 18% or greater without sacrificing cell viability.

The observation of L-glutamic acid accumulation in fermentation broth of Δ*pgi* mutants with the concommitant production of 3.6 ± 0.2 g/L kanosamine with D-glucose-only feed may suggest increased L-glutamate levels have a beneficial effect on kanosamine production in *E. coli* expressing *Bacillus* genes. L-Glutamate is a substrate for the *ntdA*-encoded 3-keto-D-glucose-6-phosphate:L-glutamate aminotransferase. Exogenous L-glutamic acid did not improve

kanosamine production, but increasing carbon flux through L-glutamate biosynthesis in *E. coli* might lead to greater substrate availability and improved kanosamine production.

REFERENCES

REFERENCES

1. Mehta, C. M.; Palni, U.; Franke-Whittle, I. H.; Sharma, A. K. Compost: Its Role, Mechanism and Impact on Reducing Soil-Borne Plant Diseases. *Waste Manag.* **2014**, *34* (3), 607–622.

2. Handelsman, J.; Stabb, E. V. Biocontrol of Soilborne Plant Pathogens. *Plant Cell* **1996**, *8* (10), 1855–1869.

3. Caulier, S.; Gillis, A.; Colau, G.; Licciardi, F.; Liépin, M.; Desoignies, N.; Modrie, P.; Legrève, A.; Mahillon, J.; Bragard, C. Versatile Antagonistic Activities of Soil-Borne *Bacillus* spp. and *Pseudomonas* spp. against *Phytophthora infestans* and Other Potato Pathogens. *Front. Microbiol.* **2018**, *9*, 143.

4. Liu, L.; Liang, M.; Li, L.; Sun, L.; Xu, Y.; Gao, J.; Wang, L.; Hou, Y.; Huang, S. Synergistic Effects of the Combined Application of *Bacillus subtilis* H158 and Strobilurins for Rice Sheath Blight Control. *Biol. Control* **2018**, *117*, 182–187.

5. Mora, I.; Cabrefiga, J.; Montesinos, E. Cyclic Lipopeptide Biosynthetic Genes and Products, and Inhibitory Activity of Plant-Associated *Bacillus* against Phytopathogenic Bacteria. *PLoS One* **2015**, *10* (5), e0127738.

6. Shrestha, B. K.; Karki, H. S.; Groth, D. E.; Jungkhun, N.; Ham, J. H. Biological Control Activities of Rice-Associated *Bacillus* sp. Strains against Sheath Blight and Bacterial Panicle Blight of Rice. *PLoS One* **2016**, *11* (1), e0146764.

7. Jacobsen, B. J.; Zidack, N. K.; Larson, B. J. The Role of *Bacillus*-Based Biological Control Agents in Integrated Pest Management Systems: Plant Diseases. *Phytopathology* **2004**, *94* (11), 1272–1275.

8. Ongena, M.; Jourdan, E.; Adam, A.; Paquot, M.; Brans, A.; Joris, B.; Arpigny, J.-L.; Thonart, P. Surfactin and Fengycin Lipopeptides of *Bacillus subtilis* as Elicitors of Induced Systemic Resistance in Plants. *Environ. Microbiol.* **2007**, *9* (4), 1084–1090.

9. Jourdan, E.; Henry, G.; Duby, F.; Dommes, J.; Barthélemy, J. P.; Thonart, P.; Ongena, M. Insights into the Defense-Related Events Occurring in Plant Cells Following Perception of Surfactin-Type Lipopeptide from *Bacillus subtilis*. *Mol. Plant. Microbe. Interact.* **2009**, *22* (4), 456–468.

10. Lim, J.-H.; Kim, S.-D. Synergistic Plant Growth Promotion by the Indigenous Auxins-Producing PGPR *Bacillus subtilis* AH18 and *Bacillus licheniforims* K11. *Hanguk Ungyong Saengmyong Hwahakhoe Chi* **2009**, *52* (5), 531–538.

11. Drahos, D. J.; West, L. *Bacillus lichenformis* Biofungicide.US 6,569,425 B2 , 2003.

12. Guilhabert-Goya, M.; Zhu, H. Method of Increasing Abiotic Stress Resistance in a Plant. US 2014/0066302 A1 , 2014.

13. Brannen, P. M.; Kenney, D. S. Kodiak—a Successful Biological-Control Product for Suppression of Soil-Borne Plant Pathogens of Cotton. *J. Ind. Microbiol. Biotechnol.* **1997**, *19*, 169–171.

14. Williams, J. A.; Guicherit, O. M.; Zaharian, B. I.; Xu, Y.; Chai, L.; Wichterle, H.; Kon, C.; Gatchalian, C.; Porter, J. A.; Rubin, L. L.; et al. Identification of a Small Molecule Inhibitor of the Hedgehog Signaling Pathway: Effects on Basal Cell Carcinoma-like Lesions. *Proc. Natl. Acad. Sci. U. S. A.* **2003**, *100* (8), 4616–4621.

15. Ryu, C.-M.; Farag, M. A.; Hu, C.-H.; Reddy, M. S.; Kloepper, J. W.; Paré, P. W. Bacterial Volatiles Induce Systemic Resistance in *Arabidopsis*. *Plant Physiol.* **2004**, *134* (3), 1017–1026.

16. Yu, X.; Ai, C.; Xin, L.; Zhou, G. The Siderophore-Producing Bacterium, *Bacillus subtilis* CAS15, Has a Biocontrol Effect on *Fusarium* Wilt and Promotes the Growth of Pepper. *Eur. J. Soil Biol.* **2011**, *47* (2), 138–145.

17. Gao, Z.; Zhang, B.; Liu, H.; Han, J.; Zhang, Y. Identification of Endophytic *Bacillus velezensis* ZSY-1 Strain and Antifungal Activity of Its Volatile Compounds against *Alternaria solani* and *Botrytis cinerea*. *Biol. Control* **2017**, *105*, 27–39.

18. Yu, G. Y.; Sinclair, J. B.; Hartman, G. L.; Bertagnolli, B. L. Production of Iturin A by *Bacillus amyloliquefaciens* Suppressing *Rhizoctonia solani*. *Soil Biol. Biochem.* **2002**, *34* (7), 955–963.

19. Skarbek, K.; Milewska, M. J. Biosynthetic and Synthetic Access to Amino Sugars. *Carbohydr. Res.* **2016**, *434*, 44–71.

20. Milner, J. L.; Silo-Suh, L.; Lee, J. C.; He, H.; Clardy, J.; Handelsman, J. Production of Kanosamine by *Bacillus cereus* UW85. *Appl. Environ. Microbiol.* **1996**, *62* (8), 3061–3065.

21. Iwai, Y.; Tanaka, H.; Oiwa, R.; Shimizu, S.; Omura, S. III. 3-Amino-3-Deoxy-D-Glucose, an Inhibitor of Bacterial Cell Wall Biosynthesis. *Biochim. Biophys. Acta* **1977**, *498*, 223–228.

22. Janiak, A. M.; Milewski, S. Mechanism of Antifungal Action of Kanosamine. *Med. Mycol.* **2001**, *39* (5), 401–408.

23. Silo-Suh, L. A.; Lethbridge, B. J.; Raffel, S. J.; He, H.; Clardy, J.; Handelsman, J. Biological Activities of Two Fungistatic Antibiotics Produced by *Bacillus cereus* UW85. *Appl. Environ. Microbiol.* **1994**, *60* (6), 2023–2030.

24. Silo-Suh, L. A.; Stabb, E. V.; Raffel, S. J.; Handelsman, J. Target Range of Zwittermicin A, an Aminopolyol Antibiotic from *Bacillus cereus*. *Curr. Microbiol.* **1998**, *37* (1), 6–11.

25. Vetter, N. D.; Langill, D. M.; Anjum, S.; Boisvert-Martel, J.; Jagdhane, R. C.; Omene, E.; Zheng, H.; van Straaten, K. E.; Asiamah, I.; Krol, E. S.; et al. A Previously Unrecognized Kanosamine Biosynthesis Pathway in *Bacillus subtilis*. *J. Am. Chem. Soc.* **2013**, *135* (16), 5970–5973.

26. a) van Straaten, K. E.; Ko, J. B.; Jagdhane, R.; Anjum, S.; Palmer, D. R. J.; Sanders, D. A. R. The Structure of NtdA, a Sugar Aminotransferase Involved in the Kanosamine Biosynthetic Pathway in *Bacillus subtilis,* Reveals a New Subclass of Aminotransferases. *J. Biol. Chem.* **2013**, *288* (47), 34121–34130. b) van Straaten, K. E.; Langill, D. M.; Palmer, D. R. J.; Sanders, D. A. R. Purification, Crystallization and Preliminary X-Ray Analysis of NtdA, a Putative Pyridoxal Phosphate-Dependent Aminotransferase from *Bacillus subtilis*. *Acta Crystallogr. Sect. F Struct. Biol. Cryst. Commun.* **2009**, *65* (4), 426–429.

27. Vetter, N. D.; Palmer, D. R. J. Simultaneous Measurement of Glucose-6-Phosphate 3-Dehydrogenase (NtdC) Catalysis and the Nonenzymatic Reaction of Its Product: Kinetics and Isotope Effects on the First Step in Kanosamine Biosynthesis. *Biochemistry* **2017**, *56* (14), 2001–2009.

28. Milner, J. L.; Silo-Suh, L.; Lee, J. C.; He, H.; Clardy, J.; Handelsman, J. Production of Kanosamine by *Bacillus cereus* UW85. *Appl. Environ. Microbiol.* **1996**, *62* (8), 3061–3065.

29. Umezawa, S.; Umino, K.; Shibahara, S.; Omoto, S. Studies of Aminosugars. XVII. Production of 3-Amino-3-Deoxy-D-Glucose by *Bacillus* Species. *Bull. Chem. Soc. Jpn.* **1967**, *40* (10), 2419–2421.

30. Umezawa, S.; Shibahara, S.; Omoto, S.; Takeuchi, T.; Umezawa, H. Studies on the Biosynthesis of 3-Amino-3-Deoxy-D-Glucose. *The Journal of Antibiotics* **1968**, *21* (8), 485–491.

31. Kim, C.-G.; Kirschning, A.; Bergon, P.; Zhou, P.; Su, E.; Sauerbrei, B.; Ning, S.; Ahn, Y.; Breuer, M.; Leistner, E.; et al. Biosynthesis of 3-Amino-5-Hydroxybenzoic Acid, the Precursor of mC7N Units in Ansamycin Antibiotics. *J. Am. Chem. Soc.* **1996**, *118* (32), 7486–7491.

32. Ventura, M.; Canchaya, C.; Tauch, A.; Chandra, G.; Fitzgerald, G. F.; Chater, K. F.; van Sinderen, D. Genomics of *Actinobacteria*: Tracing the Evolutionary History of an Ancient Phylum. *Microbiol. Mol. Biol. Rev.* **2007**, *71* (3), 495–548.

33. Yu, T. W.; Muller, R.; Muller, M.; Zhang, X.; Draeger, G.; Kim, C. G.; Leistner, E.; Floss, H. G. Mutational Analysis and Reconstituted Expression of the Biosynthetic Genes Involved in the Formation of 3-Amino-5-Hydroxybenzoic Acid, the Starter Unit of Rifamycin Biosynthesis in *Amycolatopsis mediterranei* S699. *J. Biol. Chem.* **2001**, *276* (16), 12546–12555.

34. August, P. R.; Tang, L.; Yoon, Y. J.; Ning, S.; Muller, R.; Yu, T.-W.; Taylor, M.; Hoffmann, D.; Kim, C.-G.; Zhang, X.; et al. Biosynthesis of the Ansamycin Antibiotic Rifamycin: Deductions from the Molecular Analysis of the Rif Biosynthetic Gene Cluster of *Amycolatopsis mediterranei* S699. *Chem. Biol.* **1998**, *5* (2), 69–79.

35. Wilson, M. C.; Gulder, T. A. M.; Mahmud, T.; Moore, B. S. Shared Biosynthesis of the Saliniketals and Rifamycins in *Salinispora arenicola* Is Controlled by the sare1259-Encoded Cytochrome P450. *J. Am. Chem. Soc.* **2010**, *132* (36), 12757–12765.

36. Guo, J.; Frost, J. W. Biosynthesis of 1-Deoxy-1-Imino-D-Erythrose 4-Phosphate: A Defining Metabolite in the Aminoshikimate Pathway. *J. Am. Chem. Soc.* **2002**, *124* (4), 528–529.

37. Guo, J.; Frost, J. W. Kanosamine Biosynthesis: A Likely Source of the Aminoshikimate Pathway's Nitrogen Atom. *J. Am. Chem. Soc.* **2002**, *124* (36), 10642–10643.

38. Lim, H. N.; Lee, Y.; Hussein, R. Fundamental Relationship between Operon Organization and Gene Expression. *Proc. Natl. Acad. Sci. U. S. A.* **2011**, *108* (26), 10626–10631.

39. Chubukov, V.; Sauer, U. Environmental Dependence of Stationary-Phase Metabolism in *Bacillus subtilis* and Escherichia Coli. *Appl. Environ. Microbiol.* **2014**, *80* (9), 2901–2909.

40. Frost, J. W.; Hansen, C. A. Synthesis of 1,2,3,4-Tetrahydroxybenzenes and 1,2,3,-Trihydroxybenzenes Using *myo*-Inositol-1-Phosphate Synthase and *myo*-Inositol-2-Dehydrogenase. US 6,750,049, 2004.

41. Tegel, H.; Ottosson, J.; Hober, S. Enhancing the protein production levels in *Escherichia coli* with a strong promoter. *FEBS J.* **2011**, *278*, 729-739.

42 Murarka, A.; Clomburg, J. M.; Moran, S.; Shanks, J. V.; Gonzalez, R. Metabolic Analysis of Wild-Type *Escherichia coli* and a Pyruvate Dehydrogenase Complex (PDHC)-Deficient Derivative Reveals the Role of PDHC in the Fermentative Metabolism of Glucose. *J. Biol. Chem.* **2010**, *285* (41), 31548–31558.

43. Lessmann, D.; Schimz, K.-L.; Kurz, G. D-Glucose-6-Phosphate Dehydrogenase (Entner-Doudoroff Enzyme) from *Pseudomonas fluorescen*s. *Eur. J. Biochem.* **1975**, *59*, 545–559.

44. Morita, T.; El-Kazzaz, W.; Tanaka, Y.; Inada, T.; Aiba, H. Accumulation of Glucose 6-Phosphate or Fructose 6-Phosphate Is Responsible for Destabilization of Glucose Transporter mRNA in *Escherichia coli*. *J. Biol. Chem.* **2003**, *278* (18), 15608–15614.

45. Kogure, T.; Wakisaka, N.; Takaku, H.; Takagi, M. Efficient Production of 2-Deoxy-*Scyllo*-Inososе from D-Glucose by Metabolically Engineered Recombinant Escherichia Coli. *J. Biotechnol.* **2007**, *129* (3), 502–509.

46. A. Dean, unpublished results

47. Charusanti, P.; Conrad, T. M.; Knight, E. M.; Venkataraman, K.; Fong, N. L.; Xie, B.; Gao, Y.; Palsson, B. Ø. Genetic Basis of Growth Adaptation of *Escherichia coli* after Deletion of *pgi*, a Major Metabolic Gene. *PLoS Genet.* **2010**, *6* (11), e1001186.

48. Brockman, I. M.; Prather - Biotechnology and, K.; 2015. Improving Product Yields on D−glucose in *Escherichia coli* via Knockout of *pgi* and *zwf* and Feeding of Supplemental Carbon Sources. *Wiley Online Library* **2015**.

49. Bren, A.; Park, J. O.; Towbin, B. D.; Dekel, E.; Rabinowitz, J. D.; Alon, U. Glucose Becomes One of the Worst Carbon Sources for *E.coli* on Poor Nitrogen Sources due to Suboptimal Levels of cAMP. *Sci. Rep.* **2016**, *6*, 24834.

49. Guo, J. Biosynthesis of Precursors to the Aminoshikimate Pathway and Microbial Synthesis of 5-Amino-5-Deoxyshikimate. Doctor of Philosophy, Michigan State University, 2004.

51. Floss, H. G.; Yu, T.-W.; Arakawa, K. The Biosynthesis of 3-Amino-5-Hydroxybenzoic Acid (AHBA), the Precursor of mC7N Units in Ansamycin and Mitomycin Antibiotics: A Review. *J. Antibiot.* **2011**, *64* (1), 35–44.

52 Puigbò, P.; Guzmán, E.; Romeu, A.; Garcia-Vallvé, S. OPTIMIZER: A Web Server for Optimizing the Codon Usage of DNA Sequences. *Nucleic Acids Res.* **2007**, *35* (Web Server issue), W126–W131

53. Jensen, K. F. The *Escherichia coli* K-12 “Wild Types” W3110 and MG1655 Have an Rph Frameshift Mutation That Leads to Pyrimidine Starvation Due to Low *pyrE* Expression Levels. *Journal of Bacteriology* **1993**, *175* (11), 3401–3407.

54. Li, K.; Mikola, M. R.; Draths, K. M.; Worden, R. M.; Frost, J. W. Fed-Batch Fermentor Synthesis of 3-Dehydroshikimic Acid Using Recombinant *Escherichia coli*. *Biotechnol. Bioeng.* **1999**, *64* (1), 61–73.

55. Vemuri GN, Altman E, Sangurdekar DP, Khodursky AB, Eiteman MA. Overflow metabolism in *Escherichia coli* during steady-state growth: transcriptional regulation and effect of the redox ratio. *Appl Environ Microbiol* **2006**, *72,* 3653–3661.

56. Hansen, C. Chemo-enzymatic synthesis of aromatics via non-shikimate pathway intermediates. Doctor of Philosophy, Michigan State University, 2002.
57. Lee, T. S.; Krupa, R. A.; Zhang, F.; Hajimorad, M.; Holtz, W. J.; Prasad, N.; Lee, S. K.; Keasling, J. D. BglBrick Vectors and Datasheets: A Synthetic Biology Platform for Gene Expression. *J. Biol. Eng.* **2011**, *5*, 12.

58. Pittard, J.; Wallace, B. J. Distribution and Function of Genes Concerned with Aromatic Biosynthesis in *Escherichia coli*. *J. Bacteriol.* **1966**, *91* (4), 1494–1508.

CHAPTER THREE: EXPERIMENTAL

General methods

General chemistry

All reactions sensitive to air and moisture were carried out in oven-dried glassware under a positive atmosphere of nitrogen or in a Parr high pressure reaction vessel. All reagents sensitive to air and moisture were handled under a positive nitrogen atmosphere and transferred to reaction flasks fitted with rubber septa via oven-dried syringes or cannula. Unless otherwise specified, all reactions were carried out at room temperature. Solvents were removed using a Büchi rotary evaporator at water aspirator pressure or under high vacuum (0.5 mm Hg).

Toluene, *m*-xylene, and bis(methoxypropyl) ether were dried over 4 Å molecular sieves. 1,4-Dioxane was distilled from sodium metal under a positive nitrogen atmosphere. Water was glass-distilled and deionized. All other reagents and solvents were used as available from commercial sources. Organic solutions of products were dried over anhydrous $MgSO_4$. The sodium salt of 3-(trimethylsilyl)propionic-*2*,*2*,*3*,*3*-d_4 acid (TSP) was purchased from Sigma-Aldrich. $BOB(OAc)_4$ was prepared and characterized previously by this laboratory.[1]

Analytical methods

^1H NMR spectra were recorded on a 500 MHz spectrometer. For 1H NMR experiments, the relaxation delay parameter (d_1) was adjusted to 10 s for 2-HMA-containing samples or 25 s for kanosamine-containing samples. Chemical shifts are reported (in parts per million) relative to residual non-deuterated solvent in CD_3OD (δ = 3.31 ppm) and DMSO-d_6 (δ = 2.50 ppm).

When D_2O was used as the solvent, chemical shifts are reported (in parts per million) relative to internal sodium 3-(trimethylsilyl)propionate-*2*,*2*,*3*,*3*-d_4 (TSP, δ = 0.00 ppm). The following abbreviations are used to describe spin multiplicity: s (singlet), d (doublet), t (triplet), q (quartet), dd (doublet of doublets), ddd (doublet of doublet of doublets), dt (doublet of triplets) m (unresolved multiplet). ^{13}C NMR spectra were recorded at 126 MHz and chemical shifts are reported (in parts per million) relative to CD_3OD (δ = 49.0 ppm) or DMSO-d_6 (δ = 39.5 ppm). When D_2O was used as the solvent, chemical shifts are reported (in parts per million) relative to internal sodium 3-(trimethylsilyl)propionate-*2*,*2*,*3*,*3*-d_4 (TSP, δ = 0.0 ppm). Concentrations of fermentation and cell-free reaction products were determined by comparison of the integrals corresponding to each compound with the integral corresponding to TSP (δ = 0.0 ppm) or maleic acid (δ = 6.32 ppm) in the ^1H NMR. Response factors were determined as follows: A known quantity of each compound was dissolved in 5 mL D_2O to obtain a stock solution. Compounds with exchangeable protons were concentrated to dryness under reduced pressure and redissolved in an equal volume of D_2O a total of three times. Various known volumes were then concentrated to dryness and redissolved in 1 mL D_2O containing 1 mM TSP or maleic acid and their ^1H NMR spectra were recorded. Compounds were quantified using the following resonances: 2-hydroxymuconic acid (2-HMA, δ 7.71, dd, 1H), α-keto acid **24** (δ 6.97, dt, 2H), α-keto acid **23** (δ 6.89, dt, 2H), formic acid (δ 8.26, s, 1H), HOAc (δ 1.92, s, 3H), pyruvic acid (δ 2.41, s, 3H), lactic acid (δ 1.35, s, 3H), L-glutamic acid (δ 2.35, dt, 2H), 3-dehydroquinic acid (δ 4.38, d, 1H) , 3-dehydroshikimic acid (δ 4.28, d, 1H), gallic acid (δ 7.02, s 2H). The concentrations of formic acid, HOAc, pyruvic acid, lactic acid, and L-glutamic acid were calculated by application of the following response factors derived from standards taken using

reagent-grade samples. The concentrations of gallic acid, 3-dehydroshikimic acid, and 3-dehydroquinic acid were calculated by application of the following response factors derived from laboratory stock samples:

$$[\text{glutamic acid mM}]_{\text{actual}} = 0.93[\text{L-glutamic acid mM}]_{\text{NMR}}$$

$$[\text{acetic acid mM}]_{\text{actual}} = 1.12[\text{L-glutamic acid mM}]_{\text{NMR}}$$

$$[\text{pyruvic acid mM}]_{\text{actual}} = 0.85[\text{L-glutamic acid mM}]_{\text{NMR}}$$

$$[\text{formic acid mM}]_{\text{actual}} = 0.91[\text{L-glutamic acid mM}]_{\text{NMR}}$$

$$[\text{gallic acid mM}]_{\text{actual}} = 1.36[\text{L-glutamic acid mM}]_{\text{NMR}}$$

$$[\text{lactic acid mM}]_{\text{actual}} = 1.21[\text{L-glutamic acid mM}]_{\text{NMR}}$$

$$[\text{3-dehydroquinic acid mM}]_{\text{actual}} = 0.95[\text{3-dehydroquinic acid mM}]_{\text{NMR}}$$

$$[\text{3-dehydroshikimic acid mM}]_{\text{actual}} = 1.31[\text{3-dehydroshikimic acid mM}]_{\text{NMR}}$$

The concentrations of 2-hydroxymuconic acid, α-keto acid **23**, and α-keto acid **24** were calculated by application of a response factor derived from standards taken using laboratory-synthesized 2-hydroxymuconic acid: $[\text{mM}]\text{actual} = 1.02[\text{mM}]_{\text{NMR}}$

The concentrations of glucosamine and kanosamine were calculated by application of a calibration formula derived from standards taken using reagent-grade D-glucosamine hydrochloride (Alfa Aesar): $[\text{mM}]_{\text{actual}} = 1.01[\text{mM}]_{\text{NMR}}$

Kanosamine and glucosamine concentrations were calculated from integration of anomeric resonances. The ratio of α- and β-anomers of each aminosugar varied somewhat between samples [kanosamine (δ 5.27, d, 0.3-0.5H and δ 4.73, d, 0.5-0.7H), glucosamine (δ 5.43,

d, 0.3-0.5H and δ 4.96, d, 0.5-0.7H)]. Therefore, the integration of both anomeric peaks were combined and applied to the calibration formulae for the respective compounds. When this was not possible due to overlap of the α-anomeric proton peak, an average ratio was used: α:β = 0.45:0.55 for both kanosamine and glucosamine.

UV and visible measurements were recorded on an Agilent 8453 UV-Vis spectrophotometer with a Dell Dimension 8100 equipped with ChemStation operating software or a ThermoFisher NanoDrop™ One^{C} microvolume UV-Vis spectrophotometer.

HPLC analysis was performed on an Agilent 1100 instrument. Terephthalic acid and phthalic acid was quantified by HPLC using an Agilent ZORBAX SB-C18 column (4.6 x 150 mm, 5 μm particle size) with isocratic elution of 15/85 (v/v) CH_3CN/H_2O (100 mM NH_4HCO_2, pH 2.5). The ZORBAX column was received in a solution of 85/15 (v/v) CH_3OH/H_2O and was subsequently washed with 1 L HPLC-grade CH_3CN (0.2 mL/min) prior to use. Analytical standards were obtained from Sigma-Aldrich. Requisite buffers were prepared with degassed, deionized, distilled water which had been filtered through a DURAPORE® 0.45 μm HV filter. (MILLIPORE). The eluent buffer and HPLC-grade CH_3CN was mixed online. All samples analyzed by HPLC were previously filtered through 0.45 μm disc filters (Whatman).

Bacterial strains and plasmids

E. coli DH5α([F$^-$ *endAl glnV44 thi-1 recA1 gyrA96 deoR nupG purB20* ϕ80d*lacZ*ΔM15 Δ(*lacZYA-argF*)$_{U169}$ *hsdR17*($r_K^-m_K^+$) λ$^-$] was previously obtained by this laboratory from Invitrogen. The laboratory strain *E. coli* WN1 [F$^-$ *tsx-352 glnV42 aroE353 malT352*(λ^R) λ$^-$

serA::*aroBaroZ lacZ*::*tktAaroZ*] was previously constructed by Wei Niu in the Frost group.[2] The laboratory strain RB791*serA* (W3110 *lacL8I*^{q}*serA*) was previously constructed by this laboratory.[3] *E. coli* KM1 (WN1 *pptA*::FRT) was prepared using λ Red recombinase-mediated homologous recombination.[4] *Paenibacillus* sp. JJ-1b (ATCC 35889) was obtained from ATCC.[5] Plasmids pBbA1a-RFP and pBbA7k-RFP were obtained from Addgene.[6] Plasmids pWN1.262,[2] pWN1.28,[2] pMF63,[2] and pJG7.246[7] were constructed previously by this laboratory.

Plasmids were transformed into *E. coli* DH5α for long-term storage. All bacterial strains were stored at −80°C in glycerol. Glycerol samples were prepared by adding 0.75 mL of a stationary phase culture to a sterile vial containing 0.25 mL 80% (v/v) glycerol. The solution was mixed by inversion, incubated at rt for 2 h, then stored at −80°C.

Plasmid construction via BglBrick assembly standard

All plasmids described in this work were constructed using the BglBrick Assembly Standard developed by Anderson and Keasling.[6] A general outline for the method of plasmid construction is shown in Figure 106 and described herein. Before genes could be combined into an expression plasmid, a BglBrick part was created for each gene of interest. This was done by inserting the PCR-amplified or synthetic genes between the *Bgl*II and *Bam*HI sites in a standard BglBrick cloning vector, pBbA1a (Figure 107).

Once each gene had been inserted, two genes were concatenated following the prefix-insertion method described in Figure 105. The gene to be inserted (Gene 1, Fig. 106) is liberated by digestion with *Eco*RI and *Bam*HI while the recipient vector is digested with *Eco*RI and *Bgl*II. Gene 1 is inserted upstream of Gene 2 in the vector following ligation of the digested DNA

fragments. The *Eco*RI site is reformed upstream of Gene 1 in the product plasmid while compatible BamHI/BglII sticky ends form a two amino acid scar sequence between Gene 1 and Gene 2 encoding glycine-serine (Figure 106). The final plasmid retains the *Eco*RI, *Bgl*II, *Bam*HI, and *Xho*I sites that the original BglBrick parts contained. Therefore, any gene can be inserted upstream of any other by following this method of digestion and ligation.

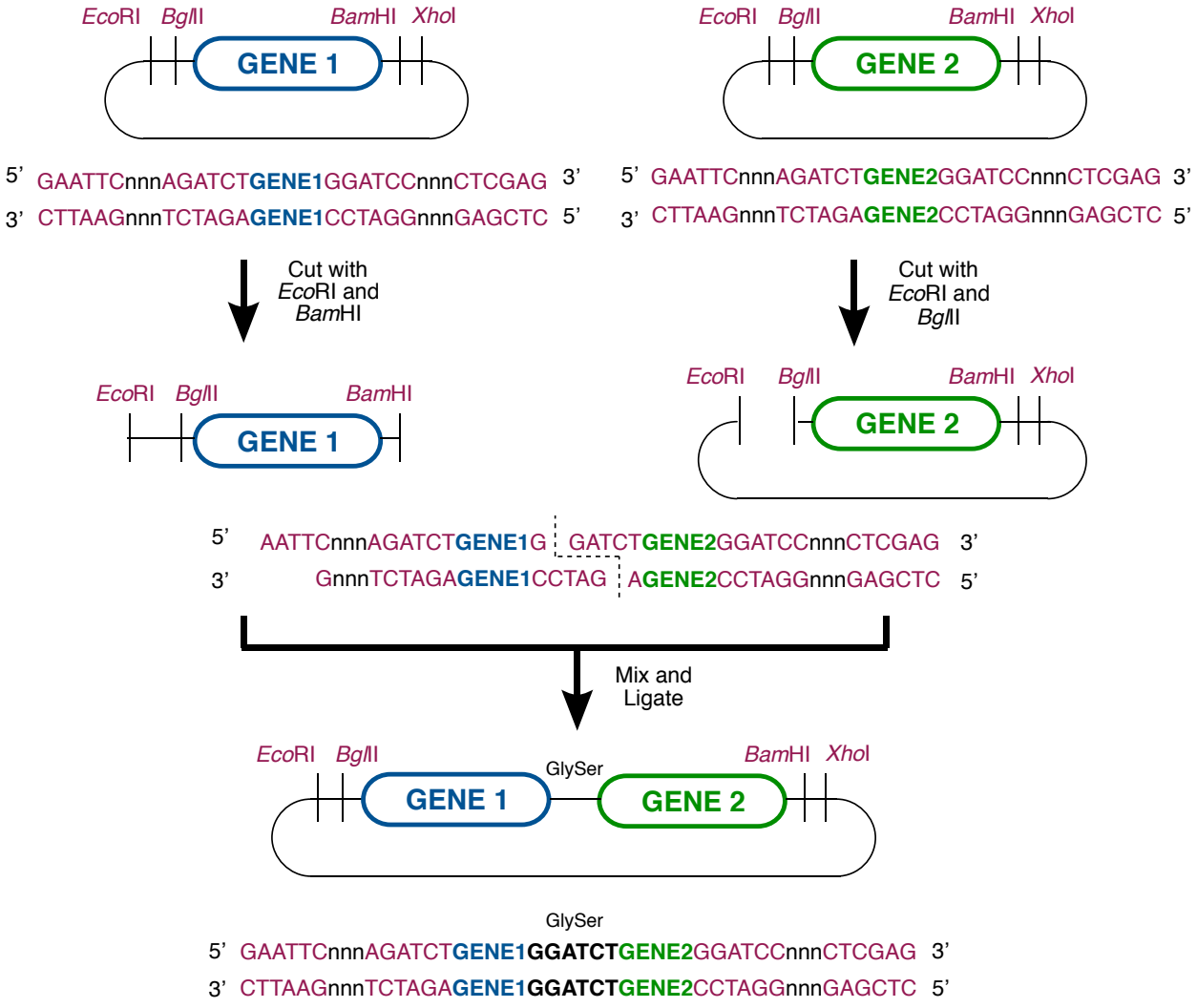

Figure 106. BglBrick plasmid assembly workflow.

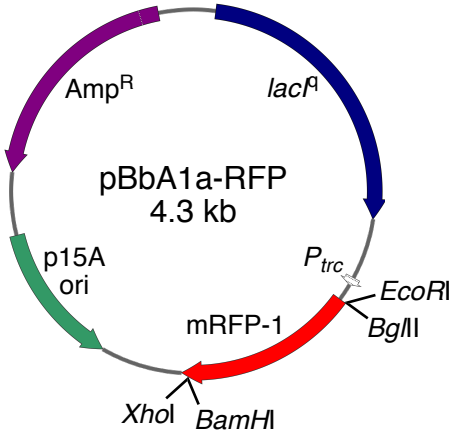

Figure 107. BglBrick vector pBbA1a-RFP.

Culture medium

Bacto™ tryptone, Difco™ yeast extract, and Bacto™ agar were obtained from BD Diagnostic Systems. Ampicillin, thiamine hydrochloride, 2,3-dihydroxybenzoic acid, 4-aminobenzoic acid, and 4-hydroxybenzoic acid were obtained from Spectrum. Isopropyl-β-D-thiogalactopyranoside (IPTG) was obtained from Gold Biotechnology. Ammonium heptamolybdate tetrahydrate was obtained from Mallinckrodt. Aromatic amino acids (L-phenylalanine, L-tyrosine, and L-tryptophan), iron(III) ammonium citrate, and kanamycin were purchased from Sigma Aldrich. All solutions were prepared in distilled, deionized water.

LB medium[8] (1 L) contained Bacto™ tryptone (10 g), Difco™ yeast extract (5 g), and NaCl (10 g). 2×Yeast-tryptone (2×YT) (1 L) contained Bacto™ tryptone (16 g), Difco™ yeast extract (10 g), and NaCl (5 g). Modified SOB medium (1 L) contained Bacto™ tryptone (20 g), Difco™ yeast extract (5 g), and NaCl (5 g). These modifications deviated from the standard recipe[9] by omitting KCl (2.5 mM, 0.186 g/L), $MgCl_2$ (10 mM, 0.952 g/L), and $MgSO_4$ (10 mM, 1.204 g/L). Modified SOC medium was prepared from modified SOB medium (1 L) with the

additions of 250 mM KCl (10 mL), 2 M $MgCl_2$ (5 mL), and 1 M D-glucose (20 mL). These modifications deviated from the standard recipe[9] by omitting $MgSO_4$ (10 mM, 1.204 g/L).[8] ATCC medium 1416 4-hydroxybenzoic acid medium, pH 7.2 (1 L) contained 4-hydroxybenzoic acid (1 g), $K_2HPO_4 \cdot 3H_2O$ (4.25 g), $NaH_2PO_4 \cdot H_2O$ (1 g), NH_4Cl (2 g), nitrilotriacetic acid (0.1 g, adjusted to alkaline pH with concentrated NaOH), $MgSO_4 \cdot 7H_2O$ (0.2 g), $FeSO_4 \cdot 7H_2O$ (0.012 g), $MnSO_4 \cdot H_2O$ (0.003 g), $ZnSO_4 \cdot 7H_2O$ (0.003 g), and $CoSO_4$ (0.001 g). M9 salts[9] (1 L) contained Na_2HPO_4 (6 g), KH_2PO_4 (3 g), NH_4Cl (1 g), and NaCl (0.5 g). Modified M9 media[8] was prepared by adding D-glucose (10 g), $MgSO_4$ (0.24 g), and thiamine hydrochloride (0.001 g) to 1 L M9 salts. These modifications increased the percentage of D-glucose from 0.4% to 1% (w/v), increased the amount of $MgSO_4$ by two-fold, and omitted 0.1 mM $CaCl_2$ from the recipe described by Sambrook and Russell.[9] Where appropriate, modified M9 media (1 L) was supplemented with L-phenylalanine (0.040 g), L-tyrosine (0.040 g), L-tryptophan (0.040 g), 4-hydroxybenzoic acid (0.010 g), 4-aminobenzoic acid (0.010 g), and 2,3-dihydroxybenzoic acid (0.010 g). L-Serine was added to a final concentration of 40 mg/L where indicated. Antibiotics were also added where required to the following concentrations: ampicillin (Ap), 50 µg/mL; kanamycin (Kan), 50 µg/mL; chloramphenicol (Cm), 20 µg/mL (in 95% EtOH); and tetracycline (Tc), 12.5 µg/mL (in 1:1 H_2O:EtOH). IPTG was added to culture medium of strains carrying inducible promoters: P_{trc}, P_{T7}, P_{T5}. Solutions of LB media, M9 salts, $MgSO_4$ (1 M), D-glucose (20% w/v), initial glucose (18-30 g/L), feed glucose (60% w/v), D-fructose (20% w/v), mixed D-glucose/D-fructose feed (60% w/v, 1:1 glucose:fructose), modified SOB media, KCl (250 mM), and $MgCl_2$ (1 M) were sterilized by autoclaving. Solutions of aromatic vitamins (containing 4-hydroxybenzoic acid, 4-aminobenzoic acid, and 2,3-dihydroxybenzoic acid),

aromatic amino acids (containing L-phenylalanine, L-tyrosine, and L-tryptophan), L-serine, antibiotics, and IPTG were sterilized by filtration through 0.22 μm membrane. Solid media was prepared by adding 1.5% (w/v) Bacto™ agar to liquid media.

The standard *E. coli* fermentation medium[10] (1 L) contained K_2HPO_4 (7.5 g), anhydrous citric acid (1.92 g), ammonium iron (III) citrate (0.3 g), conc. H_2SO_4 (1.2 mL), and concentrated NH_4OH (4.1 mL). Where appropriate, fermentation media was supplemented with L-phenylalanine (0.7 g), L-tyrosine (0.7 g), and L-tryptophan (0.35 g). The following supplements were added to the medium immediately prior to inoculation of the vessel and initiation of fermentation: D-glucose (18 g, 20 g, or 30 g), $MgSO_4$ (0.24 g), and trace minerals including $(NH_4)_6(Mo_7O_{24})\cdot 4H_2O$ (0.0037 g), $ZnSO_4\cdot 7H_2O$ (0.0029 g), H_3BO_3 (0.0247 g), $CuSO_4\cdot 5H_2O$ (0.0025 g), and $MnCl_2\cdot 4H_2O$ (0.0158 g). For fermentations requiring aromatic vitamin supplementation, 4-hydroxybenzoic acid (0.01 g), 2,3-dihydroxybenzoic acid (0.01 g), and 4-aminobenzoic acid (0.01 g) were added alongside initial glucose supplements.

Fermentation conditions

General

Fermentations were conducted in a B. Braun BIOSTAT® B-DCU system controlled by a DCU tower with 2 L working capacity fermentor vessel. Data was acquired on a Digilink personal computer utilizing MFCS/Win 3.0 software. PID control loops were used to maintain temperature (33°C) and pH (7.0 ± 0.1). pH was maintained via addition of 2 N H_2SO_4 and concentrated NH_4OH. Glucose was added as a 60% (w/v) solution using a Matson Marlow 101U/R peristaltic pump. A mixed carbohydrate feed consisting of equimolar amounts of D-

glucose (30% w/v) and D-fructose (30% w/v) was similarly added as a 60% (w/v) aqueous solution. Dissolved oxygen (D.O.) was monitored using a Hamilton OxyFerm FDA 225 sterilizable O_2 sensor fitted with an Optiflow FDA O_2-permeable membrane. pH was measured using a Hamilton EasyFerm Plus K8 200 sterilizable probe. Glucose concentrations were measured with a GlucCell™ meter and test strip (CESCO Bioengineering Co., Ltd.). Antifoam 204 (Sigma-Aldrich) was added manually as needed to mitigate foam accumulation.

Growth of an inoculant was initiated by introduction of a fresh, single colony into a culture tube (18 mm × 150 mm) containing 5 mL modified M9 medium. Cultures were grown with agitation at 250 rpm for 18-24 h. 2-Hydroxymuconic acid (2-HMA)-producing strains were cultured at 37°C while kanosamine-producing strains were cultured at 35°C. An appropriate amount of the 5 mL culture was used to inoculate 100 mL M9 medium in a 500 mL three-baffled Kimble™ KIMAX™ culture flask to an initial OD_{600} = 0.05. The 100 mL cultures were incubated with agitation at 37°C, 250 rpm for 2-HMA-synthesizing strains or 35°C, 250 rpm for kanosamine-producing strains, for 6-8 h. After an appropriate OD_{600} was reached (1.0-1.5) the culture was transferred into the fermentation vessel. The initial glucose concentrations in the fermentation medium was 18-20 g/L for glucose-limited conditions and 30 g/L for glucose-rich conditions.

Glucose-rich fermentations

For fermentations which employed glucose-rich conditions, a stainless steel baffle cage containing four 1/4″ × 4″ baffles was fitted to the fermentation vessel. Fermentation runs used three staged methods to maintain D.O. concentrations at 10% air saturation. Mass flow

controller settings for the first stage are presented in Figure 108 while settings for the second stage are presented in Figure 109. With the airflow at an initial setting of 0.06 L/L/min, the D.O. was maintained by increasing the impeller speed from an initial set point of 50 rpm to a preset maximum of 750 rpm. With the impeller rate constant at 750 rpm, the mass flow controller then maintained D.O. concentration by increasing airflow from its initial setting to a preset maximum of 1.0 L/L/minutes. After the preset maxima of 750 rpm and 1.0 L/L/min were reached, the third stage of the fermentation was entered in which glucose (60% w/v) was added at a rate sufficient to maintain 20-30 g/L D-glucose concentration throughout the run. During this stage, the impeller speed was allowed to vary between 400-1800 rpm in order to maintain D.O. concentration at 10% air saturation.

Deadband 0.5% saturation							
CASCADE							
1	STIR						
2	AIRFLOW						
Parameter	**Minimum**	**Maximum**	**X_P**	**τ_I**	**τ_D**	**Hysterese**	**Mode**
STIR	2.5%	37.5%	150.0%	100.0 s	0.0 s	01:00 m:s	auto
AIRFLOW	2.0%	33.3%	90.0%	50.0 s	0.0 s	01:00 m:s	auto

Figure 108. Mass flow controller settings for first stage of glucose-rich fermentations. Stir settings: 2.5% (50 rpm), 37.5% (750 rpm). Airflow settings: 2.0% (0.06 L/L/min), 33.3% (1.0 L/L/min).

Deadband 0.5% saturation							
CASCADE							
1	AIRFLOW						
2	STIR						
Parameter	**Minimum**	**Maximum**	**X_P**	**τ_I**	**τ_D**	**Hysterese**	**Mode**
STIR	37.5%	90.0%	150.0%	100.0 s	0.0 s	01:00 m:s	auto
AIRFLOW	33.3%	33.3%	90.0%	50.0 s	0.0 s	01:00 m:s	auto

Figure 109. Mass flow controller settings for second stage of glucose-rich fermentations. Stir settings: 37.5% (750 rpm), 90.0% (1,800 rpm). Airflow settings: 2.0% (0.06 L/L/min), 33.3% (1.0 L/L/min).

Glucose-limited fermentations

All glucose-limited fermentations did not utilize a fermentation vessel outfitted with a stainless steel baffle cage. During a fermentation, the following three stages were used to maintain D.O. concentration at 10% air saturation. With the airflow at an initial set point of 0.06 L/L/min, the D.O. concentration was maintained by varying the impeller speed from an initial setting of 50 rpm to a preset maximum of 850 rpm. Once the preset maximum was reached, the airflow was allowed to increase from its initial setting to a preset maximum of 1.0 L/L/minutes. At a constant impeller speed of 850 rpm and airflow rate of 1.0 L/L/min, the D.O. concentration was maintained at 10% air saturation for the remainder of the run by oxygen-sensor-controlled glucose feeding. PID control parameters for oxygen-sensor-controlled glucose feeding were set to 0.0 (off) for the derivative control (τ_D) and 999.9 s (minimum control action) for integral control (τ_I). The proportional response (X_p) was set to 950.0% to achieve a proportional gain (K_c) of 0.1. Mass flow controller settings for stir speed and airflow are shown in Figure 110.

Deadband 0.5% saturation							
CASCADE							
1	STIR						
2	AIRFLOW						
Parameter	**Minimum**	**Maximum**	**X_P**	**τ_I**	**τ_D**	**Hysterese**	**Mode**
STIR	2.5%	42.5%	175.0%	100.0 s	0.0 s	01:00 m:s	auto
AIRFLOW	2.0%	33.3%	90.0%	50.0 s	0.0 s	01:00 m:s	auto

Figure 110. Mass flow controller settings for second stage of glucose-rich fermentations. Stir settings: 2.5% (50 rpm), 42.5% (850 rpm). Airflow settings: 2.0% (0.06 L/L/min), 33.3% (1.0 L/L/min).

General procedure for processing fermentation broth

Cells were removed from fermentation broth by centrifugation (6,000*g*, 20 min, 4°C). Proteins were removed by filtration through a Sartocon® ECO Hydrostart® membrane 10 kD cut-off cassette using a SartoJet® 4-piston Diaphragm Pump. Tangential flow filtration was performed with 25 ± 5 psig toward the membrane and a 7 ± 1 psig back-pressure. When approximately 200 mL broth remained unfiltered, the volume was insufficient to sustain flow and the filtration ceased.

Analysis of fermentation cultures

Samples (5-15 mL) were removed at indicated intervals and cell densities of *E. coli* were determined by dilution of an aliquot of fermentation broth with water (1:50, 1:100, or 1:200; 1 mL total volume of diluted sample) followed by measurement of absorption at 600 nm. Dry cell weight for *E. coli* was obtained using a conversion coefficient of 0.43 g/L/OD_{600}. The remaining

fermentation broth was centrifuged (11,300 *g*, 5 min, rt for 5 mL samples or 7,600 *g*, 15 min, 4°C for 15 mL samples) and the cell-free supernatant was used to determine solute concentrations. Cell pellets from 15 mL samples were frozen at −80°C for later use.

Solute concentrations in cell-free broth were determined by ^{1}H NMR with application of formulae described above. Kanosamine containing solutions were concentrated to dryness under reduced pressure, concentrated to dryness one additional time from D_2O, and redissolved in D_2O containing a known quantity of the sodium salt of 3-(trimethylsilyl)propionic-*2*,*2*,*3*,*3*-d_4-acid (TSP). Solutions containing 2-hydroxymuconic acid were acidified to pH 4 with 10% (v/v) H_2SO_4 and concentrated to dryness under reduced pressure. The yellow oil was redissolved in CD_3OD containing a known amount of maleic acid.

Genetic manipulations

General methods

E. coli DH5α was used as the host strain for plasmid manipulations. Restriction enzymes, T4 DNA ligase, and Q5 DNA polymerase were purchased from New England BioLabs, Inc. (Ipswich, MA). Agarose (electrophoresis grade) was purchased from Invitrogen and dNTPs were purchased from Promega. PCR amplifications were performed following the recommended protocol as described by New England BioLabs (NEB). Each reaction (50 µL) contained 5× Q5 reaction buffer (10 µL), dNTPs (0.2 mM), forward and reverse primers (0.5 µM), template DNA (100-500 ng), and 1 unit of Q5 DNA polymerase. Primers were synthesized by Integrated DNA Technologies (Coralville, IA). The PCR reaction was performed using a Bio-Rad DNA Engine® Peltier Thermal Cycler.

PCR products and digested DNA fragments were isolated and purified from 0.7% (w/v) agarose gel (TAE buffer, pH 8.3) using the Zymoclean™ Gel DNA Recovery kit (Zymo Research) or the Monarch® DNA Gel Extraction kit (NEB) following manufacturer's protocol. TAE buffer contained trishydroxymethylaminomethane (Tris base, 40 mM), HOAc (20 mM), and sodium ethylenediaminetetraacetate (EDTA, 50 mM). Ligation reaction mixtures were purified prior to transformation using the Zymo Research DNA Clean & Concentrator™-25 kit or the Monarch® PCR & DNA Cleanup kit (NEB) following manufacturer's protocol. DNA concentration was determined by measuring the absorbance at 260 nm. An absorbance of 1.0 at 260 nm corresponds to 50 μg/μL of double-stranded DNA. Protein contamination was estimated by measuring the absorbance of DNA sample at 280 nm. A ratio of A_{260}:A_{280} of 1.8-2.0 indicates pure DNA.

Preparation and transformation of electrocompetent *E. coli*

Electrocompetent cells were prepared using modified procedures from Sambrook and Russell.[9] A single colony was used to inoculate LB media (5 mL). The liquid culture was incubated overnight at 37°C, 250 rpm. An appropriate amount of overnight culture was used to inoculate a 1 L six-baffled Kimble™ KIMAX™ culture flask containing 200 mL 2×YT media to an initial OD_{600} = 0.015. Cells were cultured at 37°C, 250 rpm for 2-3 h until mid-exponential growth phase (OD_{600} = 0.5-0.7) at which point the flask containing the cell culture was chilled on ice for 30 minutes. Cells were harvested by centrifugation (5 min, 2,800*g*, 4°C) and the supernatant was discarded. All subsequent manipulations were carried out on ice. The cell pellet was resuspended in 200 mL sterile ice-cold water and harvested by centrifugation (10 min,

2,800*g*, 4°C). The supernatant was discarded and cells resuspended in 100 mL sterile ice-cold water. Cells were harvested again by centrifugation (10 min, 2,800*g*, 4°C). The supernatant was discarded and the cells were resuspended in 100 mL sterile, ice-cold 10% (v/v) glycerol. Resuspended cells were chilled on ice for 30 min prior to centrifugation (10 min, 2,800*g*, 4°C). The supernatant was discarded and the cells were resuspended in 0.5 mL sterile, ice-cold 10% (v/v) aqueous glycerol solution. Aliquots (50 μL) were dispensed into sterile, ice-cold microcentrifuge tubes and flash-frozen in liquid nitrogen. Frozen electrocompetent cells were stored at −80°C.

Plasmid DNA (dissolved in sterile water, 1-3 μL; 10-100 ng) or purified, de-salted DNA ligation reaction solutions (3 μL) was mixed with 50 μL of thawed electrocompetent cells. The mixture of cells and DNA was transferred to a Bio-Rad Gene Pulser cuvette (0.2 cm electrode gap). Electroporation was performed using a Bio-Rad Gene Pulser II electroporator set to 2.5 kV, 25 μF, and 200 Ω. A single pulse was applied across the cuvette containing cells and DNA which resulted in a time constant of 5.16-5.30 ms. SOC medium (950 μL) was added into the cuvette and the cell-containing mixture was transferred into a sterile glass culture tube (20 × 150 mm). Cells were cultured in a rotary shaker (37°C, 250 rpm) for 1 h and plated onto appropriate medium. Before plating onto M9 medium, cells were washed with M9 salts (1 mL, 3×). Washed, pelleted cells were resuspended in M9 salts before plating.

Small-scale purification of plasmid DNA

A single colony of freshly transformed *E. coli* was used to inoculate 5 mL LB media containing the appropriate antibiotic. Inoculated cultures were incubated with shaking at 37°C,

250 rpm overnight. Cells were harvested from 3 mL of stationary-phase cultures by microcentrifugation (2,400*g*, 3 min, rt). Isolation and purification of plasmid DNA used the Qiagen QIAprep® Spin Miniprep kit following the manufacturer's protocol. Plasmid DNA was eluted from the spin column with 50 µL sterile water.

Large-scale purification of plasmid DNA

A single, fresh colony of *E. coli* was used to inoculate 100 mL LB media containing the appropriate antibiotic in a 500 mL three-baffled Kimble™ KIMAX™ culture flask. Inoculated cultures were incubated with shaking at 37°C, 250 rpm overnight. Cells were harvested by centrifugation (2,800*g*, 5 min, 4°C). Isolation and purification of plasmid DNA used the Qiagen Plasmid Midiprep kit following the manufacturer's protocol. The purified air-dried plasmid DNA pellet was dissolved in 200 µL sterile water and stored at 4°C.

Restriction enzyme digestion of DNA

A typical restriction enzyme DNA digest (20 µL) contained 2 µL restriction enzyme buffer (10× concentration), 5-10 µL purified DNA stock (0.1-1.0 µg), 1 µL of restriction enzyme, and 7-13 µL sterile water. Double-digestions used 1 µL each of the required restriction enzymes. When sequential restriction digests involved enzymes requiring buffers of varying salt concentrations, the first digest was performed in the low-salt buffer followed by addition of 1 µL 1.7 M NaCl and 1 µL of high-salt restriction enzyme before the second digest. Reactions were incubated a 37°C for 1 h. When pJG7.246 was used as the vector, 1 unit of calf intestinal alkaline phosphatase (CIAP) was added following *Bam*HI digestion and the reaction mixture

incubated for an additional hour at 37°C. Digests were terminated by addition of 4 μL DNA gel loading dye containing SDS (6× concentration, NEB) and subsequently analyzed by agarose gel electrophoresis.

Ligation of DNA

Most DNA ligations were designed so that the molar ratio of insert DNA to vector DNA was 3:1. When inserting a fragment into pJG7.246, however, the molar ratio of insert DNA to vector DNA was increased to 10:1. A typical ligation reaction contained 0.01-0.02 pmol of vector DNA and 0.03-0.1 pmol insert DNA. This mixture was brought to 17 μL using sterile water before adding 2 μL 10× T4 ligase buffer and 1 μL of T4 DNA ligase (2 units). Ligations were conducted for 2 h at rt. Reactions were terminated by incubation at 65°C for 10 min before purifying the reaction mixture with a Zymo Research DNA Clean & Concentrator™-25 kit or the Monarch® PCR & DNA Cleanup kit (NEB) following the manufacturer's protocol. Purified ligation mixtures were eluted from the spin column in 6 μL sterile water.

Agarose gel electrophoresis

Agarose gel electrophoresis was performed in TAE buffer containing trishydroxymethylaminomethane (Tris base, 40 mM), HOAc (20 mM), and sodium ethylenediaminetetraacetate (EDTA, 50 mM). A constant voltage of 97 V was applied for 1 h. Gels typically contained 0.7% (w/v) agarose in TAE buffer. Lower concentrations of agarose (0.35 %) were used to resolve genomic DNA. Ethidium bromide (0.5 μg/mL) was added to the agarose to allow visualization of DNA fragments under a UV lamp. The size of the DNA

fragments were determined by comparison to DNA fragments present in 10 μL 1 kb DNA ladder (NEB, 500-10,000 bp).

Polyacrylamide gel electrophoresis (SDS-PAGE)

Polyacrylamide gels were run under denaturing conditions in SDS-PAGE buffer (pH 8.3) containing sodium dodecyl sulfate (SDS, 0.1% w/v), L-glycine (192 mM), and Tris base (25 mM). Protein analysis used 4-20% (w/v) acrylamide Mini-PROTEAN® TGX™ precast gels purchased from Bio-Rad Laboratories, Inc. Each protein sample (60 μL) was diluted with Laemmli sample buffer (60 μL) consisting of 4% (w/v) SDS, 20% (v/v) glycerol, dithiothreitol (100 mM), 0.004% (w/v) bromophenol blue, and 125 mM Tris-HCl (pH 6.8). Diluted protein samples were incubated at 90-95°C for 5 min and microcentrifuged (11,300 *g*, 2 min, rt). Samples (30 μL) and Precision Plus Protein™ All Blue ladder (Bio-Rad) were loaded into sample wells and the gel was run under constant voltage at 200 V. When the blue tracking dye reached the bottom of the gel, the gels were removed from the cassettes and stained in a solution containing 0.1% (w/v) Coomassie Brilliant Blue R, 45% (v/v) MeOH, and 10% (v/v) HOAc in H_2O for at least 2 h. Gels were destained in a solution of 45% (v/v) MeOH and 10% (v/v) HOAc in H_2O.

CHAPTER ONE

Synthetic procedures

Diethyl 2-hydroxyhexa-2,4-dienedioate **22**

A 500 mL three-neck flask equipped with a thermometer was charged with *t*-butanol (39 mL, 420 mmol) which was stirred under a nitrogen atmosphere. Finely sliced potassium metal (3.9 g, 100 mmol) was added gradually. The mixture was allowed to stir at rt for 1 h after which dry toluene (30 mL, 284 mmol) was added via syringe. An ice bath was used to cool the reaction mixture to 0°C where it was maintained for 30 min before adding a solution of diethyl oxalate (13.5 mL, 100 mmol) in dry toluene (8 mL, 76 mmol). Diethyl oxalate was added slowly to ensure the temperature was maintained between 0-5°C during which time the solution developed a bright yellow-orange color. Upon complete addition of diethyl oxalate, the solution was stirred at 0°C for 30 min before a solution of ethyl crotonate (12.4 mL, 100 mmol) in dry toluene (8 mL, 76 mmol) was added via a syringe. The ethyl crotonate solution was similarly added to ensure the temperature was maintained between 0-5°C. The resultant red-orange solution was stirred at 0°C for 1 h before the ice bath was removed and the reaction mixture allowed to warm gradually to rt. A mustard yellow precipitate was observed beginning 1 h after addition of ethyl crotonate. The reaction mixture was allowed to stir at rt for 15 h after which time no further formation of yellow precipitate was observed.

The mustard-yellow solids were dissolved in 5% HOAc (250 mL) to afford a red solution. Dilute H_2SO_4 was used to acidify the solution to pH 5, whereupon crude diethyl 2-hydroxyhexa-2,4-dienedioate **22** was extracted into EtOAc (3 x 250 mL). The organic extracts

were pooled and dried with anhydrous $MgSO_4$ before concentrating under reduced pressure. The pale yellow solids were dried overnight under reduced pressure at rt to afford diethyl 2-hydroxyhexa-2,4-dienedioate **22** (15.2 g, 71 mmol, 71% yield). ^{1}H NMR (500 MHz, CD_3OD) δ 7.72 (dd, *J* = 15.6, 11.7 Hz, 1H), 6.26 (dd, *J* = 11.7, 0.9 Hz, 1H), 6.01 (dd, *J* = 15.5, 0.9 Hz, 1H), 4.29 (q, *J* = 7.1 Hz, 2H), 4.19 (q, *J* = 7.1 Hz, 2H), 1.33 (t, *J* = 7.1 Hz, 3H), 1.29 (t, *J* = 7.1 Hz, 3H). ^{13}C NMR (126 MHz, CD_3OD) δ 168.7, 165.1, 147.9, 139.1, 122.1, 109.3, 63.1, 61.5, 14.6, 14.4.

6-Carboxy-2-pyrone **19**

Diethyl 2-hydroxyhexa-2,4-dienedioate **22** (3.2 g, 15 mmol) was dissolved in an aqueous solution (17.5 mL total volume) of conc. H_2SO_4 (2.5 mL, 47 mmol) and glacial HOAc (10 mL, 175 mmol) in a 50 mL round-bottom flask equipped with a thermometer and reflux condenser. The bright yellow solution was heated to reflux for 3 h during which time a red-brown color developed. After allowing to cool to rt, the acidic solution was neutralized with NaOH and extracted with EtOAc (3 x 20 mL). The organic extracts were pooled and dried with anhydrous $MgSO_4$ before concentrating under reduced pressure. After drying overnight under reduced pressure at rt, 6-carboxy-2-pyrone **19** was obtained as light brown solids (1.8 g, 12.8 mmol, 85% yield). ^{1}H NMR (500 MHz, D_2O) δ 7.73 (dd, *J* = 9.4, 6.7 Hz, 1H), 7.27 (dd, *J* = 6.7, 1.0 Hz, 1H), 6.66 (dd, *J* = 9.4, 1.0 Hz, 1H). ^{13}C NMR (126 MHz, DMSO-d_6) δ 160.4, 160.0, 149.5, 143.6, 120.0, 110.1.

2-Hydroxymuconic acid

A rust-colored solution of 6-carboxy-2-pyrone **19** (0.5 g, 3.6 mmol) dissolved in 2 M NaOH (18 mL) was stirred at rt for 12 h in a round bottom flask. The solution was transferred to a beaker on ice and chilled to 0°C. Acidification of the ice-cold solution to pH 2 with conc. H_2SO_4 resulted in the formation of a pale-yellow precipitate. Solids were removed by filtration and dried under reduced pressure to afford 2-hydroxymuconic acid (2-HMA, 0.32 g, 64% yield). An alternative method of preparation utilized a solution of 2-hydroxyhexa-2,4-dienedioate **22** (7.0 g, 33 mmol) in 2 M NaOH (200 mL) following the described procedure resulting in 2-HMA in 59% isolated yield (2.77 g, 19.5 mmol). ^{1}H NMR (500 MHz, CD_3OD) δ 7.72 (dd, J = 15.6, 11.8 Hz, 1H), 6.26 (d, J = 11.7 Hz, 1H), 5.96 (d, J = 15.5 Hz, 1H). ^{13}C NMR (126 MHz, DMSO-d_6) δ 167.7, 165.0, 147.2, 137.5, 121.8, 107.9.

Derivatization of 2-hydroxymuconic acid to 2-hydroxydimethylmuconate

A solution of 2-hydroxymuconic acid (10 mg, 0.06 mmol) in MeOH (0.2 mL) was stirred in a pear-shaped flask at rt. Trimethylsilyldiazomethane (TMSD, 2 M in diethyl ether, 0.3 mL) was added via syringe and the mixture was stirred at rt for 1 h. Upon completion of the reaction, solvent was removed by passing a stream of nitrogen over mouth of reaction vessel. The oily residue was dissolved in a solvent mixture of EtOAc:hexanes (1:4) and purified by silica gel chromatography. Fractions containing 2-hydroxydimethylmuconate were pooled and used for nuclear Overhauser effect experiments. ^{1}H NMR (500 MHz, DMSO-d_6) δ 7.61 (dd, J = 15.4, 11.8 Hz, 1H), 6.29 (d, J = 11.8 Hz, 1H), 6.13 (d, J = 15.5 Hz, 1H), 0.95 (s, 3H), 0.94 (s, 3H).

General procedure for cycloaddition of 2-hydroxymuconic acid with ethylene **2**

Cycloadditions of 2-HMA with ethylene were conducted in a Series 4560 Titanium Mini-reactor Stirred Vessel (Parr Instrument Co.). Solvent, catalyst (where indicated), and 2-HMA were added to the reactor vessel in a glove bag under a positive nitrogen atmosphere. The reactor head was attached and secured by tightening the collar bolts finger-tight in the glove bag. The sealed reactor vessel was brought to a fume hood and secured to the instrument mount. Bolts were tightened further with a torque wrench to 15 psi. While stirring at low speed (50 rpm), the reactor vessel was flushed with ethylene gas (3x) before pressurizing with ethylene gas to the reaction pressure (500 psig unless otherwise indicated). A heating mantle was lifted into place surrounding the reactor vessel and the impeller speed was increased to 200 rpm. Approximately 1.5 h was required to reach reaction temperature (t = 0) during which time the internal reactor pressure rose by 350 psig. An additional 100 psig increase of pressure was observed during the course of the reaction. To terminate the reaction, the heating mantle was removed and the reactor was allowed to cool to rt. Approximately 2.5 h were required to cool reactor completely. Pressure was released by slowly opening the vent valve and the reactor head was removed in air. The reactor chamber, impeller, and thermoprobe were rinsed with acetone followed by copious amounts (200-300 mL) of *N*,*N*-dimethylacetamide (DMA). Acetone and DMA solutions were analyzed separately by NMR and HPLC.

General procedure for cycloaddition of propiolic acid **18** and 6-carboxy-2-pyrone **19**

A three-neck flask equipped with a stir bar, thermometer, and jacketed condenser was charged with solvent (5 mL) and propiolic acid (0.9, 14 mmol). Catalyst (20 mol%) was added

and the mixture stirred at rt for 2 minutes. 6-Carboxy-2-pyrone (0.5 g, 3.6 mmol) was added and the reaction mixture was heated to reflux. After 12 h, the reaction was cooled to rt and quenched with H_2O. The solvent was removed under reduced pressure and the crude reaction material analyzed by NMR and HPLC.

Conversion of 2-hydroxymuconic acid isomer mixture to 6-carboxy-2-pyrone **19** in fermentation broth

Cell-free, protein-free fermentation broth containing 2-HMA, α-keto acid **23** and α-keto acid **24** (700 mL) was combined with HOAc (560 mL) and conc. H_2SO_4 (136 mL) in a 2 L three-neck flask equipped with stir bar, thermometer, and jacketed condenser. The solution was stirred under a nitrogen atmosphere at 95°C for 5 h. Upon cooling to rt, the dark brown reaction crude was concentrated under reduced pressure and analyzed by ^{1}H NMR.

D-Erythrose-4-phosphate

Synthesis of D-erythrose-4-phosphate followed procedures described by Sieben.[11] Glacial HOAc (500 mL) was stirred in a 1 L three-neck flask under a stream of nitrogen for 15 min at rt. A solution of D-glucose-6-phosphate, disodium salt hydrate (0.56 g, 2 mmol) in 4 mL H_2O was added via syringe. Dropwise addition of a suspension of $Pb(OAc)_4$ (1.51 g, 3.4 mmol) in HOAc (60 mL) with 6 N H_2SO_4 (1.2 mL) employed an addition funnel affixed to the 1 L three-neck flask. Complete addition of $Pb(OAc)_4$ required 1.5 h during which time a white precipitate developed in the reaction flask. The precipitate was removed by filtration through Celite® 545. The clarified solution was concentrated to 1/5 volume under reduced pressure and

the excess HOAc was removed by azeotropic distillation with H_2O (5×). The resulting solution was applied to a cation exchange resin at rt (Dowex® 50WX8, 1.5 in × 6 in, 50 mL, hydrogen form) and eluted with H_2O (300 mL). D-Erythrose 4-phosphate (E4P) was quantified using a transketolase coupled enzyme assay described below.

Isolation of *Paenibacillus* sp. JJ-1b (ATCC 35889) genomic DNA

Lyophilized *Paenibacillus* sp. JJ-1b (ATCC 35889) was rehydrated with 250 µL of ATCC #1416 media and streaked onto ATCC #1416 agar plates. Cells were grown at 30°C for 36 h. A single colony was used to inoculate ATCC #1416 media (5 mL) and the culture was incubated at 30°C, 250 rpm overnight. Genomic DNA was isolated from growing cells following a procedure described by Wecke.[12] A 250 mL three-baffle flask containing 50 mL ATCC #1416 media was inoculated with 1 mL overnight culture. Cells were incubated at 30°C, 250 rpm for 16 h to a final OD_{600} = 1.3. Cells were harvested by centrifugation (5 min, 2,000 *g*, 4°C) and the supernatant was discarded. The cell pellet was suspended in 400 µL TEN buffer (10 mM Tris-HCl, pH 8.0, 10 mM EDTA, 150 mM NaCl) and transferred into a microcentrifuge tube. Lysozyme (0.4 mg) was added and the mixture was incubated for 20 min at 37°C. RNase A (0.04 mg) was added and the mixture was incubated for 3 min at 65°C. SDS (0.004 mg) and proteinase K (0.15 mg) was added along with 550 µL TEN* buffer (10 mM Tris-HCl, pH 8.0, 1 mM EDTA, 50 mM NaCl) and the mixture was incubated for 2 h at 60°C. Tris-buffered phenol (450 µL) was added and the microcentrifuge tube vortexed briefly to mix. Organic and aqueous layers were separated by microcentrifugation (5 min, 11,300 *g*, rt). The aqueous layer was decanted into a new microcentrifuge tube and phenol extraction was repeated. After

microcentrifugation (5 min, 11,300 *g*, rt) phenol was discarded and the aqueous layer was washed with chloroform:isoamyl alcohol (24:1, 900 µL). The aqueous phase was then transferred into a test tube containing 95% EtOH (10 mL, −20 °C). Precipitated DNA was collected on the tip of a Pasteur pipette and dried in air at rt for 5 minutes. Genomic DNA was then dissolved in 100 µL sterile water. The DNA concentration was 1.4 µg/µL based on the absorbance at 260 nm.

Bacterial strains and plasmids

Strain generation: *E. coli* KM1

E. coli KM1 was prepared by inactivation of genomic *pptA* from *E. coli* WN1 using λ Red mediated homologous recombination following the procedure of Wanner.[4] Plasmid pKD46 allows cell growth in the presence of ampicillin and carries a temperature-sensitive replicon and the λ Red recombinase genes behind an arabinose-inducible promoter. This plasmid was transformed into WN1 and electrocompetent WN1/pKD46 cells were prepared as described above. A kanamycin resistance gene (Kan^R) flanked by flippase recognition targets (FRT) was PCR-amplified from plasmid pKD4 using Q5 high-fidelity DNA polymerase. The FRT-flanked Kan^R PCR product was treated with DpnI to remove template DNA and purified using the Zymo Research DNA Clean & Concentrator™-25 kit. Purified PCR product was transformed into electrocompetent WN1/pKD46. Cells were plated onto LB/Kan and grown at 37°C for 24 h, during which time homologous recombination events led to insertion the FRT-flanked Kan^R cassette into the genomic *pptA* locus. Transformants were re-streaked onto LB agar and grown at 37°C for 24 h. Single colonies from these LB plates were replicate plated onto LB, LB/Ap, and

LB/Kan plates. Colonies that grew in the presence of kanamycin and ampicillin were selected to prepare electrocompetent cells, WN1*pptA*::FRT-Kan^R/pKD46. Plasmid pCP20, which carries a thermally-induced yeast Flp recombinase gene and a temperature-sensitive replicon, was transformed into electrocompetent WN1*pptA*::FRT-Kan^R/pKD46 and plated onto LB/Ap. Cells were grown at 30°C for 24 h. Transformants were re-streaked onto LB agar before growth at 43°C. Loss of antibiotic resistance was tested by replicate plating colonies from LB plates onto LB, LB/Kan, and LB/Cm. An inability to grow in the presence of kanamycin, chloramphenicol, or ampicillin implied loss of FRT-flanked kanamycin resistance gene and λ Red helper plasmids simultaneously. Loss of genomic *pptA* was verified by PCR followed by agarose gel electrophoresis.

BglBrick parts and plasmids

All plasmids used in this Chapter are presented in Table 23. All "parts" are genes inserted into pBbA1a (Figure 107). All insertions followed the method of cloning described above (Figure 106). The sequence for all BglBrick parts were confirmed by Sanger sequencing.

Table 25. Plasmids used and constructed in Chapter 1 of this work.

Strain/plasmid	Relevant characteristics	Source or reference
pBbA1a-RFP	Ap^R, *lacI*^{q}, P_{trc}*rfp* p15A replicon	Addgene #35334[6]
pWN1.028A	*aroF*^{FBR} source	lab[2]
pWN1.162A	*serA* source	lab[2]
pMF63A	P_{aroF} source	lab[13]
pKM6.196	P_{trc}*praA* in pBbA1a	this work
pKM6.200	P_{trc}*praB* in pBbA1a	this work
pKM6.201	P_{trc}*praH* in pBbA1a	this work
pKM6.208	P_{trc}*praHpraA* in pBbA1a	this work
pKM6.232	P_{trc}*praBpraHpraA* in pBbA1a	this work
pKM6.240	P_{trc}*serA* in pBbA1a	this work
pKM6.241	$P_{trc}P_{aroF}$ in pBbA1a	this work
pKM6.261	P_{trc}*serA*P_{aroF} in pBbA1a	this work
pKM6.268	P_{trc}*aroF*^{FBR} in pBbA1a	this work
pKM6.274	P_{trc}*aroF*^{FBR}*serA*P_{aroF} in pBbA1a	this work
pKM6.280	P_{trc}*praBpraHpraAaroF*^{FBR}*serA*P_{aroF} in pBbA1a	this work

Plasmid pKM6.274

Plasmid pKM6.274 contained a P_{trc}*aroF*^{FBR}*serA*P_{aroF} cassette. It was created by first inserting *serA* from plasmid pKM6.240 upstream of P_{aroF} in plasmid pKM6.241 to afford plasmid pKM6.261. The *aroF*^{FBR} gene was then inserted upstream of *serA* to afford plasmid pKM6.274.

Plasmid pKM6.232

Plasmid pKM6.232 contained a P_{trc}*praBpraHpraA* cassette. It was created by first inserting *praH* from plasmid pKM6.201 upstream of *praA* in plasmid pKM6.196 to afford

plasmid pKM6.208. The *praB* gene was then inserted upstream of *praA* to afford plasmid pKM6.232.

Plasmid pKM6.280

Plasmid pKM6.280 contained a P_{trc}*praB*p*raH*p*raA*a*roF*^{FBR}*serA*P_{aroF} cassette. It was created by inserting the *praB*p*raH*p*raA* gene fragment from plasmid pKM6.232 upstream of *aroF*^{FBR} in plasmid pKM6.274.

Enzyme assays

Transketolase assay

Estimation of laboratory-synthesized E4P concentration employed the transketolase assay using the method of Paoletti.[14] A dilute solution of E4P was concentrated four-fold by rotary evaporation and the pH adjusted to 7.0 with 5 N KOH. The assay mixture (1 mL) contained 150 mM triethanolamine (pH 7.6), 5 mM $MgCl_2$, 0.1 mM thiamine pyrophosphate, 0.4 mM $NADP^+$, 0.4 mM β-hydroxypyruvate, 50 μL E4P solution, glucose-6-phosphate dehydrogenase (8 units, Roche), and phosphoglucose isomerase (4 units, Sigma-Aldrich). The solution was allowed to equilibrate at rt for 3-5 min during which time the unreacted D-glucose-6-phosphate remaining in solution from the synthesis of E4P had been consumed. After no change in absorbance was observed, a solution containing purified *E. coli* transketolase (10 units, Sigma-Aldrich) was added and the increase in absorbance at 340 nm was monitored until the absorbance was no longer increasing (5 min). The difference in absorbance at 340 nm due to formation of NADH (ε = 6,220 M^{-1} cm^{-1}) was used to estimate the concentration of laboratory-synthesized E4P.

DAHP synthase ($AroF^{FBR}$) assay

DAHP synthase activity was assayed according to the procedure described by Schoner.[15] A dilute solution of E4P was concentrated to 12 mM under reduced pressure and neutralized with 5 N KOH. Two different solutions were prepared and incubated separately at 37°C for 5 minutes. The first solution (1 mL) contained E4P (6 mM), phosphoenolpyruvate (PEP, 12 mM), ovalbumin (1 mg/mL), and potassium phosphate buffer (25 mM, pH 7.0). The second solution (0.5 mL) contained 1,3-propanediol (250 mM), PEP (0.5 mM), and an appropriate amount of protein sample diluted in potassium phosphate buffer (50 mM, pH 7.0). After the two solutions were mixed (time = 0), aliquots (0.15 mL) were removed at timed intervals and quenched with 0.1 mL trichloroacetic acid (10% w/v). Precipitated protein was removed by microcentrifugation (11,300*g*, 2 min, rt) and the amount of DAHP in each sample was determined using a thiobarbituric acid assay.

The reagents used in the thiobarbituric acid assay[16] include solution A: 0.2 M $NaIO_4$ in 8.2 M H_3PO_4; solution B: 0.8 M $NaAsO_2$ and 0.5 M Na_2SO_4 in 0.1 M H_2SO_4; and solution C: 0.04 M thiobarbituric acid in 0.5 M Na_2SO_4 (pH 7.0). An aliquot (0.1 mL) of DAHP-containing sample was reacted with 0.1 mL of solution A in a glass test tube (13 mm × 100 mm) at 37°C for 5 minutes. The reaction was quenched by addition of 0.5 mL solution B and briefly vortexed until a brown color disappeared. Upon addition of 3 mL solution C, the sample was heated at 100°C for 15 minutes. Samples were briefly cooled and the pink chromophore was extracted into 4 mL of cyclohexanone. The aqueous and organic layers were separated by centrifugation (2,000 *g*, 15 min). The absorbance of the organic layer was measured at 549 nm (ε = 68,000 M^{-1} cm^{-1}).

2-Hydroxymuconic acid extraction solvent screening

Cell-free, protein-free fermentation broth containing 2-hydroxymuconic acid, α-keto acid **23** and α-keto acid **24** was concentrated to 1/4 original volume under reduced pressure and acidified to pH 2 with conc. H_2SO_4. Extraction screens were performed in 1 dram glass vials with screw caps. Each vial contained 0.5 mL concentrated broth and 0.5 mL extraction solvent. The solvent and broth were mixed by continuously rotating (7 rpm) for 12 h at rt using a hybridization incubator. The concentration of 2-HMA, α-keto acid **23** and α-keto acid **24** in the organic and aqueous layers were determined by ^{1}H NMR.

CHAPTER TWO

Plasmid construction

BglBrick parts and plasmids

A list of the BglBrick parts used in this Chapter are presented in Table 26. All "parts" are genes inserted into pBbA1a (Figure 107). All insertions followed the method of cloning described above (Figure 106). The sequence for all BglBrick parts was confirmed by Sanger sequencing.

Table 26. Plasmids used and constructed in Chapter 2 of this work.

Strain/plasmid	Relevant characteristics	Source or reference
pBbA1a-RFP	Ap^R, *lacI*^{q}, P_{trc}*rfp* p15A replicon	Addgene #35334[6]
pBbA7k-RFP	Kan^R, *lacI*^{q}, P_{T7}*rfp*, p15A replicon	Addgene #35318[6]
pKM6.240	P_{trc}*serA* in pBbA1a	Chapter 1
pSN1.294	P_{trc}*ntdC*^{sub}	lab (described herein)
pSN1.295	P_{trc}*ntdB*^{sub}	lab (described herein)
pSN1.296	P_{trc}*ntdA*^{sub}	lab (described herein)
pSN1.119	P_{trc}*ntdC*^{sub}*ntdA*^{sub} in pBbA1a	lab (described herein)
pSN1.139	P_{trc}*ntdC*^{sub}*ntdA*^{sub}*ntdB*^{sub} in pBbA1a	lab (described herein)
pSN1.292	P_{trc}*ntdC*^{sub}*ntdA*^{sub}*ntdB*^{sub}*serA* in pBbA1a	lab (described herein)
pJG7.246	Ap^R, P_{T5}, His_6, *lacI*^{q}, ColE1 replicon	lab[7]
pKM9.279C	$P_{T5}$$His_6$-*ntdC*^{sub} in pJG7.246	this work
pKM10.82A	P_{T7}*ntdC*^{sub}*ntdA*^{sub}*ntdB*^{sub}*serA* in pBbA7k	this work
pKM10.204A	P_{trc}*ntdA*^{sub}*serA* in pBbA1a	this work
pKM10.204B	P_{trc}*ntdB*^{sub}*serA* in pBbA1a	this work

Table 26 (cont'd)

pKM10.204C	P_{trc}*ntdC*^{sub}*serA* in pBbA1a	this work
pKM10.214CA	P_{trc}*ntdC*^{sub}*ntdA*^{sub}*serA* in pBbA1a	this work
pKM10.214CB	P_{trc}*ntdC*^{sub}*ntdB*^{sub}*serA* in pBbA1a	this work
pKM10.214AB	P_{trc}*ntdA*^{sub}*ntdB*^{sub}*serA* in pBbA1a	this work
pKM10.214BC	P_{trc}*ntdB*^{sub}*ntdC*^{sub}*serA* in pBbA1a	this work
pKM10.220ABC	P_{trc}*ntdA*^{sub}*ntdB*^{sub}*ntdC*^{sub}*serA* in pBbA1a	this work
pUCIDT(Kan)-rifK	Kan^{R}, P_{lac}, codon optimized *rifK*, ColE1 replicon	IDT
pUCIDT(Kan)-rifL	Kan^{R}, P_{lac}, codon optimized *rifL*, ColE1 replicon	IDT
pUCIDT(Kan)-rifM	Kan^{R}, P_{lac}, codon optimized *rifM*, ColE1 replicon	IDT
pKM10.254K	P_{trc}*rifK* in pBbA1a	this work
pKM10.254L	P_{trc}*rifL* in pBbA1a	this work
pKM10.254M	P_{trc}*rifM* in pBbA1a	this work
pKM10.268K	P_{trc}*rifKserA* in pBbA1a	this work
pKM10.268L	P_{trc}*rifLserA* in pBbA1a	this work
pKM10.268M	P_{trc}*rifMserA* in pBbA1a	this work
pKM10.278KM	P_{trc}*rifKrifMserA* in pBbA1a	this work
pKM10.284L	P_{T5}His$_6$-*rifL* in pJG7.246	this work
pKM11.9	P_{trc}*rifLrifKrifMserA* in pBbA1a	this work
pKM11.46	P_{T7}*rifLrifKrifMserA* in pBbA7k	this work
pUCIDT(Kan)-ntdA	Kan^{R}, P_{lac}, *ntdA*^{pum}, ColE1 replicon	IDT
pUCIDT(Kan)-ntdB	Kan^{R}, P_{lac}, *ntdB*^{pum}, ColE1 replicon	IDT
pUCIDT(Kan)-ntdC	Kan^{R}, P_{lac}, *ntdC*^{pum}, ColE1 replicon	IDT
pKM11.121A	P_{trc}*ntdA*^{pum} in pBbA1a	this work
pKM11.121B	P_{trc}*ntdB*^{pum} in pBbA1a	this work
pKM11.121C	P_{trc}*ntdC*^{pum} in pBbA1a	this work
pKM11.125	P_{trc}*ntdB*^{pum}*serA* in pBbA1a	this work
pKM11.130	P_{trc}*ntdC*^{pum}*ntdA*^{pum} in pBbA1a	this work
pKM11.135	P_{trc}*ntdC*^{pum}*ntdA*^{pum}*ntdB*^{pum}*serA* in pBbA1a	this work

Plasmid pSN1.292

Plasmid pSN1.292 contained a P_{trc}*ntdC*^{sub}*ntdA*^{sub}*ntdB*^{sub}*serA* cassette. It was created by first inserting *ntdC*^{sub} from plasmid pSN1.294 upstream of *ntdA* in plasmid pSN1.296 to afford plasmid pSN1119. The *ntdC*^{sub}*ntdA*^{sub} gene was then inserted upstream of *ntdB*^{sub} in plasmid pSN1.295to afford plasmid pSN1.139, which carried a P_{trc}*ntdC*^{sub}*ntdA*^{sub}*ntdB*^{sub} cassette. Finally, the *ntdC*^{sub}*ntdA*^{sub}*ntdB*^{sub} gene fragment was inserted upstream of *serA* in plasmid pKM6.240 to afford plasmid pSN1.292.

Plasmid pKM10.220ABC

Plasmid pKM10.220ABC contained a P_{trc}*ntdA*^{sub}*ntdB*^{sub}*ntdC*^{sub}*serA* cassette. It was created by first inserting *ntdC*^{sub} from plasmid pSN1.294 upstream of *serA* in plasmid pKM6.240 to afford plasmid pKM10.204C. The *ntdB*^{sub} gene was then inserted upstream of *ntdC*^{sub} to afford plasmid pKM10.214BC, which carried a P_{trc}*ntdB*^{sub}*ntdC*^{sub}*serA* cassette. Finally, *ntdA*^{sub} was inserted upstream of *ntdB*^{sub} to afford plasmid pKM10.220ABC.

Plasmid pKM10.214CA

Plasmid pKM10.214CA contained a P_{trc}*ntdC*^{sub}*ntdA*^{sub}*serA* cassette. It was created by first inserting *ntdC*^{sub} from plasmid pSN1.294 upstream of *ntdA*^{sub} in plasmid pKM10.204A to afford plasmid pKM10.214CA.

Plasmid pKM10.214CB

Plasmid pKM10.214CB contained a P_{trc}*ntdC*^{sub}*ntdB*^{sub}*serA* cassette. It was created by first inserting *ntdC*^{sub} from plasmid pSN1.294 upstream of *ntdB*^{sub} in plasmid pKM10.204B to afford plasmid pKM10.214CB.

Plasmid pKM10.214AB

Plasmid pKM10.214AB contained a P_{trc}*ntdA*^{sub}*ntdB*^{sub}*serA* cassette. It was created by first inserting *ntdA*^{sub} from plasmid pSN1.296 upstream of *ntdB*^{sub} in plasmid pKM10.204B to afford plasmid pKM10.214AB.

Plasmid pKM10.82A

Plasmid pKM10.82A contained a P_{T7}*ntdC*^{sub}*ntdA*^{sub}*ntdB*^{sub}*serA* cassette. The *ntdC*^{sub}*ntdA*^{sub}*ntdB*^{sub}*serA* fragment was removed from pSN1.292 by *Eco*RI and *Bam*HI digestion. BglBrick plasmid pBbA7k (Figure 111) was linearized also with *Eco*RI and *Bam*HI digestion. Ligation of the two DNA fragments afforded pKM10.82A.

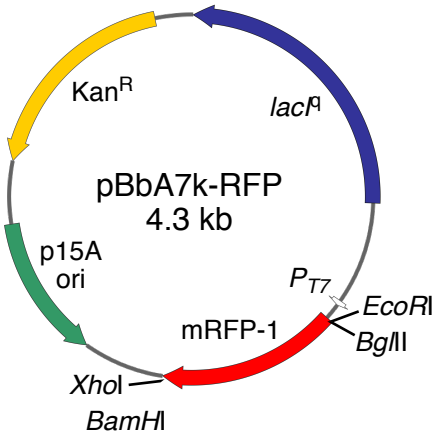

Figure 111. BglBrick plasmid pBbA7k-RFP.

Plasmid pKM11.9

Plasmid pKM11.9 contained a P_{trc}*rifLrifKrifMserA* cassette. It was created by first inserting *rifM* from plasmid pKM10.254M upstream of *serA* in plasmid pKM6.240 to afford plasmid pKM10.268M. The *rifK* gene was then inserted upstream of *rifM* to afford plasmid pKM10.278KM, which carried a P_{trc}*rifKrifMserA* cassette. Finally, *rifL* was inserted upstream of *rifK* to afford plasmid pKM11.9.

Plasmid pKM11.46

Plasmid pKM11.46 contained a P_{T7}*rifLrifKrifMserA* cassette. The *rifLrifKrifMserA* fragment was removed from pKM11.9 by *Eco*RI and *Bam*HI digestion. BglBrick plasmid pBbA7k (Figure 114) was linearized also with *Eco*RI and *Bam*HI digestion. Ligation of the two DNA fragments afforded pKM11.46.

Plasmid pKM11.135

Plasmid pKM11.135 contained a P_{trc}*ntdC*^{pum}*ntdA*^{pum}*ntdB*^{pum}*serA* cassette. It was created by first inserting *ntdB*^{pum} from plasmid pKM11.121B upstream of *serA* in plasmid pKM6.240 to afford plasmid pKM11.125. The *ntdC*^{pum} gene was inserted upstream of *ntdA*^{pum} in plasmid pKM11.121A to afford plasmid pKM11.130. Finally, the *ntdC*^{pum}*ntdA*^{pum} fragment was inserted upstream of *ntdB*^{sub} in plasmid pKM11.125 to afford plasmid pKM11.135.

Plasmid pKM10.284

The *rifL* gene was PCR-amplified from pKM10.254L without its native ATG start codon and the addition of *Bam*HI sites at the 5' and 3' end. The PCR product was inserted into the *Bam*HI site of pJG7.246 to afford plasmid pKM10.284. The relevant gene and vector sequences are shown in Figure 112.

5' — **ATG** AGA GGA TCG **CAT CAC CAT CAC CAT CAC** **GGA TCC** GCA — 3'

Figure 112. Beginning gene sequence for plasmid pKM10.284. Vector codons are in blue, the BamHI site is in black, *rifL* codon is in green. The transcription start codon and the His_6 sequence on vector pJG7.246 are underlined.

Plasmid pKM9.297C

The *ntdC*^{sub} gene was PCR-amplified from pSN1.294 without its native ATG start codon and the addition of *Bam*HI sites at the 5' and 3' end. The PCR product was inserted into the *Bam*HI site of pJG7.246 to afford plasmid pKM9.279C. The relevant gene and vector sequences are shown in Figure 113.

5’ — **ATG** AGA GGA TCG **CAT CAC CAT CAC CAT CAC** **GGA TCC** TCT — 3’

Figure 113. Beginning gene sequence for plasmid pKM9.279C. Vector codons are in blue, the *Bam*HI site is in black, *ntdC*^{sub} codon is in green. The transcription start codon and the His_6 sequence on vector pJG7.246 are underlined.

RB791*serA*/pSN1.292 growth study with exogenous kanosamine

A culture of RB791*serA*/pSN1.292 in 5 mL modified M9 media was grown at 35°C with agitation at 250 rpm for 11 h. An aliquot of this culture was used to inoculate three 20 mL cultures of the same media in 100 mL three-baffled flasks to an initial OD_{600} = 0.05. Growth continued at 35°C with agitation at 250 rpm until OD_{600} = 0.4. An appropriate amount of a 300 mM aqueous solution of kanosamine hydrochloride (pH 8.0) was added to each of the three flasks to achieve the desired final concentration of 0, 25, or 50 mM. Growth continued at 35°C with agitation at 250 rpm and was monitored once every hour until stationary phase. Growth rates were determined during exponential phase by using the conversion factor of $OD_{600}(1.0)$ = 1.0 x 10^8 cells/mL. The logarithm of the number of cells measured between 4 h and 8 h was used to compare the rate of growth for each culture.

Cell-lysate preparations

E. coli cells were harvested from flask cultures by centrifugation at 4,000*g* for 5 min at 4°C. Cell samples removed from fermentation runs were collected by centrifugation at 11,300*g* for 20 min at 4°C. Cell lysis was achieved by two passages through a French® pressure cell (SLM Aminco) at 17,400 psi. Cellular debris was removed from the lysate by centrifugation (38,500*g*, 30 min, 4°C). Protein concentrations were determined using the Bradford dye-binding procedure[11] using a protein assay solution purchased from Bio-Rad (1× concentration). Assay

solution (1 mL) was combined with 20 µL protein containing solution and incubated at rt for 3 minutes. The absorbance was measured at 595 nm and the protein concentration determined by comparison to a standard curve prepared using bovine serum albumin.

Protein purifications

B. subtilis ntdC-encoded D-glucose-6-phosphate 3-dehydrogenase

D-Glucose-6-phosphate (G6P) 3-dehydrogenase[17] was purified from *E. coli* DH5α/ pKM9.279C (P_{T5}, *lacO*, His_6, *ntdC*, Amp^R) on a Ni-NTA Agarose column (Qiagen). Buffers used in the purification included buffer A: Tris-HCl (20 mM), NaCl (500 mM), imidazole (5 mM), glycerol (20% v/v), pH 7.9; buffer B: Tris-HCl (20 mM), NaCl (500 mM), imidazole (60 mM), glycerol (20% v/v), pH 7.9; buffer C: Tris-HCl (20 mM), NaCl (500 mM), imidazole (5 mM), EDTA (50 mM), glycerol (20% v/v), pH 7.9; buffer D: Tris-HCl (25 mM), NaCl (150 mM), glycerol (50% v/v), pH 8.0.

A single colony of *E. coli* DH5α/pKM9.279C was used to inoculate 5 mL LB containing ampicillin. Cells were grown with agitation at 250 rpm, 37°C for 14 h. An appropriate amount of culture was used to inoculate 500 mL LB containing ampicillin to an initial OD_{600} = 0.01. Growth continued at 250 rpm, 37°C for 3 h until the OD_{600} reached 0.6. IPTG was added to a final concentration of 1 mM. After an additional 4 h of growth, cells (4.8 g) were harvested by centrifugation (5,500*g*, 10 min, 4°C), resuspended in buffer A (2 mL/g wet cells), and lysed by two passages through a French® pressure cell at 17,400 psi. Cellular debris was removed by centrifugation (38,500*g*, 30 min, 4°C). To the supernatant was added a 50% (w/v) slurry of Ni-NTA agarose resin (1 mL resin per 4 mL crude lysate) that had been equilibrated in buffer A and

the mixture was gently stirred at 4°C for 1 h. The lysate–resin slurry was transferred to a polypropylene column (Qiagen) and the column was washed with buffer B (2 × 4 mL per mL of Ni-NTA agarose resin). The His_6-tagged protein was eluted from the column by washing with buffer C (4 × 0.5 mL per mL of Ni-NTA agarose resin). Fractions were analyzed by sodium dodecyl sulfate–polyacrylamide gel electrophoresis (SDS–PAGE), and those containing pure protein were combined and dialyzed twice against buffer D at 4°C. Enzyme was stored in 100 µL aliquots at −20°C.

Amycolatopsis mediterranei rifL-encoded UDP-D-glucose 3-dehydrogenase

UDP-D-glucose 3-dehydrogenase was purified from *E. coli* DH5α/pKM10.284 (P_{T5}, *lacO*, *His*$_6$, *rifL*, Amp^R) on an ÄKTAstart FPLC. Buffers used in the purification included buffer A: NaH_2PO_4 (20 mM, pH 7.4), NaCl (500 mM); buffer B: NaH_2PO_4 (20 mM, pH 7.4), NaCl (500 mM), imidazole (500 mM) buffer C: Tris-HCl (25 mM), NaCl (150 mM), glycerol (50% v/v), pH 8.0.

A single colony of *E. coli* DH5α/pKM10.284 was used to inoculate 5 mL LB containing ampicillin (50 µg/mL). Cells were grown with agitation at 250 rpm, 37°C for 14 h. An appropriate amount of culture was used to inoculate 500 mL LB containing ampicillin to an initial OD_{600} = 0.01. Growth continued at 250 rpm, 37°C for 3 h until the OD_{600} reached 0.6. IPTG was added to a final concentration of 1 mM. After an additional 4 h of growth, cells (5.3 g) were harvested by centrifugation (5,500*g*, 10 min, 4°C), resuspended in buffer A (2 mL/g wet cells), and lysed by two passages through a French® pressure cell at 17,400 psi. Cellular debris was removed by centrifugation (38,500*g*, 30 min, 4°C). The supernatant was loaded onto a

HisTrap Fast Flow Sepharose column (16 x 25 mm, 1.0 mL) which had been equilibrated with buffer A. The column was washed with buffer A (20 mL) and eluted with a linear gradient (4%-100%) of buffer A and buffer B. Fractions were analyzed by sodium dodecyl sulfate–polyacrylamide gel electrophoresis (SDS–PAGE), and those containing pure protein were combined and dialyzed twice against buffer C at 4°C. Enzyme was stored in 100 µL aliquots at −20°C.

Enzyme assays

D-glucose-6-phosphate 3-dehydrogenase assay ($NtdC^{sub}$ and $NtdC^{pum}$)

Enzyme activity was determined spectrophotometrically by monitoring increase in absorption at 340 nm due to the formation of NADH (ε = 6,220 M^{-1} cm^{-1}). The reaction was carried out in 2-amino-1-methylpropanol (AMP, 100 mM) buffer (pH 9.5) using a mixture (1 mL) consisting of D-glucose-6-phosphate (5 mM), NAD^+ (5 mM), and an appropriate amount of enzyme at rt. One unit of D-glucose-6-phosphate 3-dehydrogenase activity was defined as the amount which catalyzed the formation of 1 µmol of NADH per min.

UDP-D-glucose 3-dehydrogenase assay (RifL)

Enzyme activity was determined spectrophotometrically by monitoring increase in absorption at 340 nm due to the formation of NADH (ε = 6,220 M^{-1} cm^{-1}). The reaction was carried out in sodium phosphate buffer (50 mM, pH 7.0) using a mixture (1 mL) consisting of UDP-D-glucose (5 mM), NAD^+ (5 mM), and an appropriate amount of enzyme at rt. One unit of

UDP-D-glucose 3-dehydrogenase activity was defined as the amount which catalyzed the formation of 1 μmol of NADH per min.

Purification of kanosamine from fermentation broth

After completion of a fermentation run, cells were harvested by centrifugation (6,400 *g*, 4°C, 20 min). Cell-free broth was then passed through a tangential flow filtration apparatus (10 kD) (Sartorius) to remove proteins. The clarified broth was then treated with activated charcoal (10 g L, Darco KB-B, 100 mesh) at 37°C for 1 h and filtered through a layer of Celite 545. The colorless filtrate was loaded onto a cation exchange column (Dowex 50WX8, H^+-form, 50-100 mesh) and washed with four column volumes of water. Kanosamine was eluted as the hydrochloride salt with a linear gradient of HCl (0-0.5 N). Kanosamine containing fractions were combined and adjusted to pH 7.0 with KOH (5 N). Water was removed under reduced pressure and the pale yellow solids extracted into methanol (2 x 30 mL). Insoluble salts were removed by filtration. The filtrate was evaporated under reduced pressure to afford kanosamine hydrochloride as a white solid. ^{1}H NMR (500 MHz, D_2O, TSP = 0.00 ppm): δ 5.27 (d, J = 3.5 Hz, 1H), 4.73 (d, J = 7.7 Hz, 1H), 3.94-3.73 (m, 6H), 3.67 (dt, J = 9.9, 2.9 Hz, 2H), 3.58 (ddd, J = 9.7, 5.4, 2.2 Hz, 1H), 3.47-3.39 (m, 2H), 3.24 (t, J = 10.4 Hz, 1H). ^{13}C NMR (126 MHz, D_2O, TSP = 0.0 ppm): δ 98.9, 94.0, 79.6, 74.1, 73.4, 71.0, 68.9, 68.8, 63.0, 62.8, 60.7, 57.9.

REFERENCES

REFERENCES

1. Zhang, P.; Kriegel, R. M.; Frost, J. W. B–O–B Catalyzed Cycloadditions of Acrylic Acids. *ACS Sustainable Chem. Eng.* **2016**, *4* (12), 6991–6995.

2. Niu, W.; Draths, K. M.; Frost, J. W. Benzene-Free Synthesis of Adipic Acid. *Biotechnol. Prog.* **2002**, *18*, 201–211.

3. Frost, J. W.; Hansen, C. A. Synthesis of 1,2,3,4-Tetrahydroxybenzenes and 1,2,3,-Trihydroxybenzenes Using Myo-Inositol-1-Phosphate Synthase and *myo*-Inositol-2-Dehydrogenase. US 6,750,049, 2004.

4. Datsenko, K. A.; Wanner, B. L. One-Step Inactivation of Chromosomal Genes in Escherichia Coli K-12 Using PCR Products. *Proc. Natl. Acad. Sci. U. S. A.* **2000**, *97* (12), 6640–6645.

5. Kasai, D.; Fujinami, T.; Abe, T.; Mase, K.; Katayama, Y.; Fukuda, M.; Masai, E. Uncovering the Protocatechuate 2,3-Cleavage Pathway Genes. *J. Bacteriol.* **2009**, *191* (21), 6758–6768.

6. a) Lee, T. S.; Krupa, R. A.; Zhang, F.; Hajimorad, M.; Holtz, W. J.; Prasad, N.; Lee, S. K.; Keasling, J. D. BglBrick Vectors and Datasheets: A Synthetic Biology Platform for Gene Expression. *J. Biol. Eng.* **2011**, *5*, 12. b) Anderson, J.; Dueber, J. E.; Leguia, M.; Wu, G. C.; Goler, J. A.; Arkin, A. P.; Keasling, J. D. BglBricks: A Flexible Standard for Biological Part Assembly. *J. Biol. Eng.* **2010**, *4* (1), 1.

7. Guo, J. Biosynthesis of Precursors to the Aminoshikimate Pathway and Microbial Synthesis of 5-Amino-5-Deoxyshikimate. Doctor of Philosophy, Michigan State University, 2004.

8. Miller, J. H. *Experiments in Molecular Genetics*; Cold Spring Harbor Laboratory: Cold Spring Harbor, NY, 1972.

9. Sambrook, J.; Russell, D. W. *Molecular Cloning: A Laboratory Manual* 3rd ed.; Cold Spring Harbor Laboratory: Cold Spring Harbor, NY, 2001.

10. Knop, D. R.; Draths, K. M.; Chandran, S. S.; Barker, J. L.; von Daeniken, R.; Weber, W.; Frost, J. W. Hydroaromatic Equilibration During Biosynthesis of Shikimic Acid. *J. Am. Chem. Soc.* **2001**, *123* (42), 10173–10182.

11. Sieben, A. S.; Perlin, A. S.; Simpson, F. J. An Improved Preparative Method for D-Erythrose 4-Phosphate. *Canadian Journal of Chemistry* **1966**, *44* (6), 663–669.

12. Wecke, T. Isolation of genomic DNA from Bacillus http://2012.igem.org/wiki/images/6/6b/LMU-Munich_2012_Isolation_of_genomic_DNA_from_Bacillus_%28for_PCR....%29.pdf (accessed Jan 2018).

13. Farabaugh, M. A. Biocatalytic Production of Aromatics from D-glucose. Master of Science, Michigan State University, 1996.

14. Paoletti, F.; Williams, J. F.; Horecker, B. L. An Enzymic Method for the Analysis of D-Erythrose 4-Phosphate. *Anal. Biochem.* **1979**, *95*, 250–253.

15. Schoner, R.; Herrmann, K. M. 3-Deoxy-D-*arabino*-Heptulosonate 7-Phosphate Synthase. Purification, Properties, and Kinetics of the Tyrosine-Sensitive Isoenzyme from *Escherichia coli*. *J. Biol. Chem.* **1976**, *251* (18), 5440–5447.

16. Gollub, E.; Zalkin, H.; Sprinson, D. B. Assay for 3-Deoxy-D-*arabino*-Heptulosonic Acid 7-Phosphate Synthase. *Methods in Enzymology* **1971**, *17*, 349–350.

17. Vetter, N. D.; Palmer, D. R. J. Simultaneous Measurement of Glucose-6-Phosphate 3-Dehydrogenase (NtdC) Catalysis and the Nonenzymatic Reaction of Its Product: Kinetics and Isotope Effects on the First Step in Kanosamine Biosynthesis. *Biochemistry* **2017**, *56* (14), 2001–2009.